Rickettsia-Macrophage Tropism: A Link To Rickettsial Pathogenicity?

Pedro Tiago Cardoso Curto

UNIVERSIDADE D COIMBRA

UNIVERSIDADE D
COIMBRA

Pedro Tiago Cardoso Curto

Rickettsia-Macrophage Tropism: A Link To Rickettsial Pathogenicity?

Tese no âmbito do Doutoramento em Biologia Experimental e Biomedicina, especialidade em Biotecnologia e Saúde orientada pela Doutora Isaura Isabel Gonçalves Simões e pelo Doutor Juan J. Martinez e apresentada ao Instituto de Investigação Interdisciplinar da Universidade de Coimbra.

Julho de 2018

Instituto de Investigação Interdisciplinar da Universidade de Coimbra

RICKETTSIA-MACROPHAGE TROPISM: A LINK TO RICKETTSIAL PATHOGENICITY?

Pedro Tiago Cardoso Curto

Tese no âmbito do programa doutoral em Biologia Experimental e Biomedicina, na área de Biotecnologia e Saúde orientada pela Doutora Isaura Isabel Gonçalves Simões e pelo Doutor Juan J. Martinez e apresentada ao Instituto de Investigação Interdisciplinar da Universidade de Coimbra.

Julho de 2018

UNIVERSIDADE D
COIMBRA

Este trabalho foi realizado no grupo biotecnologia molecular e microbiana do Centro de Neurociências e Biologia Celular (Universidade de Coimbra, Portugal) e no departamento de ciências patobiológicas da Universidade do Estado de Louisiana, orientado pela Doutora Isaura Simões e Doutor Juan J. Martinez.

Pedro Tiago Cardoso Curto é um estudante do programa doutoral em biologia experimental e biomedicina do Centro de Neurociências e Biologia Celular da Universidade de Coimbra, Portugal.

Este trabalho foi elaborado ao abrigo de uma bolsa de doutoramento financiada pela Fundação para a Ciência e Tecnologia (FCT, SFRH/BD/96769/2013) suportada por Fundos nacionais do Ministério da Ciência, Tecnologia e Ensino Superior e pelo Fundo Social Europeu através do POCH – Programa Operacional Capital Humano. Parte do trabalho foi financiado pelo projeto com a referência POCI-01-0145-FEDER-029592, financiado pelo Programa Operacional Competitividade e Internacionalização na sua componente FEDER e pelo orçamento da Fundação para a Ciência e a Tecnologia na sua componente OE; por fundos FEDER através do Programa Operacional Factores de Competitividade – COMPETE 2020 e por Fundos Nacionais através da FCT – Fundação para a Ciência e a Tecnologia no âmbito do projeto Estratégico com referência atribuída pelo COMPETE: POCI-01-0145-FEDER-007440 (ref.; UID/NEU/04539/2013); pelo projeto PTDC/SAU-MII/107942/2008; e pelo "National Institute of Allergy and Infectious Diseases of the National Institutes of Health" através dos projetos R01AI072606 and 5R21AI111086-02.

Agradecimentos / Acknowledgments

Uma tese de doutoramento consiste em uma busca incessante pelo conhecimento. Para mim, desde que me lembro de conseguir pensar, que me fascina entender o que ainda não é compreendido. Contudo, descobrir algo novo é um processo longo, duro, com obstáculos e que requer muita persistência, apoio e suporte de várias pessoas. Desta forma, gostaria de deixar algumas palavras de profundo e sincero agradecimento a todos aqueles que, de alguma forma, deixaram o seu contributo durante este percurso.

Em primeiro lugar, gostaria de deixar um agradecimento especial à minha orientadora Doutora Isaura Simões. No entanto, sinto que as palavras que escolherei serão sempre poucas. Muito obrigado por todos estes momentos de partilha e amizade. Irei, para sempre, apreciar ter tido a oportunidade de trabalhar consigo. A sua forma de ver e fazer ciência é algo que me fascina. Obrigado por todo o seu apoio, ajuda e amizade ao longo destes anos. O caminho nem sempre tem sido fácil mas, é quando assim é, que se vêm os verdadeiros laços. Muito obrigado por tudo. Faço votos para o caminho que iremos percorrer seja carregado de sucesso.

To Doctor Juan J. Martinez, who kindly welcomed me in his lab, I deeply appreciate the opportunity to perform science in a different country and environment. Working alongside you allowed me to immerse myself in diversity by operating with different people, different backgrounds, and different mentalities. Additionally, our collaboration gave me a chance to be in touch with different methods of doing science. Thank you for your friendship and you are always welcome in Portugal.

Gostaria também de extender os meus sinceros agradecimentos a todos os membros que partecem, ou em algum momento perteceram, ao laboratório de Biotecnologia Molecular do CNC por terem dado o seu contributo no meu crescimento enquanto cientista e pessoa. Assim, deixo um agradecimento especial ao Doutor Pedro Castanheira, Doutor Rui Cruz, Doutor André Soares, Doutora Ana Sofia Lourenço, Carla Almeida, Liliana Antunes, Paulo Santo, Ana Rita Leal e a todos os outros, pelos bons momentos de amizade e boa disposição.

I would also like to extend my acknowledgments to everyone who made my experience at LSU so meaningful. Thus, I would like to thank Doctor Sean Riley, Doctor Kevin Macaluso and his lab members, Doctor Abbie Fish, Doctor Emma Harris, Daniel Garza, Nam, Bee, Ryan Avery and all the others that made Baton Rouge a welcoming home.

To Matt, I don't have the words to describe how important you were during my time in the States. Thanks for all the moments of joy and sharing that I will forever carry with me. You made my life in Baton Rouge so much easier and enjoyable. Because of the moments we shared, returning home was nothing short of arduous. I will always miss those moments and I have high hopes that our friendship stays strong. Saudades

Gostaria de agradecer aos restantes colegas e amigos do UC-Biotec pelas boas recordações e momentos vividos. Assim, agradeço a todos os membros do laboratório do Doutor Ricardo Pires e do Doutor Bruno Manadas. Não poderia passar sem deixar um agradecimento especial à Cátia Santa e a Doutora Sandra Anjo pela ajuda e apoio na interpretação dos resultados de espectrometria de massa.

A todos os meus amigos, um enorme obrigado por estarem sempre presentes e por partilharem comigo muitos momentos especiais. Assim, gostaria de deixar um agradecimento especial à Isabel, Luís, Carla, Daniela Faria, Joana Novo e à sua princesa Benedita, Andreia Filipa |risinhos daqueles| e Daniela Filipa.

Por fim, gostaria de agradecer a toda a minha família por me ensinarem a ser quem sou. Aos meus Pais, Avós, Irmão, Tia Rosa e primo Marcelo deixo um grande obrigado por toda esta força e momentos de partilha. As batalhas têm sido duras, mas os bons momentos serão, para sempre, parte de nós. A força e a persistência que nos caracteriza está também presente neste documento.

Resumo

Os membros do género *Rickettsia* são bactérias intracelulares obrigatórias, cuja transmissão a humanos pode ocorrer através de vetores artrópodes. São responsáveis por infeções severas, das quais se destacam a febre maculosa das montanhas rochosas (*Rickettsia rickettsii*) e a febre escaro-nodular (*Rickettsia conorii*). Embora o papel das células endoteliais no desenvolvimento de doenças provocadas por *Rickettsia* esteja bem estudado, nenhuma função foi até agora atribuída a outros tipos celulares para o desenvolvimento da infeção. Contudo, evidências obtidas em modelos animais demonstraram a presença de bactérias intactas em vários tipos de células, tais como macrófagos, neutrófilos e hepatócitos, levantando diversas questões acerca da função desempenhada por estas células no desenvolvimento de rickettsioses. Curiosamente, evidências experimentais com mais de quarenta anos mostram que estirpes de *Rickettsia* do grupo tifo, com diferentes graus de patogenicidade em humanos, apresentam padrões de crescimento distintos em culturas celulares de macrófagos. No entanto, estes resultados permaneceram por explorar e os mecanismos moleculares que definem e distinguem patogenicidade entre espécies do género *Rickettsia* continuam por esclarecer.

Este trabalho mostra que duas espécies de *Rickettsia* do grupo das febres exantemáticas, com diferentes graus de patogenicidade em humanos, também apresentam fenótipos intracelulares distintos em células THP-1 diferenciadas em macrófagos. Especificamente, a bactéria patogénica (*R. conorii*) sobrevive e prolifera dentro destas células fagocitárias, enquanto que a bactéria não patogénica (*R. montanensis*) é rapidamente eliminada. Estes resultados reforçam uma possível correlação entre patogenicidade no género *Rickettsia* e a capacidade de sobreviver e proliferar em macrófagos, e sugerem o reposicionamento dos macrófagos como elementos centrais no desenvolvimento da infeção. Assim, o estudo detalhado dos mecanismos moleculares que regulam a interação de bactérias do género *Rickettsia* com macrófagos é fundamental para uma melhor compreensão da doença.

Usando *R. conorii* e *R. montanensis* como modelos de estudo, demonstrámos também que estas duas espécies de *Rickettsia* apresentam requisitos distintos no que respeita aos fatores de sinalização do hospedeiro recrutados durante o processo de invasão de células do tipo macrófago. O

processo de entrada da bactéria patogénica *R. conorii* revela uma maior dependência da atividade da cinase PAK1 e de trocadores de N+/H+ (NHE), características de mecanismos de endocitose do tipo macropinocitose. Os nossos resultados sugerem assim que a bactéria *R. conorii* usa um mecanismo alternativo de entrada do tipo macropinocitose, envolvendo o eixo de sinalização PAK-NHE-TK. A utilização de diferentes vias de sinalização entre espécies de *Rickettsia* poderá contribuir para explicar o tropismo observado em macrófagos.

Este trabalho demonstra ainda que a bactéria *R. conorii* é capaz de induzir alterações substanciais na célula hospedeira (demonstradas em perfis transcricionais e proteicos) muito cedo no processo de infeção, por forma a escapar aos mecanismos de defesa das células fagocitárias e estabelecer o seu nicho de infeção. Para além de interferir com a resposta inflamatória e a função do proteassoma, a bactéria *R. conorii* induz a expressão de diversos genes com funções antiapoptóticas e interfere com a resposta ao stress no retículo endoplasmático. Esta mobilização do hospedeiro poderá, por um lado, auxiliar a bactéria a escapar à capacidade de defesa e vigilância do sistema imunitário e, por outro, manter a viabilidade do hospedeiro durante a infeção. Os nossos resultados também sugerem que a bactéria *R. conorii* tira partido da elevada plasticidade metabólica dos macrófagos para induzir alterações substanciais em diversas vias metabólicas. Esta bactéria patógenica modula ainda a expressão de diversos elementos reguladores da expressão génica, sugerindo que a interferência com um número tão elevado de processos celulares decorra da sua capacidade de manipulação dos programas transcricionais na célula hospedeira.

Este trabalho contribui para o avanço do conhecimento acerca dos mecanismos moleculares responsáveis pela patogenicidade entre diferentes espécies de *Rickettsia*. Pela primeira vez, é revelada a capacidade da bactéria patogénica *R. conorii* de subverter os mecanismos de defesa de macrófagos e de estabelecer o seu nicho de infeção nestas células fagocitárias. Estes resultados contribuem para posicionar a infeção em macrófagos como um elemento chave para o desenvolvimento de patologia provocada por *Rickettsia*. Numa perspetiva mais geral, este trabalho abre portas ao desenvolvimento de novas linhas de investigação na área das interações patógeno-célula hospedeira, que poderão contribuir para a descoberta de terapias alternativas para o tratamento de infeções provocadas por bactérias intracelulares.

Palavras-chave: *Rickettsia*; Macrófago; Agentes patogénicos intracelulares; Interações hospedeiro-agente patogénico;

Abstract

Members of the genus *Rickettsia* are obligate intracellular bacteria that are transmitted to humans by arthropod vectors, causing severe human infections like epidemic typhus (*Rickettsia prowazekii*), Rocky Mountain spotted fever (*Rickettsia rickettsii*), and Mediterranean spotted fever (*Rickettsia conorii*). Although the role of endothelial cells during rickettsioses is well studied and established, no functional role in promoting the development of rickettsial diseases has been attributed to cells other than the endothelium. Using several animal models, different research groups have demonstrated the presence of intact bacteria within macrophages and neutrophils, raising several questions about the role of phagocytic cells in rickettsial diseases. Moreover, over 40 years ago, it was demonstrated that typhus group *Rickettsia* strains with different levels of virulence possessed distinct abilities to proliferate in macrophage cell cultures. However, these findings remained unexplored, and the attributes that distinguish pathogenic and non-pathogenic rickettsial species continued elusive.

In this work, we demonstrate that two members of spotted fever group *Rickettsia* with different pathogenicity attributes to humans have completely distinct intracellular fates within THP-1 macrophages. More specifically, the pathogenic *R. conorii* can survive and proliferate in these phagocytic cells, whereas the non-pathogenic *R. montanensis* is rapidly destroyed. Therefore, these findings have raised several provocative questions including the possibility that pathogenicity in rickettsial species may be correlated with the ability to proliferate in macrophages, thereby positioning macrophages as central players in the development of rickettsial diseases. Thus, the understanding of the molecular determinants involved in the rickettsiae-macrophage interface is critical to a better understanding of the disease.

Interestingly, we provide evidence that the two members of SFG *Rickettsia* species (*R. conorii* and *R. montanensis*) differentially target different host signaling components during the entry process. Remarkably, we have identified P21-activated kinase (PAK1) as a core host factor for *R. conorii* entry into macrophage-like cells, together with an unrecognized sensitivity to amiloride compounds such as DMA, EIPA, and zoniporide which, combined, are key hallmarks of macropinocytosis. Collectively, our findings suggest that *R. conorii* uses a novel PAK-NHE-TK-dependent macropinocytosis-like

mechanism to invade macrophage-like cells, which may contribute to rickettsiae tropism in macrophages.

Moreover, the work herein presented also demonstrated that very early in infection, *R. conorii* can substantially reprogram multiple signaling pathways to escape host immune defenses and establish its replicative niche in macrophage-like cells (in sharp contrast with *R. montanensis*). In addition to the modulation of host inflammatory responses and proteasome function, which may help the bacteria to escape immune defenses and surveillance, the pathogenic *R. conorii* was also able to specifically modulate pro-survival and ER stress response pathways to maintain the integrity of its replicative niche. Furthermore, our results also suggest that *R. conorii* takes advantage of the high metabolic plasticity of macrophages to substantially reprogram several host cell metabolic pathways, rendering the intracellular environment apparently more favorable for *Rickettsia* replication. The capacity of *R. conorii* to interfere with this multiplicity of host functions, likely stems from the observed modulation of the expression of several gene expression modulators such as non-coding RNAs and transcription factors, which may substantially affect transcriptional programs during infection in macrophage-like cells.

Overall, these findings provide the research community with novel insights on the molecular attributes that help distinguishing pathogenicity requirements between rickettsial species. With this work, we revealed the sophisticated molecular strategies employed by the pathogenic *R. conorii* to modulate host cellular functions to establish its replicative niche in macrophages, contributing to a better understanding of the disease. We firmly believe that this work not only helps to position infection of macrophages as a central node in the development of rickettsial diseases but also opens several avenues of research in host-pathogen interactions that may contribute to the development of alternative and more efficacious therapies for intracellular bacterial infections.

Keywords: Intracellular pathogens; Rickettsia; Macrophages; Host-pathogen interactions;

Table of contents

List of abbreviations

AG	Ancestral Group
ATBF	African Tick Bite Fever
BMDCs	Bone-Marrow-derived DCs
CNS	Central Nervous System
dpi	Days Post-Infection
DC	Dendritic Cells
ELISA	Enzyme-linked Immunosorbent assay
ER	Endoplasmic Reticulum
EU	European Union
FAO	Fatty-Acid Oxidation
FAS	Fatty-Acid Synthesis
hpi	Hours Post-Infection
IDA	Information Dependent Acquisition
IFA	Indirect Immunofluorescence assay
IHC	Immunohistochemistry
IPA	Ingenuity Pathway Analysis
lncRNAs	Long non-coding RNAs
LPS	Lipopolysaccharide
MHC	Major Histocompatibility Complex
MIC	Mean Inhibitory Concentration
MIF	IFA microimmunofluorescence
miRNAs	Micro-RNAs
MOI	Multiplicity of Infection
MSF	Mediterranean Spotted Fever
ncRNAs	Non-Coding RNAs
NO	Nitric Oxid
OGs	Orthologous Groups
ORFs	Open Reading Frames
OXPHOS	Oxidative Phosphorylation
PAMPs	Pathogen-Associated Molecular Patterns
PFA	Paraformaldehyde
PMA	Phorbol 12-Myristate 13-Acetate
PPP	Pentose Phosphate Pathway
PRRs	Pattern Recognition Receptors
RET	Reverse Electron Transport
RMSF	Rocky Mountain Spotted Fever

RNAseq	RNA sequencing
ROS	Reactive Oxygen Species
rpm	Rotation per Minute
scaRNAs	Small Cajal-Body RNAs
SFG	Spotted Fever Group
snoRNAs	Small Nucleolar RNAs
STRING	Search Tool for Retrieval of Interacting Genes/Proteins
SWATH-MS	Sequential Window Acquisition of all Theoretical Mass Spectra
TA	Toxin-antitoxin
TCA	Tricarboxylic Acid
TEM	Transmission Electron Microscopy
TG	Typhus Group
TRG	Transitional Group
UPR	Unfolded Protein Response
U-RNA	Small Nuclear RNA
WB	Western Blot
WHO	World Health Organization
XIC	Extracted-Ion Chromatography
5S rRNA	5S Ribosomal RNA
7SL RNA	Signal Recognition Particle RNA

Chapter I

Introduction

I.1 | *Rickettsiae* and rickettsioses

I.1.1 | Bacteriology

Rickettsia are obligate intracellular, small (0.3-0.5 x 0.8-2.0 µm) bacilli with a gram-negative cell wall that has a typical bilayer with inner and outer membranes separated by a periplasmic layer (Walker, 2007). *Rickettsia* reside free in the cytosol (and occasionally in the nucleus) where they replicate by binary fission (Walker, 2007). They stain poorly with conventional Gram techniques but retain basic fuchsin when stained using the Gimenez method (Gimenez, 1964).

I.1.2 | Phylogeny and taxonomy

Bacterial species belonging to the order *Rickettsiales* are an early-branching lineage of the *Alphaproteobacteria*, forming a sister clade with all known alphaproteobacterial species (Williams et al., 2007). *Rickettsiales* lineages (excluding "*Candidatus Pelagibacter*" spp.) are obligate intracellular species that are dependent on one or more eukaryotic hosts (Gillespie et al., 2012b). Before the implementation of DNA sequence-based systematics, species within the order *Rickettsiales* were primarily distinguished based on five characteristics: (i) energy production and biosynthesis; (ii) human disease and geographic distribution; (iii) natural vertebrate and invertebrate hosts and other biological reservoirs; (iv) experimental infections and serological reactions and cross-reactions; and (v) strain cultivation, stability, and maintenance (Gillespie et al., 2012b). By convention, obligate or facultative intracellular bacterial species have long been classified into nine genera within three families in the order *Rickettsiales*: (i) family *Rickettsiaceae* (genera *Rickettsia*, *Coxiella*, *Rochalima*, and *Ehrlichia*), (ii) family *Anaplasmataceae* (genus *Anaplasma*), and (iii) family *Bartonellaceae* (genera *Bartonella*, *Haemobartonella*, *Eperythrozoon*, and *Grahamella*) (Gillespie et al., 2012b). However, DNA sequence-based phylogenetic methodologies have resulted in an extensive re-organization of the *Rickettsiales* classification, which significantly differs from this traditional classification scheme (Gillespie et al., 2012b). After reorganization, the order *Rickettsiales* consists now of the family *Rickettsiaceae* and the family *Anaplasmataceae* (Gillespie et al., 2012b) **(Figure I.1)**. The family *Rickettsiaceae* are short rods or coccobacilli, while the family *Anaplasmataceae* are small pleomorphic cocci. The family

Rickettsiaceae contains now the genus *Rickettsia* and the genus *Orientia*. Interestingly, of the four genera originally classified in the *Rickettsiaceae* family, only the genus *Rickettsia* has remained (Gillespie et al., 2012b).

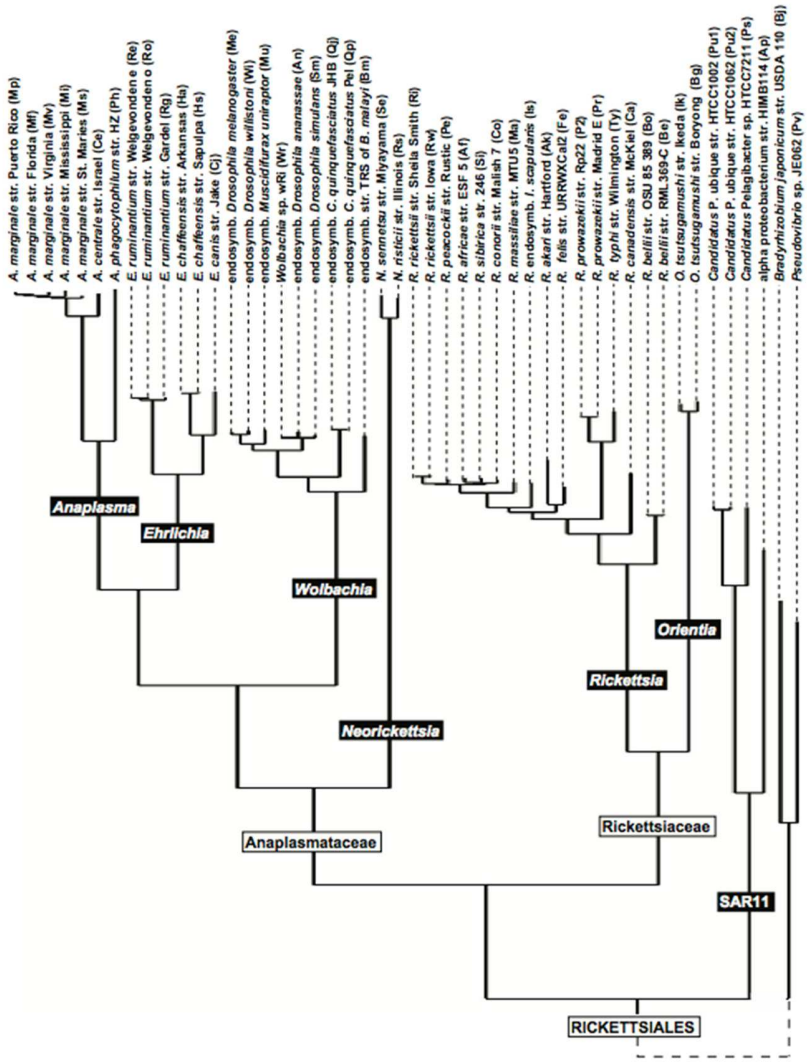

Figure I.1 | Whole-genome-based phylogeny estimation for 46 *Rickettsiales* taxa. Adapted from (Gillespie et al., 2012b).

As for other prokaryotes, members of the genus *Rickettsia* have been traditionally classified based on the comparison of morphological, ecological, epidemiological and clinical characteristics, which has resulted in the separation into spotted fever group (SFG) and typhus group (TG) rickettsiae (Fournier and Raoult, 2009). However, phylogenetic classification based on these criteria was highly unreliable, and some *Rickettsia* species did not fit well in this grouping.

After considerable sequencing efforts of several genomes of rickettsial species, phylogeny in the genus *Rickettsia* has been addressed by sequence analysis of different genes, varying from housekeeping genes to genes that are under evolutionary pressure, such as those that encode variable immunodominant outer-membrane proteins (Fournier et al., 2003; Fournier and Raoult, 2009; Merhej and Raoult, 2011). Thus, the use of genetic criteria supported the revision of the classification within the genus *Rickettsia*. In 2008, *Gillespie et al.*, established orthologous groups (OGs) of open reading frames (ORFs) that distinguished the core rickettsial genes and other group of specific genes, which have resulted in the reclassification of the genus *Rickettsia* into AG (ancestral group), TG (typhus group), TRG (transitional group), and SFG (spotted fever group) rickettsiae (Gillespie et al., 2008). According to this revision, TG is represented by the highly pathogenic and insect-associated *Rickettsia prowazekii* and *Rickettsia typhii*, which are the etiological agents of the epidemic and murine typhus, respectively (Gillespie et al., 2008). SFG *Rickettsia* comprises rickettsial tick-borne species, such as *Rickettsia rickettsii* (the causative agent of Rocky Mountain spotted fever), *Rickettsia conorii* (the agent of Mediterranean spotted fever), *Rickettsia helvetica*, which has unconfirmed human pathogenicity, among others (Gillespie et al., 2008). The AG consists of *Rickettsia belli* and *Rickettsia canadensis*, both of which are tick-borne with unrecognized human pathogenicity; while the TRG consists of mite-borne *Rickettsia akari* (the causative agent of rickettsialpox), tick-borne *Rickettsia australis* (the agent of Queensland tick typhus), and flea-borne *Rickettsia felis* (the causative agent of flea-borne spotted fever) (Gillespie et al., 2008). Thus, the TRG *Rickettsia* emerges as a distinct lineage that shares immediate ancestry with the members of the SFG rickettsiae (Gillespie et al., 2007).

However, even phylogenies based on molecular markers have resulted in conflicting tree topologies due to the incongruity between phylogenetic reconstructions using different portions of the genome. In 2016, *Murray et al.*, have reconstructed the *Rickettsia* phylogeny based on whole-genome sequence data **(Figure I.2)** (Murray et al., 2016). Using such approach, several phylogenetic changes were proposed, as the example of *R. helvetica*, which does not fit in the SFG *Rickettsia* (Murray et al., 2016). Thus, regardless all efforts, taxonomic classification of the genus

Rickettsia is still not consensual and alternative phylogenetic classifications have constantly been proposed throughout time (Gillespie et al., 2008; Murray et al., 2016; Weinert et al., 2009).

Currently, the genus *Rickettsia* comprises 32 species (http://www.bacterio.net), and more species are being added to the genus every year due to the advent of molecular techniques and cost reductions associated to new molecular tools (Abdad et al., 2018). Interestingly, DNA sequence-based phylogenetic analyses have allowed the establishment of a link between *Rickettsiales* and the eubacterial ancestor of the mitochondria (Andersson et al., 1998).

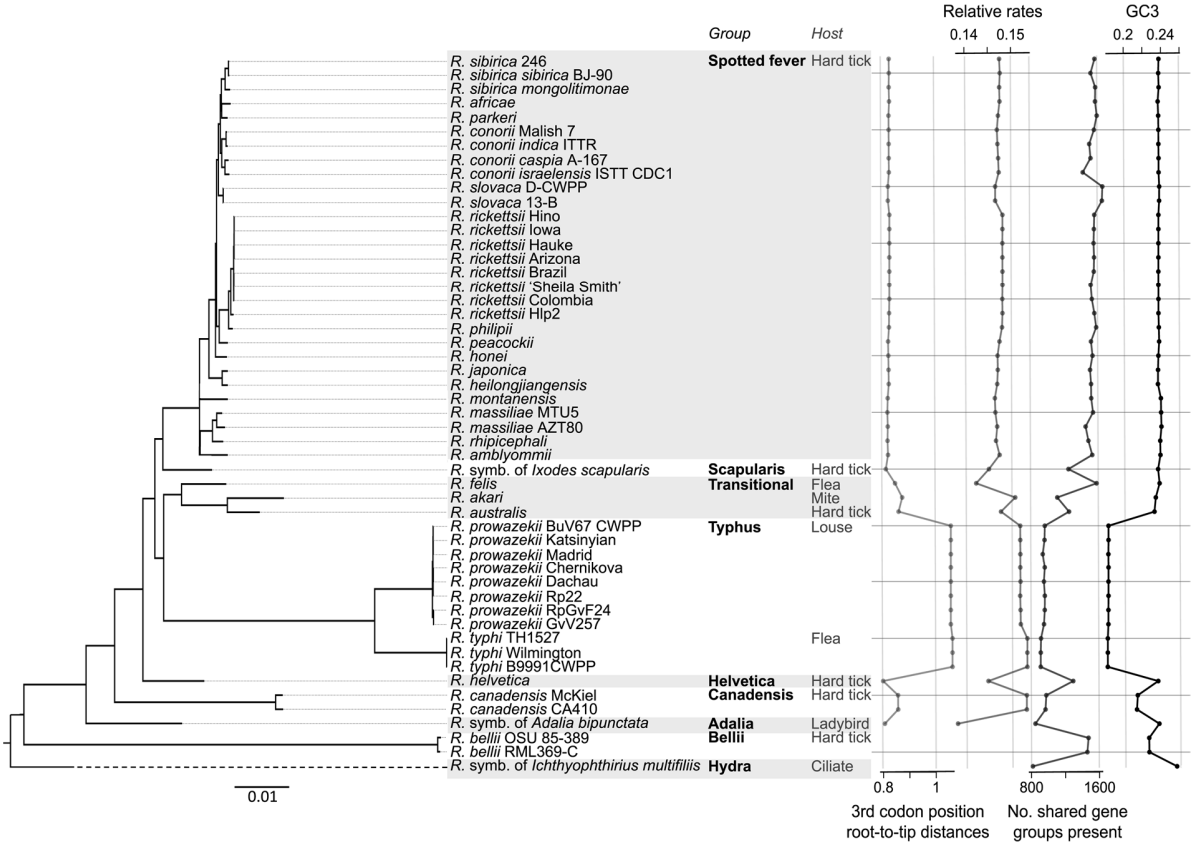

Figure I.2 | Revision of *Rickettsia* phylogeny using whole-genome data. Adapted from (Murray et al., 2016).

Although the placement of the eubacterial ancestor within the phylogenic tree is still controversial (Williams et al., 2007), complex interactions between modern rickettsiae with their eukaryotic host are envisioned to occur, such as the bacterial import of proteins (as well as other molecules) that are targeted for the mitochondria as well as the secretion of several bacterial effectors into the host cell cytoplasm and organelles (Emelyanov, 2001, 2009).

I.1.3 | Genomics

Analysis of complete genome sequences of bacterial pathogens has revealed that those are very dynamic, with three main forces shaping genome evolution: gene gain, gene loss and gene change (that is, any changes that affect the sequences or order of the existing gene) (Pallen and Wren, 2007). Although most prokaryotic genomes remain about the same size throughout evolution (acquisition of new genes over time by lateral gene transfer or gene gain is balanced with gene loss), obligate intracellular bacteria such as *Chlamydia*, *Ehrlichia*, *Mycoplasma*, *Spirochaetes*, and *Rickettsia* have much more reduced genome sizes compared to their free-living relatives (McCutcheon and Moran, 2011; Sakharkar et al., 2004; Weinert and Welch, 2017; Wixon, 2001). The transition from a free-living existence to a close relationship with eukaryotic cells was accompanied by the loss of many genes (justified by the presence of orthologous genes in the host cells that compensate the function of those genes that have been discarded), resulting in a reductive genome evolution (Blanc et al., 2007; Wixon, 2001).

Interestingly, *Rickettsia* genomes present substantial inter-species variations in size (1.1 Mb for the TG, 1.2-1.4 Mb for the SFG, and 1.5 Mb for AG) and gene content (about 900-1500 genes) providing an excellent model to investigate the process of reductive genome evolution (Blanc et al., 2007; Ogata et al., 2001; Renesto et al., 2005). Genes involved in biosynthetic pathways are a particular example of genes that were lost throughout evolution, but that can be compensated by the ability of bacteria to import proteins or metabolites from the host cell (Weinert and Welch, 2017; Wixon, 2001). The replacement of many biosynthetic pathways present in free-living bacteria for transport systems in *Rickettsia* has resulted in a complete dependence of the bacteria in the host cell to survive and proliferate (Weinert and Welch, 2017; Wixon, 2001).

Paradoxically, reductive genome evolution in *Rickettsia* and other bacteria has been associated with increased pathogenicity (Weinert and Welch, 2017). Indeed, it is known for several years that pathogenic bacteria often have smaller genomes and fewer genes than their nearest non-pathogenic or less-pathogenic relatives (Diop et al., 2017; Weinert and Welch, 2017). This has been noted for several pathogens, from a diverse range of bacterial phyla, including *Shigella flexneri*, *Yersinia pestis*, *Salmonella typhi*, *Mycobacterium tuberculosis*, and *Rickettsia*. The loss of

genes associated with transcriptional regulators has been reported, whereas high preservation of toxin-antitoxin (TA) modules, and recombination and DNA repair proteins have been observed (Diop et al., 2017; Weinert and Welch, 2017). However, the complete understanding of the association between reductive genome evolution and pathogenicity is still an ongoing research topic, and it may help explain why and how bacteria become pathogens (Diop et al., 2017; Weinert and Welch, 2017).

It has also been noted that although horizontal gene transfer is a common driving source of evolution between prokaryotic organisms, either with bacteriophages, transposons, or other bacteria, rickettsiae minimize their exposure to horizontally transferred DNA likely due to their obligate intracellular lifestyle, which results in few recent gene transfers and genome rearrangements (El Karkouri et al., 2016; Merhej and Raoult, 2011). However, the few evidence for lateral gene transfer in *Rickettsia* has been provided by the identification of large fractions of mobile genetic elements, including plasmids (El Karkouri et al., 2016; Gillespie et al., 2012a). To our knowledge, the presence of plasmids has been identified in 11 rickettsial species, including *R. felis*, *R. australis*, *R. helvetica*, and *Rickettsia monacensis*, which suggests that conjugation may play a role in the evolution of rickettsial genomes (El Karkouri et al., 2016; Gillespie et al., 2007).

Overall, reductive genome evolution in *Rickettsia* associated with the relatively low rate of lateral gene transfer has resulted in highly conserved genomes exhibiting similar gene synteny, and content, which has been correlated with a gain of pathogenicity for rickettsial species (Diop et al., 2017; Mendonca et al., 2011).

I.1.4 | Epidemiology

Rickettsioses represent some of the oldest recognized pathologies transmissible from animals to humans. In 1906, Howard T. Ricketts (an American pathologist) demonstrated that *R. rickettsii* was the etiological agent of Rocky Mountain spotted fever and that it could be transmitted to healthy animals by the bite of a tick (Gross and Schafer, 2011; Weiss and Strauss, 1991). However, until advances in electron microscopy field, it was not clear what kind of organism the pathogen was, whether bacteria, virus or something in between (Gross and Schafer, 2011). Three

years later, Ricketts and his assistant studied a major outbreak of epidemic typhus in Mexico City and they found that it was transmitted by the body louse (*Pediculus humanus*) and they were able to locate the disease-causing organism both in the blood of the victims and in the bodies of the lice (Gross and Schafer, 2011). Tragically, while isolating the organism causing the disease (*R. prowazekii*), he got himself infected and died shortly after (Weiss and Strauss, 1991). Given his contributions to the field, both the taxonomic family (*Rickettsiaceae*) and the order (*Rickettsiales*) were named after him (Gross and Schafer, 2011).

Rickettsial organisms are endemic worldwide, existing in all continents except Antarctica, and they can be found in diverse habitats associated with a variety of arthropod vectors including fleas, lice, ticks, and mites **(Figure I.3)** (Abdad et al., 2018). The geographic distribution of these zoonoses is determined by the distribution of the infected arthropod, which for most of the rickettsial species is the reservoir host (Parola et al., 2013; Richards, 2012).

I.1.4.1 | Typhus group rickettsioses

The clinical disease described as typhus fever includes epidemic typhus (*R. prowazekii*, which is spread by body lice), murine typhus (*R. typhi*, which is spread by fleas), and scrub typhus (*Orientia tsutsugamushi* spread by chiggers) (the latter belonging to the genus *Orientia*). Although both epidemic and murine typhus have many clinical similarities, infections with *R. prowazekii* are generally considered more severe with high mortality rates (around 30% before antibiotic era), whereas fatalities associated with *R. typhi* are rarely reported. Interestingly, typhus group *Rickettsia* are ubiquitously found in various geographic areas of the world **(Figure I.3)** (Abdad et al., 2018).

Epidemic typhus is so named because the disease often causes epidemics when conditions favor human-to-human transmission of the body louse (*P. humanus corporis*), as is the case of war, extreme cold, and poverty (Bechah et al., 2008a). Historically, epidemic typhus has killed millions of people, particularly during or immediately after World Wars I and II, potentially affecting the outcome of the war (Raoult et al., 2004). The epidemic form of the disease is now rarely reported in developed countries, and when it occurs is usually associated with settings of close crowding and poor sanitary conditions (e.g., prisons, refugee camps, or among homeless

people), which are situations where the body louse infestations may occur (Bechah et al., 2008a). Nevertheless, epidemic typhus continues to have an endemic focus in developing countries with possible contexts of socio-political instability, famine, civil wars or natural disasters, with situations, for example, still being reported in the Peruvian Andes and western Rwanda (Abdad et al., 2018; Fang et al., 2017). In 1997, a massive outbreak estimated to have affected over 100 000 persons was reported in Burundi (Raoult et al., 1998). In contemporary settings, *R. prowazekii* human infections are only sporadically reported in the United States being mostly associated with contact with flying squirrel *Glaucomuys volans* (Bechah et al., 2008a; Duma et al., 1981).

Murine typhus, caused by *R. typhii*, is spread to people through contact with infected fleas (*Xenopsylla cheopis*) (Civen and Ngo, 2008). Murine typhus occurs in tropical and subtropical climates around the world where rats and their fleas live (Civen and Ngo, 2008). Cat fleas found on domestic cats and opossums have been associated with cases of murine typhus in the United States, with most cases being reported in people from California, Hawaii, and Texas (Civen and Ngo, 2008). Although it is not a contemporary public health concern in the US, murine typhus is still a risk in many parts of the world, since its principal mammalian reservoir (*Rattus spp.)* has a worldwide distribution, especially in Africa and Indonesia (McQuiston and Paddock, 2012). Interestingly, exposure to or infection with *R. typhi* is thought to be more common than currently reported since seropositivity to the bacteria ranges from 3 to 9% in Spain, 32% in South Korea and 35% in Indonesia (Bolanos-Rivero et al., 2011; Jang et al., 2005; Nogueras et al., 2006; Richards et al., 1997).

I.1.4.2 | Spotted Fever Group Rickettsioses

SFG *Rickettsia* display a widespread distribution including the Americas, Europe, Africa, Asia and Australia **(Figure I.3)** (Abdad et al., 2018).

Rocky Mountain spotted fever (RMSF) is caused by *R. rickettsii,* and it is the most commonly diagnosed spotted fever rickettsial infection in the United States (Dantas-Torres, 2007). *Dermacentor variabilis* (the American dog tick is the primary vector in the eastern half of the country), *Dermacentor andersoni* (the Rocky Mountain wood tick is responsible for most of the

infections in the western part of the country), *Rhipicephalus sanguineus* (primary tick vector in focal geographic areas such as eastern Arizona), and *Amblyomma americanum* (lone star tick is responsible for a reported case in North Carolina) have been identified as primary tick vectors of *R. rickettsii* (Dantas-Torres, 2007; Demma et al., 2006; Demma et al., 2005). RMSF has also been reported in several other countries in North, Central and South America, including Brazil where the infection is transmitted by Cayenne tick (*Amblyomma cajennense*) and the disease is known as Brazilian spotted fever (Parola et al., 2005). In Mexico, RMSF has been reported in several states with hyper-endemic foci repeatedly described in communities, mainly due to unchecked populations of stray and free-ranging dogs, with associated historical and contemporary case fatality rates ranging 27-80% (Alvarez-Hernandez et al., 2017).

One of the most widely distributed SFG *Rickettsia* is *R. conorii* (the causative agent of MSF), which has been found throughout southern Europe, northern Africa, the Middle East, and central Asia and it is transmitted by *Rh. sanguineus* (Abdad et al., 2018; Rovery and Raoult, 2008). Although *R. conorii* is endemic in southern Europe, it is also sporadically found in central and northern Europe (ECDC, 2013). Most of the MSF cases in Europe are reported during the summer mainly due to increased temperatures and lower rainfall, which seems to be related with a warming-mediated increase in the aggressiveness of *Rh. sanguineus* ticks to bite humans (Parola et al., 2008; Tomassone et al., 2018). In addition to *R. conorii*, which is the most prevalent rickettsial causing-disease in Europe, other *Rickettsia* species have also been widely documented in this continent (Brouqui et al., 2007; Rovery et al., 2008). This is the case of *Rickettsia massiliae* (transmitted by *Rh. sanguineus*); *R. helvetica* and *R. monacensis* (transmitted by *Ixodes ricinus*); *Rickettsia slovaca* and *Rickettsia raoultii* (transmitted by *Dermacentor marginatus* and *Dermacentor reticulatus*), together with other non-tick transmitted *Rickettsia* species such as *R. felis*, *R. akari*, the louse-borne *R. prowazeki* and the flea-borne *R. typhi* (Brouqui et al., 2007; Rovery et al., 2008) (ECDC, 2013). *Rickettsia* species with uncertain pathogenicity to humans have also been found in Europe, which may suggest that rickettsial infections are probably not well recognized and there is a need to assess their impact at the European Union (EU) level (Tomassone et al., 2018).

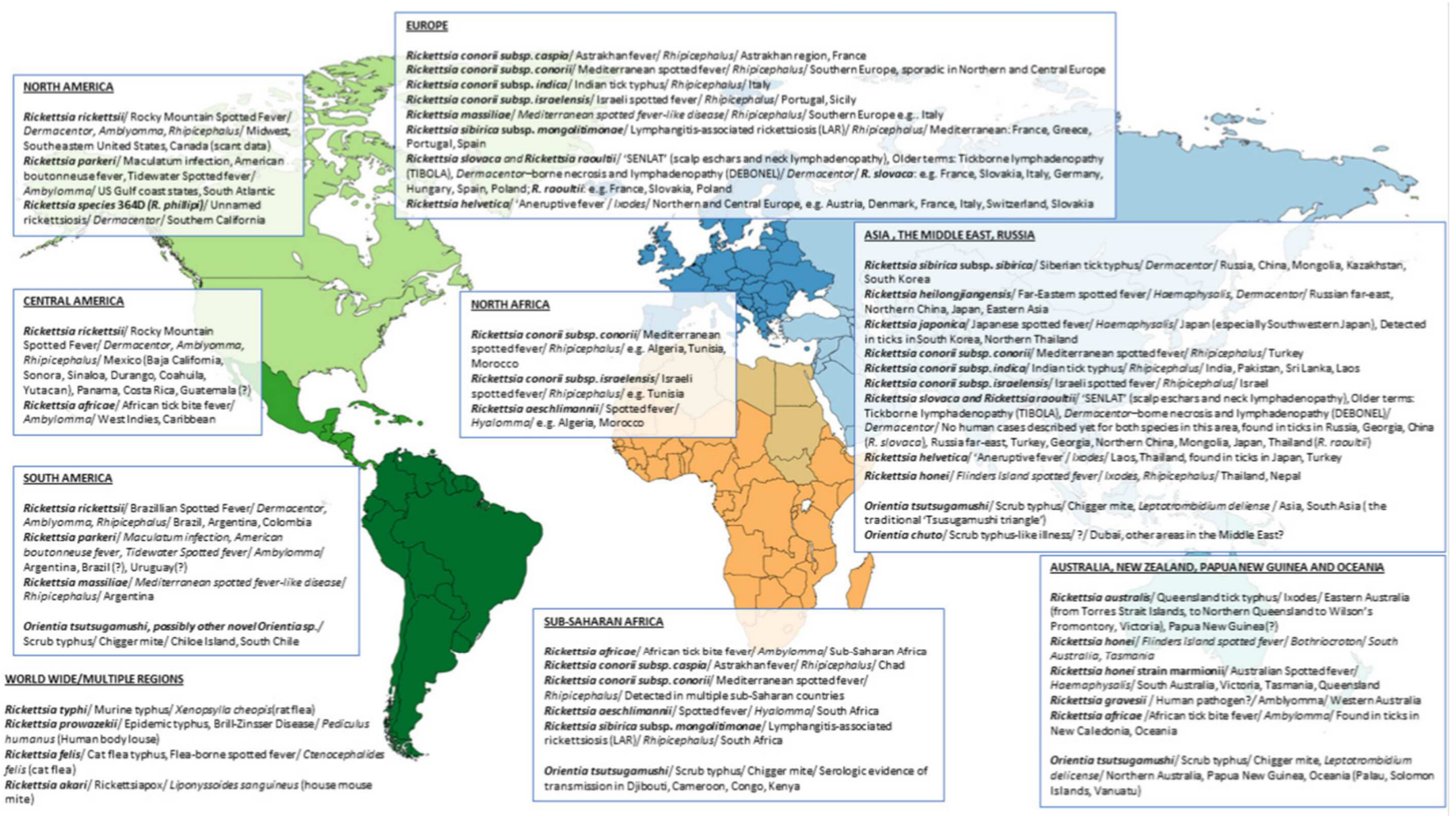

Figure I.3 | Geographical distribution of rickettsial species (Abdad et al., 2018).

New SFG rickettsial species have recently been diagnosed and demonstrated to be associated with human disease in EU, as is the case of *R. slovaca* and *R. raoulti*, both cause tick-borne lymphadenopathy and *Dermacentor*-borne necrosis lymphadenopathy (TIBOLA/DEBONEL), *R. sibirica mongolotimonae*, which causes a mild rickettsioses called Lymphangitis-Associated Rickettsioses, and *R. monanencis*, which is the cause of a MSF-like syndrome (Chmielewski et al., 2011; Fournier et al., 2005; Madeddu et al., 2012; Oteo and Portillo, 2012; Parola et al., 2009).

African tick bite fever (ATBF) is another example of a spotted fever caused by a member of SFG *Rickettsia*, *R. africae* (Tsai et al., 2008). The disease occurs in sub-Saharan Africa, the West Indies and Oceania, and it is relatively common among travelers to sub-Saharan Africa (Eldin et al., 2011; Jensenius et al., 2003; Jensenius et al., 1999; Tsai et al., 2008).

I.1.4.3 | Transitional Group Rickettsioses

Members of TRG *Rickettsia* are also responsible for rickettsial diseases with distinctive clinical onsets. *Rickettsia australis*, which is transmitted by *Ixodes* spp ticks, are responsible for Queensland tick typhus and it is increasingly recognized as a cause of community-acquired acute febrile illness in eastern Australia (Stewart et al., 2017). Rickettsialpox (which is caused by *R. akari* and transmitted by the mite (*Liponyssoides sanguineus*)) was originally described after an outbreak in 1946 in a New York City apartment complex (Paddock et al., 2003). Humans get rickettsialpox when receiving a bite from an infected mite, and those dwelling in urban areas with rodent problems have a higher risk of contracting the disease, being one of the few spotted fever rickettsioses with a cosmopolitan distribution (Radulovic et al., 1996). Cases of rickettsialpox have been reported in several countries around the world, including Ukraine, Croatia, Turkey, South Korea, and Mexico (Ozturk et al., 2003; Radulovic et al., 1996; Zavala-Castro et al., 2009).

Rickettsia felis, the causative agent of flea-borne spotted fever, was first described in the US but is now identified throughout the world due to the equally widespread occurrence of cat fleas (*Ctenocephalides felis* is the primary vector and reservoir of this rickettsial species) (Brown and

Macaluso, 2016). *Rickettsia felis* is an important cause of febrile illness in Africa (Mourembou et al., 2015).

I.1.4.4 | Contemporary concerns in rickettsioses

The re-emerging nature of tick-borne pathogens mainly as a result of climate and behavioral changes (increasing traveling and recreational activities associated with nature), expanding cohorts of immunocompromised individuals, and ageing of societies is expected to be a burden factor for rickettsioses in the public health context in near future (ECDC, 2013; Randolph, 2010; Tomassone et al., 2018). In respect to global warming, the increase in temperatures is expected to impact the activity and aggressiveness of *Rh. sanguineus*, increasing human attacks and the possibility of transmission of severe rickettsioses (Parola et al., 2008). Moreover, the fact that birds (possible dispersers of *Rickettsia*) are able to respond to environmental changes adjusting their timing of migration according to climate is also expected to affect transmission patterns of tick-borne pathogens (Elfving et al., 2010; Lommano et al., 2014). Social changes regarding human behavior including the increase of outdoor activities or international trade and travel are also expected to impact vector dynamics and alter pathogen adaptation and evolution (ECDC, 2013; Tomassone et al., 2018). Thus, in order to tackle emerging threats, surveillance and data collection/notification should be promptly strengthened. At this moment, the last technical report on tick-borne rickettsioses from the “European Centre for Disease and Prevention and Control” dates from 2013 and it includes data up to 2010 (ECDC, 2013). Therefore, major efforts and inter-disciplinary collaborations for epidemiological studies worldwide should be promptly achieved (Tomassone et al., 2018).

I.1.5 | Life cycle

Bacteria within the order *Rickettsiales* are acquired, maintained, and transmitted to humans, non-human mammals, and birds by hematophagous arthropod vectors (Ceraul, 2012). Arthropod vectors can act as reservoirs and vectors for many intracellular endosymbiotic bacteria being estimated that around 24% of terrestrial arthropod species are infected with *Rickettsia*

endosymbionts (Weinert et al., 2015). Most SFG *Rickettsia* species are transmitted by the family of hard ticks known as the *Ixodidae* (Ceraul, 2012), but the presence of rickettsiae in soft ticks (Argasidae) has also been reported (Tomassone et al., 2018). However, the role of soft ticks in transmitting rickettsiae to vertebrates and possible implications in human health is still a matter of debate (Tomassone et al., 2018). Associations of *rickettsiae* with tick genera can largely differ between rickettsial species. Some *rickettsiae* seem to be strictly linked to one tick vector, as is the case of *R. conorii* and the vector *Rh. sanguineus*, whereas others like *R. rickettsii* are associated with a broad spectrum of tick species belonging to different genera (Parola et al., 2013; Raoult and Roux, 1997). *Rickettsia* species are maintained within tick populations by vertical (transovarial from female to offspring or transstadial, in which the bacteria is maintained throughout different stages of the tick life cycle (from egg to larva, to nymph, to adult) and/or horizontal (acquired during feeding) transmission **(Figure I.4)** (Burgdorfer and Brinton, 1975; Eremeeva and Dasch, 2015; Hayes et al., 1980; Socolovschi et al., 2009a; Socolovschi et al., 2009b).

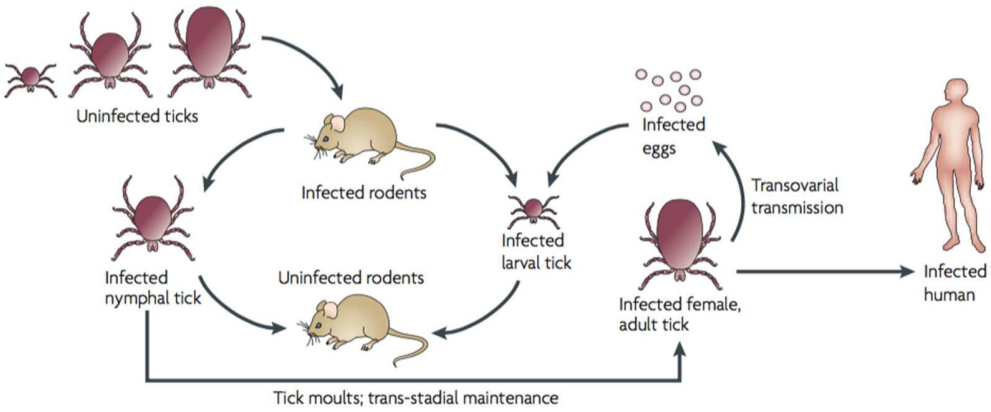

Figure 4 | The life cycle of tick-borne rickettsiae. Spotted-fever-group rickettsiae are maintained in nature by transovarial and transstadial transmission in ticks and horizontal transmission to uninfected ticks that feed on rickettsemic rodents and other animals. Adapted from (Walker and Ismail, 2008).

To establish an endosymbiotic relationship with their hosts, rickettsiae struggles to survive by adopting a proactive and reactive stance, having developed sophisticated strategies throughout evolution to evade tick immune defenses (Ceraul, 2012; Socolovschi et al., 2009b). The

pathological effect of different rickettsiae on ticks largely differs between rickettsial species, with deleterious effects on invertebrate hosts being more evident for pathogenic species (e.g., *R. rickettsii* and *R. conorii*) compared to less or non-pathogenic species (e.g., *R. montanensis*, *R. belli* and *R. rhipicephalli*) (Harris et al., 2017; Niebylski et al., 1999; Socolovschi et al., 2009b; Tomassone et al., 2018). The endosymbiotic interaction between rickettsial species within ticks and with other pathogens within ticks, as well as among different pathogens has been emerging as a hotspot of scientific research in this field (Tomassone et al., 2018). Unlike the pathogenic *R. rickettsii,* which is lethal for ticks, infection with *R. peacockii* has not been reported to affect tick viability but instead might be even beneficial for ticks by preventing the adverse effects of secondary infections with pathogenic rickettsiae (Niebylski et al., 1999; Walker and Ismail, 2008). Thus, infection of a tick with one SFG rickettsial species seems to interfere with a secondary rickettsial infection, and this process of rickettsial "interference" might affect the frequency and distribution of different pathogenic rickettsiae (Macaluso et al., 2002). In fact, the low incidence of *R. rickettsii* (less than 1% of wood ticks) in the eastern part of the Bitterroot Valley (Montana, USA) is attributed to the high infection rate (70%) of female wood ticks (*D. andersoni*) with the non-virulent rickettsiae*, R. peacockii* (Mansueto et al., 2012; Niebylski et al., 1997; Walker and Ismail, 2008). On the other hand, the simultaneous occurrence of multiple pathogens within ticks has also been reported suggesting that coinfection might be frequent for both vectors and wild reservoir hosts, and their concurrent transmission to vertebrate hosts can have severe health consequences for patients (Lommano et al., 2012). Thus, manipulation of tick microbiome has been suggested as a fascinating strategy to decrease tick vectorial competence in order to control the maintenance and transmission of rickettsial pathogens (Tomassone et al., 2018).

Humans are considered accidental hosts for *Rickettsia*, with the exception of *R. prowazekii*, for which they are reservoirs (Olano, 2005). The transmission of SFG *Rickettsia* occurs when an infected tick encounters the skin of a human host, inserts its mouthparts (which cut the epidermis and dermis), creates a small pool of blood into which the hypostome is inserted, and through which blood is ingested, and saliva containing anticoagulants, anesthetic, host defense-inhibiting molecules, and rickettsiae is injected (Brossard and Wikel, 2004; Fang et al., 2017). The blood

meal for ticks and mites takes place over a period of 3 to 14 days (Ceraul, 2012). The components of tick saliva that are injected during the blood meal play important functions by modulating the host immune system to facilitate rickettsial infections. It has been reported that tick saliva components are able to inhibit neutrophil function, interfere with complement system, natural killer (NK) cell and macrophage activity, and decrease cytokines (IL-12 and IFN-γ) production, as well as T-cell proliferation (Brossard and Wikel, 2004; Ferreira and Silva, 1999; Gillespie et al., 2001; Kotsyfakis et al., 2006; Montgomery et al., 2004; Valenzuela, 2004). The suppression of dendritic cells (DC) maturation and subsequently influence in acquired immunity against tick-transmitted rickettsioses have also been suggested as a crucial role for tick saliva components in increasing host susceptibility to severe and fatal rickettsial diseases (Cavassani et al., 2005; Sa-Nunes et al., 2007). Therefore, immunity to tick salivary components has already been raised as a promising strategy to act as an adjuvant with specific rickettsial antigens in the design of an effective anti-rickettsial vaccine (Walker and Ismail, 2008).

On the other hand, *R. prowazekii* and *R. typhi* are transmitted to the human host throughout the feces of human body lice and fleas, respectively, which are deposited on the skin during the blood meal (Bechah et al., 2008a; Civen and Ngo, 2008). The insect feces containing rickettsiae can then enter the skin throughout the site of the wound bite, or by rubbing onto mucous membranes, such as conjunctivae (Fang et al., 2017).

I.1.6 | *Rickettsia*-endothelial cell interactions

Upon transmission, the success of an obligate intracellular bacteria is governed by the ability to adhere, invade and adapt to the intracellular environment of a target cell (Olano, 2005). In rickettsial pathogenesis, endothelial cells are considered the main target cells of rickettsiae and the mechanisms by which *Rickettsia* adhere and subsequent invade endothelial cells have already been a subject of several studies **(Figure I.5)** (Valbuena and Walker, 2009; Walker and Ismail, 2008). Two different mechanisms have been shown to facilitate the entry of intracellular bacterial pathogens into non-phagocytic cells: the “zipper” and the “trigger” mechanisms (Alonso and Garcia-del Portillo, 2004). The “zipper” invasion mechanism is a receptor-mediated invasion strategy,

whereby bacterial proteins can induce host intracellular signaling through the extracellular stimulation of a membrane receptor, whereas the "trigger" mechanism relies on the bacterial secretion systems to deliver bacterial effectors into the host cell to modulate the invasion process (Alonso and Garcia-del Portillo, 2004; Cossart, 2004).

As obligate intracellular pathogens, rickettsial species have also evolved mechanisms to invade non-phagocytic cells (Chan et al., 2010). Transmission electron micrographs of non-phagocytic cells in the presence of *R. conorii* have demonstrated intimate localized cellular plasma membrane rearrangements around the bacteria that morphologically resembled a zipper-induced entry process (Gouin et al., 1999; Teysseire et al., 1995), suggesting that adherence of *R. conorii* to non-phagocytic cells must require an effective recognition and interaction between bacteria surface proteins and specific cellular receptors in the host cell.

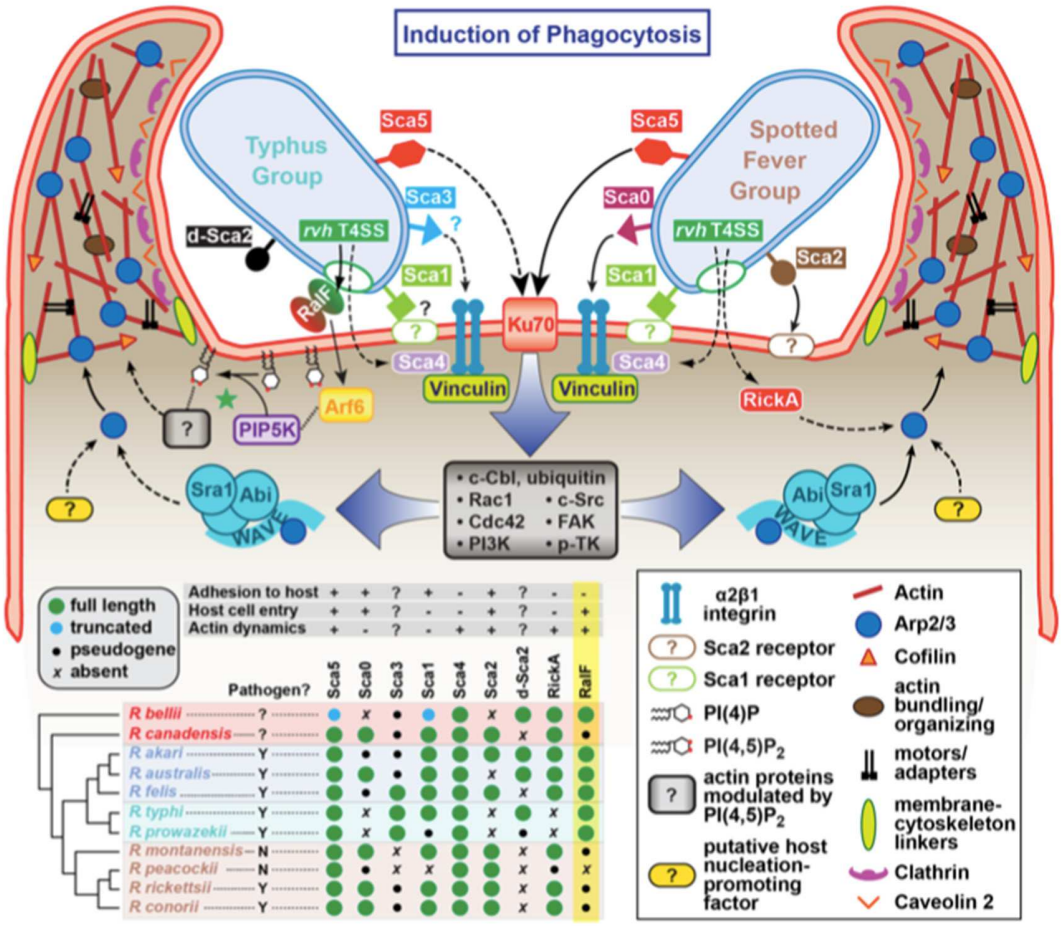

Figure I.5 (previous page) | Model for the variable pathways utilized by different *Rickettsia* species for host cell entry. General pathways for Typhus Group (TG, left) and Spotted Fever Group (SFG, right) rickettsiae species are inferred primarily from previous work on SFG rickettsiae species *R. conorii* and *R. parkeri* or *R. typhi*. Adapted from (Rennoll-Bankert et al., 2015).

In order to identify potential candidate *Rickettsia* surface proteins that potentiate this rickettsial-host cell interaction, a bioinformatics analysis of several sequenced rickettsial species allowed the identification of several predicted outer surface proteins, designated as Sca (surface cell antigen) proteins, with homology to the autotransporter proteins of gram-negative bacteria (Blanc et al., 2005). Among these, the genes encoding rOmpA (Sca0), Sca1, Sca2, and rOmpB (Sca5), are conserved across the SFG, whereas rOmpA and Sca2 genes are missing or appear fragmented in many of TG rickettsial species, respectively (Blanc et al., 2005). Three members of this family, the rickettsial outer membrane proteins A (rOmpA), B (rOmpB) and Sca2 have already been identified as playing a role in the adhesion and/or invasion process of *Rickettsia* into non-phagocytic mammalian cells (Cardwell and Martinez, 2009; Chan et al., 2009; Li and Walker, 1998). The identity of a mammalian receptor for *R. conorii* was first revealed by *Martinez et al.*, using a biochemical affinity approach with intact and purified rickettsiae incubated with detergent-soluble host cell lysates, revealing Ku70 (a component of DNA-dependent protein kinase) as a mammalian receptor for *R. conorii* (Martinez et al., 2005). Moreover, the ability of recombinant and purified rOmpB to interact directly with Ku70 and to competitively inhibit rOmpB-mediated bacterial adherence to cultured mammalian cells revealed rOmpB-Ku70 as a bona fide adhesion-receptor pair involved in the entry of rickettsial species (Chan et al., 2009). However, blockage of Ku70 with antisera directed against an N-terminal epitope of Ku70 results in a reduction of 50-60% in the ability of *R. conorii* to invade non-phagocytic cells (Martinez et al., 2005), which suggests that other factors besides the pair Ku70-rOmpB may contribute to the entry process, through a still unknown interaction. Furthermore, mammalian receptors for Sca1, Sca2 and/or other still unidentified rickettsiae adhesion molecules remain to be revealed.

Once the interaction between bacterial ligand and the mammalian receptor is achieved, signal transduction cascades are activated leading to internalization of the bacteria through a process known as “induced phagocytosis”. It is already known that binding of rOmpB to its host

receptor Ku70, triggers a host-signaling cascade involving c-Cbl-mediated ubiquitination of Ku70, Rho-family GTPases Cdc42 and Rac1, phosphoinositide 3-kinase (PI3K) activity, and activation of tyrosine kinases (e.g., c-Src, FAK and p-TK) and their phosphorylated targets **(Figure I.5)** (Chan et al., 2009; Martinez and Cossart, 2004). Signaling by this pathway leads to the recruitment of factors that activate the actin-nucleating complex (Arp2/3), which leads to host actin polymerization, extensive membrane ruffling and filopodia formation, and subsequently bacteria internalization in a clathrin- and caveolin-dependent process (Chan et al., 2009; Martinez and Cossart, 2004). However, diverse *Rickettsia* species are predicted to utilize different mechanisms to adhere to and invade host cells, since some adhesins and effectors that are reported to be involved in the host cell entry are differentially encoded in diverse *Rickettsia* species genomes (Blanc et al., 2005; Ogata et al., 2001). One particular example is RalF (a sec7 domain-containing protein that functions as a guanine nucleotide exchange factor of ADP-ribosylation factors (Arfs)), which was shown to be critical for *R. typhii* entry but it is pseudogenized or absent in SFG *Rickettsia* genomes (Rennoll-Bankert et al., 2015; Rennoll-Bankert et al., 2016). It is known that RalF is secreted during *R. typhii* infection and that its localization to the host plasma membrane and interaction with host ADP-ribosylation factor 6 (Arf6) leads to the regulation of phosphatidylinositol 4-phosphate 5-kinase (PIP5K), which is critical for *R. typhii* entry into mammalian cells (Rennoll-Bankert et al., 2015; Rennoll-Bankert et al., 2016).

Following internalization of rickettsiae, both SFG and TG *Rickettsia* reside in the cytosol and are not enclosed in a membrane-bound phagosome, implying that bacteria must escape from the phagosome after cell invasion (Teysseire et al., 1995). The first study into the mechanism and kinetics of invasion of *R. conorii* in Vero cells, including phagosome escape, revealed that the process is completed in the first 20 minutes upon infection (Teysseire et al., 1995). Escape from the phagosome in other bacterial pathogens, such as *Listeria monocytogenes*, involves the secretion and activation of membrane disrupting factors including phospholipases and hemolysins (Ray et al., 2009). Phospholipase A2 (PLA2), hemolysin C (TlyC), and phospholipase D (PLD) can be found in the genome of rickettsial species and a role in phagosomal membrane degradation and subsequent bacteria escape from the phagosome has been proposed (Driskell et al., 2009;

Silverman et al., 1992; Welch et al., 2012; Whitworth et al., 2005). Indeed, the expression of *R. prowazekii* phospholipase D (RP819) in *Salmonella typhimurium* enabled bacteria to escape from the phagosome but *R. prowazekii* Δpld mutant showed no difference from wild-type in the timing of escape, suggesting that a redundancy in activities may be involved in this process (Driskell et al., 2009; Whitworth et al., 2005).

Once in the cytoplasm, rickettsiae explore the host-cell actin cytoskeleton to move within and spread between mammalian host cells (Goldberg, 2001). Intracellular spreading mechanisms have long been considered a major characteristic difference distinguishing SFG and TG *Rickettsia* (Goldberg, 2001). Members of TG *Rickettsia* are non-motile within host cells, and the infection of adjacent cells takes place when the bacterial load increases and induction of host cells lysis occurs (Goldberg, 2001). In contrast, SFG *Rickettsia* exploit the host cell actin cytoskeleton to promote intracellular motility *via* active propulsion by means of directionally polymerized actin (Goldberg, 2001). Two rickettsial proteins, RickA and Sca2, have already been studied as bacterial proteins that function in actin-based motility (Haglund et al., 2010; Jeng et al., 2004). Interestingly, the RickA (a surface Wiskott-Aldrich syndrome (WASP)-like protein) gene appears to be limited to the genomes of rickettsial species that exploit host actin-based motility during infection (present in SFG *Rickettsia*, but absent in TG genomes), and its role in activating the Arp2/3 complex and mediating actin-based motility in SFG *Rickettsia* has already been demonstrated (Jeng et al., 2004; Ogata et al., 2001). A random transposon mutagenesis screening in *R. rickettsii*, in which the Sca2 gene was disrupted, provided the first evidence for its role in actin-based motility since the Sca2 mutant did not make actin tails and showed a defect in intra- and intercellular spread during infection (Kleba et al., 2010). Moreover, the sequence of Sca2 from SFG, TG, and AG *Rickettsia* species is quite divergent, suggesting potential differences in the mechanism by which it contributes to actin assembly and motility between species (Welch et al., 2012). Interestingly, *Reed et al.* have shown that RickA and Sca2 proteins direct an independent mode of *R. parkeri* actin-based motility at different times during infection (Reed et al., 2014). Early in infection, *Rickettsia* motility requires RickA and Arp2/3 complex and it is slow and meandering, generating short and curved actin tails that are enriched with Arp2/3 complex and cofilin (Reed et al., 2014). However, later in infection,

motility is independent of Arp2/3 complex and RickA but requires Sca2, and motility is faster and directionally persistent, which results in long and straight actin tails (Reed et al., 2014). The ability of SFG *Rickettsia* to exploit two actin assembly pathways may allow bacteria to establish an intracellular niche and spread between different cells throughout a prolonged infection (Reed et al., 2014).

I.1.7 | Host responses to infection

Rickettsial infections, with the exception of *R. akari*, are characterized by their affinity to preferentially infect vascular endothelial cells lining the small and medium-sized blood vessels in human and also animal models of infection (Olano, 2005; Walker et al., 1994). As a consequence, rickettsiae are able to disseminate through the endothelium, damaging vascular networks, which leads to disseminated inflammation, loss of barrier function and altered vascular permeability (collectively referred to as rickettsial vasculitis), and infection of multiple organs, such as brain, liver, lungs, among others (Sahni et al., 2013). Indeed, most of the clinical features of rickettsial diseases have been attributed to disseminated infection of the endothelium, where *Rickettsia* are able to proliferate and cause oxidative stress, thereby causing injury to the endothelial cells (Walker and Ismail, 2008). However, during infection, endothelial cells are not merely injured but are also able to launch an array of adaptive cellular responses switching from basal and nonthrombogenic phenotype to a state known as “endothelial activation” **(Figure I.6)** (Sahni et al., 2012). The responses that characterize an “activated endothelial” state have been the subject of several studies from different laboratories and hallmark features include, but are certainly not limited to, higher expression of pro-thrombotic, pro-adhesive and pro-inflammatory genes (Sahni et al., 2012; Walker and Ismail, 2008). More specifically, expression of tissue factor and E-selectin increased synthesis of plasminogen activator inhibitor-1, the release of von Willebrand factor from Weibel-Palade bodies, and changes in endothelial cell surface adhesiveness molecules, among others (Sahni et al., 2012). The stability of rickettsiae to evade the immune system has been linked with the inhibition of endothelial cell apoptosis by a mechanism involving nuclear factor-κB (NF-κB), which enables bacteria to maintain their replicative niche (Joshi et al., 2003, 2004). Moreover, the

involvement of two major host signaling pathways (NF-κB and MAPK) in the expression of many inflammatory genes during rickettsial infections has also been reported (Clifton et al., 2005a; Clifton et al., 2005b; Rydkina et al., 2007; Rydkina et al., 2005a).

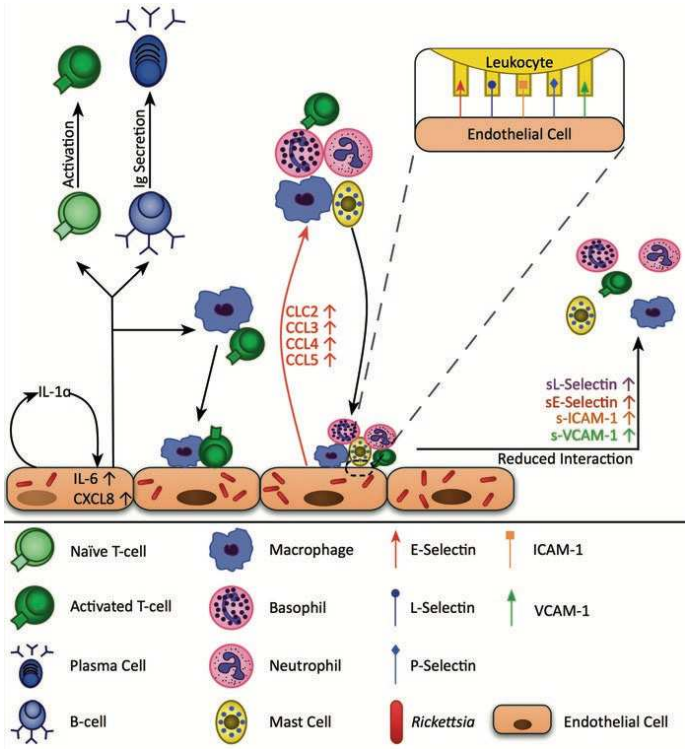

Figure I.6 | Endothelial cell activation and inflammatory response to rickettsial infection. A summary of the current state of knowledge regarding endothelial cell activation post-rickettsial infection and subsequent inflammatory response. Activation of host endothelium leads to activation of lymphocytes and recruitment of leukocytes through the secretion of pro-inflammatory cytokines. Adapted from (Schroeder et al., 2016).

Endothelial cells have emerged as key immunoreactive cells that participate in a diverse array of cellular processes by both producing and/or reacting to a broad range of mediators (Galley and Webster, 2004). Indeed, the production of inflammatory cytokines, such as IL-1α, IL-6, and IL-8 by rickettsiae-infected endothelial cells has been correlated with the expression of cell adhesion molecules, such as intercellular-adhesion molecule 1 and vascular-cell-adhesion molecule 1, which support the recruitment of T cells to the site of infection. Although chemokines are expressed at relatively low levels in endothelial cells, increased levels of interleukins and chemokines have been reported upon infection with rickettsiae. For example, increased expression of CCL2, CCL3, CCL4, and CCL5 has been correlated with macrophage and monocyte interactions with endothelial cells,

while increased levels of CXCL5 and CXCL8 are reported to act in recruitment of monocytes, macrophages, lymphocytes, and other polymorphonuclear leukocytes to the site of infection, and CXCL9 and CXCL10 as T-cell chemoattractants (Kaplanski et al., 1995; Rydkina et al., 2005a, b; Valbuena et al., 2003; Valbuena and Walker, 2004). In fact, the peak of expression of chemokines correlates with maximal T-cell infiltration (mainly CD8+ T cells) at the site of infection. However, it is still not completely clear whether this contributes to protection against rickettsial infection or more to the pathogenesis of the disease (Walker and Ismail, 2008).

Several studies have suggested that innate immune responses play a role in limiting the proliferation and subsequently spread of rickettsiae **(Figure I.7)**.

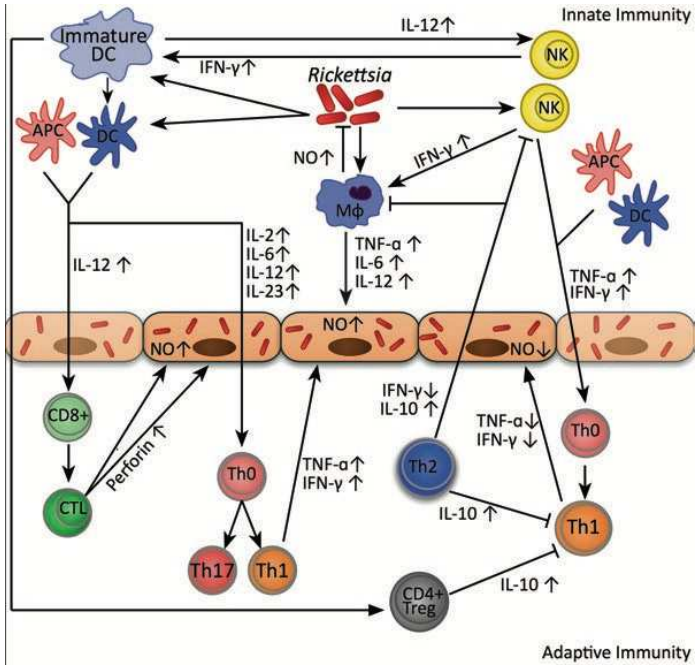

Figure I.7 | Innate and adaptive immune response to rickettsial infection. A schematic representation depicting the host's innate (*top*) and adaptive (*bottom*) response to rickettsioses. The response is delicately balanced through the secretion of both pro-inflammatory and anti-inflammatory cytokines. Adapted from (Schroeder et al., 2016).

For example, the role of IFN-γ and TNFα in primary defense against rickettsial infections was demonstrated when IFN-γ and TNFα-depleted C3H/HeN mice were infected with a sublethal dose of *R. conorii* that resulted in an overwhelming and lethal infection (Feng et al., 1994). Moreover, using animal models of infection, it was also shown that depletion of NK cell activity in the already

susceptible C3H/HeN and C57BL/6 mice increased the susceptibility of mice to infection by *R. conorii* and *R. typhi*, respectively (Billings et al., 2001). Using C3H/HeN mice models, *Jordan et al.* have demonstrated that rickettsiae stimulate dendritic cells (DCs) through Toll-like Receptor 4 (TLR4) leading to enhanced NK cell activation and recruitment to draining lymph nodes (Jordan et al., 2009). Interestingly, increased IFN-γ production by NK cells was also correlated with a role in mediating the protective T_H1 response in anti-rickettsial immunity and macrophage activation (Billings et al., 2001; Walker and Ismail, 2008). Moreover, activated macrophages have also been shown to play a role in restricting rickettsial proliferation via the production of hydrogen peroxide and tryptophan starvation (Feng and Walker, 2000).

Dendritic cells are antigen-presenting cells, and their primary function is to process antigen material and present it on the cell surface to the T cells of the immune system. Thus, they act as messengers between the innate and the adaptive immune system. Rickettsiae have been shown to efficiently enter and localize in both phagosomes and the cytosol of bone-marrow-derived DCs (BMDCs) from resistant C57BL/6 and susceptible C3H/HeN mice (Fang et al., 2007). It has been reported that the dual localization of rickettsiae within BMDCs may favor the access of rickettsial antigen to both major histocompatibility complex (MHC) class I and II pathways, thus promoting the activation of *Rickettsia*-specific $CD8^+$ and $CD4^+$ T cells, respectively (Fang et al., 2007; Walker and Ismail, 2008). *Rickettsia*-infected DCs have been shown to induce DC maturation and activate *in vitro* $CD8^+$ T lymphocytes in the absence of $CD4^+$ T-cell help (Fang et al., 2007; Jordan et al., 2007). Mature *Rickettsia*-infected DCs can then enter lymph nodes through afferent lymphatic vessels, where they display antigens to naïve antigen-specific $CD4^+$ and $CD8^+$ T cells and provide co-stimulatory signals that activate antigen-specific T cells (Walker and Ismail, 2008). A critical role for $CD8^+$ T lymphocytes during rickettsial infections has been already demonstrated in several studies comprising $CD8^+$ T cells depletion, immune $CD8^+$ T cell adoptive transfer, and experiments in mice with knockout of selected immune response genes (Feng et al., 1997; Walker et al., 2001). $CD8^+$ T lymphocytes are able to recognize MHC class I molecules on the surface of antigen presenting cells aiding in bacterial clearance. Interestingly, MHC class-I deficient C57/BL/6 mice are 50 000-fold more susceptible than wild-type mice to *R. australis* infection, demonstrating that cytotoxic

activity of $CD8^+$ T lymphocytes is an effective mechanism of the immune system in fighting rickettsial infections (Walker et al., 2001). Moreover, a strategy involving nucleofection of antigen-presenting cells targeting the MHC class I pathway with clones expressing *R. prowazekii* genes stimulated cross-protection reducing the bacterial load in liver of mice infected with an ordinarily lethal dose of *R. typhi*, further supporting the contribution of $CD8^+$ T lymphocytes in rickettsial immunity (Caro-Gomez et al., 2014; Gazi et al., 2013). On the other hand, it has been reported that BMDCs from susceptible murine hosts that are infected *in vitro* with *Rickettsia* fail to stimulate *Rickettsia*-specific $CD4^+$ T-cell differentiation into Th1 or Th2 cells, and suppressed effects on $CD4^+$ T-cell responses have been associated with IL-10 production by DCs as well as increased numbers of $CD4^+CD25^+Foxp3^-$ T-regulatory (T_{Reg}) cells that also secrete IL-10 (Fang et al., 2009; Walker and Ismail, 2008). Thus, this mechanism of immune suppression of $CD4^+$ T-cell responses in rickettsial infections seems to contribute to the progression and development of a fatal disease.

Humoral immunity, often called antibody-mediated immunity, is part of the immune system that protects the extracellular space, in which the antibodies produced by B cells cause the destruction of extracellular organisms and prevent the spread of intracellular infections (Casadevall, 2018). Due to their intracellular lifestyle, it is presumed that *Rickettsia* are able to evade the humoral immune response by residing within a host cell. However, some studies have already shown that antibodies against rickettsial OmpA and OmpB, but not rickettsial lipopolysaccharide, protected susceptible C3H/HeN mice from lethal doses of *R. conorii* (Feng et al., 2004; Valbuena et al., 2002). However, it is known that in rickettsial infections antibodies usually do not appear until before 2 weeks after the onset of clinical symptoms, suggesting that antibody-mediated killing in rickettsial infections may be more important in preventing re-infection and in vaccine-induced immunity than in clearance of primary infections (Fournier et al., 2002; Mansueto et al., 2012). However, it was recently demonstrated that the complement system is activated during *R. australis* infection and genetic ablation of the complement system increases susceptibility to infection, which may suggest that humoral responses may also have a role in rickettsial clearance during rickettsioses (Riley et al., 2018).

I.1.8 | Virulence factors

Several efforts have been made to identify which rickettsial effectors are involved in the infectious process. Rickettsial-endothelial cell interactions have been a target of several studies from different research groups, which have allowed the identification of several (host and rickettsial) molecular components that are involved in this process, such as rickettsial adhesins, host cell receptors, components of signal transduction that affect rickettsial entry, apparent mediators of phagosomal escape, manipulation of NF-κB to inhibit apoptosis, actin-based motility and cell-to-cell spread (Walker and Ismail, 2008).

Table I.1 | Candidate rickettsial virulence genes (update from (Walker and Ismail, 2008).

Rickettsial Gene	Encoded product	Potential function	Reference
pat1	Patatin B1 precursor	Membranolytic phospholipase A host cell escape	(Rahman et al., 2013)
tlyA	Haemolysin A	Membranolytic traversal of host cell membrane	(Whitworth et al., 2005)
tlyC	Haemolysin C	Membranolytic phagosomal escape	(Whitworth et al., 2005)
Pld	Phospholipase D	Membranolytic phagosomal escape	(Whitworth et al., 2005)
invA	Dinucleoside polyphosphate hydrolase	Hydrolysis of toxic dinucleoside polyphosphates to ATP	(Gaywee et al., 2002a; Gaywee et al., 2003; Gaywee et al., 2002b)
coxAB	Cytochrome c oxidase	Aerobic respiration under optimal aerobic conditions	(McLeod et al., 2004)
cydAB	Cytochrome d oxidase	Aerobic respiration under low-oxygen conditions	(Narra et al., 2016)
sodB	Superoxide dismutase	Neutralizes oxidative stress of reactive oxygen species	(Walker and Ismail, 2008)
Lipopolysaccharide synthesis genes	Lipopolysaccharide	Endotoxin-mediated inflammation	(Driscoll et al., 2017; Fodorova et al., 2005)
ompA	Outer-membrane protein A	Spotted-fever-group rickettsial attachment to host cell	(Cardwell and Martinez, 2009; Li and Walker, 1998)
ompB	Outer-membrane protein B	Rickettsial attachment to host cell	(Chan et al., 2009)
virB4, virB6, virB7, virB8, virB9, virBro, virB11 and others	Type IV secretion system	Transport of rickettsial proteins or DNA into host cytosol	(Gillespie et al., 2009; Gillespie et al., 2015b)
rickA	Actin-tail polymerization gene	Formation of actin tail and mediation of intracellular and intercellular rickettsial spread	(Harris et al., 2018; Jeng et al., 2004)
rc1339 APRc	Retropepsin-like aspartic protease	*In vitro* processing of two autotransporter adhesin/invasion proteins, Sca5/OmpB and Sca0/OmpA	(Cruz et al., 2014; Li et al., 2015)
ralF	Bacterial Sec7-domain-containing proteins	Controls *R. typhi* invasion into non-phagocytic cells	(Rennoll-Bankert et al., 2015; Rennoll-Bankert et al., 2016)

We have herein summarized and updated a list of candidate rickettsial virulence genes, which was previously published by Walker et al. **(Table I.1)**. Although all of these efforts, the identification of virulence genes, elucidation of their role on the host cell, and their validation in an *in vivo* system has mainly been hampered by the genetic manipulation intractability of rickettsial species (McClure et al., 2017). Nevertheless, recent studies have highlighted important roles of rickettsial proteins such as ralF, which functions in the invasion process of *R. typhi* into non-phagocytic cells or APRc, an HIV-like retropepsin protease, that may act on the proteolytic processing of rOmpA and rOmpB (important proteins for rickettsiae infectious process) (Cruz et al., 2014; Rennoll-Bankert et al., 2015). Due to the limitations in genetic manipulation in rickettsial species, other approaches such as comparative genomics between virulent and avirulent strains have also been carried out to identify putative virulence factors (Clark et al., 2015; Ellison et al., 2008). However, although research has generated a wealth of data, information about crucial virulent factors and the subsequent mechanism of action that, for example, modulate inflammatory responses, mediate immune evasion or modulate intracellular survival during infection are still elusive.

I.1.9 | Disease symptoms, diagnostics and therapeutics

Rickettsioses present an array of clinical signs and symptoms that generally are manifested 2 to 14 days upon bacterial inoculation (Faccini-Martinez et al., 2014). Rickettsioses vary in severity from self-limited mild infections to fulminating life-threating diseases. The disease is generally characterized by an acute onset of high fever, and there is a considerable variation in the range and severity of the associated symptoms (Dumler, 2012). Such symptoms can include severe headaches, prominent neck muscle myalgia, malaise, nausea/vomiting, or neurological signs (Faccini-Martinez et al., 2014). In RMSF or epidemic typhus, a characteristic macular or maculopapular rash appear 3 to 5 days after the onset of the disease in most infected patients (≈80%) (Fang et al., 2017). Rare in RMSF, focal skin necrosis with a dark scab (eschar) at the site of tick feeding is a common feature of MSF, African tick bite fever, North Asian tick typhus, Queensland tick typhus, Japanese spotted fever, Flinders Island spotted fever, Rickettsialpox, and tick-borne lymphadenopathy (Faccini-Martinez et al., 2014; Fang et al., 2017; Mahajan, 2012). If

untreated, rickettsioses originated from highly pathogenic species are lethal and severe injury can develop, and sometimes progress into multi-organ failure. Systemic vascular infection in RMSF is also known to result in encephalitis which can lead to stupor, coma and seizures, interstitial pneumonia, non-cardiogenic pulmonary edema and adult respiratory distress syndrome (Walker and Ismail, 2008). In severe cases, hypovolaemia and hypotensive shock result in acute renal failure (Walker and Ismail, 2008).

R. prowazekii infection causes latent infection in convalescent individuals, and recrudescence of latent infection is known to result in Brill-Zinsser disease, which is characterized by fever, rash, and less-severe illness. Under this condition, infection of feeding lice may occur and ignite an epidemic (McQuiston et al., 2010).

Currently, diagnostic assays for rickettsial diseases comprise immunohistochemistry (IHC) analysis, molecular detection, isolation and culture of pathogens, and serology tests (Luce-Fedrow et al., 2015). Determination of the most appropriate diagnostic assay to request for a suspected rickettsial infection requires consideration of several factors, which includes the suspected pathogen and timing relative to the onset of symptoms **(Figure I.8)** (Fang et al., 2017; Luce-Fedrow et al., 2015).

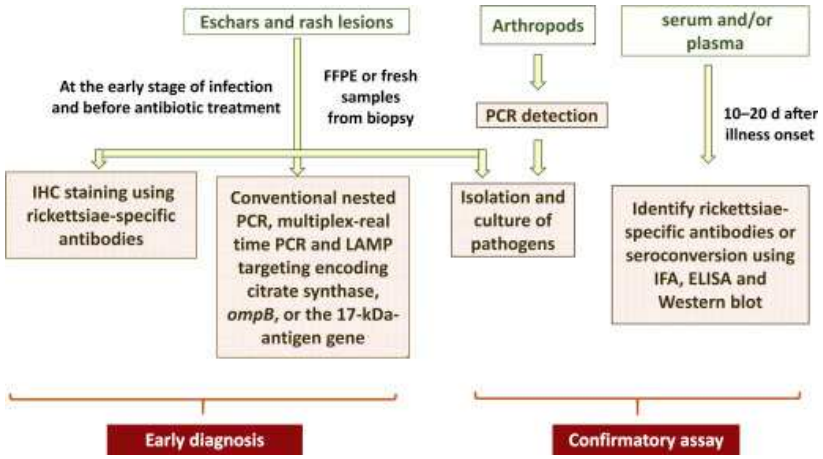

Figure I.8 | A diagnostic algorithm for laboratory diagnosis of rickettsial diseases. ELISA, enzyme-linked immunosorbent assay; FFPE, formalin-fixed, paraffin-embedded; IFA, immunofluorescence assay; IHC staining, immunohistochemical staining; LAMP, loop mediated isothermal amplification; OmpB, outer membrane protein B; PCR, polymerase chain reaction. Adapted from (Fang et al., 2017).

During the acute phase of the disease, and because rickettsial infections often present rash or eschars, analysis of skin biopsy samples by immunohistochemical staining using antibodies directed or cross-reactive against rickettsiae and/or detection of nucleic acid molecules of rickettsiae using molecular approaches (PCR) are the recommended diagnostic tests (La Scola and Raoult, 1997).

Isolation and culture of pathogens from a suspected patient can also be used but requires technical expertise, and specialized facilities (biosafety level-3 laboratories) since a small number of aerosolized rickettsiae can cause illness (Angelakis et al., 2012).

Ten to twenty days after illness onset, detection of antibodies in the serum or plasma of patients infected with rickettsiae is a gold-standard method to confirm the diagnosis of rickettsial infections (Luce-Fedrow et al., 2015). Rickettsial antigen-specific antibodies can be detected by enzyme-linked immunosorbent assay (ELISA), indirect immunofluorescence assay (IFA), and Western blot (WB) (Fang et al., 2017). Although WB is a technique that allows a specific identification of a causative agent, only some reference laboratories have a robust rickettsial antigen collection that allows such identification and the kits on the market lack specificity and sensitivity relying on a few established rickettsial species antigens such as *R. rickettsii* and *R. conorii* (Abdad et al., 2018). Thus, in the cases that rickettsiae are suspected to be distinct from those, some laboratories have in-house IFA microimmunofluorescence (MIF) for a broader range of rickettsial species. MIF can detect antibodies up to 9 antigens within a single well containing multiple antigen dots, and it can be a useful method for areas where several rickettsial species coexist and cause human disease (La Scola and Raoult, 1997; Philip et al., 1976; Robinson et al., 1976). Seroconversion or a 4-fold increase in titers of IgG from acute-phase to convalescent-phase samples confirms the diagnostic of rickettsial disease (Brouqui et al., 2004).

Due to the limitations of current laboratory diagnostic assays for rickettsial diseases, empirical knowledge about eliciting historical factors such as patient's symptoms, travel or recreational activities in endemic areas that favor possible exposure to infected vectors is essential in the diagnostics (Fang et al., 2017). This knowledge is key due to the rapidly progressive

expansion of certain rickettsial species and because empirical antibiotics for other infections (e.g., penicillins, cephalosporins, and sulfamides) are ineffective against *Rickettsia* species (Rolain et al., 1998).

Due to rapid progression of the disease, it is also recommended that antibiotic prescription should never be delayed while waiting for laboratory confirmation of a rickettsial illness (Botelho-Nevers and Raoult, 2011; Botelho-Nevers et al., 2012). Tetracyclines are the class of antibiotics of choice in the treatment of all SFG and TG rickettsioses, and the mean inhibitory concentration (MIC) of tetracyclines for *Rickettsia* species is 0.06 to 0.25 µg/mL with doxycycline being the preferred agent (Fang et al., 2017). Chloramphenicol is considered an alternative with MICs of 0.25 to 2.0 µg/mL (Fang et al., 2017).

I.2 | Macrophage-pathogens interactions

I.2.1 | Macrophages as a component of the immune system

The immune system is a host defense system that comprises many biological structures and processes within an organism protecting it against disease (Parkin and Cohen, 2001). Functioning properly, the immune system must be able to detect a wide variety of disease-causing agents, which are known as pathogens (it can be viruses, bacteria, fungus or parasites), and distinguish them from the organism's own healthy tissue (Parkin and Cohen, 2001). In humans, the immune system can be classified into subsystems, such as the innate and adaptive immune system (the latter comprising both humoral and cell-mediated immunity) (Husband, 2001). Innate immunity is characterized by the ability of phagocytic cells to engulf and digest microorganisms providing defenses against infection that are not specific, whereas adaptive immunity is a specific response against infection characterized by the ability to generate an immunological memory after an initial response to a specific pathogen, leading to an enhanced response to subsequent encounters with that pathogen (Bonilla and Oettgen, 2010; Turvey and Broide, 2010). Humoral immune response (or antibody-mediated response) is characterized by the protection of extracellular spaces (lymph or blood) by the ability of antibodies produced by B cells to help to destroy extracellular microorganisms and their products, and subsequently prevent the spread of intracellular infection, whereas the cell-mediated response involves mostly T cells and responds to any cell that displays aberrant MHC markers, which includes infected cells, tumor cells, or transplanted cells (McNeela and Mills, 2001; Shishido et al., 2012).

Macrophages (in Greek: big eaters) are a type of white blood cells, originated from monocytes, that engulf and digest cellular debris, foreign substances, microbes, cancer cells, and anything else that do not have the type of proteins specific to healthy body cells on its surface in a process called phagocytosis (Epelman et al., 2014). Human macrophages are about 21 micrometers in diameter and can be identified using flow cytometry or immunohistochemical staining by the expression of specific proteins at the surface (Epelman et al., 2014; Krombach et al., 1997). These large phagocytes are relatively long-lived cells, found in virtually all tissues, where they patrol for potential pathogens, adopting various forms (with different names) throughout the

body (e.g., microglial cells in neural tissue, Kupffer cells in the liver or alveolar macrophages in the lung) (Murray and Wynn, 2011). The substantial heterogeneity among macrophage population, which reflects the required level of specialization within the environment of specific tissues, is characterized by the diverse morphologies they adopt, the type of pathogens they can recognize, as well as the levels of inflammatory cytokines they produce (Amit et al., 2016; Murray and Wynn, 2011). Macrophages express a limited number of invariant innate recognition receptors at their surface called pattern recognition receptors (PRRs), which allow them to recognize pathogens or the damage caused by them (Mogensen, 2009). PRRs are able to recognize simple molecules and regular patterns of molecular structures known as pathogen-associated molecular patterns (PAMPs) that are part of many microorganisms but not of the host body's own cells (Mukhopadhyay et al., 2009). These recognition patterns comprise the ability of mannose, glucan or scavenger receptors to bind cell-wall carbohydrates of bacteria, yeast, and fungi, or the TLR-1/TLR-2 heterodimer to bind certain lipopeptides from Gram-positive bacteria, or TLR-4 to bind both lipopolysaccharides (LPS) from Gram-negative and lipoteichoic acids from Gram-positive bacteria, or even the cytoplasmic proteins, the NOD-like receptors, that sense intracellular bacterial invasion (Mukhopadhyay et al., 2009). After sensing a pathogen, sensor cells can either directly respond with effector activity or producing inflammatory mediators to amplify the immune response (Hirayama et al., 2017).Thus, activation of PRRs in macrophages can lead to effector functions on these cells by inducing phagocytosis of the pathogen and subsequently production of toxic chemical mediators, such as degradative enzymes or reactive oxygen intermediates, to kill the pathogen (an essential role in innate immunity) (Hirayama et al., 2017). In addition, sensing of pathogens can also trigger macrophages for the production of inflammatory mediators such as cytokines and chemokines that serve to amplify the immune response by increasing the permeability of blood vessels, which allow fluid, proteins and other inflammatory cells to pass into the tissues helping to destroy the pathogen (Leick et al., 2014; Murphy and Weaver, 2017). Inflammation also increases the flow of lymph to nearby lymphoid tissues, where the adaptive immune response is initiated, and inflammation can also serve to recruit effector components of adaptive immunity to the site of infection (Twigg, 2004). Another important function of macrophages

is to act as antigen presenting cells displaying antigen peptides on the MHC molecules, thus playing a role in presenting antigens derived from phagocytized infectious organisms (Unanue, 1984). Hence, when B or T lymphocytes encounter antigens, adaptive immune responses are initiated, and appropriate inflammatory signals are provided to support activation of adaptive immune responses (Murphy and Weaver, 2017).

Overall, besides playing an essential role in non-specific defense (innate immunity) by engulfing and destroying pathogens, macrophages can also help initiating specific defense mechanisms (adaptive immunity) by orchestrating immune responses and recruiting other immune cells to the site of infection as well as serve as antigen presenting cells to lymphocytes (Murphy and Weaver, 2017).

Although phagocytosis and microbial killing were the first functions attributed to macrophages, a much more complex and broad range of functions have emerged for macrophages in host defense, together with important roles in tissue homeostasis and repair, pathology, and development (Murray and Wynn, 2011). In tissues, macrophages mature and can be activated by combinations of stimuli to acquire specific functional phenotypes to accommodate their varied functional repertoire (Epelman et al., 2014). As for the lymphocyte system, a dichotomy has been proposed to classify the macrophage activation states: M1 (or classic) vs. M2 (or alternative) (Martinez and Gordon, 2014). M1 macrophages (also called “killer macrophages”) are typically activated by PAMPs (e.g., LPS), damage-associated molecular patterns (DAMPs), and inflammatory cytokines such as TNF and IFNγ, secrete high levels of IL-12 and low levels of IL-10, and are classified by their pro-inflammatory, bactericidal, and phagocytic characteristics (Martinez and Gordon, 2014; Murray et al., 2014). IFNγ activated macrophages are characterized by high expression of antimicrobial GTPases such as p47 and guanylate-binding proteins (GPB) family members, which strongly induce macrophage antimicrobial defenses, particularly autophagy and reactive nitrogen intermediates (Kim et al., 2012). Therefore, stimulation of macrophages by IFNγ almost invariably renders a macrophage completely inhospitable to invading pathogens due to the combination of antimicrobial responses induced by this cytokine (Pollard et al., 2013). However, the potential of IFNγ for collateral tissue damage leads to the need of tightly controlling its

expression in order to maintain homeostasis and avoid autoimmunity, limiting the use of this pathway to fully control intracellular parasitism (Schroder et al., 2004). In contrast, M2 macrophages (also called “repair” macrophages) arise in response to stimuli, such as the Th2-cell-associated cytokines IL-4 and IL-13, bacterial molecules such as LPS in combination with immune complexes, and glucocorticoids, among others (Martinez and Gordon, 2014; Murray et al., 2014). M2 macrophages are characterized by the production of anti-inflammatory cytokines like IL-10, participating in constructive processes like wound healing and tissue repair due to their ability to turn off the activation of damaging immune system. (Martinez and Gordon, 2014; Murray et al., 2014).

Although useful to understand extreme polarization states, the classification of macrophages in the opposite binary activation states (M1 vs. M2) is currently accepted to be oversimplified. Indeed, *in vivo,* macrophages are subjected to a plethora of stimuli and nutrient environments that often do not entirely fit in the binary classification but in a spectrum of phenotypes allowing macrophages to exert a diverse array of cellular activities (Price and Vance, 2014). Therefore, to face the entire spectrum of cellular activities and phenotypes, macrophages present a high degree of plasticity, adopting different metabolic states **(Table I.2)** (Van den Bossche et al., 2017). Thus, the metabolic reprogramming of macrophages is crucial to regulating their phenotype. One of the main metabolic differences between the contrasting macrophage activation states is the ability of M1 macrophages to convert arginine into the “killer” molecule nitric oxide (NO) through inducible NO synthase (iNOS) activity, whereas M2 macrophages have the ability to metabolize arginine to the “repair” molecule ornithine through arginase-1 (Corraliza et al., 1995; Modolell et al., 1995; Munder et al., 1998). In parallel with distinct arginine metabolism, differences in several metabolic pathways such as glycolysis, pentose phosphate pathway (PPP), fatty-acid synthesis (FAS), fatty-acid oxidation (FAO), and oxidative phosphorylation (OXPHOS) also characterize the distinctive features of macrophage activation states, which will be discussed in detail henceforth **(Table I.2)** (O'Neill and Pearce, 2016).

Table I.2 | Metabolic reprogramming in macrophage subsets. Adapted from (Van den Bossche et al., 2017).

	M1/M[LPS(+IFNγ)]	M2/M[IL-4]
Amino acid metabolism	Arginine is converted to NO by iNOS. Glutamine metabolism regulates trained innate immunity.	Arginase-1 metabolizes arginine.
Glycolysis	Strongly induced and supports pro-inflammatory macrophage functions in distinct ways.	Induced and crucial for IL-4 induced macrophage activation.
OXPHOS	Impaired by NO and itaconate. Electrons flow backwards, driving ROS production, HIF1α stabilization, and IL-1β expression.	Induced and supports the phenotype of IL-4-induced macrophages.
PPP	Induced and required for ROS generation via NADPH oxidase, NO production, and nucleotide and protein synthesis.	Not required/suppressed by the sedoheptulose kinase CARKL.
FAS	Citrate accumulation is required for FAS, supporting inflammatory signaling and increased NO and TNF production.	Suggested to fuel FAO.
FAO	Needed for NLRP3 inflammasome activation and IL-1β secretion.	CPT1a is needed for M2 polarization. CPT2 is not needed. Effects of the CPT1 inhibitor etomoxir appear highly context dependent.

To fuel their bioenergetics demands, inflammatory macrophages have an enhanced glycolytic metabolism, which is tied to the increased production of reactive oxygen species and the biosynthesis of cytokines (Pearce and Pearce, 2013). Upregulation of glycolytic metabolism in M1 macrophages serves not only to swiftly produce ATP to sustain their high secretory and phagocytic functions, but also to feed the PPP, which supports inflammatory macrophage responses by generating amino acids for protein synthesis, ribose for nucleotides, and NADPH for the production of reactive oxygen species (ROS) by NADPH oxidase (Haschemi et al., 2012; O'Neill et al., 2016). In fact, increased glycolysis is considered a hallmark metabolic change in most immune cells undergoing rapid activation (e.g., DCs, in activated NK cells, activated effector T cells, and activated B cells) in response to diverse stimuli like PRRs, cytokine or antigen receptors (Donnelly et al., 2014; Doughty et al., 2006; Krawczyk et al., 2010; Michalek et al., 2011; Rodriguez-Prados et al., 2010). Inflammatory macrophages are also characterized by a disrupted TCA cycle with breaks in two places: (i) at isocitrate dehydrogenase 1 (IDH1) resulting in the accumulation of citrate and (ii) at succinate dehydrogenase resulting in the accumulation of succinate (O'Neill et al., 2016). The citrate that accumulates in M1 macrophages has been shown to meet the biosynthetic demands of inflammatory macrophages including the synthesis of fatty acids, lipids and prostaglandins and support increased NO and TNF production (Infantino et al., 2011; Moon et al.,

2015; Wei et al., 2016). Excess of citrate can also result in increased production of itaconate via immune-responsive gene 1 (Irg1), which has been shown to have direct antimicrobial effects on several species such as *Salmonella enterica* subsp. *enterica* serovar Typhimurium and *Mycobacterium tuberculosis* (Michelucci et al., 2013). Moreover, an increase of itaconate and NO production can both inhibit succinate dehydrogenase (SDH), thereby inducing the second break that causes accumulation of succinate (O'Neill et al., 2016). Succinate acts as a pro-inflammatory metabolite that stabilizes the transcription factor hypoxia-inducible factor 1 alpha (HIF1α) through inhibition of prolyl hydroxylase (PHD) activity and promotion of reactive oxygen production and leading to increased expression of the pro-inflammatory IL-1β (Tannahill et al., 2013). Accumulation of itaconate and NO in inflammatory macrophages also results in impaired OXPHOS, which contributes to increased ROS levels via reverse electron transport (RET) through complex I (Mills et al., 2016). Overall, M1 macrophages are characterized by high glycolytic and PPP activity, while the TCA cycle is broken at two points, and OXPHOS is impaired (O'Neill et al., 2016).

In sharp contrast with the metabolic characteristics of inflammatory macrophages, M2 macrophages are characterized by an intact TCA cycle coupled with an enhanced mitochondrial OXPHOS (Van den Bossche et al., 2015; Van den Bossche et al., 2016). This allows the generation of UDP-GlcNAc intermediates that are necessary for the glycosylation of M2-associated receptors, such as the mannose receptor (Jha et al., 2015; O'Neill et al., 2016). Moreover, and in contrast to the aerobic glycolysis observed in inflammatory macrophages, M2 macrophages rely on FAO to support mitochondrial oxidative metabolism (Jha et al., 2015). Furthermore, increased FAO can also result in reduced lipid accumulation and consequently reduced production of inflammatory cytokines, which may be an approach to reduce the inflammatory potential of macrophages (Malandrino et al., 2015). Recently, it has also been demonstrated that production of α-ketoglutarate (αKG) via glutaminolysis promotes M2 activation via a Jmjd3-dependent metabolic and epigenetic reprogramming (Liu et al., 2017). Interestingly, high αKG/succinate ratio has been correlated with an M2-promoting mechanism, whereas a low ratio of αKG/succinate strengthens the pro-inflammatory phenotype of M1 macrophages (Liu et al., 2017).

The understanding of metabolic reprogramming in macrophages has emerged in recent years and provided new insights into the complex interplay between macrophage activation states and their role in immunity and disease.

1.2.2 | "The macrophage paradox"

Although macrophages display a diverse array of functions, it is clear that one of their specialized roles is to orchestrate the elimination of microbes (Hirayama et al., 2017). Nevertheless, many bacterial pathogens are able to subvert macrophage defense mechanisms and establish a niche of infection in these professional phagocytic cells **(Table I.3)**. This has been termed "the macrophage paradox": "why do so many bacterial pathogens replicate in macrophages, given that macrophages are a cell type that appears adapted to kill and eliminate bacteria?" (Price and Vance, 2014). To better understand this question, a number of distinct possibilities have been addressed. Interestingly, although macrophages are known to encode numerous antimicrobial activities, they also have distinctive features that make their intracellular environment very attractive for pathogens (Eisenreich et al., 2017; Price and Vance, 2014). These features comprise the fact that macrophages are long-lived cells (being a stable niche), have a rich nutrient pool associated with a high degree of metabolic diversity and plasticity (that can be quickly remodeled by pathogens), and are able to induce inflammation and traffic throughout the body (that can be beneficial for pathogen dissemination (Price and Vance, 2014). Moreover, it is practically inevitable that an invading pathogen will eventually find itself in a macrophage due to the localization of macrophages in virtually every tissue in the body, combined with their intrinsic ability to phagocyte (Epelman et al., 2014; Perdiguero and Geissmann, 2016). Indeed, even pathogens that preferentially invade non-macrophage cells or the most devoted intracellular pathogens will eventually find themselves in a macrophage when their primary host cell undergoes apoptosis or during their experience in the extracellular space (Mansueto et al., 2012; Price and Vance, 2014). Therefore, success as a pathogen may require the ability to avoid macrophage-killing mechanisms and to replicate, or at least survive, within the intracellular environment of a macrophage (Price and Vance, 2014). Indeed, it is now known that several successful pathogens have evolved sophisticated strategies

to subvert the macrophage defense system and promote their survival and replication within the hostile environment of these professional phagocytes.

Table I.3 | Replicative niches of intracellular bacterial pathogens. Adapted from (Price and Vance, 2014).

Name of Bacteria	Human Diasease	Replication in macrophages?	Replication in other cell type(s)?	Intracellular niche	Virulence factors[a]
Anaplasma phagocytophilum	granulocytic anaplasmosis; tick-borne fever	mainly granulocytes	granulocytes and endothelial cells	membrane-bound ‘‘inclusion’’	T4SS
Bartonella henselae	cat-scratch disease	Yes	endothelial cells; erythrocytes in cats	membrane-bound vacuole	T4SS
Brucella abortus	brucellosis	Yes	mainly in macrophages; also placental trophoblasts	ER-like vacuole	T4SS
Burkholderia pseudomallei	melioidosis	Yes	yes, including neutrophils	cytosol	T3SS; T6SS
Chlamydia pneumoniae	pneumonia	Yes	yes, but mainly macrophages	membrane-bound “inclusion”	T3SS
Chlamydia trachomatis	trachoma, pelvic inflammatory diasease, etc.	poorly if at all	epithelial cells	membrane-bound “inclusion”	T3SS
Coxiella burnetti	Q fever	Yes	yes, but mainly professional phagocytes	phagolysosome-like compartment	T4SS
Edwardsiella tarda	rare; typically gastroenteritis	Yes	yes, e.g., epithelial cells	phagosome-derived compartment	T3SS;T6SS
Ehrlichia chaffeensis	monocytic ehrlichiosis	Yes	mainly monocytes and macrophages	early endosome-like “inclusion”	T4SS
Francisella tularensis	Tularemia	Yes	mainly macrophages? Also epithelial and other cells	cytosol	T6-like SS (FPI)
Legionella pneumophila	Legionnaires’ disease	Yes	mainly macrophages in mammals, but also protozoa	ER-like vacuole	T4SS
Listeria monocytogenes	gastroenteritis; bacteremia	Yes	CD8α dendritic cells	cytosol	Listeriolysin O. ActA
Mycobacterium tuberculosis	tuberculosis	Yes	mainly macrophages	membrane bound compartment	T7SS (ESX)
Rickettsiae	Rocky Mountain spotted fever, typhus, etc	yes, but mainly endothelial cells	primarily vascular endothelial	cytosol	Various
Salmonella enterica	typhoid fever, gastroenteritis	Yes	dendritic cells, gut epithelial cells	late endosomal compartment	T3SS
Shigella flexneri	Diarrhea	poorly if at all	mainly intestinal epithelial cells	cytosol	T3SS

[a]Abbreviations are as follows: T3SS, type III secretion system; T4SS, type IV secretion system; T6SS, type VI secretion system; T7SS, type VII secretion system.

It has been reported that *Mycobacterium tuberculosis* (Mtb), the causative agent of tuberculosis, is able to downregulate IL-12 expression and thereby reduces optimal Th1 differentiation and subsequent IFNγ production (Chandran et al., 2015). Another study has also demonstrated that Mtb exploits different molecular strategies to switch off the immune system by downregulating host genes that are involved in pathogen sensing, phagocytosis, degradation within the phagolysosome, and antigen processing and presentation, thus contributing to increase intracellular survival and subsequent replication (von Both et al., 2018). Remarkably, Mtb has been pointed as a microorganism that developed a myriad of genetic and epigenetic reprogramming strategies to interfere with the macrophage activation status, thus promoting an M2 activation state, which is more favorable for its survival and replication (Chandran et al., 2015; von Both et al., 2018). In fact, it has been suggested that some pathogenic bacteria have the ability to directly influence the polarization and the metabolism of macrophages to suit their own metabolic needs, whereas other bacteria exploit the pre-existing diversity of macrophages to find a metabolically optimal niche of replication. Several studies have suggested that intracellular bacteria such as *L. monocytogenes, S. Typhimurium,* and *Francisella tularensis* can induce an M2 activation state in host macrophages and/or establish its niche of infection in M2 macrophages (Abdullah et al., 2012; Eisele et al., 2013; Ketavarapu et al., 2008). Interestingly, infection of macrophages with *S. Typhimurium* was shown to induce the expression of PPAR*γ*, which is known to promote M2 activation status in macrophages (Eisele et al., 2013). The induction of an M2 activation state by *S. Typhimurium* has been associated with an enhancement of fatty-acid β-oxidation and OXPHOS activity. The resulting increased levels of unconsumed glucose may allow *Salmonella* to capitalize the glucose for its own consumption (Eisele et al., 2013). On the other hand, the highly activated glycolytic pathway of M1 macrophages may withdraw glucose needed for bacterial metabolism. Another example of a pathogen that preferentially survives and proliferates within M2 macrophages is *Brucella abortus*, which also explores the abundance of glucose, characteristic of this activation state, for its consumption (Xavier et al., 2013). Similarly, M2 macrophages have also been considered a preferred replicative niche for *Chlamydophila pneumonia*, which contrasts with the complete

incapacity of the bacteria to proliferate within M1 macrophages, demonstrating that macrophage polarization also plays a role in *C. pneumonia* proliferation (Buchacher et al., 2015).

However, manipulation of the macrophage activation state and metabolic environment are not the only strategies employed by pathogens to survive and proliferate within phagocytic cells. In fact, the ability of Mtb to block the recruitment of inducible nitrite oxide synthase to the phagosomal membrane, which possibly limits the exposure to nitric oxide and subsequent reduces bacterial killing, has also been demonstrated (Davis et al., 2007). Moreover, it has been reported that Mtb interferes with intracellular signaling pathways in order to inhibit the phagolysosome fusion, which results in the ability of virulent Mtb to persist within the immature phagosomal compartment, protecting itself from the microbicidal challenges within macrophages (Deretic et al., 2006; Sun et al., 2010; Vergne et al., 2005). Inhibition of the lysosome fusion with the phagosome has also been highlighted as a tool developed by other pathogens such as *Salmonella*, *Legionella*, and the *chlamydiae* to prevent the discharge of lysosomal contents into the phagosome environment, thus shielding the bacteria (Buchmeier and Heffron, 1991; Eissenberg and Wyrick, 1981; Fernandez-Moreira et al., 2006). In *Chlamydia*, elements of the bacterial cell wall have been suggested to play a role in the modification of the phagosome membrane to avoid fusion with the lysosome (Eissenberg and Wyrick, 1981). Moreover, it has also been suggested that intracellular bacterial pathogens may be able to translocate effector protein(s) before or shortly after internalization that specifically counteracts the antimicrobial activities (e.g., ROS or reactive nitrogen intermediates) escaping macrophage immune defenses (Price and Vance, 2014).

Thus, despite the well-characterized antimicrobial activity of macrophages, several successful pathogens devote considerable genetic and energetic resources in diverse strategies to suppress or escape macrophage defenses. Consequently, macrophages should not be envisioned as simple antimicrobial effector cells, but instead as a permissive niche that provides a diversity of metabolic and cellular states for intracellular pathogens to survive, replicate and disseminate infection (Price and Vance, 2014).

I.3 | Thesis scope

Vector-borne infectious diseases are emerging or resurging worldwide, being responsible for more than 17% of all infectious diseases and 700 000 deaths annually, thus contributing for a significant fraction of the global infectious disease burden (Source: World Health Organization (WHO), 2017). Rickettsioses are listed among the globally emerging communicable diseases and are expected to result in a burden factor in public health, due to behavioral changes (increasing traveling and recreational activities associated with nature), climate changes, expanding cohorts of immunocompromised individuals, and aging societies (ECDC, 2013). In addition to the emerging character of rickettsioses, difficulties associated with diagnostics, lack of a protective vaccine, life-threating nature of some forms of the disease, and the potential use of *Rickettsia* as bioterrorism weapons strengthen the need to better understand the pathogenesis of the disease.

Although it is long known that different rickettsial species are responsible for very distinctive clinical onsets, the molecular determinants that contribute to differences in pathogenicity between rickettsial species remain elusive. While endothelial cells have long been considered the primary target for rickettsiae, infection of certain immunoregulatory cells (macrophages and peripheral monocytes), parenchymal cells (hepatocytes), and perivascular smooth muscle have also been reported (Schroeder et al., 2016). However, very little is still known about the contribution of the interaction between rickettsiae and cells other than the endothelium for the pathogenesis and complications of rickettsial diseases.

Therefore, the present study is focused on bringing new insights into the molecular details governing rickettsiae-macrophage interactions and their potential contribution to the pathogenesis of rickettsial diseases.

Successful intracellular bacterial pathogens are characterized by their ability to escape macrophage killing and establish a niche of infection within these phagocytic cells (Price and Vance, 2014). In line with this, our first goal with this study was to evaluate the ability of two SFG *Rickettsia* species, associated with distinct degrees of pathogenicity to humans, to establish an infection in THP-1 macrophages. As our working models, we have used *R. conorii*, which is one of the most pathogenic *Rickettsia* species to humans and endemic in Europe, and *R. montanensis*

which has not been associated with disease. In Chapter II, we explore the behavior of these two SFG *Rickettsia* species through the discrete steps of an *in vitro* infection, which includes the ability of the bacteria to bind to the target cell, invade, and once in the intracellular environment, escape macrophage intracellular defenses and subsequently survive and proliferate.

Sensing of a pathogen by the host cell and the subsequently activated signaling cascades have been correlated with the intracellular fate of intracellular pathogens. To start dissecting the molecular determinants that may help to explain the drastic differences in the intracellular fate of these two SFG *Rickettsia* species in THP-1 macrophages (observed in Chapter II), we employed a pharmacological study to evaluate the early signaling events involved in rickettsiae-macrophage interactions. The goal of this study was to assess the differences (if any) in the host factors required for invasion of *R. conorii* and *R. montanensis* in these phagocytic cells. Chapter III compiles these results, where we have highlighted several host proteins that play a role in the entry process of the two SFG *Rickettsia* species in THP-1 macrophages.

To better understand the molecular factors that contribute for the different intracellular fates of *R. conorii* and *R. montanensis* in macrophage-like cells (proliferation vs. death, respectively), we have next employed comprehensive transcriptomic profiling of early host cell responses to infection by RNA sequencing (RNA-Seq). The goal of this analysis was to understand how THP-1 macrophages respond transcriptionally to infection by SFG *Rickettsia* species: how the cells respond to fight the infection as well as if and which host transcriptional programs are modulated by the pathogenic rickettsiae to establish a replicative niche. A detailed analysis of the observed host transcriptomic alterations and the contribution of this modulation for the successful establishment of a rickettsial infection within macrophages is presented and discussed in Chapter IV.

Substantial alterations in the protein content of THP-1 macrophages are also expected to occur upon infection with rickettsial species, that may likely reflect differential macrophage responses to either favor (*R. conorii*) or restrict (*R. montanensis*) intracellular bacterial proliferation. To gain deeper insights into the molecular mechanisms underlying these responses, we have employed a label-free quantitative proteomics approach (SWATH-MS) (sequential window

acquisition of all theoretical mass spectra) to profile proteomic alterations that occur upon infection of THP-1 macrophages with *R. conorii* and *R. montanensis*. The detailed analysis of the differential proteomic signatures triggered by these two SFG *Rickettsia* species and the potential impact of these host responses for the establishment (or not) of a stable niche is presented and discussed in Chapter V.

We expect that the results from this integrative study may contribute to expanding our understanding of the complex network of rickettsiae-macrophage interactions and may provide new insights into the potential role of macrophages in rickettsial pathogenesis.

Chapter II

Differences in intracellular fate of two spotted fever group *Rickettsia* in macrophage-like cells

The work presented in this chapter has been published with the following reference:

Curto, P., Simões, I., Riley, S.P., Martinez, J.J. 2016. Differences in Intracellular Fate of Two Spotted Fever Group Rickettsia in Macrophage-Like Cells. Front. Cell. Infect. Microbiol. 6:80. doi: 10.3389/fcimb.2016.00080

II.1 | Abstract

Spotted fever group (SFG) rickettsiae are recognized as important agents of human tick-borne diseases worldwide, such as Mediterranean spotted fever (*R. conorii*) and Rocky Mountain spotted fever (*R. rickettsii*). Recent studies in several animal models have provided evidence of non-endothelial parasitism by pathogenic SFG *Rickettsia* species, suggesting that the interaction of rickettsiae with cells other than the endothelium may play an important role in pathogenesis of rickettsial diseases. These studies raise the hypothesis that the role of macrophages in rickettsial pathogenesis may have been underappreciated.

Herein, we evaluated the ability of two SFG rickettsial species, *R. conorii* (a recognized human pathogen) and *R. montanensis* (a non-virulent member of SFG) to proliferate in THP-1 macrophage-like cells, or within non-phagocytic cell lines. Our results demonstrate that *R. conorii* was able to survive and proliferate in both phagocytic and epithelial cells *in vitro*. In contrast, *R. montanensis* was able to grow in non-phagocytic cells, but was drastically compromised in the ability to proliferate within both undifferentiated and PMA-differentiated THP-1 cells. Interestingly, association assays revealed that *R. montanensis* was defective in binding to THP-1-derived macrophages; however, the invasion of the bacteria that are able to adhere did not appear to be affected. We have also demonstrated that *R. montanensis* which entered into THP-1-derived macrophages were rapidly destroyed and partially co-localized with LAMP-2 and cathepsin D, two markers of lysosomal compartments. In contrast, *R. conorii* was present as intact bacteria and free in the cytoplasm in both cell types.

These findings suggest that a phenotypic difference between a non-pathogenic and a pathogenic SFG member lies in their respective ability to proliferate in macrophage-like cells, and may provide an explanation as to why certain SFG rickettsial species are not associated with disease in mammals.

II.2 | Introduction

Rickettsiae are small Gram-negative, obligate intracellular α-proteobacteria transmitted to humans through arthropod vectors (Hackstadt, 1996). The rapid increase in *Rickettsia* genome sequences allowed their classification into several distinct genetic groups including the ancestral group (AG), spotted fever group (SFG), typhus group (TG), and transitional group (TRG) (Fournier and Raoult, 2009; Gillespie et al., 2008; Goddard, 2009; Weinert et al., 2009). Many rickettsial species belonging to the TG and SFG are pathogenic to humans, causing serious illness such as epidemic typhus (*Rickettsia prowazekii*), Rocky Mountain spotted fever (RMSF) (*Rickettsia rickettsii*), and Mediterranean spotted fever (MSF) (*Rickettsia conorii*) (Parola et al., 2005; Walker, 2007; Walker and Ismail, 2008). However, it has been reported that members of each group can drastically differ in their ability to cause disease (Uchiyama, 2012; Wood and Artsob, 2012). The SFG *Rickettsia* species, *R. montanensis,* has been detected in *Dermacentor variabilis* ticks throughout the United States and Canada, but is considered an organism with limited or no pathogenicity to humans (Ammerman et al., 2004; Carmichael and Fuerst, 2010; McQuiston et al., 2012). A previous report has demonstrated that prior exposure to *R. montanensis* may confer protective immunity to mammalian hosts that are subsequently infected by *R. rickettsii*, possibly by preventing these mammals from becoming amplifying hosts for virulent rickettsial species (Moncayo et al., 2010). Conversely, *R. conorii* the causative agent of MSF (considered as a highly pathogenic organism) is associated with morbidity, and fatality rates varying from 21% to 33% in Portugal (de Sousa et al., 2003; Galvao et al., 2005; Walker, 1989). MSF is endemic to Southern Europe, North Africa and India (Rovery et al., 2008); however, recent evidence has unveiled that MSF exhibits an expansive geographic distribution, now including central Europe and central and southern Africa (Wood and Artsob, 2012).

Although the progression of rickettsial diseases in humans has been the subject of several studies over the last years, the underlying mechanisms that are responsible for differences in pathogenicity by different rickettsiae species are still to be understood. The establishment of a successful infection by a pathogen involves the recognition and invasion of target cells in the host, adaptation to the intracellular environment, replication, and ultimately dissemination within the host

(Walker and Ismail, 2008). Although endothelial cells have long been considered the main target cells for rickettsiae, infection of monocytes/macrophages and hepatocytes has also been previously reported (Walker et al., 1997; Walker and Gear, 1985; Walker et al., 1999; Walker et al., 1994). Additionally, mouse and Rhesus macaque models of SFG *Rickettsia* infection have provided evidence of non-endothelial parasitism by *R. conorii* and *R. parkeri*, respectively (Banajee et al., 2015; Riley et al., 2016). Using C3H/HeN mice as a fatal murine model of MSF, *Riley et al.* have demonstrated evidence of numerous bacteria within the cytoplasm of macrophages and neutrophils, both in tissues and within the blood circulation. In the Rhesus macaque model, *R. parkeri* was present at cutaneous inoculation sites, primarily within macrophages and occasionally neutrophils. These results suggest that the interaction of rickettsiae with cells other than the endothelium may play an important role in the pathogenesis of rickettsial diseases, and is an underappreciated aspect of rickettsial biology. There are a few reports studying the interaction of different rickettsial species with macrophages *in vitro* (Feng and Walker, 2000; Gambrill and Wisseman, 1973a, b); however, the role of macrophages in rickettsial pathogenesis remains to be clarified. Therefore, more studies are required to better understand the biological function of macrophages during rickettsial infections.

In this work, we report that *R. conorii,* a pathogenic member of SFG rickettsiae, is able to invade and proliferate within THP-1-derived macrophages, whereas *R. montanensis*, a non-pathogenic member of SFG *Rickettsia*, is drastically compromised in the ability to proliferate within these cells. These findings suggest that the intracellular fate in macrophages may provide an explanation as to why certain SFG rickettsial species are not associated with disease.

II.3 | Materials and Methods

II.3.1 | Cell lines, *Rickettsia* growth and purification

Vero and EA.hy926 cells were grown in Dulbecco's modified Eagle's medium (DMEM) (Gibco) supplemented with 10% heat-inactivated fetal bovine serum (Atlanta Biologicals), 1x non-essential amino acids (Corning), and 0.5 mM sodium pyruvate (Corning). THP-1 (ATCC TIB-202^{TM}) cells were grown in RPMI-1640 medium (Gibco) supplemented with 10% heat-inactivated fetal bovine serum. Differentiation of THP-1 cells into macrophage-like cells was carried out by the addition of 100 nM of phorbol 12-myristate 13-acetate (PMA) (Fisher). Cells were allowed to differentiate and adhere for 3 days prior to infection. All cell lines were maintained in a humidified 5% CO_2 incubator at 34 ºC. *R. conorii* isolate Malish7 and *R. montanensis* isolate M5/6 were propagated in Vero cells and purified as previously described (Ammerman et al., 2008; Chan et al., 2009; Chan et al., 2011)

II.3.2 | Antibodies

Anti-Rc$_{PFA}$, rabbit polyclonal antibody that recognizes *R. conorii*, was generated as previously described (Cardwell and Martinez, 2012; Chan et al., 2011). Anti-*Rickettsia* rabbit polyclonal antibody that recognizes *R. montanensis* (NIH/RML I7198) was kindly provided by Dr. Ted Hackstadt (Rocky Mountain Laboratories). Alexa Fluor 488- and 546-conjugated goat anti-rabbit IgG, Texas Red-X-phalloidin, and DAPI (4', 6'-diamidino-2-phenylindole) were purchased from Thermo Scientific. Anti-LAMP2 [H4B4] and anti-cathepsin D [CTD19] antibodies were purchased from Abcam.

II.3.3 | Assessment of *Rickettsia* growth dynamics

Growth curves were performed by inoculating *R. conorii* and *R. montanensis* at a multiplicity of infection (MOI) of 2.5 into Vero, EA.hy926, or PMA-differentiated THP-1 cells monolayers at a confluency of 2 x 10^5 cells per well, in 24 well plates, with 3 wells infected for each day of the growth curve. Plates were centrifuged at 300 x g for 5 minutes at room temperature to induce contact between rickettsiae and host cells, and incubated at 34 ºC and 5% CO_2. At each

specific time point post inoculation, cells were scraped and samples were stored in PBS at -80 ºC. For undifferentiated THP-1 cells, 2 x 10^5 cells were infected with *R. conorii* and *R. montanensis* at a multiplicity of infection (MOI) of 2.5 in a total volume of 100 µL. Samples were centrifuged at 300 x g for 5 minutes at room temperature to induce contact between rickettsiae and host cells, and then transferred to 96 well plates and incubated at 34 ºC and 5% CO_2 (3 samples infected for each day of the growth curve). At each specific time point post inoculation, samples were stored in PBS at -80 ºC. Genomic DNA was extracted using the PureLink Genomic DNA kit (Life Technologies) according to the manufacturer's instructions. The extracted DNA was subjected to quantitative PCR analysis using LightCylcer 480 II (Roche). Bacterial growth was queried by quantitative PCR using TaqMan Master Mix at 95 ºC, with a 10 min incubation followed by 50 cycles of 95 ºC 15 sec and 58 ºC 1 min. The rickettsial *sca1* gene was amplified using the primers sca1-F, sca1-R and Sca1-Fam and the mammalian *actin* gene was amplified using the primers actin-F, actin-R and actin-Hex(Vic) **(Table II.1)**. Growth is presented as the ratio of *sca1* versus *actin*. All unknowns were quantified by ΔΔCt as compared to molar standards. Experiments were done in triplicate with duplicates for each experiment.

Table II.1 | Primers and probes used in q-PCR assays.

Primer name	Primer sequence	Concentration of primer or probe in PCR reaction
Actin-F420	5'-CCTGTATGCCTCTGGTCGTA-3'	300 nM
Actin-R681	5'-CCATCTCCTGCTCGAAGTCT-3'	300 nM
Actin-Hex	5'-/5MAXN/ACTGTGCCC/ZEN/ATCTAC-3'	200 nM
Sca1-F5271	5'-CAAGCTCGTTATTACCCCGAAT-3'	300 nM
Sca1-R5371	5'-CTACCGCTCCTTGGAATGTTAGACC -3'	300 nM
Sca1-Fam	5'-/56-FAM/TCGGCTTAA/ZEN/GATACGGGAAGT-3'	200 nM

Growth dynamics were also assessed by immunofluorescence. Briefly, PMA-differentiated THP-1, Vero, and EA.hy926 cells were seeded onto glass coverslips in 24-well plates at 2 x 10^5 cells per well. Infections were performed as described above. At each indicated time point post inoculation, infected monolayers were washed with PBS and fixed in 4% paraformaldehyde (PFA) for 20 minutes. For undifferentiated THP-1 cells, the cells were harvested, washed with PBS,

attached to slides by centrifugation (800 rpm, 8 minutes), and cells were fixed in 4% PFA for 20 minutes. All samples were then permeabilized with 0.1% Triton X-100 and blocked with 2% BSA. *R. conorii* growth dynamics were assessed by staining with anti-Rc$_{PFA}$ (1:1,000) followed by Alexa Fluor 488-conjugated goat anti-rabbit IgG (1:1,000), DAPI (1:1,000), and Texas Red-X-phalloidin (1:200). For *R. montanensis*, staining was carried out with NIH/RML I7198 (1:1,500) followed by Alexa Fluor 488-conjugated goat anti-rabbit IgG (1:1,000), DAPI (1:1,000) and Texas Red-X-phalloidin (1:200). After washing with PBS, glass coverslips were mounted in Mowiol mounting medium and preparations were viewed on a LEICA DM 4000 B microscope equipped with Nuance FX multispectral imaging system using a final X100 optical zoom and processed with Image J software.

II.3.4 | Electron microscopy

For transmission electron microscopy, 12 wells of PMA-differentiated THP-1 cells in 6 well plates were inoculated with *R. conorii* (MOI=2.5). After 5 days in culture, cells were scraped, centrifuged at 10,000 x g for 7 minutes at room temperature and washed with PBS. After this washing step, cells were centrifuged under the same conditions, fixed in primary fixative solution (1.6% paraformaldehyde, 2.5% glutaraldehyde, 0.03% $CaCl_2$ in 0.05 M cacodylate buffer, pH 7.4), pelleted, and embedded in 3% agarose. Agar blocks were cut in 1 mm^3 cubes and transferred to a fresh portion of the fixative for 2 hours at room temperature. Samples were then washed in 0.1 M cacodylate buffer supplemented with 5% sucrose, postfixed in 1% osmium tetroxide for 1 hour, washed in water, and in-block stained with 2% uranyl acetate in 0.2 M sodium acetate buffer, pH 3.5. Specimens were dehydrated in ascending ethanol series and propylene oxide, and embedded in Epon-Araldite mixture. Blocks were sectioned with the Ultratome Leica EM UC7. Thin (80 nm) sections were stained with lead citrate for 5 min and examined in JEOL JEM 1011 microscope with the attached HAMAMATSU ORCA-HR digital camera. All reagents for electron microscopy were from EMS (Hatfield, PA).

II.3.5 | Cell association and invasion assays

Cell association and invasion assays were performed as previously described with some modifications (Martinez and Cossart, 2004). Briefly, mammalian cells (THP-1 and Vero) were seeded on glass coverslips in 24-well plates at 2 x 10^5 cells per well. PMA-differentiated THP-1 and Vero cells were infected with *R. conorii* and *R. montanensis* (MOI = 10), the plates were centrifuged at 300 x g for 5 minutes at room temperature to induce contact, and subsequently incubated for 60 minutes at 34 ºC and 5% CO_2. Infected monolayers were washed 1x with 1 mL PBS, and fixed in 4% PFA for 20 minutes prior to staining. For cell association assays, after permeabilization with 0.1% Triton X-100 and blocking with 2% BSA, *R. conorii* were stained with anti-Rc_{PFA} (1:1,000) followed by Alexa Fluor 488-conjugated goat anti-rabbit IgG, DAPI (1:1,000) and Texas Red-X-phalloidin (1:200). For *R. montanensis,* staining was carried out with NIH/RML I7198 antibody (1:1,500) followed by Alexa Fluor 488-conjugated goat anti-rabbit IgG, DAPI (1:1,000) and Texas Red-X-phalloidin (1:200). Experiments were done in triplicate and results of each experiment were expressed as the ratio of rickettsiae cells to mammalian cells (nuclei). At least 200 nuclei were counted for each experiment. For invasion assays, infected monolayers were processed for differential staining to distinguish between extracellular and intracellular rickettsia. Briefly, extracellular *R. conorii* were stained with anti-Rc_{PFA} (1:1,000) followed by Alexa Fluor 546-conjugated goat anti-rabbit IgG (1:1,000), prior to permeabilization of the mammalian cells with 0.1% Triton X-100. After permeabilization, the total *R. conorii* cells were then stained with anti-Rc_{PFA} (1:1,000) followed by Alexa Fluor 488-conjugated goat anti-rabbit IgG (1:1,000). Invasion assays of *R. montanensis* were assessed using the same procedure, and *R. montanensis* staining was carried out with NIH/RML I7198 antibody (1:1,500). Bacteria staining positive for Alexa Fluor 546-conjugated goat anti-rabbit IgG were considered as external while bacteria stained for both secondary antibodies were considered as total bacteria present. The number of internalized rickettsiae was determined by the difference between total and external rickettsiae, and results are expressed as percentages of internalized rickettsiae. As for association assays, experiments were done in triplicate with at least 200 nuclei for each experiment. Images were digitally captured with an OLYMPUS IX71 inverted microscope (Tokyo, Japan) equipped with an OLYMPUS DP72

camera (Tokyo, Japan) using a final X40 optical zoom. Rickettsiae and mammalian nuclei were counted using the cell counter analysis tool from ImageJ (http:/rsb.info.nih.gov/ij). Statistical analysis was performed by unequal variance *t*-test (Welch's *t*-test) using Prism software package (GraphPad Software Inc).

II.3.6 | LAMP-2 and cathepsin D immunostaining and confocal microscopy

Mammalian cells (THP-1 and Vero) were seeded into 24-well plates under coverslips for a cell confluency of 2 x 10^5 cells per well. PMA-differentiated THP-1 and Vero cells were infected with *R. conorii* and *R. montanensis* (MOI = 10), the plates centrifuged at 300 x g for 5 minutes at room temperature to induce contact, and subsequently incubated for 60 minutes or 24 hours at 34 ºC and 5% CO_2. Infected monolayers were washed with PBS, and fixed in 4% PFA for 20 minutes prior to staining. After permeabilization, the cells were incubated with primary antibodies anti-Rc_{PFA} (1:1,000) (*R. conorii*); NIH/RML I7198 antibody (1:1,500) *(R. montanensis)*, and mouse anti-LAMP-2 (1:100) or anti-cathepsin D (1:5,500) (lysosome markers), followed by Alexa Fluor 546-conjugated goat anti-rabbit IgG (1:1,000) and Alexa Fluor 488-conjugated goat anti-mouse (IgG) (1:1,000). Images were acquired using a confocal laser scanning microscope Leica TCS SP2 microscope with a ×100 oil immersion objective and processed using ImageJ software. Analysis of fluorescence intensity was performed with the RGB profiler plugin within the ImageJ software package (https://imagej.nih.gov/ij/).

II.4 | Results

II.4.1 | *R. conorii* is able to invade and grow inside macrophage-like cells

Infection of endothelial cells by spotted fever group (SFG) rickettsiae has been previously reported by several groups (Bechah et al., 2008c; Colonne et al., 2011; Walker, 1997; Walker et al., 1994). In addition, evidence of non-endothelial parasitism of *R. conorii in vivo* has also been recently reported, suggesting that the interaction with cells other than endothelial cells could be relevant to rickettsial pathogenesis (Riley et al., 2016). To further evaluate the growth dynamics of *R. conorii* in macrophage-like cells, human THP-1 monocytes were differentiated into macrophages by incubation with PMA, and infected with *R. conorii* at a MOI of 2.5. Samples were collected from these cultures at several time-points post inoculation, and total genomic DNA was extracted. As illustrated in **Figure II.1A**, q-PCR analysis of the ratio of *R. conorii* (*sca1*) to Vero (*actin*) DNA content clearly demonstrated that *R. conorii* was able to grow in PMA-differentiated THP-1 cultures. This successful ability of *R. conorii* to proliferate in THP-1-derived macrophages was also confirmed by immunofluorescence microscopy of cells 3 days post inoculation, with the clear presence of anti-Rc_{PFA}-positive intact bacteria dispersed within the mammalian cells **(Figure II.1B)**.

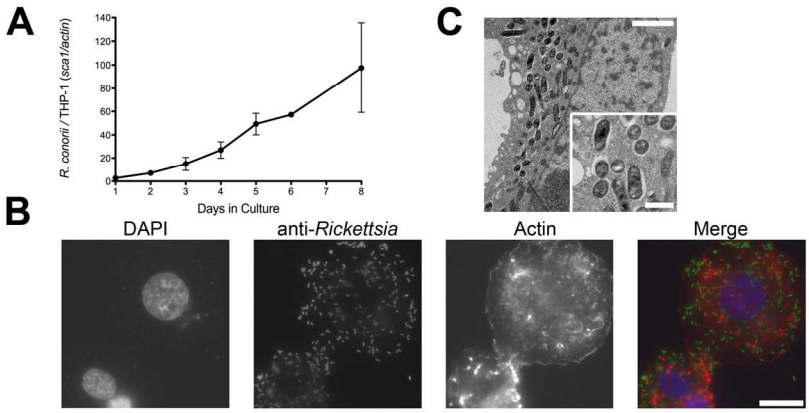

Figure II.1 | Ability of *R. conorii* to invade and proliferate within THP-1-derived macrophages. **(A)** PMA-differentiated THP-1 cells were infected with *R. conorii* and genomic DNA was extracted at different time-points after infection. Quantitative PCR data are expressed as the ratio of *R. conorii sca1* versus *actin* DNA content. **(B)** Immunofluorescence microscopy of THP-1-derived macrophages cells infected with *R. conorii* at 3 days post-infection. Cells were stained with DAPI (blue) to identify host nuclei, Phalloidin (red) to stain actin and anti-*Rickettsia* antibody (RcPFA) followed by Alexa Fluor 488 (green) to identify *R. conorii*. Scale bar = 10 µm. **(C)** Ultrastructure of THP-1-derived macrophages after 5 days post inoculation with *R. conorii* by transmission electron microscopy (TEM). Scale bar = 2 µm (top) and 500 nm (bottom).

To evaluate in more detail the morphology of *R. conorii* in THP-1-derived macrophages, transmission electron microscopy (TEM) was carried out. At day 5 post inoculation, TEM images confirmed the presence of intact bacteria spread throughout the cytoplasm of the cells **(Figure II.1C).** Interestingly, most of these bacteria displayed a normal morphology, and were not surrounded by membranes or phagolysosome-like structures but free in the cytoplasm, with an electron-lucent zone adjacent to the bacterial membrane. These results clearly indicate that *R. conorii* is able to survive and proliferate in the hostile environment of THP-1-derived macrophages.

II.4.2 | *R. montanensis* is able to grow in non-phagocytic mammalian cells but not in human macrophage-like cells

Rickettsia montanensis has traditionally been considered a nonpathogenic member of the SFG rickettsiae, and only a limited number of human infections have been previously reported with this organism (McQuiston et al., 2012). We sought to determine if *R. montanensis* would behave similarly to *R. conorii* and proliferate within epithelial and macrophage-like cells. Both THP-1-derived macrophages and Vero cells were infected with *R. montanensis* at a MOI of 2.5, and samples were collected from these cultures at several time-points post-inoculation for q-PCR analysis. As previously described, the ratio of *R. montanensis* (*sca1*) to mammalian cell (*actin*) DNA content was used to evaluate the growth dynamics of *R. montanensis* in both cell lines over time.

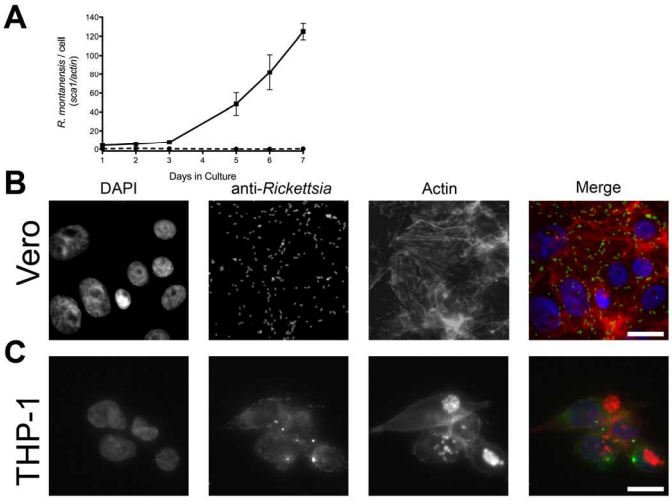

Figure II.2 (previous page) | *R. montanensis* is able to grow inside epithelial cells (Vero) but not in THP-1 derived macrophages. (A) PMA-differentiated THP-1 cells (dashed lines) and Vero cells (solid lines) were infected with *R. montanensis,* and genomic DNA was extracted at different time-points after infection. Quantitative PCR data are expressed as the ratio of *R. montanensis sca1* versus *actin* DNA content. **(B** and **C)** Immunofluorescence microscopy of Vero cells (B) and THP-1-derived macrophages (**C**) infected with *R. montanensis* at 3 days after infection. Cells were stained with DAPI (blue) to stain host nuclei, Phalloidin (red) to stain actin and rabbit anti-*Rickettsia* polyclonal antibody NIH/RML I7198 followed by Alexa Fluor 488 (green) to stain *R. montanensis*. Scale bar = 10 µm.

As shown in **Figure II.2A**, *R. montanensis* was able to grow in Vero cells, but was not able to proliferate in THP-1-derived macrophages. These results were also confirmed by immunofluorescence microscopy **(Figure II.2B-C)**. Moreover, *R. montanensis* was able to invade and proliferate in the cultured human endothelial cell line, EA.hy926 **(Figure II.3)**.

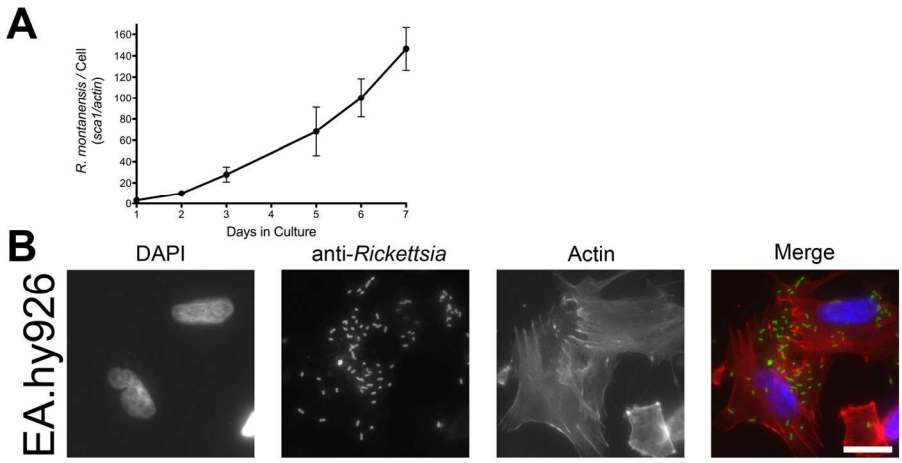

Figure II.3 | Ability of *R. montanensis* to invade and proliferate within human endothelial cells, EA.hy926. (A) EA.hy926 cells were infected with *R. montanensis* and genomic DNA was extracted at different time-points after infection. Quantitative PCR data are expressed as the ratio of *R. montanensis sca1* versus *actin* DNA content. **(B)** Immunofluorescence microscopy of EA.hy926 cells infected with *R. montanensis* at 3 days post-infection. Cells were stained with DAPI (blue) to identify host nuclei, Phalloidin (red) to stain actin and NIH/RML I7198 followed by Alexa Fluor 488 (green) to stain *R. montanensis*. Scale bar = 10 µm.

Fluorescent microscopy analysis of Vero cells infected with *R. montanensis* after 3 days post inoculation revealed intact bacilli dispersed within the host cytoplasm **(Figure II.2B)**; however, few intact bacteria were found after 3 days of inoculation of *R. montanensis* in THP-1-derived macrophages **(Figure II.2C)**. A similar phenotype was also observed when undifferentiated THP-1 cells were infected **(Figure II.4)**.

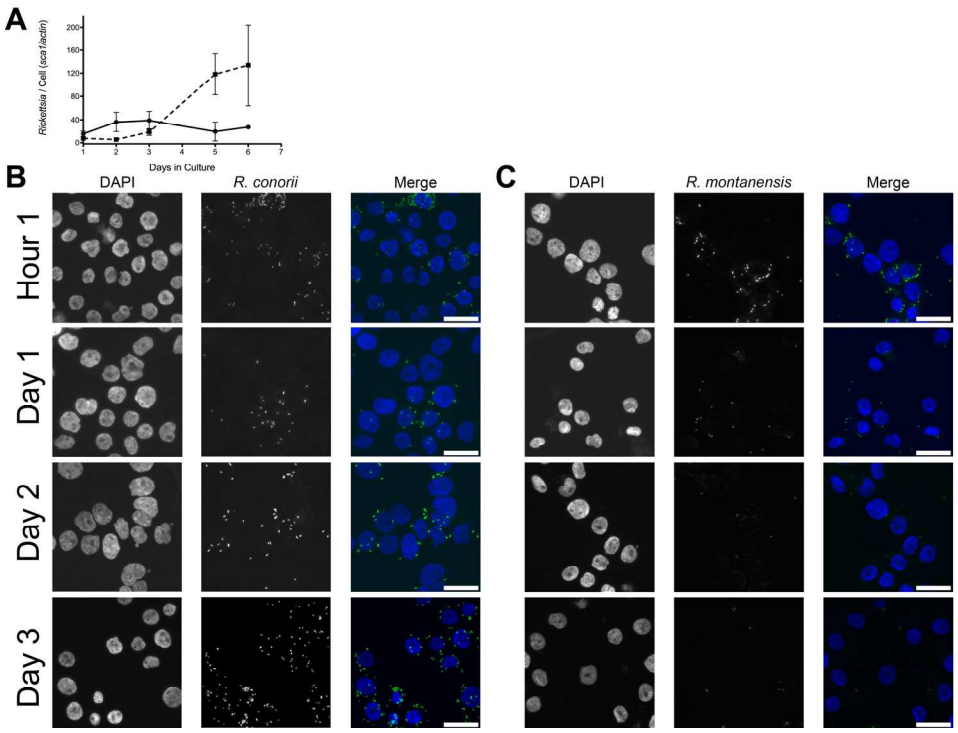

Figure II.4 | *R. conorii* and *R. montanensis* show a different ability to proliferate within undifferentiated THP-1 cells. (A) Undifferentiated THP-1 cells were infected with *R. montanensis* (solid line) and *R. conorii* (dashed line) and genomic DNA was extracted at different time-points after infection. Quantitative PCR data are expressed as the ratio of *R. montanensis* or *R. conorii sca1* versus *actin* DNA content. **(B)** Immunofluorescence microscopy of undifferentiated THP-1 cells infected with *R. conorii* at 1 h, and 1, 2, and 3 days post-infection, respectively. **(C)** Immunofluorescence microscopy of undifferentiated THP-1 cells infected with *R. montanensis* at 1 h, and 1, 2, and 3 days post-infection, respectively. Cells were stained with DAPI (blue) to identify host nuclei, and anti-Rc_{PFA} or NIH/RML I7198, followed by Alexa Fluor 488 (green) to stain *R. conorii* or *R. montanensis*, respectively. Scale bar = 10 µm.

These data demonstrate that there is a difference in the ability of *R. montanensis* to proliferate within both undifferentiated THP-1 cells (monocytic) and THP-1 derived macrophages when compared with other cell types, in contrast to the observed growth of *R. conorii*.

II.4.3 | Binding of *R. montanensis* to THP-1-derived macrophages is compromised but they still can invade

Adherence and subsequent invasion to the target cells is a critical step in the establishment of a successful rickettsial infection (Martinez and Cossart, 2004). We hypothesized that *R. montanensis* may be unable to adhere to and subsequently invade into THP-1-derived

macrophages. To test this, we initially analyzed the adherence capacity of *R. montanensis* in both cell types. Vero and THP-1 cells were inoculated with *R. montanensis* (MOI=10) for 60 minutes, and the ability to associate with cultured mammalian cells *in vitro* was assessed by immunofluorescence and quantification of the ratio of *Rickettsia* cells per mammalian cell nucleus. As shown in **Figure II.5**, the ability of *R. montanensis* to bind to THP-1-derived macrophages was significantly decreased compared to the binding to Vero cells. Representative immunofluorescence microscopy images **(Figure II.5A-B)** confirmed these differences.

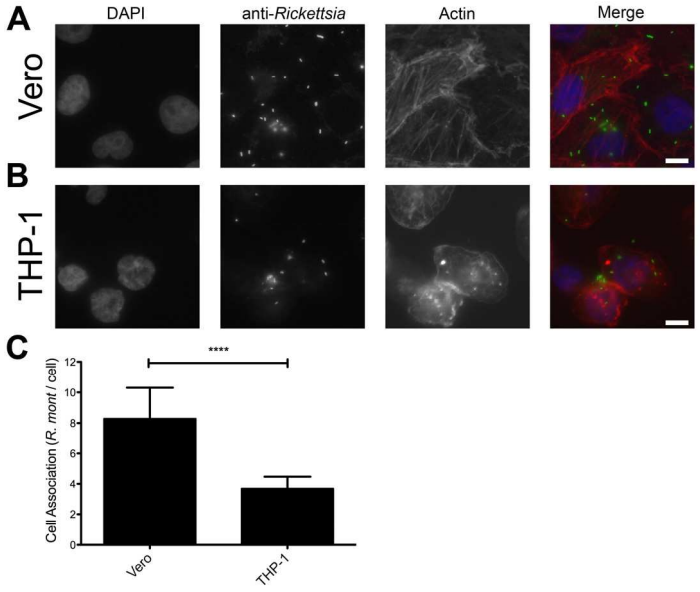

Figure II.5 | *R. montanensis* shows a defect in association with THP-1-derived macrophages. PMA-differentiated THP-1 cells and Vero cells were infected with *R. montanensis* (MOI=10). After 60 min of infection, cells were fixed and stained for immunofluorescence analysis with rabbit anti-*Rickettsia* polyclonal antibody (NIH/RML I7198), followed by Alexa Fluor 488 (green) to stain *R. montanensis*, DAPI to visualize the host nuclei (blue) and Phalloidin to illustrate the host cytoplasm (red). **(A** and **B)** Representative immunofluorescence images of *R. montanensis* association assays in Vero (A) and macrophage-like (B) cells. Each row shows, from left to right nuclei staining, rickettsia staining, actin staining, and the merged image. Scale bar = 10 µm. **(C)** *Rickettsia* and mammalian cells were counted and results are expressed as the ratio of rickettsiae to mammalian cells. At least 200 host nuclei were counted for each experimental condition. Results are shown as the mean ± SD (P values: **** <0.0001).

As a control, association assays with *R. conorii* were also performed in both cell types. Our results suggest that adherence of *R. conorii* to THP-1-derived macrophages was not compromised **(Supplementary Figure II.1)**. Together, these data suggest that *R. montanensis* are defective in binding to THP-1-derived macrophages when compared with their capacity to bind to Vero cells.

We next sought to determine whether the remaining *R. montanensis* cells bound to THP-1 cells were still capable of inducing their internalization into these phagocytic cells. To address this, we performed invasion assays of *R. montanensis* in Vero cells and THP-1-derived macrophages. Similar assays using *R. conorii* were performed as a control. Both species (MOI=10) were used to inoculate each cell-type for 60 minutes. Samples were processed for differential staining to distinguish between extracellular and intracellular rickettsiae that were then quantified to determine the percentage of internalized bacteria. As shown in **Figure II.6**, the invasion rate of *R. montanensis* into THP-1-derived macrophages was not significantly affected when compared with that observed in Vero cells. Although the ability of *R. montanensis* to bind to THP-1-derived macrophages was significantly decreased in the association assays, these results suggest that those bacteria that bind are still able to invade these cells.

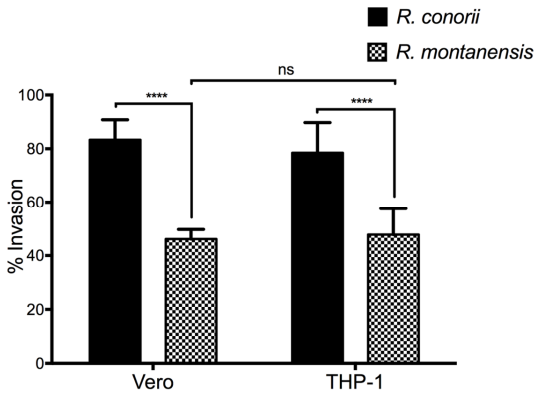

Figure II.6 | Invasion rates of *R. montanensis* into THP-1-derived macrophages is not affected when compared with Vero cells. PMA-differentiated THP-1 cells and Vero cells were infected with *R. montanensis* and *R. conorii* (MOI=10). After 60 min of infection, cells were fixed and processed for differential staining to distinguish between extracellular and intracellular rickettsiae. Results are expressed as percentage of internalized rickettsiae. At least 200 host nuclei were counted for each experimental condition. Results are shown as the mean ± SD (P values: ns – non-significant, **** <0.0001).

II.4.4 | *Rickettsia montanensis* is rapidly destroyed in THP-1-derived macrophages

We next sought to determine whether the observed lack of *R. montanensis* growth in macrophage-like cells could be attributed to destruction in phagolysosomes. Vero and THP-1-derived macrophages were infected with *R. montanensis* at a MOI of 10 for 1 hour and 24 hours, and then processed for immunofluorescence microscopy using antibodies against rickettsiae and

the lysosomal marker, LAMP-2. Again, parallel studies were also performed with *R. conorii* for comparison. Representative slices from z-stack images derived from THP-1 cells at 60 min or 24 h post infection with *R. montanensis* or *R. conorii* are shown in **Figure II.7-8**, respectively, and those from Vero cells are illustrated in **Supplementary Figure II.2-3**, respectively. *Rickettsia montanensis* in THP-1-derived macrophages at 1 hour post-infection do not appear as intact bacteria and at 24 hours post-infection, most of the *Rickettsia*-positive staining results from debris that partially localizes to LAMP-2 positive compartments **(Figure II.7)**. Analysis of the distribution of fluorescence intensity across selected regions in each panel further shows the substantial overlapping of signals, particularly at 24h. In contrast, at 1 hour and 24 hours post infection, *R. montanensis* in Vero cells appear intact with very few bacteria co-localizing with LAMP-2 positive compartments **(Supplementary Figure II.2)**.

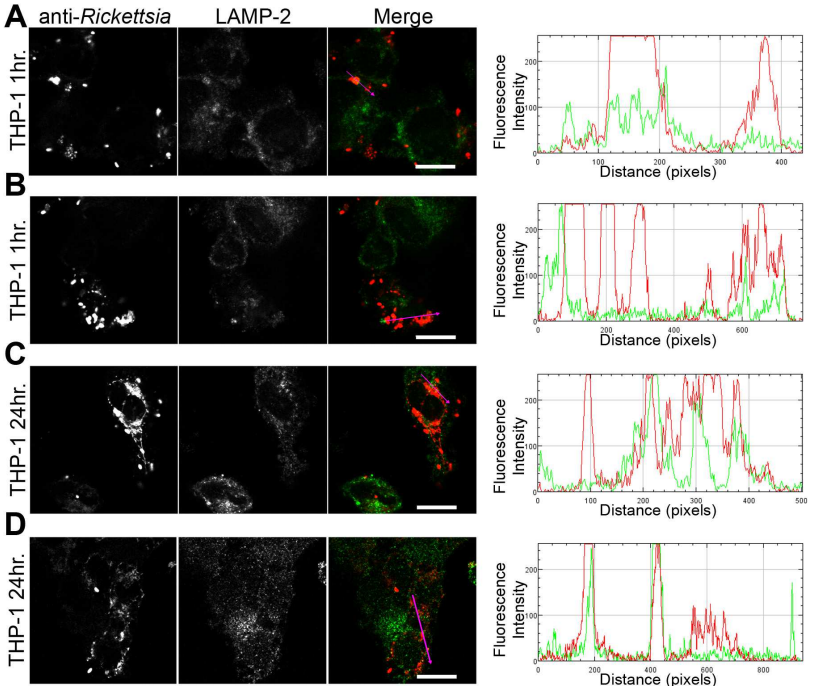

Figure II.7 | *R. montanensis* is rapidly destroyed in THP-1-derived macrophages. THP-1-derived macrophages were infected with *R. montanensis* (MOI=10). At 60 min or 24 h post infection, cells were fixed, permeabilized and double stained for immunofluorescence confocal microscopy analysis with NIH/RML I7198 followed by Alexa Fluor 546 (red) to stain *R. montanensis,* and the monoclonal antibody for LAMP-2, lysosomal membrane protein followed by Alexa Fluor 488 (green). **(A-D)** Representative images of a single slice from the z stacks. THP1-derived macrophages at 60 min post infection (**A** and **B**) and 24 h post infection (**C** and **D**). Each row shows, from left to right, *Rickettsia* staining, LAMP-2 staining, the merged image, and a RGB plot profile illustrating the fluorescence intensity along the magenta arrow. Scale bar = 10 µm. **Supplementary movies II.1-2** represent 360 degrees rotation movie of the 3D projection of the stack images shown in panels 5A and 5C, respectively (digital format).

As a control, either at 60 min or 24 h post infection in THP-1 or Vero cells, *R. conorii* maintain the morphology of intact bacteria, with no significant co-staining with LAMP-2 positive structures, and proliferate within these two cell types as depicted in an increase in rickettsial cells **(Figure II.8 and Supplementary Figure II.3)**.

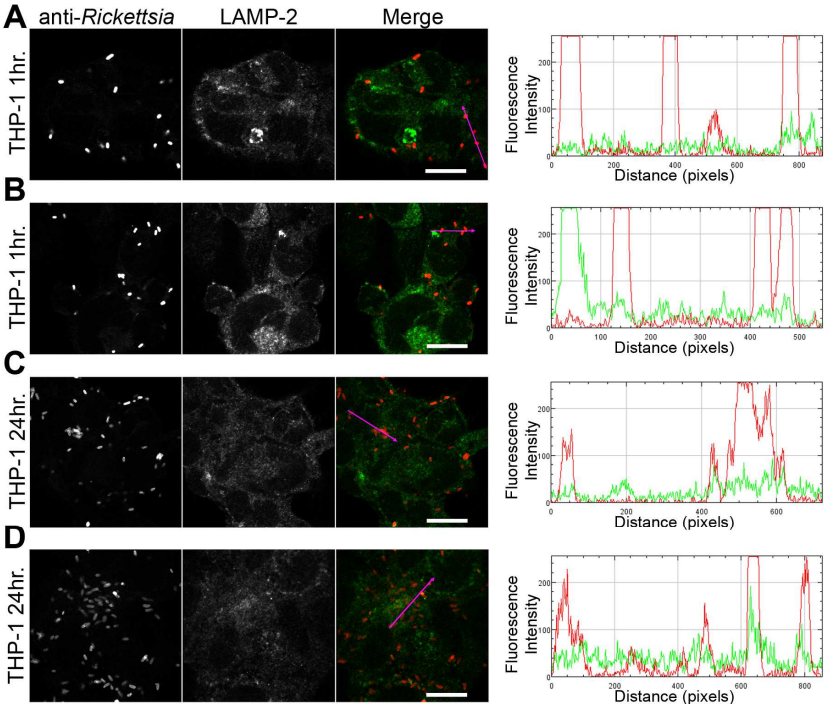

Figure II.8 | *R. conorii* is maintained as morphologically intact bacteria in THP-1-derived macrophages. THP-1-derived macrophages were infected with *R. conorii* (MOI=10). At 60 min or 24 h post infection, cells were fixed, permeabilized and double stained for immunofluorescence confocal microscopy analysis with anti-Rc$_{PFA}$ followed by Alexa Fluor 546 (red) to stain *R. conorii* and the monoclonal antibody for LAMP-2, lysosomal membrane protein followed by Alexa Fluor 488 (green). **(A-D)** Representative images of a single slice from the z stacks. THP1-derived macrophages at 60 min post infection (**A** and **B**) and 24 h post infection (**C** and **D**). Each row shows, from left to right, *Rickettsia* staining, LAMP-2 staining, the merged image, and a RGB plot profile illustrating the fluorescence intensity along the magenta arrow. Scale bar = 10 µm. **Supplementary movies II.5-6** represent 360 degrees rotation movie of the 3D projection of the stack images shown in panels 6A and 6C, respectively (digital format).

These observations were further confirmed when infected THP1-derived macrophages were immunostained with an antibody recognizing the mature form of cathepsin D (Kalamida et al., 2014; Lohoefer et al., 2014), one of the most abundant proteases active in the acidic environment of the lumen of lysosomes **(Figure II.9-10)**. *Rickettsia montanensis*-positive staining is mostly co-

localized with cathepsin D 24 h after infection **(Figure II.9C-D)**, and this is further corroborated by the fluorescence intensity profiles showing substantial overlapping between signals.

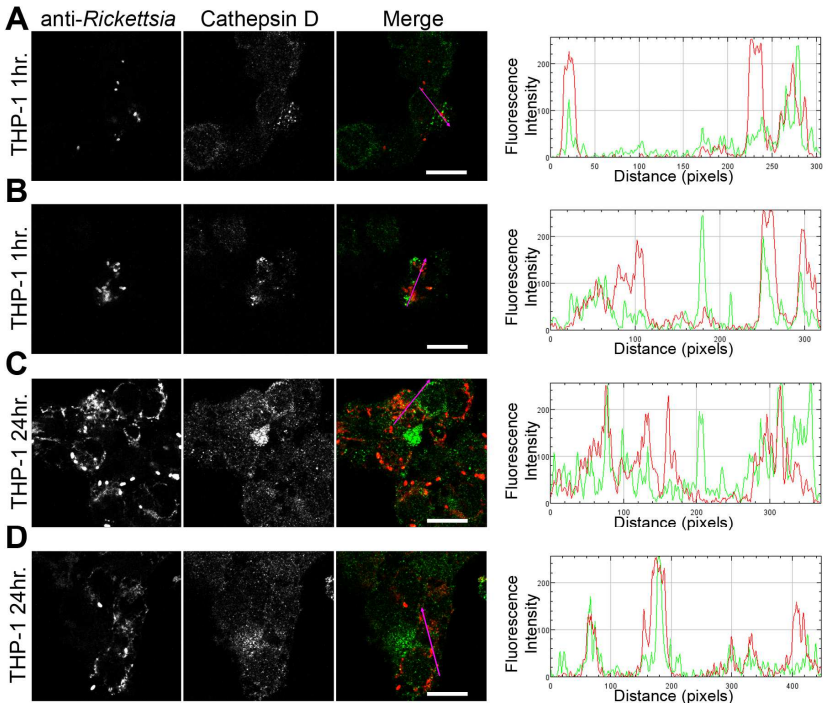

Figure II.9 | *R. montanensis* co-localizes with the lysosomal marker cathepsin D. THP-1-derived macrophages were infected with *R. montanensis* (MOI=10). At 60 min or 24 h post infection, cells were fixed, permeabilized and double stained for immunofluorescence confocal microscopy analysis with NIH/RML I7198 followed by Alexa Fluor 546 (red) to stain *R. montanensis*, and the monoclonal antibody for cathepsin D followed by Alexa Fluor 488 (green). **(A-D)** Representative images of a single slice from the z stacks of THP1-derived macrophages at 60 min post infection (**A** and **B**) and 24 h post infection (**C** and **D**). Each row shows, from left to right, *Rickettsia* staining, cathepsin D staining, the merged image, and a RGB plot profile illustrating the fluorescence intensity along the magenta arrow. Scale bar = 10 µm. **Supplementary movies II.9 -10** represent 360 degrees rotation movie of the 3D projection of the stack images shown in panels 7B and 7C, respectively (digital format).

In contrast, no significant co-staining is observed between *R. conorii* and cathepsin D at the same time point, with the representative fluorescence intensity profiles further illustrating very little superposition of signals **(Figure II.10C-D)**.

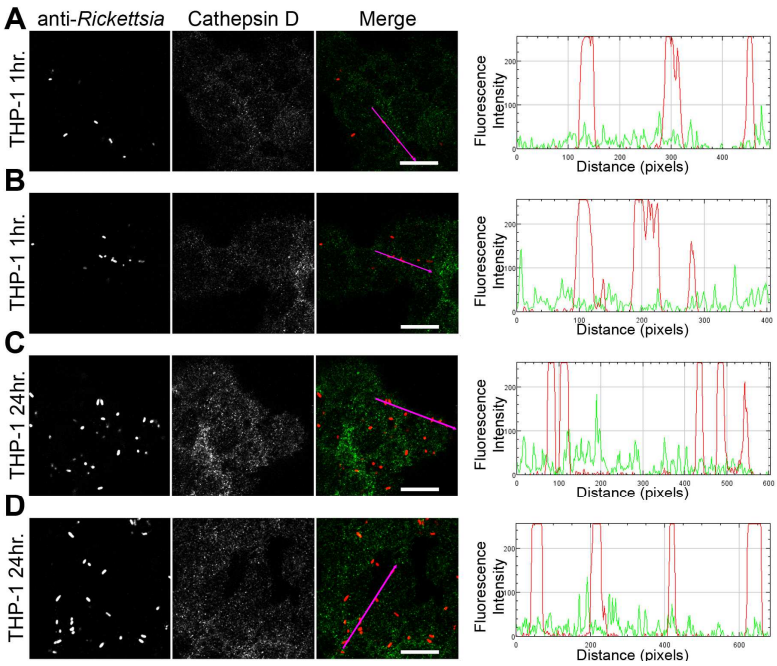

Figure II.10 | *R. conorii* shows no substantial co-localization with the lysosomal marker cathepsin D. THP-1-derived macrophages were infected with *R. conorii* (MOI=10). At 60 min or 24 h post infection, cells were fixed, permeabilized and double stained for immunofluorescence confocal microscopy analysis with anti-Rc$_{PFA}$ followed by Alexa Fluor 546 (red) to stain *R. conorii*, and the monoclonal antibody for cathepsin D followed by Alexa Fluor 488 (green). **(A-D)** Representative images of a single slice from the z stacks of THP1-derived macrophages at 60 min post infection (**A** and **B**) and 24 h post infection (**C** and **D**). Each row shows, from left to right, *Rickettsia* staining, cathepsin D staining, the merged image, and a RGB plot profile illustrating the fluorescence intensity along the magenta arrow. Scale bar = 10 µm. **Supplementary movies II.11-12** represent 360 degrees rotation movie of the 3D projection of the stack images shown in panels 8B and 8D, respectively (digital format).

Taken together, these results demonstrate a difference in the intracellular fate of *R. montanensis* between epithelial and macrophage cell types and may provide a plausible reason as to why this species is not generally considered a human pathogen.

II.5 | Discussion

Differences in pathogenicity and/or virulence between different *Rickettsia* species have been previously reported (Uchiyama, 2012; Wood and Artsob, 2012). Although several genomic, transcriptomic and proteomic studies between rickettsial species with different levels of virulence have been reported aiming to reveal putative virulence factors, no clear evidence of molecular or biochemical determinants explaining such a dramatic difference were unveiled (Bechah et al., 2010; Clark et al., 2015; Ellison et al., 2008; Ge et al., 2003).

In this work, we evaluated the ability of two SFG rickettsiae with different degrees of pathogenicity in mammals to proliferate within macrophage-like cells. The highly pathogenic, *R. conorii,* and the non-pathogenic *R. montanensis,* were used here as our models of study. Interestingly, the ability of these two SFG rickettsiae to proliferate within THP-1-derived macrophages resulted in a dramatic phenotypic difference. *R. conorii* was found to grow well within macrophage-like cells, and TEM images of THP-1-derived macrophages infected with *R. conorii* at 5 days post-inoculation showed that *R. conorii* is free in the cytoplasm of phagocytic cells, displaying a normal morphology and not surrounded by membranes or phagosome-like structures. On the other hand, the ability of *R. montanensis* to grow within macrophage-like cells was compromised, whereas its ability to grow in either an epithelial (Vero) or endothelial cell line (EA.hy926) was not affected. This phenotype prompted us to evaluate in more detail the known crucial steps of a successful rickettsial infection.

For obligate intracellular bacteria, the concept of a successful *in vitro* infection involves several steps including adherence to a target cell, invasion, avoidance of host defenses and adaptation to the host intracellular environment, multiplication and spread to neighboring cells (Walker and Ismail, 2008). Although the *in vitro* infection process of endothelial and epithelial cells by SFG rickettisae is well studied (Martinez and Cossart, 2004; Martinez et al., 2005), little is known about the molecular details governing the interactions between SFG rickettsiae and professional phagocytes such as macrophages. Our studies of fatal infections in murine models of disseminated disease suggest that the interaction of rickettsiae with cells other than the endothelium during infection may be an underappreciated aspect in rickettsial biology (Riley et al., 2015; Riley et al.,

2016). The first step for a successful infection *in vitro* is the binding to or the recognition of the target cell (Bechah et al., 2008b; Walker and Ismail, 2008). Thereby, to start understanding the reason why *R. montanensis* is unable to proliferate in macrophage-like cells, we addressed the adherence capacity of *R. montanensis* to THP-1-derived macrophages and Vero cells. Our results demonstrate that *R. montanensis* is defective in binding THP-1-derived macrophages when compared with their capacity to bind to Vero cells. In contrast, the adherence of *R. conorii* to either epithelial or macrophage-like cells is not affected. Therefore, the difference in the ability of a known human pathogen and a non-pathogenic rickettsial species to bind to macrophage-like cells constitutes a major phenotypic distinction between these two SFG rickettsiae *in vitro*. For endothelial cells, several reports have highlighted the importance of the interactions between rickettsial surface proteins such as the rickettsial surface cell antigens (Sca) (Sca0/OmpA, Sca1, Sca2, Sca5/OmpB) with mammalian host cell receptors in mediating adherence and subsequently invasion of cultured mammalian cells (Cardwell and Martinez, 2009; Chan et al., 2009; Chan et al., 2010; Hillman et al., 2013; Li and Walker, 1998; Riley et al., 2010). Amino acid sequence alignments between the rickettsial Sca protein homologs in *R. conorii* and *R. montanensis* reported to play a role in the adhesion to endothelial cells do not reveal any obvious differences sharing between 60.15% and 88.47% of sequence identity **(Supplementary Figures II.4-7)**. Nonetheless, we cannot totally rule out that these changes in amino acid sequence may still be responsible for the observed difference in adherence. A gain of function assay, with the noninvasive *E. coli* expressing individual *R. montanensis* Sca proteins, could be a useful tool to assess whether Sca proteins function similarly as has been previously demonstrated (Cardwell and Martinez, 2009; Riley et al., 2010; Uchiyama, 2003). Furthermore, the process by which SFG rickettsiae adhere to macrophage-like cells is not yet studied and we cannot discard the possibility that *R. conorii* and *R. montanensis* may use alternative routes of entry into macrophages. However, the defective ability of *R. montanensis* to bind to THP-1-derived macrophages cannot totally explain the complete lack of growth in macrophage-like cells since rickettsiae can still adhere to these cells.

We demonstrated that the *R. montanensis* cells that are able to adhere to macrophage-like cells still invade these cells. However, the invasion rates of *R. montanensis* appear to be

significantly reduced when compared with those obtained for *R. conorii* in both epithelial and macrophage cell lines, further strengthening the possibility that the route by which these two SFG rickettsiae adhere to and invade into macrophage-like cells may indeed be different. Previous reports showed that binding and recruitment of Ku70 to the plasma membrane as well as localized actin rearrangements are important events in the entry of *R. conorii* into non-phagocytic mammalian cells (Chan et al., 2009; Martinez et al., 2005). Furthermore, subsequent studies demonstrated the importance of Sca0/OmpA interactions with $\alpha 2\beta 1$ integrin in the internalization of *R. conorii* into human lung microvascular endothelial cells (Hillman et al., 2013). However, it is unknown if the same events occur upon invasion of *R. conorii* into macrophages. To our knowledge, the mechanism(s) of entry in endothelial and macrophage cells by *R. montanensis* have yet to be elucidated. Therefore, we cannot discard that different SFG rickettsiae can share distinctive mechanism(s) of entry between them. Interestingly, *Legionella pneumophila* strains with different degrees of virulence were shown to differ in their respective mechanisms of entrance into monocytes/macrophages and subsequently in their ability to proliferate within this cell type (Cirillo et al., 1999). Nonetheless, further research is required to better understand the routes of entry in macrophage cells utilized by SFG rickettsiae species of varying degrees of virulence.

We determined that the lack of *R. montanensis* growth in macrophage-like cells also results from the apparent inability of *R. montanensis* to avoid intracellular destruction. Confocal microscopy data demonstrate that intracellular *R. montanensis* are rapidly destroyed in THP-1-derived macrophages, and several bacterial cells co-localized with the lysosomal markers, LAMP-2 and cathepsin D. In contrast, infection of THP-1-derived macrophages by *R. conorii* resulted in no significant co-staining with positive structures for both lysosomal markers and the increase of intact bacteria over the time course of the experiment demonstrate their ability to grow. Interestingly, amino acid sequence alignments of homologous proteins previously reported to mediate rickettsial phagosomal escape, namely membranolytic phospholipase D and haemolysin C (Whitworth et al., 2005), do not demonstrate any obvious difference between *R. conorii* and *R. montanensis* homologues of these two proteins **(Supplementary Figure II.8-9)**. Again, as for Sca proteins, the impact of minor changes in protein sequence and putative protein function cannot be excluded.

Published comparative genomic analysis of the secretome of *R. conorii and R. montanensis* highlight major differences in several genes between these two species, including *rarp*2, encoding Rickettsia Ankyrin Repeat Protein 2 (RARP-2), which is absent in *R. montanensis* genome, and phospholipase A_2 (Pat-2), which may be present as a pseudogene in *R. conorii* (Gillespie et al., 2015a). RARP-2 homologs have been described as virulence factors in other pathogenic bacteria, and *R. typhi* Pat-2 protein was suggested to be necessary to support intracellular survival without affecting host cell integrity (Pan et al., 2008; Rahman et al., 2010; Rahman et al., 2013). Whether or not these or other SFG rickettsial gene products contribute to intracellular replication in macrophages needs to be further evaluated.

Together, our results provide supportive evidence that two SFG rickettsiae with different degrees of pathogenicity have opposite fates in macrophage-like cells. Over 40 years ago, *Grambrill et al.,* provided the first evidence that TG rickettsiae strains with different levels of virulence possessed distinct abilities to proliferate in macrophage cell cultures (Gambrill and Wisseman, 1973b). Our results further strengthen the hypothesis that the virulence of different rickettsial species in mammals may somehow be explained by their ability to proliferate within macrophages and potentially other professional phagocytes, and raises the exciting possibility of using macrophage cell cultures as a useful model to predict/understand the pathogenicity of different emerging rickettsial species.

II.6 | Acknowledgments

We would like to thank members of the Martinez lab for critical analysis of the work described herein. We would also wish to thank Dr. Yuliya Sokolova (Electron Microscopy Laboratory at the LSU SVM Department of Pathobiological Sciences) for her technical expertise and guidance in sample preparation. We would like to acknowledge Dr. Kevin Macaluso (LSU SVM Department of Pathobiological Sciences) for providing *R. montanensis* isolate M5/6.

Chapter III

Host players involved in early signaling events in rickettsiae-macrophage interactions

III.1 | Abstract

Endothelial cells have long been considered the main target cells for rickettsiae. However, several studies have provided evidence of non-endothelial parasitism by rickettsial species with numerous intact bacteria being found within the cytoplasm of macrophages and neutrophils, in both tissues and blood circulation. This evidence has raised the debate about the biological role of that interaction during rickettsial pathogenesis. We have recently reported that two members of spotted fever group *Rickettsia* (*R. conorii* and *R. montanensis*) have completely distinct intracellular fates in human THP-1-derived macrophages. Although the interaction of rickettsiae with endothelial cells is a process relatively well studied, to our knowledge, nothing is known about the interaction of rickettsial species with macrophages. In this work, we employed a pharmacological study to start understanding the host proteins involved in the rickettsial entry process into macrophages. Using PMA-differentiated THP-1 cells, and *R. conorii* and *R. montanensis* as our models of study, we were able to identify a requirement of actin polymerization, receptor and non-receptor tyrosine kinase proteins, Arp2/3 complex, and PAK1 for rickettsial entry into macrophages. Moreover, we have herein found a differential contribution of host proteins for the entry process of *R. conorii* and *R. montanensis*, which suggests that different members of SFG *Rickettsia* may use different routes of entry into macrophages. Inhibition of Na^+/H^+ exchangers and PAK1 impaired *R. conorii* association with macrophage-like cells, thus suggesting that macropinocytosis-like pathways may be utilized as an alternative route of entry of rickettsiae in macrophages.

III.2 | Introduction

The incidence of tick-borne rickettsial diseases is currently going through its second prominent increase over the last 40 years (Eremeeva and Dasch, 2015). Rickettsiae are obligate intracellular Gram-negative pathogens and infections associated with these bacteria range from mild to severe, including death (Walker and Ismail, 2008). In the human host, endothelial cells have long been considered the main target cells for rickettsioses (Walker, 1997; Walker and Ismail, 2008). The early signaling events that underlie the entry of rickettsiae into endothelial cells are relatively well studied. Indeed, several studies exploring the entry mechanisms of SFG *Rickettsia* (*R. conorii* and *R. rickettsii*) have demonstrated that mammalian proteins Ku70 and $\alpha_2\beta_1$ integrin interact with rickettsial outer membrane proteins B (OmpB) and A (OmpA), respectively, to promote rickettsial invasion into non-phagocytic mammalian host cells (Chan et al., 2009; Hillman et al., 2013). Moreover, it is known that binding of rOmpB to its host receptor Ku70, triggers host-signaling cascades involving c-Cbl-mediated ubiquitination of Ku70, Rho-family GTPases Cdc42 and Rac1, phosphoinositide 3-kinase (PI3K) activity, and activation of tyrosine kinases (e.g., c-Src, FAK and p-TK) as well as their phosphorylated targets (Chan et al., 2009; Chan et al., 2010; Hillman et al., 2013; Martinez and Cossart, 2004; Martinez et al., 2005; Reed et al., 2012). Also, the induced coordinated activation of host signaling pathways by *R. conorii* leads to the recruitment of factors that activate the actin-nucleating complex (Arp2/3), which leads to host actin polymerization, extensive membrane ruffling and filopodia formation, and subsequent bacteria internalization in a clathrin- and caveolin-dependent process (Chan et al., 2009; Martinez and Cossart, 2004).

An analysis of the host cytoskeletal proteins that play a role in *R. parkeri* (genetically similar to *R. rickettsii* and *R. conorii* but less pathogenic) invasion revealed that the molecular requirements for rickettsiae invasion differ depending on the host cell type (Reed et al., 2014). The requirement of WAVE family proteins and Rho family GTPases has been demonstrated to be more stringent to the invasion into *Drosophila melanogaster* S2R+ cells than into human endothelial cell lines, whereas the Arp2/3 complex was critical for both arthropod and mammalian cells, suggesting that invasion of *R. parkeri* in mammalian endothelial cells occurs via redundant pathways that converge on the host Arp2/3 complex (Reed et al., 2014). Also, a pharmacological study revealed several

tick proteins including PI3K, protein tyrosine kinases, Src family PTK, focal adhesion kinase, Rho GTPase Rac1, N-WASP, and Arp2/3 complex that are important for *R. montanensis* uptake into a tick cell line (*Dermacentor variabilis*) (Petchampai et al., 2015).

Animal models of SFG *Rickettsia* infection have provided evidence of non-endothelial parasitism by rickettsial species (e.g., macrophages and neutrophils), raising important questions about the biological role of cells other than the endothelium in the development of rickettsial infections (Banajee et al., 2015; Riley et al., 2016). Although the primary function of macrophages in innate immunity is to act as destroyers of pathogens, several successful intracellular bacteria and viruses have developed sophisticated strategies to overcome macrophage defenses and establish a replicative niche inside these phagocytic cells (Price and Vance, 2014). Indeed, the ability to proliferate, or at least survive, within macrophages has been described as an essential part of what it means to be a pathogen (Price and Vance, 2014). We have previously reported that two members of SFG *Rickettsia* with distinct pathogenicity attributes have completely different intracellular fates within macrophage-like cells (Chapter II) (Curto et al., 2016). The pathogenic member (*R. conorii*) survives and proliferates within the hostile environment of the cytoplasm of a phagocytic cell, whereas *R. montanensis* (a non-pathogenic member of SFG *Rickettsia*) is rapidly destroyed. These results led us to hypothesize that the ability to subvert macrophage immune defenses might be correlated with the capacity of rickettsial species to cause disease in humans. Indeed, Gambrill et al. have also provided evidence that TG rickettsiae strains with different levels of virulence possessed distinct abilities to proliferate in macrophage cell cultures (Gambrill and Wisseman, 1973b). Similarly, the virulent *R. mooseri* and the Breinl strain of *R. prowazekii* readily reached high intracellular populations, whereas the attenuated E strain of *R. prowazekii* failed to grow, thus strengthening this hypothesis (Gambrill and Wisseman, 1973b). However, little is yet known about the molecular mechanisms involved in the rickettsiae-macrophage interaction that explain the distinct intracellular fates of different *Rickettsia* species into phagocytic cells. Therefore, in addition to the in-depth understanding of the biological role of macrophages during rickettsial infections, it is also critical to start unraveling the key players governing rickettsiae-macrophage interactions.

In this work, we have employed an inhibitor-based study to start deciphering host proteins required for the early signaling events involved in the entry of *R. conorii* and *R. montanensis* into macrophage-like cells. Our results reveal differences in the contribution of several host signaling molecules for the entry process between rickettsial species, anticipating some variation in the signaling pathways that regulate actin assembly/dynamics. Moreover, we unveil a previously unrecognized role for p-21 activated kinase (PAK1) and Na^+/H^+ exchangers (NHE) in *R. conorii* invasion process, suggesting the use of a macropinocytosis-like pathway as an alternate route of entry into macrophage-like cells.

III.3 | Materials and Methods

III.3.1 | Cell lines, *Rickettsia* growth and purification.

THP-1 (ATCC TIB-202^{TM}) cells were grown in RPMI-1640 medium (Gibco) supplemented with 10% heat-inactivated fetal bovine serum. Differentiation of THP-1 cells into macrophage-like cells was carried out by the addition of 100 nM of phorbol 12-myristate 13-acetate (PMA; Fisher). Cells were allowed to differentiate and adhere for 3 days prior to infection. In this work, all experiments were carried out with PMA-differentiated THP-1 cells, and they are herein named THP-1 macrophages from now on. Cells were maintained in a humidified 5% CO_2 incubator at 34 °C. *R. conorii* isolate Malish7 and *R. montanensis* isolate M5/6 were propagated in Vero cells and purified as described previously (Ammerman et al., 2008; Chan et al., 2009; Chan et al., 2011).

III.3.2 | Antibodies

Anti-Rc$_{PFA}$, a rabbit polyclonal antibody that recognizes *R. conorii*, was generated as previously described (Cardwell and Martinez, 2012; Chan et al., 2011). Anti-*Rickettsia* rabbit polyclonal antibody that recognizes *R. montanensis* (NIH/RML I7198) was kindly provided by Dr. Ted Hackstadt (Rocky Mountain Laboratories). For immunofluorescence microscopy, Alexa Fluor 488- and 546-conjugated goat anti-rabbit IgG, Texas Red-X-phalloidin, and DAPI (4',6'-diamidino-2-phenylindole) were purchased from Thermo Scientific. For immunoblotting, the following antibodies were used: 4G10® Platinum, Anti-phosphotyrosine antibody (mouse monoclonal cocktail IgG2b) from Merck; clone AC-15, anti-β-actin antibody (mouse monoclonal) from Sigma; anti-PAK antibody (A-6) and anti-pPAK antibody (66.Thr 423) from Santa Cruz Biotechnology; and donkey anti-mouse IRDye 680 IgG from LI-COR Biosciences.

III.3.3 | Pharmacological inhibitors

5-(N,N-Dimethyl)amiloride hydrocholoride (DMA) (A4562), (5-(N-Ehtly-N-isopropyl)amiloride (EIPA) (A3085), cytochalasin D (C8273), IPA-3 (I2285), Genistein (G6649), Wiskostatin (W2270), CK869 (C9124) and zoniporide (SML-0076) were obtained from Sigma. Gö 6976 (365250), Latrunculin B (428020), Rac1 Inhibitor (553502), Src Inhibitor PP1 (567809) and

Wortmannin (681675) were obtained from Calbiochem. 8-cyclopentyl-2,3,3a,4,5,6-hexahydro-1H-pyrazino[3,2,1-jk]carbazole methanesulfonate (Pirl-1) (5137877) was purchased from ChemBridge. Jasplakinolide (11705) was obtained from Cayman Chemical.

III.3.4 | Pharmacological inhibition treatment and infection assays

THP-1 macrophages were washed 3 times with serum-free RPMI and serum starved for 30 minutes. Serum-free medium containing the specific pharmacological inhibitor (or vehicle as a control) at the respective concentration was used to pretreat the THP-1 cells at 34 °C and 5% CO_2 for 30 minutes. Pre-treated THP-1 cells were then incubated in *R. conorii* or *R. montanensis* at a multiplicity of infection (MOI) of 10 in the presence of each specific pharmacological inhibitor. Plates were then centrifuged at 300 x g for 5 minutes at room temperature to induce contact between rickettsiae and host cells, and incubated at 34 °C and 5% CO_2 for 30 minutes. Infected THP-1 cells were then washed one time with 1 mL of ice cold PBS and fixed in 4% PFA for 20 minutes prior to staining.

For cell association assays, after permeabilization with 0.1% Triton X-100 and blocking with 2% BSA, *R. conorii* were stained with anti-RcPFA (1:1,000) followed by Alexa-Fluor 488-conjugated goat anti-rabbit IgG (1:1,000), DAPI (1:1,000) and Texas Red-X-phalloidin (1:200). For *R. montanensis*, staining was carried out with NIH/RML I7198 antibody (1:1,500) followed by Alexa-Fluor 488-conjugated goat anti-rabbit IgG (1:1,000), DAPI (1:1,000) and Texas Red-X-phalloidin (1:200). Experiments were done at least in triplicate and the results of each experiment were expressed as the ratio of rickettsiae cells to mammalian cells (nuclei). If no effect was observed in association assays, invasion assays were carried out to evaluate whether pharmacological inhibition would affect the ability of rickettsiae to invade host cells. For invasion assays, infected monolayers were processed for differential staining to distinguish between extracellular and intracellular rickettsia. Briefly, extracellular *R. conorii* were stained with anti-RcPFA (1:1,000) followed by Alexa Fluor 546-conjugated goat anti-rabbit IgG (1:1,000), prior to permeabilization of the mammalian cells with 0.1% Triton X-100. After permeabilization, the total *R. conorii* cells were then stained with anti-RcPFA (1:1,000) followed by Alexa Fluor 488-conjugated goat anti-rabbit IgG

(1:1,000). Invasion assays of *R. montanensis* were assessed using the same procedure, and *R. montanensis* staining was carried out with NIH/RML I7198 antibody (1:1,500). Bacteria staining positive for Alexa Fluor 546-conjugated goat anti-rabbit IgG were considered as external while bacteria stained for both secondary antibodies were considered as total bacteria present. The number of internalized rickettsiae was determined by the difference between total and external rickettsiae, and results are expressed as percentage of internalized rickettsiae. As for association assays, experiments were done in triplicate. Images were digitally captured with an OLYMPUS IX71 inverted microscope (Tokyo, Japan) equipped with an OLYMPUS DP72 camera (Tokyo, Japan) using a final x40 optical zoom. Rickettsiae and mammalian nuclei were counted using the cell counter analysis tool from ImageJ (http:/rsb.info.nih.gov/ij). Statistical analysis was performed by One-way ANOVA using Prism software package (GraphPad Software Inc).

III.3.5 | Western blotting

THP-1 macrophages onto six-well plates were washed twice with serum-free RPMI and serum-starved for 30 minutes. THP-1 macrophages were either left uninfected or infected with *R. conorii* or *R. montanensis* (MOI=20), centrifuged at 300 x g for 5 minutes at room temperature and quickly moved to 37 °C, 5% CO_2 for the indicated time. After each time point, cells were washed three times with ice-cold PBS and then lysed in 500 µL 1% NP-40 lysis buffer (1% NP-40, 20 mM Tris, pH 8.0, 150 mM NaCl, 10% glycerol, 20 mM NaF, 3 mM Na_3VO_4, 1x Pierce inhibitors tablet (ThermoFisher Scientific)). Samples were passed 10 times through Insulin Syringe with 28-gauge needle (Becton Dickinson) and denatured using 6x SDS sample buffer (4x Tris/HCl, 30% glycerol, 10% SDS, 0.6 M DTT, 0.012% Bromophenol Blue, pH 6.8) during 10 minutes at 95 °C. Total protein content in each sample was then quantified using 2D Quant kit (GE Healthcare) and kept at -20 °C until further processing. After thawing, the same amount of protein for each sample was resolved by SDS-PAGE on Mini-PROTEAN® Tris/Tricine precast gels (Bio-Rad) and transferred to nitrocellulose. For Western immunoblotting, membranes were incubated for 1 hour at room temperature in 1x TBST with 2% BSA containing anti-phosphotyrosine antibody (1:1,000), anti-β-actin antibody (1:5,000), anti-PAK (1:100) or anti-pPAK(66Thr423) (1:50) antibody, as indicated

and then incubated in donkey anti-mouse IRDye 680 IgG (1:10,000). Proteins were visualized using an Odyssey CLx instrument (LI-COR). In some experiments, blots were stripped with Restore Stripping Buffer (Pierce) and probed with the indicated antisera to demonstrate equal protein loading. Blots shown are representative of at least three biological replicates. Statistical analysis was performed by One-sample t-test using Prism software package (GraphPad Software Inc).

III.4 | Results

III.4.1 | Involvement of actin dynamics in the entry process of rickettsiae into THP-1 cells.

Intracellular pathogens have evolved numerous strategies to modulate the host cytoskeleton, promoting several cellular events that are beneficial for the pathogen including internalization into the host (Colonne et al., 2016). To investigate the role of actin polymerization on the entry mechanisms of *R. conorii* and *R. montanensis* into macrophage-like cells, we evaluated the effect of different inhibitors. THP-1 cells were pretreated with the inhibitors at different concentrations and then independently challenged with *R. conorii* or *R. montanensis* (MOI=10), and evaluated at 30 minutes post-infection for rickettsiae association to and/or invasion into host cells. The first compound tested was cytochalasin D, which blocks actin polymerization by occupying fast growing end filaments. Our results demonstrate that, at the concentrations used in this study, treatment of THP-1 macrophages with cytochalasin D had no significant effect on the ability of *R. conorii* to associate with host cells, but significantly reduced the ability of the bacteria to invade (42 % relative invasion observed in the presence of 5 µM cytochalasin D) **(Figure III.1A-B, Table III.1)**. On the other hand, *R. montanensis* displayed a significantly reduced ability to associate with host cells in the presence of this inhibitor (at both concentrations used) **(Figure III.1C, Table III.1)**, suggesting somewhat different requirements on actin polymerization between *R. conorii* and *R. montanensis* in the early signaling events in these cells. Treatment of THP-1 macrophages with Latrunculin B that sequesters G-actin and prevents F-actin assembly as well as with jasplakinolide, that stabilizes F-actin by stimulating actin filament nucleation, significantly reduced the capacity of both *R. conorii* and *R. montanensis* to associate with host cells **(Figure III.1A and 1C, Table III.1)**. These results strengthen the impact of host actin polymerization for the entry process of SFG *Rickettsia* into macrophage-like cells.

Table III.1. Summary of pharmacological inhibitors used on this work and their effect on the ability of *R. conorii* and *R. montanensis* to associate and invade to THP-1 macrophages.

Host target	Inhibitor	Mode of action	Concentrations used in this work	% *R. conorii* / cell	% relative invasion *R. conorii* (internal / total)	% *R. montanensis* / cell	% relative invasion *R. montanensis* (internal / total)
Actin	Cytochalasin D	Blocks actin polymerization by occupying fast growing end filaments	0.2 µM	ns	ns	77%**	-
			5 µM	ns	42% ****	61% ****	-
	Latrunculin B	It sequestres G-actin and prevents F-actin assembly	0.5 µM	36% ****	-	36% ****	-
			2 µM	50% ****	-	50% ****	-
	Jasplakinolide	Stabilizes F-actin by stimulating actin filament nucleation	1 µM	36% ****	-	51% ****	-
RTKs	Genistein	Tyrosine kinase inhibitor	20 µM	54% ****	-	62% ****	-
			60 µM	35% ****	-	64%****	-
c-Src	PP1	c-Src kinase inhibitor	25 µM	41% ****	-	63% ****	-
			50 µM	51%****	-	ns	-
Pak1	IPA-3	Inhibits p21 associated kinase-1 (Pak1)	10 µM	14%****	-	52% **	-
			20 µM	15%****	-	48%***	-
Rac1	Rac1 ihn	Rho GTPase Rac inhibitor	50 µM	(127%) **	80% ****	(114%) *	92% *
			100 µM	(129%) ***	83% ****	ns	ns
Cdc42	Pirl-1	Acts by inhibiting guanine nucleotide exchange on Cdc42	5 µM	85% **	-	ns	-
			10 µM	64% ****	-	72% ***	-
N-WASP	Wiskostatin	Regulate the actin cytoskeleton by directly interacting with actin in the Arp2/3 complex	1 µM	46% ****	-	83% *	-
Arp2/3 complex	CK-689	pparently the compound binds to the hydrophobic core of Arp3 and alters its conformatic	10 µM	66% ****	-	68% *	-
			20 µM	76% ****	-	53% *	-
PI(3)K	Wortmannin	PI(3)K inhibitor	20 nM	ns	(131%) ***	ns	ns
			150 nM	ns	(134%) ***	ns	ns
PKC	Gö 6976	Protein kinase inhibitor (α and β1 isoforms)	0.5 µM	ns	(117%) **	ns	87% *
			2 µM	ns	ns	ns	84% *
Na^+/H^+ exchangers	DMA	Blocks Na^+/H^+ channels altering cytosolic pH	20 µM	12% ****	-	ns	ns
			50 µM	25% ****	-	ns	ns
			100 µM	15% ****	-	ns	76% **
	EIPA	Blocks Na^+/H^+ channels altering cytosolic pH	25 µM	20% ****	-	46% ***	-
			50 µM	32% ****	-	42% ***	-
	Zoniporide	Potent and selective inhibitor of Na^+/H^+ exchanger isoform 1 (NHE-1)	10 µM	86% *	-	(114%) *	-
			100 µM	60% *	-	78% ****	-

Results are shown as the mean for each respective experimental condition (ns, non-significant, * P ≤ 0.05, ** P ≤ 0.001, *** P ≤ 0.0001, **** P ≤ 0.00001).

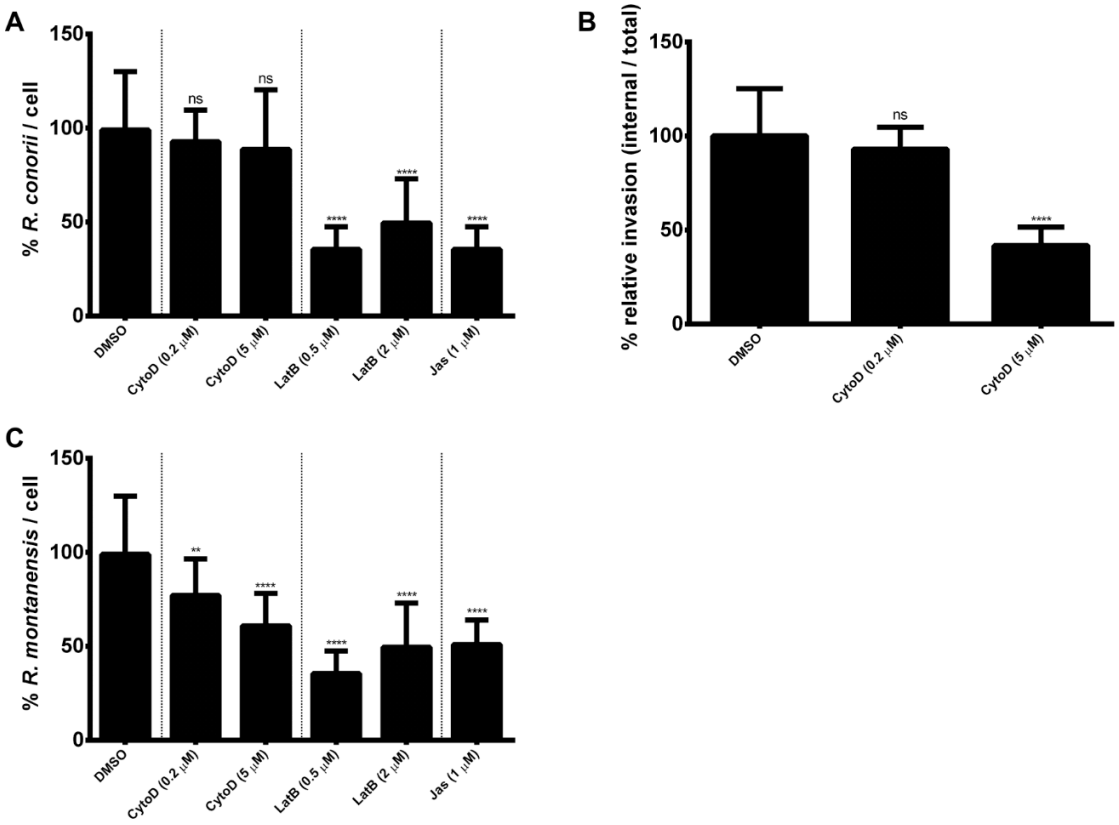

Figure III.1 | Involvement of actin polymerization in rickettsiae entry process into THP-1 macrophages. THP-1-derived macrophages were pre-treated with the following actin polymerization inhibitors: cytochalasin D, Latrunculin B and jasplakinolide in serum-free RPMI media at the indicated concentrations. Pre-treated THP-1 macrophages were then independently challenged with *R. conorii* and *R. montanensis* (MOI=10) for 30 minutes in the presence of the respective pharmacological inhibitor. Cells were then washed and fixed in 4% PFA and prepared for microscopy analysis, as described in Methods. Results were normalized for the respective control condition with DMSO. At least 200 mammalian nuclei were counted for each experimental condition and experiments were done in triplicate. Results are shown as the mean ± SD (ns, non-significant, ** $P \leq 0.01$, **** $P \leq 0.00001$). **A)** Effect of actin polymerization inhibitors in the ability of *R. conorii* to associate with THP-1 macrophages. **B)** Effect of cytochalasin D in the ability of *R. conorii* to invade THP-1 macrophages. **C)** Effect of actin polymerization inhibitors in the ability of *R. montanensis* to associate with THP-1 macrophages.

III.4.2 | Receptor and non-receptor tyrosine kinases participate in the entry process of SFG *Rickettsia* in THP-1 macrophages.

The importance of tyrosine phosphorylation of host proteins in the activation of signaling cascades upon pathogen attachment has been extensively reported (Han et al., 2016; Martinez and Cossart, 2004; Schmutz et al., 2013). We herein started by evaluating the participation of receptor tyrosine kinase proteins (RTKs) in *R. conorii* and *R. montanensis* entry process into THP-1 macrophages. Treatment with genistein, a potent general tyrosine kinase inhibitor, resulted in a drastic reduction in the association of both *R. conorii* and *R. montanensis* to the host cells **(Figure III.2A-B, Table III.1)**, suggesting that RTKs are required in the SFG *Rickettsia* entry process into macrophage-like cells. Moreover, it has been reported that under activation, a cytoplasmic pool of Src (a non-receptor tyrosine Src-family kinase) is shuttled to the sites of ruffling where it can activate the Ras-effectors Arp2/3, Rac1, and PI3K, therefore synergistically enhancing RTK signaling (Amyere et al., 2000; Bougneres et al., 2004; Donepudi and Resh, 2008; Sandilands et al., 2004). In this work, we evaluated the contribution of Src family of tyrosine kinases through pharmacological treatment with PP1. As shown in **Figure III.2C-D (Table III.1)**, a decrease in association was observed upon treatment for both rickettsial species; however, the differential effect observed for each PP1 concentration also suggests that *R. conorii* entry process might be more susceptible to the inhibition of Src kinases than that of *R. montanensis*. Overall, these results suggest the participation of different families of protein tyrosine kinases in *R. conorii* and *R. montanensis* entry into THP-1 macrophages, highlighting the importance of protein phosphorylation in these early signaling events. To further corroborate this, we next sought to evaluate if the infection of THP-1 macrophages with SFG *Rickettsia* would result in changes in the phosphorylation state of host proteins. To this end, total protein extracts of infected and uninfected THP-1 cells were subjected to Western blotting analysis with anti-phosphotyrosine antisera. Given that internalization of rickettsiae into non-phagocytic cells is a very rapid process (Martinez and Cossart, 2004), two early time points post-infection (5 min and 15 min) were also evaluated in this work. As shown in **Figure III.2E**, both *R. conorii* and *R. montanensis* infection induced tyrosine phosphorylation of several host proteins with different predicted molecular weight (125/130 kDa; 60 kDa; 30 kDa).

Receptor tyrosine kinases can indirectly lead to the initiation of several parallel signaling pathways (Bar-Sagi and Feramisco, 1986; Bar-Sagi et al., 1987). One of these pathways involves PI3K, which is capable of phosphorylating the 3-position hydroxyl group of the inositol ring of phosphatidylinositol, acting as an intracellular signal transducer enzyme (Vanhaesebroeck et al., 2012).

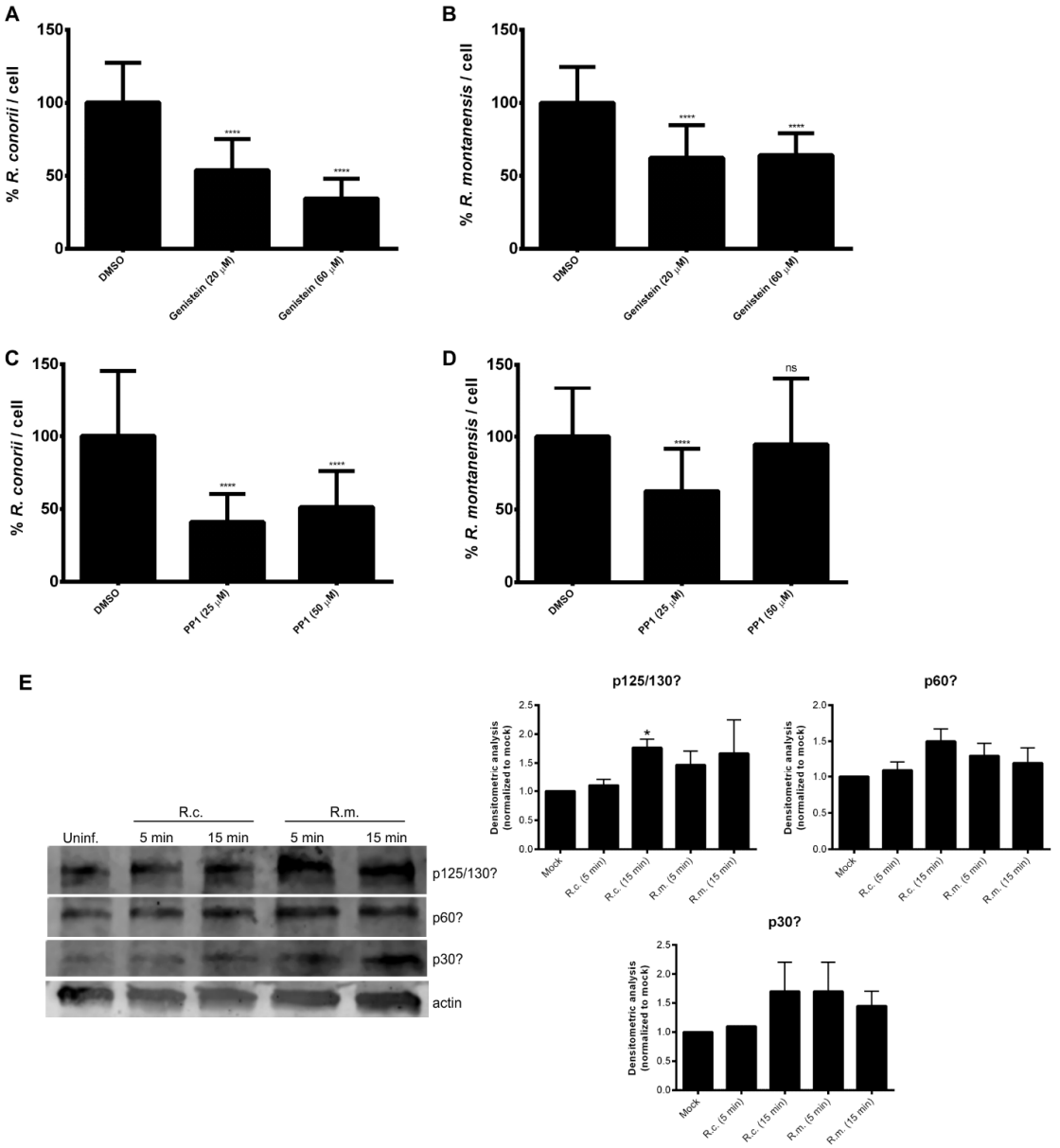

Figure III.2 (previous page) | Contribution of host protein tyrosine phosphorylation for rickettsiae entry process into THP-1 macrophages. THP-1-derived macrophages were pre-treated with a receptor tyrosine kinase inhibitor (Genistein) and a non-receptor tyrosine kinase inhibitor (PP1) in serum-free RPMI media at the indicated concentrations. Pre-treated THP-1 cells were then independently challenged with *R. conorii* and *R. montanensis* (MOI=10) for 30 minutes in the presence of the respective pharmacological inhibitor. Cells were washed and fixed in 4% PFA and prepared for microscopy analysis, as described in Methods. Results were normalized for the respective control condition with DMSO. At least 200 mammalian nuclei were counted for each experimental condition and experiments were done in triplicate. Results are shown as the mean ± SD (ns, non-significant, **** $P \leq 0.00001$). Requirement of receptor tyrosine kinase proteins for *R. conorii* **(A)** and *R. montanensis* **(B)** association with THP-1 cells. Contribution of non-receptor tyrosine kinase proteins in the ability of *R. conorii* **(C)** and *R. montanensis* **(D)** to associate with THP-1 cells. **(E)** Changes in the phosphorylation state of host proteins with different predicted molecular weight range (125/130 kDa; 60 kDa; 30 kDa) at 5 and 15 minutes post-infection of THP-1 macrophages *with R. conorii* (R.c.) or *R. montanensis* (R.m.) (MOI=20) were monitored by Western blotting analysis using anti-phosphotyrosine antibody. Immunoblot analysis with anti-actin antibody was used as protein loading control and densitometric analysis of at least two biological replicates is also shown. Results of the densitometric analysis are shown as mean ± SD and differences were considered as significant at $*P < 0.05$.

Several studies have demonstrated that PI3Ks can lead to the activation of host signaling cascades, predominantly through tyrosine phosphorylation of proteins and, in this way, contribute to the internalization of pathogens into the host cell (Amyere et al., 2000; Krachler et al., 2011; Oviedo-Boyso et al., 2011). Thus, we next sought to determine the impact of PI3K inhibition using wortmannin in *R. conorii* and *R. montanensis* entry process. For both concentrations tested in this work, we found no effect in association for both *R. conorii* **(Figure III.3A, Table III.1)** and *R. montanensis* **(Figure III.3 C, Table III.1)**. Moreover, invasion assays were performed under similar wortmannin concentrations, and our results revealed a significant increase in the ability of *R. conorii* **(Figure III.3B, Table III.1)** to invade THP-1 cells, whereas no effect was observed for *R. montanensis* **(Figure III.3D, Table III.1)**. The protein kinase C (PKC) is a Ca^{2+}- and diacylglycerol-dependent serine/threonine kinase that can also be activated by RTKs or PI3K (Amyere et al., 2000; Miyata et al., 1989).

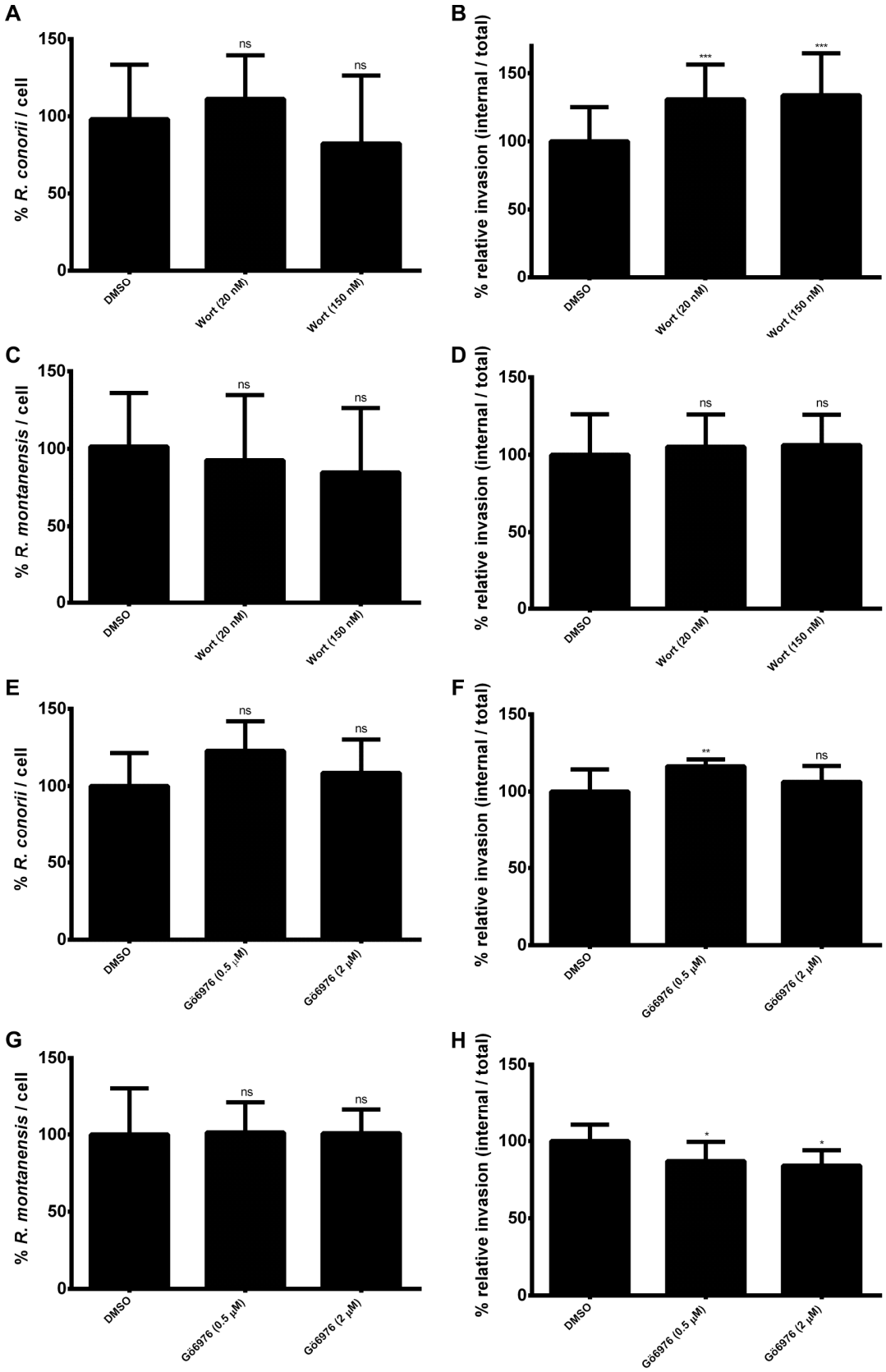
A
% R. conorii / cell
150
100
50
0
ns
ns
DMSO
Wort (20 nM)
Wort (150 nM)
B
% relative invasion (internal / total)
150
100
50
0
***
***
DMSO
Wort (20 nM)
Wort (150 nM)
C
% R. montanensis / cell
150
100
50
0
ns
ns
DMSO
Wort (20 nM)
Wort (150 nM)
D
% relative invasion (internal / total)
150
100
50
0
ns
ns
DMSO
Wort (20 nM)
Wort (150 nM)
E
% R. conorii / cell
150
100
50
0
ns
ns
DMSO
Gö6976 (0.5 μM)
Gö6976 (2 μM)
F
% relative invasion (internal / total)
150
100
50
0
**
ns
DMSO
Gö6976 (0.5 μM)
Gö6976 (2 μM)
G
% R. montanensis / cell
150
100
50
0
ns
ns
DMSO
Gö6976 (0.5 μM)
Gö6976 (2 μM)
H
% relative invasion (internal / total)
150
100
50
0
*
*
DMSO
Gö6976 (0.5 μM)
Gö6976 (2 μM)

Figure III.3 (previous page) | Involvement of PI3K and PKC in rickettsiae entry process into THP-1 macrophages. THP-1-derived macrophages were independently pre-treated with a PI3K (Wortmannin) and PKC (Gö 6976) inhibitor in serum-free RPMI media at the indicated concentrations. Pre-treated THP-1 cells were then independently challenged with *R. conorii* and *R. montanensis* (MOI=10) for 30 minutes in the presence of the respective pharmacological inhibitor. Cells were then washed and fixed in 4% PFA and prepared for microscopy analysis, as described in Methods. Results were normalized for the respective control condition with DMSO. At least 200 mammalian nuclei were counted for each experimental condition and experiments were done in triplicate. Results are shown as the mean ± SD (ns, non-significant, * $P \leq 0.05$, ** $P \leq 0.001$). Effect of Wortmannin in the ability of *R. conorii* to associate **(A)** and to invade **(B)** THP-1 cells. Effect of Wortmannin in the ability of *R. montanensis* to associate **(C)** and to invade **(D)** THP-1 cells. Contribution of PKC in the ability of *R. conorii* to associate **(E)** and to invade **(F)** THP-1 cells. Contribution of PKC in the ability of *R. montanensis* to associate **(G)** and to invade **(H)** THP-1 cells.

The effect of PKC inhibition in rickettsial association and invasion was herein evaluated using Gö 6976, a competitive inhibitor of ATP binding to PKC isoforms α and β1 (Martiny-Baron et al., 1993; Qatsha et al., 1993). Treatment of THP-1 macrophages with Gö 6976 did not significantly affect the ability of *R. conorii* to associate **(Figure III.3E, Table III.1)** and to invade **(Figure III.3F, Table III.1)** host cells. However, although inhibition of PKC had no significant effect on the association of *R. montanensis* **(Figure III.3G, Table III.1)**, a reduction in invasion was observed **(Figure III.3H, Table III.1)**. Overall, our results suggest that the reduced effect of inhibition of either PI3Ks or PKC in rickettsial entry process into THP-1 macrophages may result from possible redundancy between different signaling pathways.

III.4.3 | PAK1 activation is necessary for SFG *Rickettsia* entry process in macrophage-like cells.

P21-activated kinase (PAK1) is a serine/threonine kinase activated by Rho GTPase Rac1 or Cdc42 with a crucial role in cell motility (Parrini et al., 2005). In this study, we evaluated the effect of the PAK1 allosteric inhibitor IPA-3, which specifically binds to the autoinhibitory domain of PAK1 and inhibits its activation. As before, host cells were pretreated with the inhibitor at different concentrations and then independently challenged with *R. conorii* or *R. montanensis* (MOI=10), and evaluated 30 minutes post-infection. Treatment of THP-1 macrophages with IPA-3 resulted in

a significant reduction in the ability of both *R. conorii* **(Figure III.4A, Table III.1)** and *R. montanensis* **(Figure III.4B, Table III.1)** to associate with host cells. However, inhibition of PAK-1 resulted in a much more drastic effect in the association of *R. conorii* (15% *R. conorii* /cell vs. 48% *R. montanensis* /cell at 20 μM IPA-3), with these results suggesting that PAK1 may have a central role in the entry process in these cells. Since PAK proteins are targets for the small GTP binding proteins Rac and Cdc42, we next sought to determine if inhibition of these upstream activators could also have an impact in rickettsial entry process into THP-1 macrophages. As shown in **Figure III.4 (Table III.1)**, the inhibition of Rac1 had only a minor effect in the association **(Figure III.4E)** and invasion **(Figure III.4F)** of *R. montanensis* into host cells. However, a somewhat different effect was observed for *R. conorii* **(Figure III.4C-D, Table III.1)**. While the capacity to associate with host cells appeared to increase when the cells were treated with the Rac1 inhibitor **(Figure III.4C)**, the opposite effect was observed in the invasion assays **(Figure III.4D)**. We have then evaluated the impact of Cdc42 inhibition with Pirl-1 **(Figure III.4G-H, Table III.1)**. Interestingly, treatment of THP-1 macrophages with Pirl-1 resulted in a significant reduction in the ability of both *R. conorii* **(Figure III.4G)** and *R. montanensis* **(Figure III.4H)** to associate with macrophage-like cells, although at different levels, suggesting that Cdc42 may play a more prominent role in the activation of PAK1 than Rac1. Given that Cdc42 catalyzes the activation of PAK1 through autophosphorylation of αPAK Thr 423, we evaluated if the infection of THP-1 macrophages with SFG *Rickettsia* would indeed result in changes in the phosphorylation state of this residue. Total protein extracts of infected and uninfected THP-1 cells were analyzed by Western blotting, at two different time points post-infection (5 min and 15 min). As illustrated in **Figure III.4I**, infection with both rickettsial species resulted indeed in an increase in the phosphorylation of PAK1 when compared with uninfected cells.

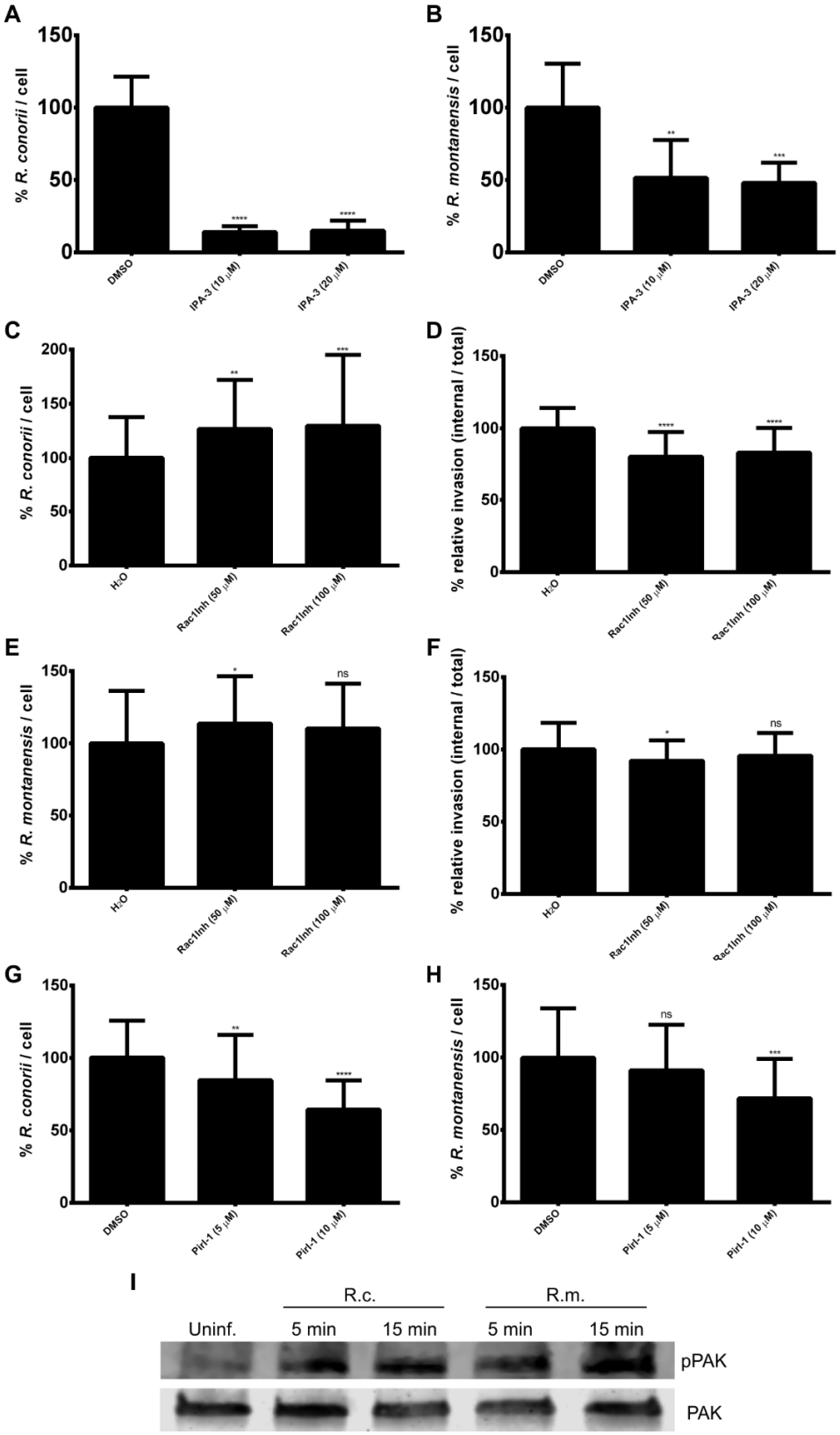
A
% R. conorii / cell
DMSO
IPA-3 (10 μM)
IPA-3 (20 μM)
B
% R. montanensis / cell
C
% R. conorii / cell
H2O
Rac1Inh (50 μM)
Rac1Inh (100 μM)
D
% relative invasion (internal / total)
E
% R. montanensis / cell
F
% relative invasion (internal / total)
G
% R. conorii / cell
Pirl-1 (5 μM)
Pirl-1 (10 μM)
H
% R. montanensis / cell
I
R.c.
R.m.
Uninf.
5 min
15 min
5 min
15 min
pPAK
PAK

Figure III.4 (previous page) | PAK1 activation is critical for rickettsiae entry into THP-1 cells. THP-1-derived macrophages were pre-treated independently with an inhibitor of PAK1 activation (IPA-3), Rac1 (Rac1 Inhibitor), and Cdc42 (Pirl-1) in serum-free RPMI media at the indicated concentrations. Pre-treated THP-1 cells were then independently challenged with *R. conorii* and *R. montanensis* (MOI=10) for 30 minutes in the presence of the respective pharmacological inhibitor. Cells were then washed and fixed in 4% PFA and prepared for microscopy analysis, as described in Methods. Results were normalized for the respective control condition with DMSO or H_2O. At least 200 mammalian nuclei were counted for each experimental condition and experiments were done in triplicate. Results are shown as the mean ± SD ns, non-significant, * $P \leq 0.05$, ** $P \leq 0.001$, *** $P \leq 0.0001$, **** $P \leq 0.00001$). Effect of IPA-3 in the ability of *R. conorii* **(A)** and *R. montanensis* **(B)** to associate with THP-1 cells. Requirement of Rac1 in the ability of *R. conorii* to associate **(C)** and to invade **(D)** THP-1 cells. Requirement of Rac1 in the ability of *R. montanensis* to associate **(E)** and to invade **(F)** THP-1 cells. Effect of Pirl-1 in the ability of *R. conorii* **(G)** and *R. montanensis* **(H)** to associate with THP-1 cells. **(I)** Changes in the phosphorylation state of PAK1 at 5 and 15 minutes post-infection of THP-1 macrophages with *R. conorii* (R.c.) or *R. montanensis* (R.m.) (MOI=20) were monitored by Western blotting analysis using anti-pPAK (66.Thr 423) antibody. Immunoblot analysis with anti-PAK antibody was used as protein loading control.

III.4.4 | A key role for N-WASP and Arp2/3 complex in rickettsiae entry process into THP-1 cells.

Neuronal Wiskott-Aldrich Syndrome protein (N-WASP) are downstream effector proteins of Cdc42 that transmits signals to the nucleation of actin filaments by Arp2/3 complex (Rohatgi et al., 2000). We have then investigated the impact of N-WASP and Arp2/3 complex proteins in rickettsiae entry process into THP-1 cells. Treatment of THP-1 macrophages with wiskostatin, a selective inhibitor of N-WASP, significantly decreased the ability of *R. conorii* **(Figure III.5A)** and *R. montanensis* **(Figure III.5B)** to associate with macrophage-like cells, although the observed effect was much more pronounced for *R. conorii*. Moreover, inhibition of the Arp2/3 complex with CK-869 also significantly diminished the association levels of *R. conorii* **(Figure III.5A)** and *R. montanensis* **(Figure III.5B)** to THP-1 macrophages, further reinforcing the role of actin reorganization in the entry process of SFG *Rickettsia* into macrophages.

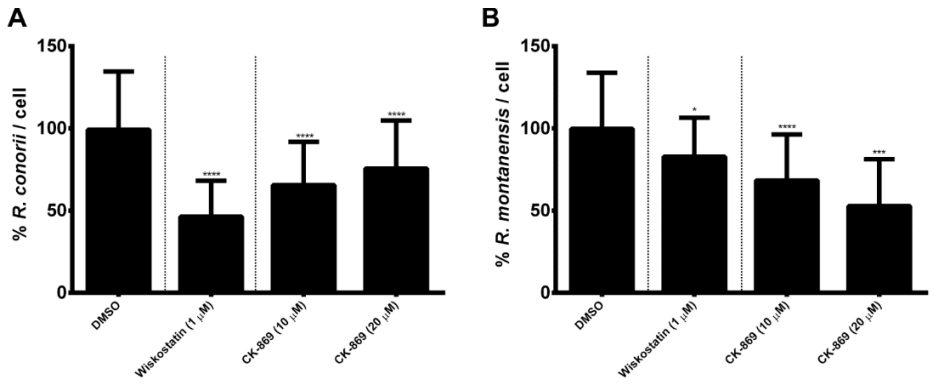

Figure III.5 | Requirement of N-WASP and Arp2/3 complex in the entry process of rickettsiae into THP-1 cells. THP-1-derived macrophages were independently pre-treated with an inhibitor of N-WASP (wiskostatin) or Arp2/3 complex (CK-869) in serum-free RPMI media at the indicated concentrations. Pre-treated THP-1 cells were then independently challenged with *R. conorii* and *R. montanensis* (MOI=10) for 30 minutes in the presence of the respective pharmacological inhibitor. Cells were then washed and fixed in 4% PFA and prepared for microscopy analysis, as described in Methods. Results were normalized for the respective control condition with DMSO. At least 200 mammalian nuclei were counted for each experimental condition and experiments were done in triplicate. Results are shown as the mean ± SD (* $P \leq 0.05$, *** $P \leq 0.0001$, **** $P \leq 0.00001$). Effect of wiskostatin and CK-869 in the ability of *R. conorii* **(A)** or *R. montanensis* **(B)** to associate with THP-1 cells.

III.4.5 | Na^+/H^+ exchangers are required for *R. conorii* entry process in macrophage-like cells.

The ability of macrophages and dendritic cells to internalize external material through its macropinocytic pathway is an essential component of the immune system (Brossart and Bevan, 1997; Kerr and Teasdale, 2009). Paradoxically, numerous infectious pathogens, such as bacteria, viruses, and protozoa, utilize macropinocytosis to invade their host cells (Carter et al., 2011; de Carvalho et al., 2015; Kalin et al., 2010; Weiner et al., 2016). The requirement of Na^+/H^+ exchangers for macropinosome formation is a hallmark of macropinocytic pathways. Therefore, the use of amiloride and its analogs by their activity in inhibiting Na^+/H^+ ion exchange pump in the plasma membrane (affecting the intracellular pH and resulting in the cessation of macropinocytosis) is frequently used as the main diagnostic test to identify macropinocytosis. Therefore, we next sought to determine the effect of several blockers of Na^+/H^+ exchangers (NHE) in the entry mechanism of SFG *Rickettsia* in macrophage-like cells.

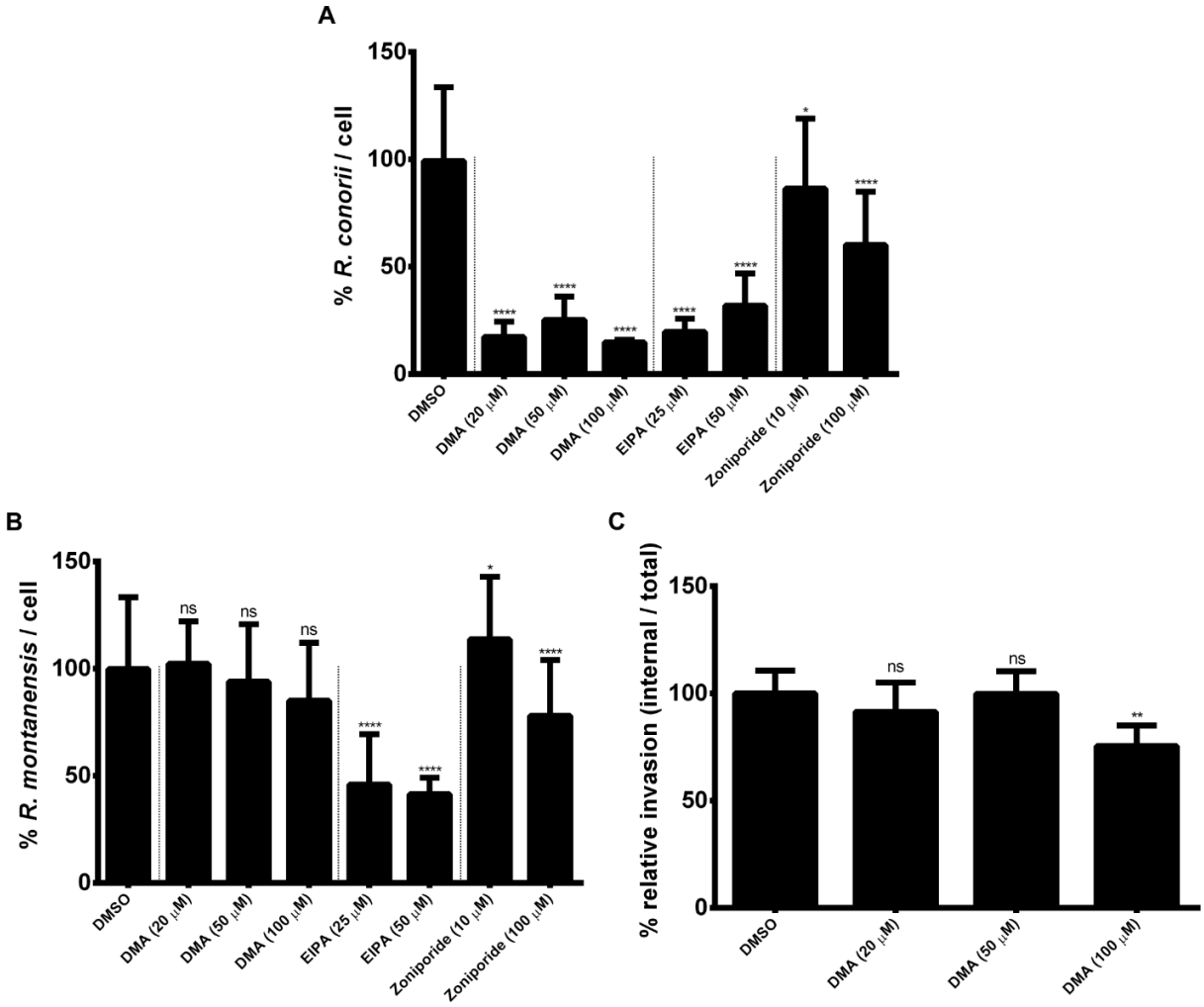

Figure III.6 | Requirement of Na^+/H^+ exchangers for rickettsiae entry process into THP-1 cells. THP-1-derived macrophages were independently pre-treated with three different inhibitors for Na^+/H^+ exchangers (DMA, EIPA and zoniporide) in serum-free RPMI media at the indicated concentrations. Pre-treated THP-1 cells were then challenged independently with *R. conorii* and *R. montanensis* (MOI=10) for 30 minutes in the presence of the respective pharmacological inhibitor. Cells were then washed and fixed in 4% PFA and prepared for microscopy analysis, as described in Methods. Results were normalized for the respective control condition with DMSO. At least 200 mammalian nuclei were counted for each experimental condition and experiments were done in triplicate. Results are shown as the mean ± SD (ns, non-significant, * $P \leq 0.05$, ** $P \leq 0.001$, *** $P \leq 0.0001$, **** $P \leq 0.00001$). Effect of Na^+/H^+ exchangers in the ability of *R. conorii* **(A)** and *R. montanensis* **(B)** to associate with THP-1 cells. **C)** Effect of DMA in the ability of *R. montanensis* to invade THP-1 cells.

Amiloride derivatives like DMA and EIPA are NHE inhibitors of the group of pyrazine derivatives that have been developed to increase the potency and selectivity towards NHE isoforms, and that are much more effective than amiloride (Masereel et al., 2003). Our results demonstrate that the ability of *R. conorii*, but not *R. montanensis*, to associate with THP-1 macrophages was completely blocked by the treatment of host cells with DMA, known as a potent inhibitor of macropinocytosis **(Figure III.6A-C)**. Similarly to DMA, treatment of THP-1 macrophages with EIPA also decreased the ability of SFG *Rickettsia* species to associate with host cells, although *R. montanensis* was again less affected by this inhibitor **(Figure III.6A-B)**. A third NHE inhibitor (zoniporide), which belongs to the group of bicyclic compounds and is a selective inhibitor of the isoform NHE1, was also tested in this study. Treatment with zoniporide also resulted in a stronger inhibitory effect on *R. conorii* association with THP-1 cells when compared with the effect observed for *R. montanensis* **(Figure III.6A-B)**. However, the stronger effect observed upon treatment with DMA and EIPA suggests that different NHE isoforms may mediate the rickettsial entry process. Together, these results indicate that macropinocytosis may be one of the pathways used by *R. conorii* to invade macrophage-like cells.

III.5 | Discussion

The identification of protein factors required for the early signaling events governing rickettsial entry into host cells has been the subject of several studies (Chan et al., 2009; Martinez and Cossart, 2004; Martinez et al., 2005; Petchampai et al., 2015; Reed et al., 2012). Comparison between studies is difficult because the invasion process of the different SFG *Rickettsia* under investigation was not systematically evaluated in all cell types. However, the evidence obtained from various host cells - including several non-phagocytic mammalian cell types (for *R. conorii* and *R. parkeri*), *Drosophila* (for *R. parkeri*) as well as tick-derived cells (for *R. montanensis*) - has shown some degree of conservation on the mechanisms utilized for the invasion of vertebrate and invertebrate cells. In all cases, rickettsiae entry was shown to depend on actin rearrangement, with the Arp2/3 complex playing a central role in actin nucleation (Martinez and Cossart, 2004; Petchampai et al., 2015; Petchampai et al., 2014; Reed et al., 2014; Reed et al., 2012). The higher degree of variation was observed on the contribution of the upstream molecules that participate in the multiple signaling pathways controlling actin rearrangement, which appear to vary depending not only on the host cell type but also between rickettsial species. Integration of the data from these studies suggests that receptor binding by *Rickettsia* triggers the activation of host tyrosine kinases. Both receptor tyrosine kinases and Src family members were shown to play a role in *R. conorii* invasion into non-phagocytic cells and *R. montanensis* invasion of tick cells, whereas the results reported for *R. parkerii* suggest no dependency in a particular tyrosine kinase signaling pathway (Martinez and Cossart, 2004; Petchampai et al., 2015; Reed et al., 2012). This leads then to activation of multiple signaling molecules (e.g. Cdc42, Rac1, PI3-K), which may cooperatively (observed for Cdc42 and Rac1, but not PI3-K in *R. parkeri* invasion studies; Cdc42 and PI3-K, but not Rac1, in *R. conorii* entry in non-phagocytic cells; and Rac1 and PI3-K in *R. montanensis* entry in tick cells) contribute to activate different members of Wiskott-Aldrich syndrome protein (WASP) family of proteins, which then regulate the activation of the Arp2/3 complex. In this case, a WAVE-dependent and N-WASP-independent process was described for *R. parkeri* invasion (Reed et al., 2012), whereas a moderate effect of N-WASP was reported in the invasion of tick cells by *R. montanensis* (Petchampai et al., 2015). Supported by our recent findings demonstrating that *R.*

conorii and *R. montanensis* can invade THP-1 macrophages (Curto et al., 2016), here we identified core host molecules involved in the early steps of invasion of these phagocytic cells. Our results reveal that several signaling molecules previously described as necessary in non-phagocytic (or tick) cells also impaired rickettsial infection of macrophage-like cells (e.g. different families of tyrosine kinases, Cdc42, N-WASP, Arp2/3), although we identified others for which a different effect was observed (e.g., PI3-K), together with new core factors as are the cases of p21-activated kinase (PAK1) and Na^+/H^+ exchangers (NHE). Moreover, our results clearly showed that *R. conorii* and *R. montanensis* differentially target several of these host components, anticipating differences in the host signaling pathways utilized by these species to promote actin rearrangement.

Consistent with previous observations, our results showed that activation of the Arp2/3 complex is important for rickettsial entry into macrophage-like cells. However, we also observed differences in the effect of actin polymerization inhibitors suggesting somewhat different requirements on host actin polymerization dynamics between *R. conorii* and R. montanensis. Further highlighting these differences is the evidence that inhibition of PAK1 with IPA-3 (10 μM) almost completely abolished *R. conorii* entry process, while having a less pronounced impact on *R. montanensis* entry (14.1% *R. conorii*/cell, $P \leq 0.00001$ *vs.* 51.5% *R. montanensis*/cell, $P \leq 0.001$). PAK1 plays a central role in regulating the dynamics of the cytoskeleton through the activation of different downstream factors (Edwards et al., 1999; Eswaran et al., 2008; Liberali et al., 2008). Regulation of F-actin organization/remodeling is one of the processes affected by PAK1-dependent signaling cascades, involving activation of LIM-1 kinase (LIMK-1) which then regulates activation of cofilin/ADF (F-actin depolymerizing and severing proteins) (Edwards et al., 1999). Based on our results on PAK1 inhibition, it is possible that F-actin organization may be differentially affected by *R. conorii* and *R. montanensis* invasion. Therefore, evaluation of the contribution of LIMK-1/cofilin/ADF signaling (as well as of other downstream targets of PAK1 affecting cytoskeletal rearrangement (Eswaran et al., 2008)) for rickettsial entry into macrophage-like cells warrants further investigation. Also, it remains to be investigated if the impact of PAK1 activation in rickettsial entry into non-phagocytic cells is similar (particularly for *R. conorii*). Evidence from *R. parkeri* invasion studies in HMEC-1 cells supports a robust recruitment of PAK1 to the sites of bacterial

invasion 5-15 min after infection (Reed et al., 2012). However, the impact of inhibition of PAK1 on invasion was not evaluated in this study.

PAK1 activation has a central role in regulating macropinocytosis (Eswaran et al., 2008; Liberali et al., 2008). Macropinocytosis is an endocytic process that is initiated by actin-driven membrane ruffling, and that can occur spontaneously or as a result of activation by external factors (e.g., growth factors and phosphatidylserine-containing residues) (Eswaran et al., 2008; John Von Freyend et al., 2017). This is considered an efficient innate immunity mechanism by which large plasma-membrane containing domains can be internalized in response to stimuli during infection (Eswaran et al., 2008). However, the utilization of macropinocytosis as an alternative entry pathway by many pathogens has been reported and suggested to be correlated with immune evasion (John Von Freyend et al., 2017; Mercer and Helenius, 2009, 2012). Entering through macropinosomes may enable pathogens to escape Toll-like receptors and other factors that trigger immune responses, as well as the endosomal compartments involved in antigen presentation (Mercer and Helenius, 2009). Indeed, it has been reported that macropinocytosis of apoptotic debris suppresses activation of innate immune responses (Albert, 2004). Notably, PAK1 is emerging as a central component of host-pathogen interactions, as its activation was shown to be essential for host invasion by many pathogens utilizing macropinocytosis-mediated pathways (John Von Freyend et al., 2017). Our observations on the robust effect of PAK inhibition, combined with the substantial impact of other macropinocytosis inhibitors (the NHE blockers DMA and EIPA) (Mercer and Helenius, 2009) impairing *R. conorii* entry into THP-1 macrophages, clearly suggest that *R. conorii* may use a macropinocytosis-dependent pathway to enter macrophage-like cells. We have previously demonstrated that *R. conorii* and *R. montanensis* display differences in the ability to bind to THP-1 cells, suggesting the possible use of alternative routes of entry into macrophages (Curto et al., 2016). The differential requirement here demonstrated for PAK activation and NHE between *R. conorii* and *R. montanensis* entry process, clearly anticipates the mobilization of different signaling pathways by these rickettsial species, further strengthening this hypothesis. Supported by our results, *R. conorii* appears to have the capacity to use different ways of interfering with actin rearrangement through signaling pathways preferentially controlled by PAK and/or, to a less extent,

by the Arp2/3 complex. Therefore, we suggest that *R. conorii* may also use a novel PAK-NHE-TK-dependent macropinocytosis-like mechanism (apparently PI3K-PKC-independent) to invade macrophage-like cells, in parallel or overlapping with Arp2/3-dependent actin nucleation (through N-WASP activation) **(Figure III.7)**.

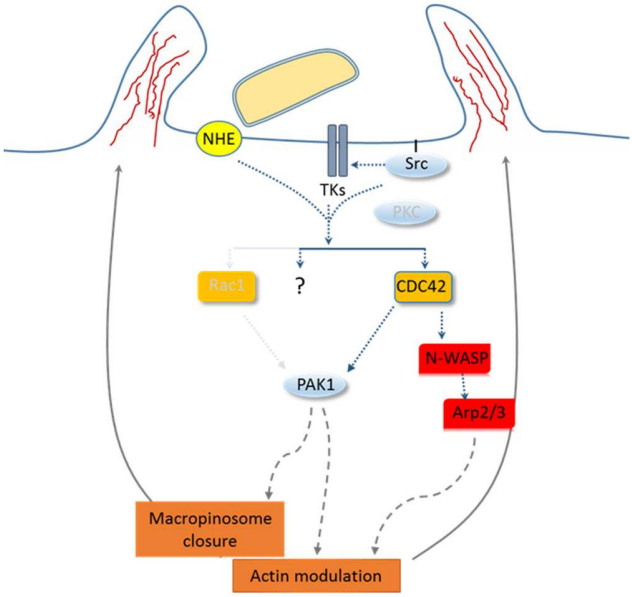

Figure III.7 | Prediction model of signaling during the early mechanism events involved in *R. conorii* entry into macrophage-like cells. The activation of macropinocytosis-like pathways through RTKs initiates a multi-branched signaling cascade that involves a diverse array of molecular players (adaptors (Src), GTPases (Cdc42), kinases (PAK1). These signaling cascades are responsible for initiating actin modulation, macropinosome closure and trafficking. A dependence of Na^+/H^+ exchangers (the main diagnostic test to identify macropinocytosis) for *R. conorii* entry process was here identified. Abbreviations: NHE - Na^+/H^+ exchangers; RTKs – receptor tyrosine kinases; Src – non-receptor tyrosine kinase protein; PKC – protein kinase C; Cdc42 – cell division control protein 42 homolog; Rac1 – Rac family small GTPase 1; PAK1 – serine/threonine-protein kinase PAK 1; N-WASP – Neural Wiskott-Aldrich syndrome protein; Arp2/3 - Arp2/3 complex.

Among upstream effectors, our results suggest a more prominent role for Cdc42 than Rac1, although we cannot exclude that other guanine nucleotide-exchange factors (or even bacterial factors) may be regulating PAK and/or other WASP family of proteins (Eswaran et al., 2008; John Von Freyend et al., 2017; Rohatgi et al., 2000). How the different signals are integrated and what induces the differential activation of the signaling molecules herein anticipated remains to be elucidated.

Supported by our findings, the ability of *R. conorii* to use a macropinocytosis-like pathway as an alternative route of entry in macrophages should be further evaluated as well as its possible contribution for the, already reported, ability of *R. conorii* to subvert macrophage immune defenses. Indeed, it is now becoming clear that gram-negative bacteria such as *Shigella flexneri*, *Salmonella enterica* serovar Typhimurium, and *Chlamydia trachomatis* take advantage of macropinocytosis-like processes to invade and subvert host cell pathways (Ford et al., 2018; Kuhn et al., 2017; Rosales-Reyes et al., 2012; Weiner et al., 2016). However, the complexity of signaling mechanisms underpinning cell entry which have now been described for several intracellular pathogens suggests a multiplicity and potentially redundant routes of entry. As a way of example, multiple entry pathways using aspects of both zipper and trigger mechanisms have been demonstrated for *Chlamydia trachomatis* and *Salmonella* (Boumart et al., 2014; Ford et al., 2018; Velge et al., 2012). Interestingly, the multiplicity of entry pathways for different *Salmonella* serovars has been correlated with different intracellular behaviors, contributing to different *Salmonella*-induced diseases and *Salmonella*-host specificity (Velge et al., 2012). Differences in the interplay between distinct forms of Coxiella (with different virulent properties) and host cell proteins have also been shown to mediate internalization rates of the bacteria, and subsequent pathogenicity attributes (Abnave et al., 2017; Cockrell et al., 2017). Among several virulence factors, *C. burnetti* lipopolysaccharide (LPS) (avirulent form harbors truncated LPS) has been described as one of the major factors contributing for the invasion process and the subsequent ability to hijack immune defenses (Abnave et al., 2017). With this work, we have demonstrated that different SFG *Rickettsia* species may also utilize different routes of entry. In non-phagocytic cells, *Rickettsia* use a zipper mechanism to facilitate infection which depends (at least in part) on the interaction between rickettsial rOmpB, rOmpA and the mammalian receptors Ku70 and $\alpha_2\beta_1$ integrin, respectively, although other bacterial ligands and host receptors may also be involved (Chan et al., 2009; Hillman et al., 2013; Martinez et al., 2005). In phagocytic cells, it remains to be clarified what the contribution of Ku70 is, and what other rickettsial and host factors trigger (differential) intracellular signaling.

Our results raise new questions about a possible correlation between the invasion mechanisms engaged by SFG *Rickettsia* species and subsequent intracellular behavior (and fate)

within macrophages. Further studies will be required to determine the detailed mechanisms of the different routes that rickettsia use to infect phagocytic cells and the relevance of the different entry processes to pathogenesis.

III.6 | Acknowledgements

We would like to acknowledge Dr. Kevin Macaluso (LSU SVM Department of Pathobiological Sciences) for providing *R. montanensis* isolate M5/6. We would like to thank Abigail Fish, Daniel Garza and Sean Riley for helpful suggestions in completion of this study.

Chapter IV

Transcriptomic profiling of macrophages infected by a pathogen and a non-pathogen Spotted Fever Group *Rickettsia* reveals differential reprogramming signatures

IV.1 | Abstract

Despite their high degree of genomic similarity, different SFG *Rickettsia* are often associated with very different clinical presentations. For example, *Rickettsia conorii* causes Mediterranean spotted fever, a life-threatening disease for humans, whereas *Rickettsia montanensis* is associated with limited or no pathogenicity to humans. However, the molecular basis responsible for these different clinical presentations are still not understood. Although killing microbes is a key function of macrophages, the ability to survive and/or proliferate within phagocytic cells seems to be a phenotypic feature of several intracellular pathogens. We have previously showed that *R. conorii* and *R. montanensis* display a differential tropism for macrophage-like cells. Herein, we have carried out a comprehensive transcriptomic profiling to further elucidate early host cell responses upon infection of THP-1 macrophages with each of these species of SFG *Rickettsia*. Our RNAseq data revealed that the pathogenic *R. conorii* was able to induce a more robust set of alterations in host gene expression profiles compared to the non-pathogenic *R. montanensis*. Transcriptional programs generated upon infection with *R. conorii* point towards a sophisticated ability of *R. conorii* to evade innate immune signals by modulating the expression of several anti-inflammatory molecules early upon infection. Moreover, *R. conorii* was also able to induce the expression of several pro-survival genes, which may result in the ability to prolong host cell survival, thus protecting its replicative niche. Remarkably, *R. conorii*-infection promoted a robust modulation of different regulators of the gene expression machinery, suggesting that regulation of host nuclear dynamics may be key to *R. conorii* tropism for THP-1 macrophages. This work provides new insights on the molecular mechanisms underlying the differential species-specific patterns of rickettsial cellular tropism and pathogenicity, opening several avenues of research in host-rickettsiae interactions.

IV.2 | Introduction

Rickettsiae are obligate intracellular bacteria that can cause mild to life-threatening diseases (Kelly et al., 2002). Advances in molecular techniques have allowed the detection of new and old rickettsial pathogens in new locations, suggesting an expanding distribution of reported cases and anticipating new regions of risk for rickettsioses (Richards, 2012). Spotted fever group (SFG) *Rickettsia* are recognized as important agents of human tick-borne diseases worldwide, with some members drastically differing in their ability to cause disease in humans (Uchiyama, 2012; Wood and Artsob, 2012). For example, *R. conorii* (the causative agent of Mediterranean spotted fever (MSF)) is highly pathogenic and associated with high morbidity and mortality rates, whereas *R. montanensis* has been considered as an organism with limited or no pathogenicity to humans (de Sousa et al., 2003; Galvao et al., 2005; McQuiston et al., 2012; Walker, 1989). However, the underlying mechanisms governing differences in pathogenicity by different SFG rickettsiae are still to be fully understood.

Several studies have provided evidence of non-endothelial parasitism of rickettsial species with intact bacteria being found in macrophages and neutrophils (both in tissues and blood circulation), raising the debate about the biological role of the rickettsiae-phagocyte interaction in the progression of rickettsial diseases (Banajee et al., 2015; Riley et al., 2016; Walker and Gear, 1985; Walker et al., 1999; Walker et al., 1994). We have recently demonstrated that the non-pathogenic *R. montanensis* and the pathogenic *R. conorii* have completely distinct intracellular fates in human THP-1 macrophages (Curto et al., 2016). *R. montanensis* are rapidly destroyed upon infection culminating in their inability to survive and proliferate in THP-1 macrophages. In contrast, *R. conorii* cells maintain the morphology of intact bacteria and establish a successful infection within these cells. Interestingly, similar survival *vs.* death phenotypes were also observed for the virulent Breinl strain and the attenuated E strain of *R. prowazekii* in macrophage cell cultures, respectively (Gambrill and Wisseman, 1973b). These results suggest that survival of rickettsial species within macrophages may be an important virulence mechanism. However, little is still known about host and rickettsial molecular determinants responsible for these differences in macrophage tropism and its relation to pathogenesis.

Due to reductive genome evolution, *Rickettsia* are obligate intracellular pathogens, making them completely dependent on their host to survive (Blanc et al., 2007; Darby et al., 2007; Sakharkar et al., 2004). Consequently, they must have evolved different strategies to manipulate host-signaling pathways making the host environment prone for their own survival and proliferation (Darby et al., 2007; Driscoll et al., 2017). Several bacterial and viral pathogens can indeed reprogram the host cell transcriptome for their own benefit in order to survive and proliferate (Ashida and Sasakawa, 2014; Goodwin et al., 2015; Hannemann and Galan, 2017; Paschos and Allday, 2010; Tran Van Nhieu and Arbibe, 2009). However, the study of host signaling reprogramming by rickettsial species is still in its infancy.

After infection of host cells, alterations on the content of transcripts are expected as a result not only of the natural host cell response but also due to the potential manipulation of host signaling pathways by the pathogen. High-throughput transcriptomic analysis using RNA-seq has become a key tool to understand these molecular changes generated by bacterial or viral infections of eukaryotic cells (Westermann et al., 2017). In this work, we evaluate the early transcriptional alterations generated upon infection of THP-1 macrophages with the pathogenic (*R. conorii*) and the non-pathogenic (*R. montanensis*) member of SFG *Rickettsia* by RNA-seq. Our transcriptomic results demonstrate that one hour after infection, a total of 470 and 86 genes were differentially regulated upon infection of THP-1 macrophages with *R. conorii* and *R. montanensis*, respectively. A detailed analysis of the pathways affected by these genes revealed that *R. conorii* elicits a global transcriptional program that results in the establishment of a replicative niche within the infected host cell. Specifically, *R. conorii* infection of THP-1 cells results in the regulation of TNFR1 and TNFR2 signaling pathways, cellular pro-survival pathways and RNA polymerase II mediated transcription that is significantly different from the transcriptional profiles induced by *R. montanensis* infection. Overall, these findings highlight the mechanisms that an obligate intracellular bacterial pathogen utilizes to manipulate a host cell at the transcriptional level early in the infection process, which can ultimately result in the ability of the bacterium to proliferate intracellularly within a phagocyte.

IV.3 | Materials and Methods

IV.3.1 | Cell lines

Vero cells (CCL-81 ATCC) were grown in Dulbecco's modified Eagle's medium (DMEM, Gibco) supplemented with 10% (v/v) heat-inactivated fetal bovine serum (Atlanta Biologicals), 1x non-essential amino acids (Corning), and 0.5 mM sodium pyruvate (Corning). THP-1 (TIB-202^{TM}, ATCC) cells were grown in RPMI-1640 medium (Gibco) supplemented with 10% (v/v) heat-inactivated fetal bovine serum. Differentiation of THP-1 cells into macrophage-like cells was carried out by the addition of 100 nM of phorbol 12-myristate 13-acetate (PMA, Fisher). Cells were allowed to differentiate and adhere for 3 days prior to infection. Both cell lines were maintained in a humidified 5% CO_2 incubator at 34°C.

IV.3.2 | Microbe strains

R. conorii isolate Malish7 and *R. montanensis* isolate M5/6 were routinely cultured in Vero cells in DMEM supplemented with 10% (v/v) heat-inactivated fetal bovine serum, 1x non-essential amino acids, and 0.5 mM sodium pyruvate and maintained in a humidified 5% CO_2 incubator at 34°C.

IV.3.3 | RNA Isolation, DNase Treatment, Ribosomal RNA depletion, and cDNA Synthesis

PMA-differentiated THP-1 cells monolayers at a cell confluency of 1.2 x 10^6 cells per well, in 6 well plates (2 wells per condition) were infected with *R. conorii, R. montanensis* at a multiplicity of infection (MOI) of 10 or maintained uninfected. Plates were centrifuged at 300 x g for 5 min at room temperature to induce contact between rickettsiae and host cells, and incubated at 34°C and 5% CO_2 for 1 hour. At the specified time point, culture medium was removed, cells were washed 1x with PBS and total RNA was purified using SurePrep True Total RNA purification kit (ThermoFisher Scientific). DNA was removed from the RNA purification using Ambion Turbo DNase according to manufacturer's instructions. Removal of DNA contamination was verified by PCR using primers specific for the human actin gene. After DNase treatment, RNA was re-isolated using PureLink RNA Mini Kit (Ambion) according to manufacturer's instructions. RNA quality control

was performed on a Fragment Analyzer (Advanced Analytical) to determine the RNA quality number (RQN). All RNA samples had a RQN > 7.2 (7.2-8.5). After confirmation of RNA structural integrity, 5 µg RNA per sample were subjected to ribosomal RNA depletion using RiboMinus™ Eukaryote System v2 (Ambion) protocols. cDNA libraries were then constructed using the Ion Total RNAseq Kit v2 (Ion torrent). Sample preparation was carried out on a total of four replicates per condition.

IV.3.4 | qRT-PCR Validation

To validate the RNAseq results, changes to the transcriptional content of specific genes were determined by quantitative RT-PCR using SYBR Select Master Mix for CFX (Applied Biosystems). Fifteen random human genes present in our RNA-seq lists were chosen, and primers that generate PCR products smaller than 90 nucleotides were designed for each specific gene. PCR reactions with the respective primer set and using human genomic DNA isolated from THP-1 cells as template were carried out as follows: 95 °C for 2 min, followed by 35 cycles of 95 °C for 15 sec, 58 °C for 15 sec and 72 °C for 60 sec. Amplified PCR products were cloned into pCR2.1 using TOPO TA cloning kit (Invitrogen) according to manufacturer's instructions and confirmed by DNA sequencing. Plasmids were used to generate standard curves for each specific gene of interest (GOI). The quantity of transcript for each gene present in each cDNA library was determined by qPCR using the following conditions: 50 °C for 2 min, 95 °C for 2 min, followed by 40 cycles of 95 °C for 15 sec, 58 °C for 15 sec and 72 °C for 60 sec followed by melting curve using a LightCycler 480 II (Roche). qRT-PCR-derived fold change values are expressed as in equation 1:

$$fold\ change = LOG2\left({Exp.cond.2}/{Exp.cond.1}\right) = \left[\frac{(GOI\ Exp.cond.2/Reference\ gene\ Exp.cond.2)}{(GOI\ Exp.cond.1/Reference\ gene\ Exp.cond.1)}\right] \quad (1)$$

Glucose-6-phosphate dehydrogenase (G6PD), ER membrane protein complex subunit 7 (EMC7) and beta-2-microglobulin (B2M) were used as reference genes to normalize the results between the different experimental conditions (Eisenberg and Levanon, 2013; Leisching et al., 2016).

IV.3.5 | Bioinformatics Analysis

Principal Component Analysis (PCA) was performed by importing the mapped read (BAM) files into a server running Partek® Flow® Software, version 6.0.17, Copyright© 2017. The Volcano Plots were created from the output from CuffDiff, with custom python and R scripts. Significantly differentially expressed genes were uploaded into DAVID Bioinformatics Resources 6.8 (https://david.ncifcrf.gov/home.jsp) to categorize genes according to biological function, host cellular pathways and cellular component gene ontology (GO) terms (Huang da et al., 2009). Significantly differentially expressed genes were also uploaded into Ingenuity Pathway Analysis (IPA) (QIAGEN Inc., https://www.qiagenbioinformatics.com/products/ingenuity-pathway-analysis) to identify significant altered canonical pathways or downstream disease/functions (Kramer et al., 2014). Activation or inhibition of predicted canonical pathways and disease/function were determined by Z-scores calculated by IPA. Positive Z-scores (> 2.0) predict activation whereas negative Z- scores (< -2.0) predict inhibition. Functional protein association networks were evaluated using STRING 10.5 (http://string-db.org/) with high confidence (0.7) parameters (Szklarczyk et al., 2017).

IV.3.6 | TNFα Activation of THP-1 cells.

PMA-differentiated THP-1 cells at 5 x 10^4 THP-1 cells per well were infected with *R. conorii* or *R. montanensis* (MOI= 10), and centrifuged at 300 x g for 5 min at room temperature to induce contact. 24 hours after infection, 5 μg/mL *Escherichia coli* O26:B6 Lipopolysaccharide (Invitrogen) in culture media or media alone was added, and incubated for 24 additional hours. 48 total hours after infection, the media was removed, and TNFα concentration was determined by ELISA with Maxisorp plates (Nunc), Human TNFα Duo Set (R&D Systems), and OptiEIA TMB substrate (BD biosciences). Absorbance was measured at 450 mn and standard curve generated with recombinant human TNFα (R&D Systems).

IV.3.7 | PARP-1 Cleavage Assay

PMA-differentiated THP-1 cells were seeded on glass coverslips in 24-well plates at 2 x 10^5 cells per well. THP-1 monolayers were then infected with *R. conorii* (MOI=2.5), the plates were centrifuged at 300 x g for 5 min at room temperature to induce contact, and subsequently incubated for 1, 3 and 5 days at 34 ˚C and 5% CO_2. As a control, uninfected THP-1 macrophages were always kept at the same experimental conditions. When mentioned, *R. conorii*-infected and uninfected cells were incubated with staurosporine (EMD Biosciences) at a final concentration of 750 nM to induce intrinsic apoptosis during 4 hours. At each specific time point, *R. conorii*-infected and uninfected THP-1 macrophages were washed 1x with 1 mL of PBS, and fixed in 4% PFA for 20 min prior to staining. After permeabilization with 0.1% Triton X-100 and blocking with 2% BSA, cells were then incubated with rabbit anti-cleaved poly(ADP-ribose) polymerase (PARP) (1:400) (Cell Signaling Technology) and mouse anti-*R. conorii* 5C7.31 (1:1,500) antibodies for 1 hour, washed 3x in PBS, and then incubated in PBS containing 2% BSA, Alexa Fluor 488-conjugated goat anti-rabbit IgG (1:1,000) (ThermoFisher Scientific), Alexa Fluor 594-conjugated goat anti-mouse (1:1,000) (ThermoFisher Scientific) and DAPI (1:1,000) (ThermoFisher Scientific). After washing 3x with PBS, glass coverslips were mounted in Mowiol mounting medium and preparations were viewed on a LEICA DM 4000 B microscope equipped with Nuance FX multispectral imaging system using a final X40 optical zoom and processed with Image J software (https://imagej.nih.gov.ij/).

IV.3.8 | RNA-seq data analysis

The samples were sequenced using an Ion Proton V2 chip on Ion Chef instrument (ThermoFisher Scientific), following manufacturer's instructions. A QAQC check of the samples showed the read lengths followed a normal distribution, with average lengths between 117 and 131 bp, and an average read quality between 22 and 23. Adapters were trimmed from the samples using cutadapt (Martin, 2011), and the first 25 bp of the reads were trimmed after it was noticed several samples had spurious reads in this region. Next, STAR was used to map splice junctions to the human transcriptome, which was downloaded from ENSEMBL on 04/15/2017 (Dobin et al., 2013). The program Cufflinks and Cuffmerge was then used to map transcripts and calculate gene

expression, and Cuffdiff was used to calculate which samples had genes which were statistically significantly differently expressed between conditions (Trapnell et al., 2013; Trapnell et al., 2012). Cuffdiff calculated a $\log_2$ fold expression for the genes in the samples using the gene expression values from Cufflinks, and a False Discovery Rate (FDR) of $p < 0.05$. In cases where the gene expression of one sample was 0, the value was set to 1×10^{-4} to prevent an undefined value for the $\log_2$ fold change calculations, and in cases where Cufflinks identified more than one isoform that mapped to reads, the first named isoform was used.

IV.3.9 | Statistical Analysis

Correlation between qRT-PCR and RNAseq results was performed by Pearson analysis of correlation in GraphPad Prism (GraphPad Software, Inc). Pearson correlations coefficients can be found in **Figure V.1A-B**.

TNFα activation assays experiments were performed twice with each individual experiment done in triplicate for each experimental condition. Statistical analysis was performed by Mann Whitney test using GraphPad Prism (GraphPad Software, Inc). Results are shown as mean ± SD and differences were considered ns (non-significant) at $P > 0.05$ or significant at * $P \leq 0.05$, ** $P \leq 0.01$, *** $P \leq 0.001$.

PARP-cleavage experiments were done in quadruplicate and at least 100 mammalian nuclei were counted for each independent experiment. Results of each experiment were expressed as the percentage of cleaved PARP-positive cells. Statistical analysis was performed by Mann Whitney test using GraphPad Prism (GraphPad Software, Inc). Results are shown as mean ± SD and differences were considered ns (non-significant) at $P > 0.05$ or significant at * $P < 0.05$.

IV.3.10 | Data availability

Raw RNA-seq data have been deposited into the Sequence Read Archive (SRA) of the National Center for Biotechnology Information (https://www.ncbi.nlm.nih.gov/sra/SRP135996) under the accession number SRP135996. Raw and processed RNA-seq data files were also

deposited into the ArrayExpress platform under the accession number E-MTAB-6724. Reviewer login information details: Username: Reviewer_E-MTAB-6724; Password: knXikq5m.

IV.4 | Results

IV.4.1 | SFG *Rickettsia* trigger considerable macrophage reprogramming early in infection

The drastic intracellular phenotypic differences between *R. montanenis* and *R. conorii* in THP-1 macrophages (Curto et al., 2016) suggest early transcriptomic alterations, either as a result of host cell response to infection or bacterial manipulation. To further elucidate the molecular determinants that contribute for this species-specific patterns of cellular tropism, we performed a global profiling of early transcriptional responses of cultured human THP-1 macrophages stimulated by *R. conorii* and *R. montanensis* infection (MOI=10). RNA harvested at 60 min post-infection was subjected to whole genome transcriptomic analysis and compared to uninfected cells, processed in parallel. Principal component analysis (PCA) was carried out to assess the sample correlations using the expression data of all genes **(Supplementary Figure IV.1)**. Cuffdiff was then used to determine significantly differentially expressed (DE) genes between infected and uninfected conditions with a p-value cutoff of <0.05 (FDR p<0.05), and results were expressed as log_2 fold change. In total, 470 genes were filtered to be expressed at significantly higher levels (n=267) or lower levels (n=203) in *R. conorii*-infected macrophages **(Figure IV.1A and Supplementary Table IV.1)**. On the other hand, 86 genes were filtered to be expressed at significantly higher levels (n=75) or lower levels (n=11) in *R. montanensis*-infected cells **(Figure IV.1B and Supplementary Table IV.2)**. These results support that considerable transcriptomic changes occurred upon infection with either the pathogenic (*R. conorii*) or the non-pathogenic (*R. montanensis*) SFG *Rickettsia* as early as 1 hour post-infection. To validate the RNA-seq results, 15 genes were chosen for individual analysis by an independent experimental method. The amount of transcript for each gene was determined for all experimental conditions and log_2 q-RT-PCR-derived fold change for each situation was determined according to equation 1 (Methods). Log_2 fold change values are shown in **Supplementary Table IV.3**. The q-PCR data for the analyzed genes was then compared to the fold change values obtained by RNA-seq and the results from each quantification method demonstrate a significant correlation between experimental methods **(Figure 1C-D)**, thereby validating the transcriptional changes obtained by RNA-seq**.**

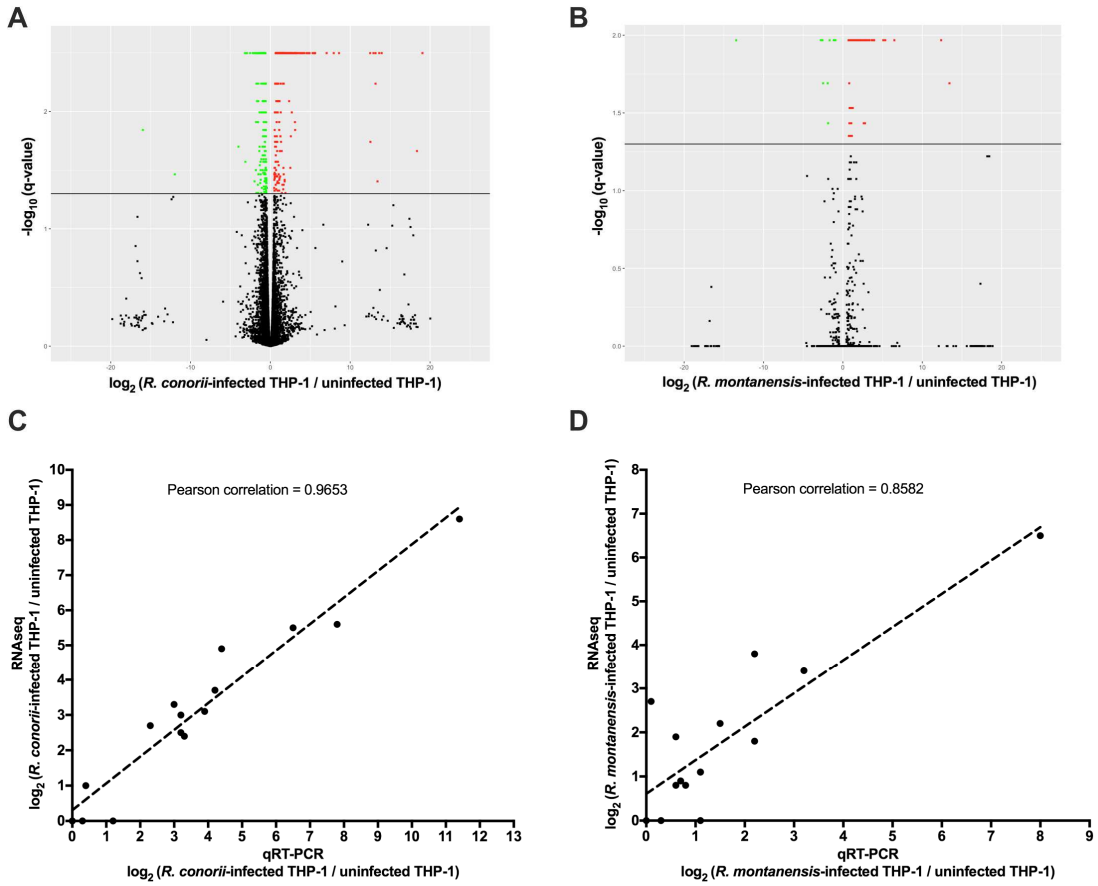

Figure IV.1 | SFG *Rickettsia* trigger considerable reprogramming in THP-1 macrophages early in infection. **(A-B)** Volcano plots of $\log_2$ fold change ratio of the expression levels in *R. conorii*- **(A)** and *R. montanensis*- **(B)** infected THP-1 macrophages over that in uninfected cells plotted against the $-\log_{10}$ (q-value). Statistically differentially upregulated and downregulated genes are represented in red and green, respectively (FDR < 0.05). See also **Supplementary Tables IV.1 and IV.2**. **(C-D)** Validation of RNA-seq data by comparing the transcriptional fold changes determined by RNA-seq and an independent method (q-RT-PCR) for *R. conorii*- **(C)** and *R. montanensis*- **(D)** infected cells. Pearson analysis of correlation was performed in GraphPad Prism. See also **Supplementary Table IV.3**.

IV.4.2 | *Rickettsia conorii* infection promotes a more robust modulation of host gene expression profiles compared to responses triggered by *R. montanensis*

Infection of THP-1 macrophages with *R. conorii* and *R. montanensis* resulted in a total of 495 host genes of which the transcript levels were considered statistically DE at 1 hour post infection when compared to uninfected cells. After sorting out this differential gene expression per experimental condition, four main different groups of genes were identified as illustrated in **Figure IV.2A (Supplementary Table IV.4)**: 409 genes were specifically regulated by *R. conorii* (214 are

upregulated and 195 are downregulated) and were designated as *R. conorii* specific; 61 genes were common to infection by both rickettsial species (53 are upregulated and 5 are downregulated), with 3 genes in this group being inversely regulated; and 25 genes (19 are upregulated and 6 are downregulated) were identified as *R. montanensis* specific.

Gene ontology (GO) analysis of the DE genes were carried out using DAVID Bioinformatics Resources (Huang da et al., 2009), in order to categorize genes according to: biological function, canonical pathways, and cellular component **(Figure IV.2 B-G and Supplementary Table IV.5)**. Analysis of the 58 DE genes commonly altered by the infection of either *R. conorii* or *R. montanensis* revealed differential regulation of genes involved in inflammatory response, cellular response to tumor necrosis factor (TNF), cellular response to lipopolysaccharide, immune response, among others **(Figure IV.2B)**. Common DE genes were also categorized into several canonical pathways, which include TNF signaling, salmonella infection, toll-like receptor, NF-κB, chemokine signaling and cytokine-cytokine receptor interaction **(Figure IV.2C)**. Moreover, a higher representation of transcripts corresponding to extracellular proteins was observed **(Figure IV.2D)**. The 3 genes that are inversely DE between *R. conorii* and *R. montanensis*-infected cells correspond to non-coding RNAs (RNU1-148P; RNU5A-1; RNU5D-1). On the other hand, analysis of the 409 DE genes uniquely altered in *R. conorii*-infected cells revealed differential regulation of several genes involved in both positive and negative regulation of transcription from RNA polymerase II promoter, inflammatory response, response to lipopolysaccharide, positive regulation of gene expression, and regulation of apoptotic process **(Figure IV.2E)**. Moreover, *R. conorii*-specific deregulated genes map to several canonical pathways, such as transcriptional misregulation in cancer, MAPK, TNF and NF-κB signaling, and viral carcinogenesis **(Figure IV.2F)**. *R. conorii*-specific DE genes showed a significant overrepresentation for nuclear localization **(Figure IV.2G)**. For the 25 DE genes specifically altered by the infection of THP-1 macrophages with *R. montanensis,* no significant enrichment was detected with very few genes categorized according to DAVID databases **(Supplementary Table IV.5)**.

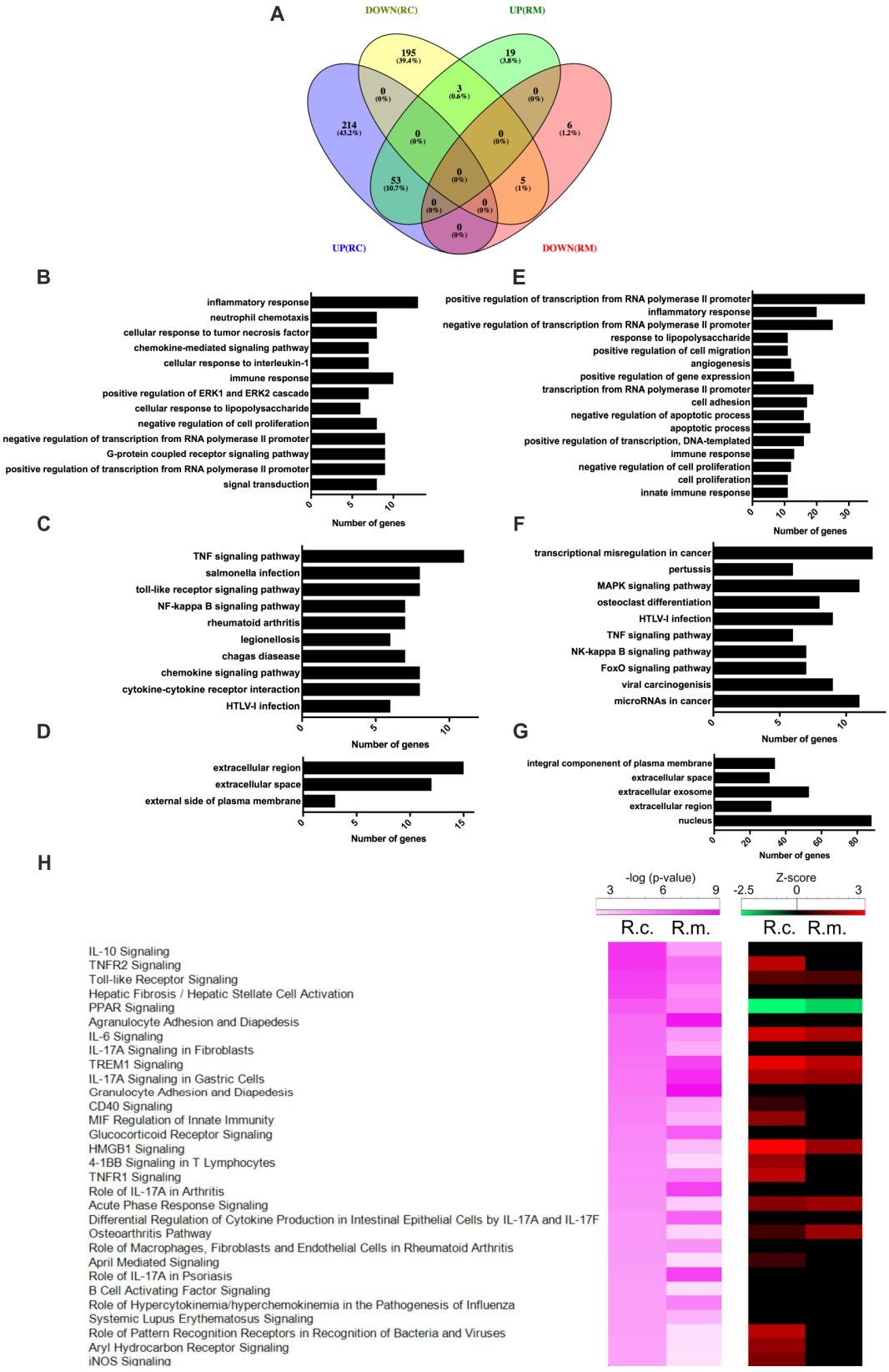
A
DOWN(RC)
UP(RM)
195 (39.4%)
19 (3.8%)
0 (0%)
3 (0.6%)
0 (0%)
214 (43.2%)
0 (0%)
0 (0%)
6 (1.2%)
53 (10.7%)
0 (0%)
5 (1%)
0 (0%)
0 (0%)
0 (0%)
UP(RC)
DOWN(RM)
B
inflammatory response
neutrophil chemotaxis
cellular response to tumor necrosis factor
chemokine-mediated signaling pathway
cellular response to interleukin-1
immune response
positive regulation of ERK1 and ERK2 cascade
cellular response to lipopolysaccharide
negative regulation of cell proliferation
negative regulation of transcription from RNA polymerase II promoter
G-protein coupled receptor signaling pathway
positive regulation of transcription from RNA polymerase II promoter
signal transduction
0 5 10
Number of genes
C
TNF signaling pathway
salmonella infection
toll-like receptor signaling pathway
NF-kappa B signaling pathway
rheumatoid arthritis
legionellosis
chagas diasease
chemokine signaling pathway
cytokine-cytokine receptor interaction
HTLV-I infection
0 5 10
Number of genes
D
extracellular region
extracellular space
external side of plasma membrane
0 5 10 15
Number of genes
E
positive regulation of transcription from RNA polymerase II promoter
inflammatory response
negative regulation of transcription from RNA polymerase II promoter
response to lipopolysaccharide
positive regulation of cell migration
angiogenesis
positive regulation of gene expression
transcription from RNA polymerase II promoter
cell adhesion
negative regulation of apoptotic process
apoptotic process
positive regulation of transcription, DNA-templated
immune response
negative regulation of cell proliferation
cell proliferation
innate immune response
0 10 20 30
Number of genes
F
transcriptional misregulation in cancer
pertussis
MAPK signaling pathway
osteoclast differentiation
HTLV-I infection
TNF signaling pathway
NK-kappa B signaling pathway
FoxO signaling pathway
viral carcinogenisis
microRNAs in cancer
0 5 10
Number of genes
G
integral componenent of plasma membrane
extracellular space
extracellular exosome
extracellular region
nucleus
0 20 40 60 80
Number of genes
H
-log (p-value)
3 6 9
Z-score
-2.5 0 3
R.c. R.m.
R.c. R.m.
IL-10 Signaling
TNFR2 Signaling
Toll-like Receptor Signaling
Hepatic Fibrosis / Hepatic Stellate Cell Activation
PPAR Signaling
Agranulocyte Adhesion and Diapedesis
IL-6 Signaling
IL-17A Signaling in Fibroblasts
TREM1 Signaling
IL-17A Signaling in Gastric Cells
Granulocyte Adhesion and Diapedesis
CD40 Signaling
MIF Regulation of Innate Immunity
Glucocorticoid Receptor Signaling
HMGB1 Signaling
4-1BB Signaling in T Lymphocytes
TNFR1 Signaling
Role of IL-17A in Arthritis
Acute Phase Response Signaling
Differential Regulation of Cytokine Production in Intestinal Epithelial Cells by IL-17A and IL-17F
Osteoarthritis Pathway
Role of Macrophages, Fibroblasts and Endothelial Cells in Rheumatoid Arthritis
April Mediated Signaling
Role of IL-17A in Psoriasis
B Cell Activating Factor Signaling
Role of Hypercytokinemia/hyperchemokinemia in the Pathogenesis of Influenza
Systemic Lupus Erythematosus Signaling
Role of Pattern Recognition Receptors in Recognition of Bacteria and Viruses
Aryl Hydrocarbon Receptor Signaling
iNOS Signaling

Figure IV.2 (previous page) | Gene expression patterns stimulated by infection of THP-1 macrophages with *R. conorii* or *R. montanensis* reveal a more robust modulation by the pathogenic species. (A) Venn diagram depicting the number and distribution of specific and common DE genes in each experimental condition. UP means upregulated, DOWN means downregulated, RC is *R. conorii*-infected cells and RM is *R. montanensis*-infected cells. See also **Supplementary Table IV.4**. **(B-G)** DE genes common to infection by both SFG *Rickettsia* or *R. conorii*-specific categorized using DAVID Bioinformatic Resources 6.8. Number of genes in each category is indicated in x-axis. Common DE genes according to GO terms: biological process **(B)**, KEGG pathways **(C)**, and cellular component **(D)**. *R. conorii*-specific DE genes acording to GO terms: biological process **(E)**, KEGG pathways **(F)**, and cellular pathways **(G)**. See also **Supplementary Table IV.5**. **(H)** Heatmap comparing the top 30 canonical pathways for *R. conorii*-infected cells and the respective prediction of activation (red)/inhibition (green) state (Z-score) in R.c. (*R. conorii*-infected cells) and R.m. (*R. montanensis*-infected cells) according to Ingenuity Pathway Analysis (IPA). See also **Supplementary Table IV.4**.

To gain more insight about the datasets, significantly DE genes were also uploaded into Ingenuity Pathway Analysis (IPA), which combines differential gene expression data with the Ingenuity Pathway Knowledge Base to determine altered canonical pathways, upstream regulators and predicted downstream disease/functions (Kramer et al., 2014). The list of altered canonical pathways and their predicted activation/inhibition scores for *R. conorii*- and *R. montanensis*-infected THP-1 macrophages can be found in **Supplementary Table IV.4**. To better understand similarities and differences on the activation/inhibition state of signaling pathways upon infection, the top 30 canonical pathways in *R. conorii*-infected cells (aligned by p-value) were compared to the corresponding p-values observed for the same pathways in *R. montanensis*-infected cells, and their predicted activation/inhibition scores (Z-score) were listed **(Figure IV.2H)**. As illustrated in the Heatmap, the pattern of altered canonical pathways differed between conditions. With differences in prediction scores, the activation of several signaling pathways such as HMGB1, TREM1, IL-6 and acute phase response signaling was predicted in both *R. conorii*- and *R. montanensis*-infected macrophage-like cells, which is consistent with an augmented inflammatory response upon infection. However, several other pathways such as TNFR1 and TNFR2 signaling, and role of pattern recognition receptors in recognition of bacteria and viruses were predicted to be activated only in *R. conorii*-infected cells.

IV.4.3 | *Rickettsia conorii* infection switches immune signals in macrophage-like cells into a hyporesponsive state

Central to the modulation of inflammatory and immune responses are Toll-like receptor (TLR), Nuclear Factor-κB (NF-κB) and Tumor Necrosis Factor (TNF) signaling pathways (Brenner et al., 2015; Kalliolias and Ivashkiv, 2016; Karin and Lin, 2002; Kawai and Akira, 2010; Li and Verma, 2002). However, pathogens have evolved strategies to modulate host immune responses and some bacteria can even benefit from host inflammation to replicate (Asrat et al., 2015; Sanchez-Villamil and Navarro-Garcia, 2015). We observed differential expression of several genes grouped to inflammatory responses in THP-1 cells infected with *R. conorii and R. montanensis* **(Figure IV.3A-B, Supplementary Table IV.6)**. Of the 33 DE genes, 13 were upregulated by both *R. conorii* and *R. montanensis* (although at different levels), and include the pro-inflammatory cytokines TNFα and IL1β, as well as the chemokines CCL20, CCL3L3, CCL3, CCL4L2, CXCL1, CXCL3 and CXCL8 that can shape the recruitment of immune cells to the site of infection (Newton and Dixit, 2012). Other genes like TNFAIP3 and NFKBZ (implicated in modulation of NF-κB signaling), or PTGS2 (involved in the synthesis of inflammatory mediators) were also induced by both rickettsial species. Importantly, twenty genes were found to be DE in *R. conorii*-infected cells only, including upregulation of cytokine IL1α and the subunit IL23a. Interestingly, eight of these genes were shown to be downregulated (CCR1, CD14, CD180, SMAD1, ADGRE5, CDO1, ECM2 and SCG2). ADGRE5 is considered a critical mediator of host defense, playing essential roles in leukocyte recruitment, activation and migration (Gray et al., 1996; Leemans et al., 2004). Moreover, it has been reported that CCR1 blocking is able to impair host defenses by perturbing the cytokine response during Herpes simplex type 2 infection (Sorensen and Paludan, 2004).

Most of the genes implicated in inflammatory responses were grouped to TLR, NF-κB or TNF signaling, together with additional genes also mapped to these pathways **(Figure IV.3C-E, Supplementary Table IV.6)**. Again, we observed differences in the regulation of genes between *R. conorii* and *R. montanensis*-infected cells. For example, in TLR-related pathways **(Figure IV.3C, Supplementary Table IV.6)**, downregulation of CD14 was observed in *R. conorii*-infected, but not in *R. montanensis*-infected cells. Bacterial lipopolysaccharide (LPS) binds to the CD14 receptor

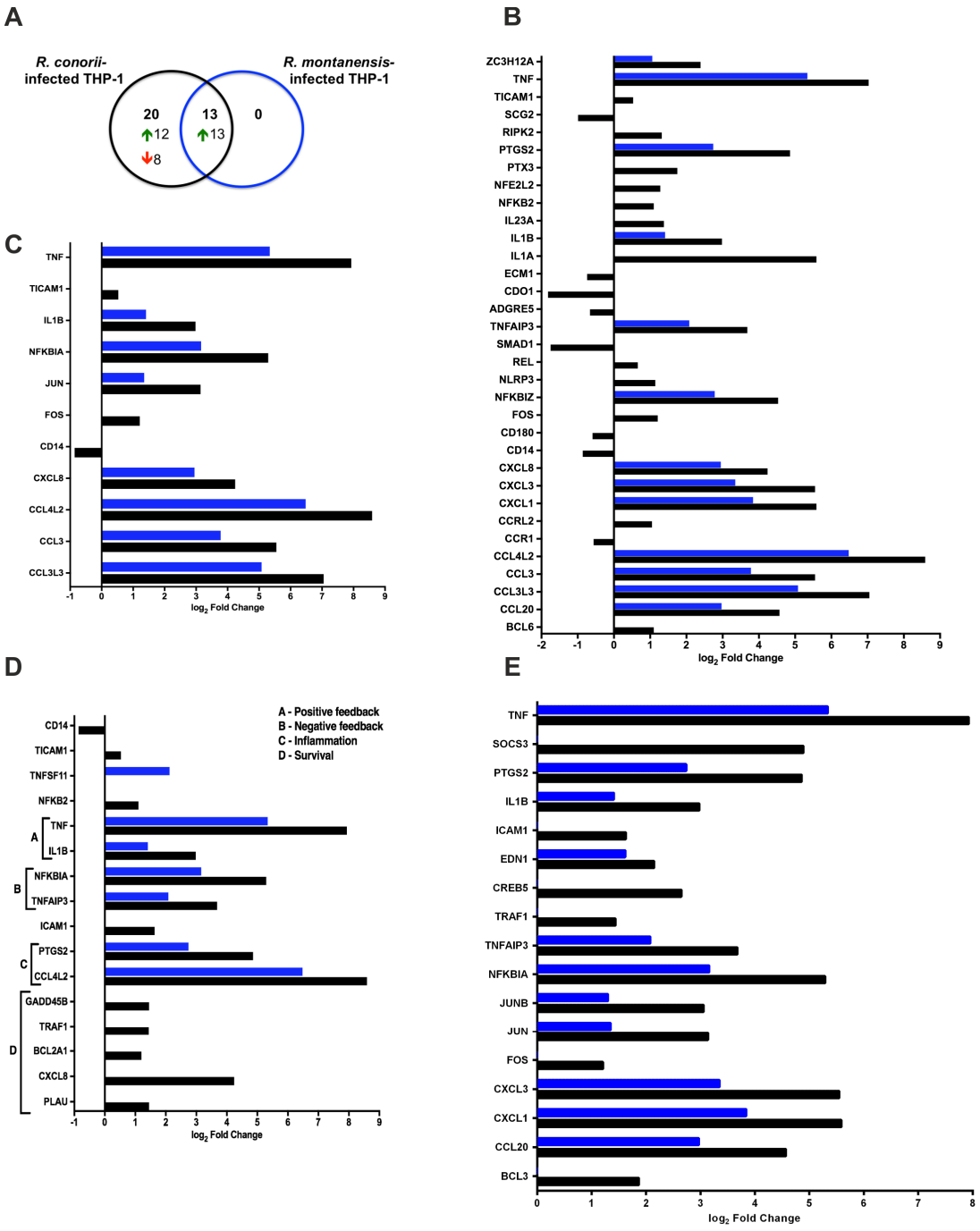

Figure IV.3 | *R. conorii* and *R. montanensis* differentially modulate innate immune responses during THP-1 macrophage infection. (A) Venn diagram depicting the number and the orientation (upregulated and downregulated) of specific and common DE genes categorized with GO term inflammatory response in *R. conorii*- and *R. montanensis*-infected cells. **(B-E)** List of the DE genes (and respective $\log_2$ fold change values) categorized with GO term inflammatory response **(B)**, and KEGG pathways: Toll-like receptor **(C)**, NF-κB signaling **(D)**, and TNF signaling **(E)** in THP-1 macrophages infected with *R. conorii* (black) and *R. montanensis* (blue). Absence of bar means that the fold change of that gene for the respective experimental condition was not considered statistically significant. See also **Supplementary Table IV.6**.

transferring it to TLR4, which in turn leads to signal transduction (Poltorak et al., 1998; Wright et al., 1990). In addition, infection by *R. conorii*, but not *R. montanensis*, resulted in the upregulation of the TLR adaptor molecule 1 (TICAM1, also known as TRIF), critical for TLR3- and TLR4-mediated signaling pathways that can lead to the activation of late-phase NF-κB and consequent induction of inflammatory cytokines (Kawai and Akira, 2010; Yamamoto et al., 2003).

Genes involved in both negative (NFKBIA and TNFAIP3) and positive (TNF and IL1B) regulatory loops of the NF-κB pathway, as well as other genes involved in inflammation (PTGS2 and CCL4L2), were upregulated in either *R. conorii*- or *R. montanensis*-infected cells, although at different levels **(Figure IV.3D, Supplementary Table IV.6)**. Interestingly, marked differences were observed in more than half of these DE genes categorized to NF-κB signaling between infection conditions. Genes that have been reported as involved in host cell survival, such as GADD45B, TRAF1, BCL2A1, CXCL8 and PLAU were specifically upregulated in THP-1 macrophages infected with *R. conorii,* but not in *R. montanensis*-infected cells.

As already mentioned, infection by either *R. conorii* or *R. montanensis* resulted in an upregulation of the TNFα transcript. TNF signaling cascades are initiated with binding of soluble TNF to either of its receptors (TNFR1 or TNFR2). However, signaling cascades generated by each receptor are markedly different (Brenner et al., 2015). Interestingly, IPA revealed that both TNFR1 and TNFR2 signaling pathways are predicted to be activated in *R. conorii*-infected THP-1 macrophages (Z-scores of 2.449; p-value of 9.77×10^{-6} and 1.15×10^{-8}, respectively), but not in *R. montanensis*-infected cells (Z-scores of 0.0; p-value of 8.51×10^{-6} (TNRF1) and 1.07×10^{-6} (TNRF2)) **(Supplementary Table IV.4)**, anticipating significant differences in host signaling responses through both pathways, between bacterial species. This was further confirmed by comparing on IPA the significantly DE genes between *R. conorii- vs. R. montanensis*-infected cells, where both TNFR1 and TNFR2 signaling pathways are also predicted to be activated in cells infected with *R. conorii* (Z-score of 2.236; p-value of 1.45×10^{-5} (TNFR1) and p-value of 2.40×10^{-8} (TNFR2) **(Supplementary Figure IV.2)**, strengthening the differences in host responses between bacterial species. It has been reported that TNFR1 signaling can result in either cell survival or cell death depending on downstream signaling events and cellular context, and TNFR2 signaling

promotes cell survival (Brenner et al., 2015; Lee and Choi, 2007; Wan et al., 2016). Interestingly, infection with *R. conorii* resulted in an upregulation of TNF receptor associated factor 1 (TRAF1) **(Figure IV.3E, Supplementary Table IV.6)**, which is reported to bind to TNFR2 (Rothe et al., 1994). Indeed, TRAF1 upregulation in *Epstein-Barr virus* (EBV)-infected cells has been documented and its role as a modulator of oncogenic signals via JNK/AP1 has been a target of study (Durkop et al., 1999; Eliopoulos et al., 2003; Siegler et al., 2003).

In addition, our RNA-seq data also revealed an upregulation of BCL3 and ICAM1 in *R. conorii*-infected cells, but no differential regulation of these genes was observed in *R. montanensis*-infected dataset **(Figure IV.3E, Supplementary Table IV.6)**. BCL3 (B-Cell lymphoma 3-encoded protein) has been documented as a regulator of classical and non-canonical NF-κB-dependent gene transcription and it is able to limit pro-inflammatory transcriptional programs (Herrington and Nibbs, 2016). On the other hand, ICAM1 (intercellular adhesion molecule-1) is a transmembrane glycoprotein reported to be upregulated in response to different inflammatory mediators and playing a role in immune surveillance (Usami et al., 2013).

Cytokine signaling through Janus kinase (Jak)-signal transducer and activator of transcription (STAT) pathway (Jak-STAT pathway) has also an important role in the control of immune responses (Shuai and Liu, 2003; Villarino et al., 2017). As shown in **Supplementary Table IV.7**, six genes categorized to this signaling process are upregulated in cells infected with *R. conorii,* but not differentially regulated in the *R. montanensis*-infected dataset. One of the products of these DE genes, SOCS3, is involved in immune evasion linked to Stat-signaling (Mahony et al., 2016), while two other gene products, OSM and MCL1, are involved in protection against mitochondrial dysfunction and inhibition of BAK-mediated apoptosis, respectively (Chang et al., 2015).

The overall prediction of inflammatory response in *R. conorii*- and *R. montanensis*-infected THP-1 macrophages was then evaluated using the downstream “Diseases and Functions” tool provided by IPA **(Figure IV.4A)**. Interestingly, contribution of DE genes associated with this response in *R. conorii*-infected cells resulted in a balance between pro- and anti-inflammatory signals with a predicted null Z-score of activation/inhibition (Z-score of -0.092; p-value of 5.29×10^{-20}). Genes coding for antimicrobial enzymes, such as cathepsin G (CTSG), elastase (ELANE) and

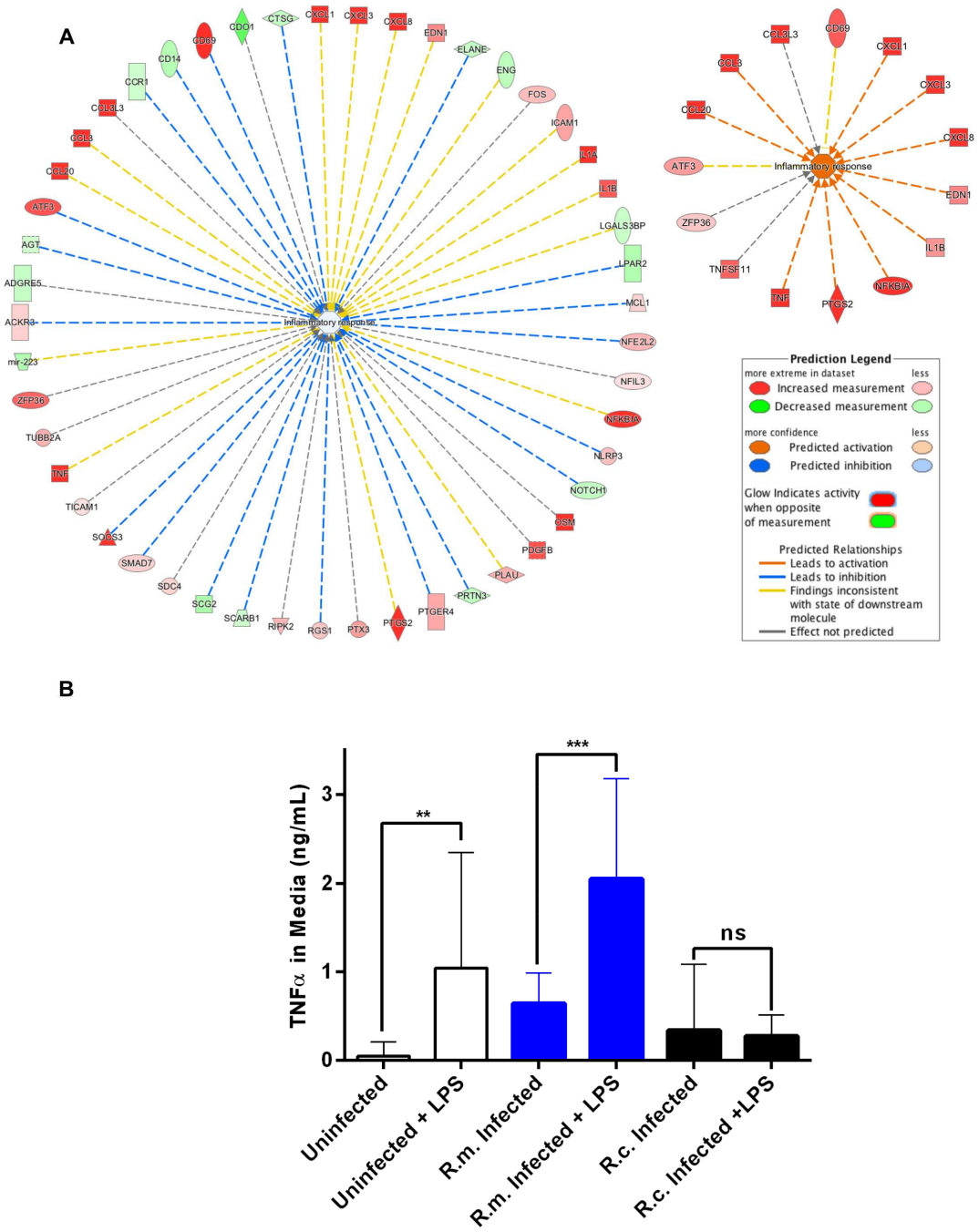

Figure IV.4 | *R. conorii* switches macrophage immune responses into a hyporesponsive state. (A) IPA "Diseases and Function" analysis predicted contribution of DE genes for inflammatory response, resulting in Z-score of -0.092 and p-value of 5.29 x 10^{-20} for *R. conorii*-infected cells (left) and Z-score of 2.664 and p-value of 1.01 x 10^{-10} for *R. montanensis*-infected cells (right). DE genes are color-graded by $\log_2$ fold change values and the contribution of DE genes is color-coded by predicted relationship (see inset legend). See also **Supplementary Table IV.11**. **(B)** Quantification of TNFα concentration in the culture media of uninfected (white), *R. conorii*-(black) and *R. montanensis*-infected (blue) THP-1 macrophages upon stimulation with *E. coli* O26:B6 LPS. Results are shown as mean ± SD and differences were considered ns (non-significant) at P > 0.05 or significant at ** P ≤ 0.01, *** P ≤ 0.001.

proteinase 3 (PRTN3), that are part of the earliest line of host inflammatory responses against pathogens (Hahn et al., 2011; Korkmaz et al., 2010), were among the downregulated genes predicted to contribute to inhibit inflammatory responses in *R. conorii*-infected cells.

Conversely, in *R. montanensis*-infected cells mainly pro-inflammatory signals were observed, resulting in the predicted activation of inflammatory response (Z-score of 2.664; p-value of 1.01 x 10^{-10}). To further characterize these differences in inflammatory response between *R. conorii* and *R. montanensis*-infected cells, we next evaluated how cells respond to a well-known pro-inflammatory stimulus (LPS) 24 hours after infection **(Figure IV.4B)**. As expected, uninfected THP-1 cells responded by increasing secretion of TNFα and a similar result was obtained in *R. montanensis*-infected cells. However, in sharp contrast *R. conorii*-infected cells were totally unresponsive to LPS stimulation, displaying levels of secreted TNFα comparable to non-stimulated cells **(Figure IV.4B)**. Overall, these results anticipate significant differences in inflammatory signaling promoted by these bacterial species and, more interestingly, suggest that the pathogenic *R. conorii* is able to modulate inflammatory responses in macrophages.

IV.4.4 | *Rickettsia conorii* actively modulates pro-survival pathways to sustain macrophage viability during infection

Apoptosis is part of the arsenal of defense mechanisms used to prevent infection. However, pathogens themselves have evolved numerous ways to modulate cell death pathways and intracellular microorganisms can subvert nearly all steps of the apoptotic cascade (Friedrich et al., 2017; Gao and Kwaik, 2000). THP-1 cells infected with *R. conorii* and *R. montanensis* showed a striking difference in the number of DE genes grouped to the negative regulation of the apoptotic process, with 16 out of the 19 DE genes being deregulated in *R. conorii*-infected cells only **(Figure IV.5A, Supplementary Table IV.8)**. Among these genes were MCL1 and BCL2A1, two Bcl-2 protein family members known as important regulators of the integrity of mitochondria by suppression of the pro-apoptotic function of BAX and BAK (Willis and Adams, 2005), PIM3 that can prevent apoptosis and promote cell survival (Mukaida et al., 2011), and the mitochondrial protein superoxide dismutase 2 (SOD2) involved in protection against oxidative stress (Drane et al., 2001).

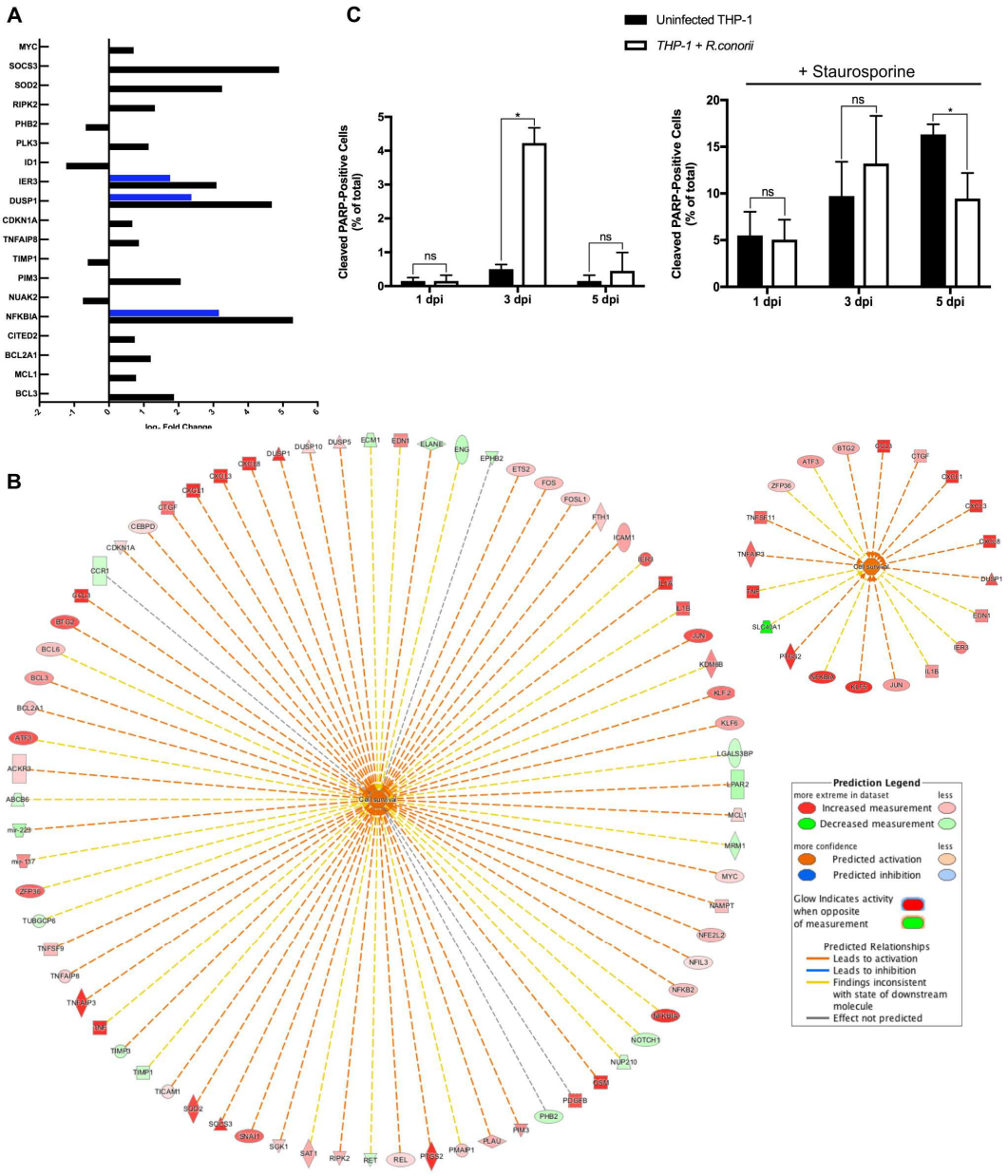

Figure IV.5 | *R. conorii* is able to control host cell viability maintaining its replicative niche. **(A)** Log_2 fold change values of DE genes categorized with GO term "negative regulation of apoptotic process" in *R. conorii*- (black) and *R. montanensis*-infected (blue) cells. Absence of bar means that the fold change of that gene for the respective experimental condition was not considered statistically significant. See also **Supplementary Table IV.8**. **(B)** IPA "Diseases and Function" analysis predicted contribution of DE genes for cell survival, resulting in Z-score of 3.661 and p-value of 1.41 x 10^{-15} for *R. conorii*-infected cells (left) and Z-score of 1.960 and p-value of 1.01 x 10^{-9} for *R. montanensis*-infected cells (right). DE genes are color-graded by log_2 fold change values and the contribution of DE genes is color-coded by predicted relationship (see inset legend). See also **Supplementary Table IV.8**. **(C)** Percentage of cleaved PARP-positive cells, a marker of intrinsic apoptosis, over the course of infection of THP-1 macrophages with *R. conorii*, without (left) and with (right) challenge with staurosporine (a potent inducer of intrinsic apoptosis). Results are shown as mean ± SD and differences were considered ns (non-significant) at $P > 0.05$ or significant at * $P < 0.05$.

Furthermore, IPA "Diseases and functions" downstream analysis identified the contribution of 73 DE genes for cell survival in cells infected with *R. conorii* (predicted activation Z-score of 3.661; p-value of 1.41 x 10^{-15}), against only 20 DE genes mapped to cell survival in *R. montanensis*-infected cells (Z-score of 1.960; p-value of 6.11 x 10^{-9}) **(Figure IV.5B)**. Globally, our results showed a *R. conorii*-specific upregulation of several genes with important functions in the control of host cell survival and modulation of responses against inflammatory cytokines, further reinforcing the trend already observed with other pro-survival genes grouped to NF-κB signaling **(Figure IV.3D)**. These results are consistent with our previously reported phenotypic differences, supporting the ability of *R. conorii* to establish a niche in THP-1 macrophages while the integrity of *R. montanensis*-infected cells was shown to be compromised (Curto et al., 2016).

To further evaluate if this pro-survival manipulation of the host cell by *R. conorii* is maintained over the course of the infection, we quantified cleaved poly(ADP-ribose) polymerase (PARP-1) (a classical marker of the terminal stages of apoptosis), in both uninfected and *R. conorii*-infected THP-1 macrophages by immunofluorescence microscopy analysis (IFA), at 24, 72 and 120 hours post-infection **(Figure IV.5C)**. We observed no significant increase in the number of cleaved PARP-positive cells at 24 and 120 hours post-infection, although a significant increase in this number was observed at the intermediate time-point (72h), suggesting a controlled (but dynamic) modulation of host cell apoptosis by *R. conorii*. We then evaluated if infection with *R. conorii* was able to protect these cells from treatment with a potent inducer of intrinsic apoptosis, staurosporine. Our results showed a significant reduction in cleaved PARP-positive THP-1 cells at 120 h post-infection when compared with uninfected control cells, confirming a protection from staurosporine-induced apoptosis triggered by *R. conorii* infection **(Figure IV.5C)**. Combined, these findings suggest that *R. conorii* actively modulates apoptotic signaling to sustain viability of the host cell over the course of infection.

IV.4.5 | *Rickettsia conorii* promotes robust changes in expression of several classes of non-coding RNAs early in macrophage infection

To face bacterial or viral infections, host cells can adjust their gene expression programs using non-coding RNAs (ncRNAs) as regulatory molecules (Duval et al., 2017; Eulalio et al., 2012). Reciprocally, pathogens can also escape host defense mechanisms using strategies that target ncRNAs-mediated regulation with favorable consequences for pathogen survival and proliferation (Bayer-Santos et al., 2017; Cullen, 2013; Das et al., 2016). In addition to protein coding transcripts, it was also possible to identify several ncRNAs differentially regulated within our datasets. Infection with each SFG *Rickettsia* resulted not only in a robust response regarding these regulatory elements, with multiple ncRNAs of different types being DE at 1 h post-infection, but also in a very different pattern of modulation between rickettsial species **(Figure IV.6A, Supplementary Table IV.9)**. Overall, 80 ncRNAs were found deregulated in *R. conorii*-infected cells, whereas only 18 were observed in *R. montanensis*-infected cells **(Figure IV.6A)**.

Micro-RNAs (miRNAs) are one class of the ncRNAs that have been extensively studied not only by playing crucial roles in the host response to infection but also as a molecular strategy exploited by pathogens to manipulate host cell pathways (Duval et al., 2017). Infection of THP-1 macrophages by *R. conorii* resulted in the upregulation of miR-137 and downregulation of miR-223 and miR-424, whereas infection with *R. montanensis* resulted in the upregulation of miR-663A **(Figure IV.6B)**. Long noncoding RNAs (lncRNAs) are also a class of ncRNAs that have been studied as playing important roles in immune responses (Duval et al., 2017; Zur Bruegge et al., 2017). In our dataset, we observe again a differential response regarding this type of ncRNAs, with 10 lincRNAs DE in *R.conorii*-infected cells (and only 1 in the *R. montanensis* dataset) **(Figure IV.6C)**. Infection with *R. conorii* resulted also in a robust modulation of the class of small nucleolar RNAs (snoRNAs) (18 snoRNAs and 3 small Cajal-body specific RNA (scaRNAs) were found specifically downregulated in this condition only) **(Figure IV.6D)**. snoRNAs are involved in the regulation of posttranscriptional modification of ribosomal RNA and it has been reported that defects in ribosome maturation and function are related with transformation of normal cells into tumor cells (Stepanov et al., 2015). Members of other non-coding RNA classes such as 7SK RNA

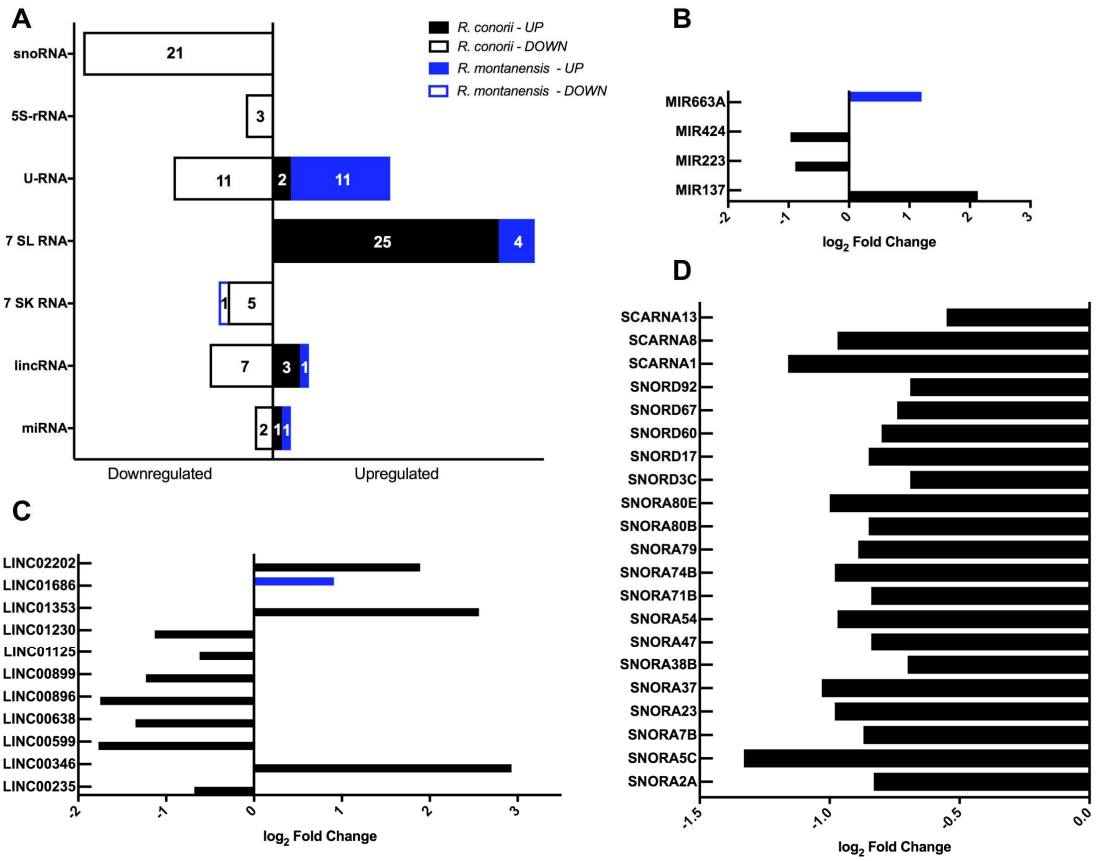

Figure IV.6 | *Rickettsial* species differentially modulate the expression of several non-coding RNAs early in infection of THP-1 macrophages. (A) Distribution of DE non-coding RNAs according to their category in *R. conorii*- (black) and *R. montanensis*- (blue) infected cells. scaRNAs (small Cajal body-specific RNAs), snoRNAs (small nucleolar RNAs), 5S-rRNAs (5S ribosomal RNAs), U-RNA (small nuclear RNAs), 7SL RNAs (signal recognition particle RNAs), 7SK RNAs (7SK small nuclear RNAs), lincRNAs (long intergenic noncoding RNAs), miRNAs (microRNAs). Number of genes for each orientation (upregulated or downregulated) is represented in each bar. **(B-D)** Log_2 fold change values of miRNAs **(B)**, lincRNAs **(C)**, and snoRNAs **(D)** in *R. conorii*- (black) and *R. montanensis*- (blue) infected cells. Absence of bar means that the fold change of that gene for the respective experimental condition was not considered statistically significant. See also **Supplementary Table IV.9**.

class, signal recognition particle RNA (7SL RNA), small nuclear RNA (U-RNA), and 5S ribosomal RNA (5S rRNA) also showed DE between infection conditions **(Supplementary Figure IV.3)**.

Together, our results show that several ncRNAs are differentially regulated in THP-1 macrophages in response to rickettsial infection by either *R. conorii* or *R. montanensis*, although a more robust and specific response to *R. conorii* infection was observed.

IV.4.6 | *Rickettsia conorii* induces an extensive modulation of genes associated with RNA polymerase II-dependent transcription

Recognition of infectious agents by host cells result in alterations of transcriptional programs in order tackle the infection (Asrat et al., 2015). However, it is now becoming clear that pathogens can reprogram host gene expression profiles by directly targeting or altering these programs at the level of transcriptional regulation (Asrat et al., 2015; Bierne and Cossart, 2012). To evaluate potential differences in pathways involved in transcriptional regulation between our data sets, we utilized the "Diseases and Functions" downstream analysis on IPA. Under both conditions, transcription was predicted to be activated (*R. conorii*-infected: Z-score of 2.428 and p-value of 5.27×10^{-1}; *R. montanensis*-infected: Z-score of 2.647 and p-value of 7.48×10^{-6}). However, the number of genes predicted to impact this process differed substantially between infected conditions **(Figure IV.7A-B)**. In cells infected with *R. conorii*, 81 DE genes were predicted to affect transcription whereas only 18 DE genes were associated with this process in *R. montanensis*-infected dataset **(Supplementary Table IV.10)**. Moreover, as also evidenced by our GO term analysis **(Figure IV.2B, E)**, a large number of these DE genes (61) were categorized as either positive or negative regulators of transcription from RNA polymerase II (RNAP II) promoter, against only 17 DE genes grouped in this category in *R. montanensis*-infected cells **(Supplementary Table IV.10)**. We further analyzed the potential relationships among these 61 DE genes found in *R. conorii* dataset using the STRING database **(Figure IV.7C)**. Of these regulators, 27 genes were categorized as transcription factors involved in positive regulation (nodes in red) and in negative regulation of transcription (nodes in blue) (RNA polymerase II transcription regulatory region sequence-specific DNA binding: GO:0001228 - Transcriptional activator activity; GO:0001227 - Transcriptional repressor activity). Moreover, members of the AP-1 transcription factor complex appear as central nodes in this interaction network **(Figure IV.7C)**. AP1 is a transcription factor that has been described as a nuclear decision-maker determining life or death cell fates (Angel and Karin, 1991). Together with the more substantial reprograming globally observed in *R. conorii*-infected cells **(**409 DE genes**, Figure IV.2A)**, this robust modulation of several different transcription factors by *R. conorii* further suggests that modification of the transcriptional machinery early in

infection might be critical to prolonging host survival and, as a result, bacterial survival and proliferation in THP-1 macrophages.

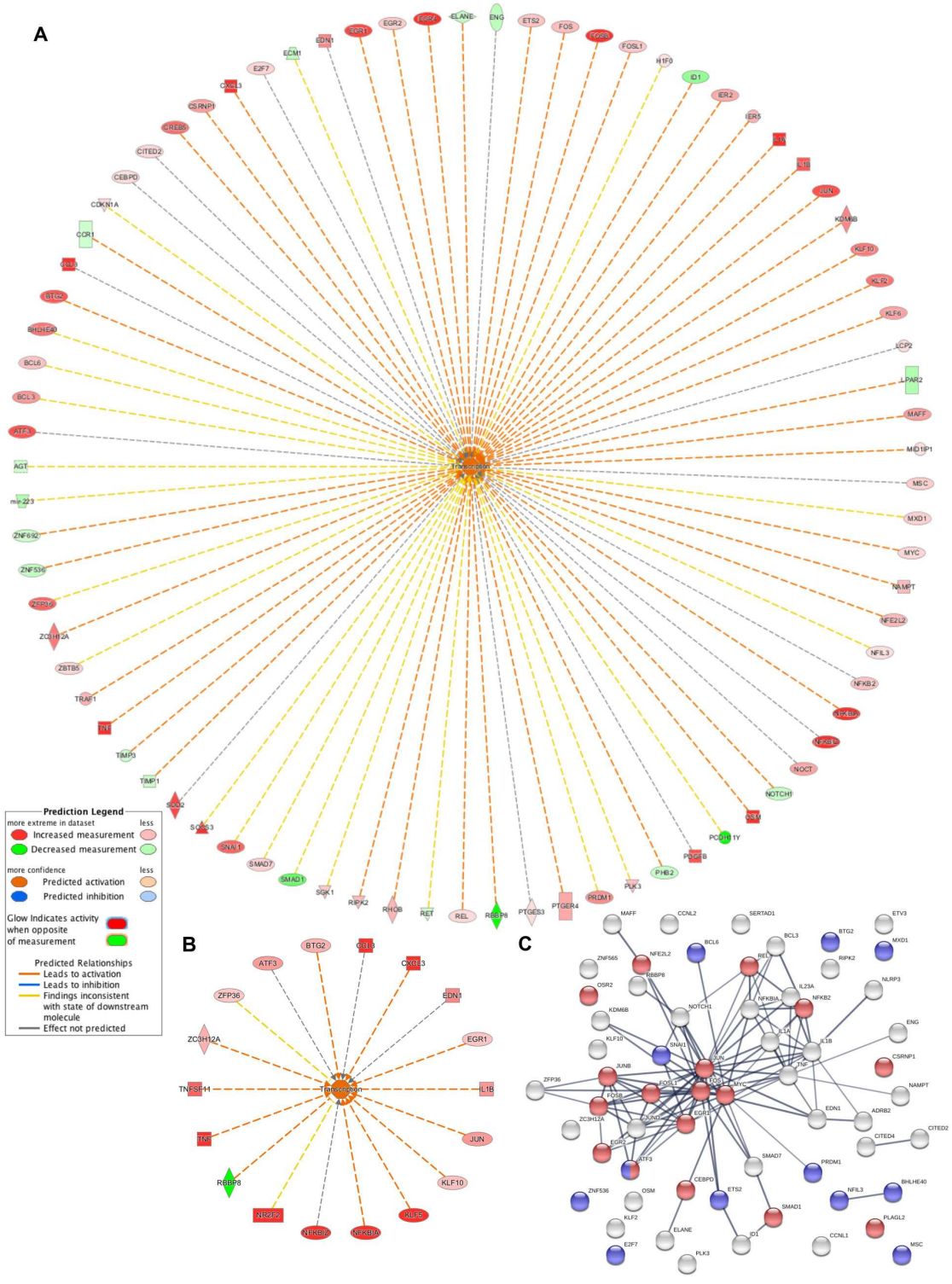

Figure IV.7 (previous page) | *Rickettsia conorii* induces an extensive modulation of genes associated with transcription. (A-B) IPA "Diseases and Function" analysis predicted contribution of DE genes for transcription resulting in Z-score of 2.428 and p-value of 5.27×10^{-14} for *R. conorii*-infected cells (A) and Z-score of 2.647 and p-value of 7.48×10^{-6} for *R. montanensis*-infected cells **(B)**. DE genes are color-graded by $\log_2$ fold change values and the contribution of DE genes is color-coded by predicted relationship (see inset legend). See also **Supplementary Table IV.10**. **(C)** STRING analysis of DE genes in *R. conorii*-infected cells categorized in the GO term "positive or negative regulators of transcription from RNA polymerase II promoter". Nodes corresponding to DE genes categorized with transcriptional activator activity (GO:0001228) are in red and with transcriptional repressor activity (GO:0001227) are in blue. See also **Supplementary Table IV.10**.

IV.5 | Discussion

The ability of many microbial and viral pathogens to modulate host transcriptional responses is a central aspect for pathogenesis (Ashida and Sasakawa, 2014; Lateef et al., 2017; Tran Van Nhieu and Arbibe, 2009). Consequently, the study of host transcriptomic alterations promoted during infection is a useful source of information to understand how pathogens are able to establish a successful niche inside host cells (Cloney, 2016). The employment of high-throughput sequencing-based transcriptomic technologies has endorsed significant advances in unraveling host-pathogen interactions that contribute for cellular tropism and pathogenicity (Saliba et al., 2017; Westermann et al., 2017; Westermann et al., 2012). We have previously showed that *R. conorii* and *R. montanensis*, two SFG *Rickettsia* with different degrees of pathogenicity to humans, display opposite intracellular fates in THP-1 macrophages (Curto et al., 2016). To further understand these variations in tropism, we herein characterized the early changes in host gene expression in these cells upon infection with the two SFG *Rickettsia*. This experimental design allowed us to determine not only the common host transcriptomic responses to different SFG *Rickettsia* but also species-specific alterations.

Our results revealed that infection with *R. conorii*, the pathogenic species, was able to specifically promote a more robust set of alterations in host gene expression when compared with *R. montanensis*, the non-pathogenic member of SFG *Rickettsia*. Remarkably, of the significantly DE genes at 1 hour post-infection, only 61 genes were found to be common to both infection conditions, whereas 409 genes were specifically regulated in *R. conorii*-infected cells and only 25 genes were specifically regulated upon infection with *R. montanensis*. These results indicate that different SFG *Rickettsia*, with distinct abilities to cause disease in humans, promoted different transcriptional responses in THP-1 macrophages, which ultimately culminate in completely distinct intracellular fates in the host cell.

We demonstrated that THP-1 cells responded to either *R. conorii* or *R. montanensis* stimuli by augmenting the expression of pro-inflammatory cytokines and chemokines in order to tackle the infection. However, differences in expression were observed for several other inflammatory-related genes between infection conditions, anticipating a differential host response to each rickettsial

species. The observed *R. conorii*-specific downregulation of CD14 is one of the examples. Physical interaction between CD14 and TLR4 has been reported and it is now assumed that a ternary complex incorporating CD14, MD-2 and TLR4 serves to activate LPS signaling (Beutler, 2004; Poltorak et al., 2000). The downregulation of CD14 observed upon infection by *R. conorii* might therefore affect LPS signaling and downstream pathways. Indeed, reduced levels of CD14 upon infection by *Porhymonas gingivalis* and *Pseudomonas aeruginosa* have been reported as being related with hyporesponsiveness to bacterial challenge (Van Belleghem et al., 2017; Wilensky et al., 2015). Another interesting difference was the *R. conorii*-specific upregulation of several genes mapped to NF-KB signaling that have been involved in cell survival, including the growth arrest and DNA damage-inducible 45 (GADD45). This protein plays essential roles in connecting NF-κB signaling to mitogen-activated protein kinase (MAPK) and it can regulate several cell activities as growth arrest, differentiation, cell survival and apoptosis (Yang et al., 2009). Moreover, differential expression of several genes related to the Jak-STAT signaling pathway were observed in *R. conorii*-infected cells only, further suggesting a specific modulation of immune responses by the pathogenic bacteria. One of these genes is SOCS3 (suppressor of cytokine signaling 3), a cytokine-induced inhibitor that suppresses cytokine receptor-mediated Stat signaling via a negative feedback loop (Mahony et al., 2016). Indeed, high expression of SOCS3 upon infection is well reported for several bacterial and viral pathogens and it has been linked to pathogenic immune evasion (Narayana and Balaji, 2008; St John and Abraham, 2009; Yokota et al., 2005; Yokota et al., 2004). Our results showed also an upregulation of OSM and MCL1. It is reported that the OSM is able to stimulate the expression of MCL1 via JAK1/2-STAT1/3 and CREB and it contributes to bioenergetics improvements and protection against mitochondrial dysfunction (Chang et al., 2015). Upregulation of MCL1 during *Leishmania donovani* infection has been documented as being essential for disease progression by preventing BAK-mediated mitochondria-dependent apoptosis (Giri et al., 2016).

Overall, the first striking difference between *R. conorii*- and *R. montanensis*-promoted changes was the observed balance between pro- and anti-inflammatory mediators induced upon infection with the pathogenic *Ri*ckettsia, which was not observed in *R. montanensis*-infected cells

where mainly pro-inflammatory signals were generated. Modulation of immune signals in the host has been described as a sophisticated strategy developed by successful pathogens to subvert host responses, switching the immune responses into a hyporesponsive state (Gogos et al., 2000). The observed differential expression of genes associated with different signaling transduction pathways (such as TLR, TNFR, NF-κB or the Jak-STAT pathway), and with other mechanisms of the earliest line of defense against pathogens (e.g. antimicrobial enzymes) in *R. conorii*-infected cells, suggests that this pathogen may be able to modulate innate immune system components at various levels, anticipating the use of complex modulatory mechanisms very early in infection to evade and subvert host responses. An example of manipulation of immune responses by a Gram-negative pathogen is the ability of *Shigella flexneri* to inhibit NF-κB signaling pathways by its Type III effector (OspI), which greatly reduces the acute inflammatory response in macrophages during invasion, as well as the ability of these cells to undergo apoptosis and communicate with other immune cells (Reddick and Alto, 2014). Members of the genus *Rickettsia* do not possess genes to encode a functional Type III secretion system (Gillespie et al., 2015a) and therefore must employ other strategies to manipulate the infected host cell. How *R. conorii* can specifically induce this program in infected cells is unclear and currently under investigation.

Another strategy that intracellular pathogens have developed to establish a niche of infection is the ability to control host cell apoptosis to its own advantage (Friedrich et al., 2017). Our results revealed that *R. conorii* promoted an upregulation of several host genes that have been implicated in pro-survival pathways. Some of these gene products (e.g. Bcl-2 protein family members) are targeted by several pathogens to modulate host apoptotic signaling to their own advantage (Friedrich et al., 2017). It has been reported that survival of *Mycobacterium tuberculosis* in host macrophages involves resistance to apoptosis by upregulating Bcl-2 and the Bcl-2 like protein Mcl-1 (Sly et al., 2003; Wang et al., 2014); and other studies have also demonstrated that Bcl-2 family members are essential for the survival of *Legionella* by preventing macrophage apoptosis (Speir et al., 2016). Therefore, upregulation of two Bcl-2 family members (MCL1 and BCL2A1) at an early time post-infection in THP-1 macrophages by *R. conorii* may be a strategy to promote host cell survival and retain a replicative niche. Upregulation of PIM3, a proto-oncogene

with serine/threonine kinase activity that can prevent apoptosis, promote cell survival and protein translation, was also observed in *R. conorii*-infected cells, but not in the *R. montanensis*-infected dataset. Interestingly, PIM3 may contribute to tumorigenesis through the delivery of survival signaling through phosphorylation of BAD, which induces release of the anti-apoptotic protein Bcl-X_L (Narlik-Grassow et al., 2014). Another interesting difference was the upregulation of SOD2 observed only in *R. conorii*-infected cells. This gene product is involved in protection against oxidative stress and, as a result, may have a protective role against cell death (Drane et al., 2001). Modulation of NF-κB signaling pathways has been already described as a strategy developed by *R. rickettsii* to modulate apoptosis over the course of infection in epithelial cells (Clifton et al., 1998; Joshi et al., 2003, 2004). Interestingly, our results point towards a well-designed ability of *R. conorii* to not only manipulate but also to sustain host cell survival early during the infection, suggesting again a complex interference with apoptotic cascades. In contrast, host cell integrity is severely disrupted in *R. montanensis*-infected THP-1 macrophages. Therefore, control of host survival appears to be another key feature exploited by *R. conorii* during THP-1 macrophage infection, and a critical distinguishing factor between these two rickettsial species.

Survival of intracellular pathogens in host cell niches depends on multiple alterations in host cell function, and these changes reflect, in part, the ability of the microbe to alter host cell gene expression (Asrat et al., 2015). In fact, our findings suggest that the drastic difference in intracellular fate of these two rickettsial species in macrophage-like cells could be the result of the differential ability of *Rickettsia* species to interfere with the regulation of gene expression programs. Indeed, the pathogenic *R. conorii* appears to interfere with a myriad of cellular processes not only to control immediate host responses but apparently modulating several transcriptional and posttranscriptional regulatory elements that may extensively impact host cell functions later in infection. One of these examples is the observed modulation of non-coding RNAs, where more substantial transcriptomic changes were found upon infection with *R. conorii*. Non-coding RNAs have been emerging as key regulatory molecules in controlling gene expression (Duval et al., 2017). Several intracellular bacterial pathogens, such as *Helicobacter pylori*, *Salmonella spp.* and *Mycobacterium tuberculosis,* and many others, are able to manipulate the expression profiles of these regulatory molecules

resulting in more favorable environmental and physiological conditions for pathogen survival (Das et al., 2016; Duval et al., 2017; Zur Bruegge et al., 2017). Regarding the miRNAs identified in this work, and to our knowledge, only miR-223 has been previously associated with responses to bacterial infection (Staedel and Darfeuille, 2013), suggesting a new role for miR-137, miRNA-424, and miR-663A in these processes. Since this study was not specifically directed to the identification of small non-coding RNAs, we cannot exclude that other miRNAs (as well as other classes of non-coding RNA) may be differentially regulated in this cell type upon infection with *Rick*ettsia. The robust and specific modulation of different snoRNAs only observed in *R. conorii*-infected cells raise also interesting questions on the role of this class of RNAs for rickettsial survival in THP-1 macrophages. Indeed, it has been reported that snoRNAs can act as mediators of host antiviral response and the activity of regulatory RNAs can be used by viruses to evade innate immunity (Peng et al., 2011; Saxena et al., 2013; Stepanov et al., 2015). We also observed a stronger modulation of 7SLRNAs in *R. conorii* infected cells. To our knowledge, the relevance of 7SL RNAs in host-pathogen interactions is still largely unknown and only previously shown during *Leishmania* infection in macrophages (Abell et al., 2004; Misra et al., 2005). Although further studies are required to understand the functional impact of the specific modulation of different ncRNAs by *R. conorii* at 1 hour post-infection, our results suggest that these regulatory molecules may also be exploited by this pathogenic bacterium as a strategy to bolster more favorable conditions for proliferation in macrophages.

Along with ncRNAs, the *R. conorii*-specific modulation of a high number genes associated with RNA polymerase II-dependent host gene expression was another noticeable difference between *R. conorii* and *R. montanensis*-infected macrophages. Interestingly, targeting of Pol II-dependent transcription by pathogens has just been recently reported in urinary tract infections as playing a role in evasion of immune activation (Ambite et al., 2016; Lutay et al., 2013) but, to our knowledge, these mechanisms of pathogen-induced transcriptional modulation are still poorly understood. Of particular importance was the observed DE of several transcription factors (both activators and repressors), which can modulate the expression of several other genes and may drastically affect host expression profiles at later stages of infection. Interestingly, changes in

expression of several transcription factors early in infection by *Salmonella typhimurium* were reported to result in unique features of the late transcriptional responses that are required for bacteria intracellular replication (Hannemann et al., 2013). Therefore, our results provide a new example of a pathogenic bacterium capable of inducing a broad effect on RNA Pol II-dependent transcription that deserves to be further studied. Furthermore, our results demonstrate that infection of THP-1 macrophages with *R. conorii* resulted in the upregulation of different members of the AP-1 complex such as FOS, JUN and JUNB (while infection with *R. montanensis* resulted in the upregulation of only JUN and JUNB). It is known that contribution of AP-1 complex to determination of cell fates critically depends on the relative abundance of AP-1 subunits, the composition of AP-1 dimers, the quality of stimulus, the cell type as well as the cellular environment (Ameyar et al., 2003; Hess et al., 2004). Heterodimers formed by FOS:JUN are more stable complexes with stronger DNA binding affinity when compared to JUN:JUN homodimers, which can further define the host gene expression profiles generated by the AP-1 complex (Halazonetis et al., 1988). Therefore, the observed differential expression of AP-1 subunits by *R. conorii* and R. *montanensis* may also affect transcriptional programs triggered by each bacterial species. Interestingly, significant manipulation of AP-1 transcription factor by *Ebolavirus* (EBOV) infection, and its role in host gene expression profiles defining EBOV pathogenesis has been documented (Wynne et al., 2017), urging for the future evaluation of the role of AP1 in *R. conorii* pathogenesis.

Herein, we provide evidence that the gene expression machinery in the host nucleus appears to be a key target of *R. conorii* interference, likely contributing to modulate host processes to establish a favorable cell environment for bacterial survival and proliferation in THP-1 macrophages. Therefore, one of the most important questions that now emerge is how *R. conorii* is regulating nuclear dynamics. Several strategies have been identified for other pathogenic bacteria, and the identification of microbial effectors that directly target and alter host gene expression programs at the level of transcriptional regulation has been emerging as a new field of research (Asrat et al., 2015; Bierne and Cossart, 2012; Reddick and Alto, 2014). In SFG *Rickettsia*, the nature and function of bacterial effectors are still mostly elusive. However, in other intracellular pathogenic bacteria of the related genera *Ehrlichia* and *Anaplasma*, recent studies identified

ankyrin repeat-containing proteins (Anks) as key virulence factors by their ability to affect host gene expression profiles (Dumler et al., 2016; Pan et al., 2008). Interestingly, the Ank gene homolog *Rickettsia* Ankyrin Repeat Protein 2 (RARP-2) is present in *R. conorii* genome but absent in *R. montanensis*, which might, in part, explain the differential expression programs generated upon infection (Gillespie et al., 2015a). Therefore, further studies exploring the potential role of RARP-2 as a virulence factor in rickettsial species should be promptly addressed.

By unraveling early alterations in host gene expression profiles upon infection of macrophage-like cells with two SFG rickettsial species with different pathogenicity attributes, this work contributes new insights on how host cell functions and multiple signaling events respond to either clear an infection or to be exploited to the own benefit of a pathogen. Combined, these findings raise the exciting hypothesis that manipulation of host nuclear dynamics may be a virulence strategy deployed by pathogenic rickettsiae to proliferate in macrophage-like cells. These results will help to guide future research with valuable resources that can be used to expand our understanding of the complex network of host-rickettsiae interactions, including deciphering the nature and function of rickettsial virulence effectors as well as the role of phagocytic cells in the pathogenesis of rickettsial diseases.

IV.6 | Acknowledgements

We would like to particularly acknowledge the efforts of Dr. John Caskey and Dr. Vladimir Chouljenko in completion of this study. We would also wish to thank Dr. Kevin Macaluso (LSU SVM Department of Pathobiological Sciences) for providing *R. montanensis* isolate M5/6. We would like to thank Abigail Fish and Daniel Garza for helpful suggestions in completion of this study.

Chapter V

Glimpse into global macrophage responses triggered by a pathogenic and a non-pathogenic species of Spotted Fever Group *Rickettsia* by systems-wide quantitative proteomics

V.1 | Abstract

We have previously reported that *Rickettsia conorii* and *Rickettsia montanensis* have distinct intracellular fates within THP-1 macrophages, suggesting that the ability to proliferate within macrophages may be a distinguishable factor between pathogenic and non-pathogenic Spotted fever group (SFG) members. To start unraveling the molecular mechanisms underlying the capacity (or not) of SFG *Rickettsia* to establish their replicative niche in macrophages, we have herein profiled the host proteomic alterations resulted by the infection of THP-1 macrophages with *R. conorii* and *R. montanensis* using a high throughput quantitative proteomics approach (SWATH-MS). Our results revealed that these two members of SFG *Rickettsia* with distinct pathogenicity attributes for humans, trigger differential proteomic signatures in macrophage-like cells. Although infection by both rickettsial species resulted in a lower abundance of enzymes of glycolysis and pentose phosphate pathway, the pathogenic *R. conorii* specifically induced the accumulation of several enzymes of the tricarboxylic acid cycle, oxidative phosphorylation, fatty acid β-oxidation and glutaminolysis, as well as of several inner and outer membrane mitochondrial transporters. These results suggest a profound metabolic rewriting of macrophages by *R. conorii* towards a metabolic signature of an M2-like (anti-inflammatory) activation program. Moreover, our results revealed that several subunits forming the proteasome and immunoproteasome are found in lower abundance upon infection with both rickettsial species, which may help bacteria to escape immune surveillance. Remarkably, *R. conorii*-infection specifically induced the accumulation of several host proteins implicated in protein processing and quality control in ER, suggesting that this pathogenic *Rickettsia* may be able to compensate the accumulation of misfolded proteins by increasing the ER protein folding capacity and subsequently restore host cell homeostasis. This work reveals novel aspects of macrophage-*Rickettsia* interactions, expanding our knowledge of how pathogenic rickettsiae explore host cells to their advantage.

V.2 | Introduction

Bacteria in the genus *Rickettsia* are small Gram-negative α-proteobacteria, which can be transmitted to humans through arthropod vectors (Hackstadt, 1996). Although rickettsial species share a high degree of genome similarity, they are associated with very different clinical outcomes (Fang et al., 2017), and the molecular determinants underlying these drastic differences in pathogenicity between *Rickettsia* species are still to be understood.

Endothelial cells have long been considered the primary target cells for *Rickettsia* (Walker and Ismail, 2008). However, even pathogens that preferentially invade non-macrophage cells might encounter macrophages during their experience in the extracellular space or when the primary host cell undergoes apoptosis, and subsequent phagocytosis by a nearby macrophage (Price and Vance, 2014; Walker, 1997; Walker and Gear, 1985). New evidence of the presence of intact *Rickettsia* within the cytoplasm of macrophages, both in tissues and within the blood circulation, has raised further questions about the exact role of these phagocytic cells in the pathogenesis of rickettsial diseases (Banajee et al., 2015; Riley et al., 2016; Walker and Gear, 1985). Over 40 years ago, it was shown that two *Rickettsia* strains of the Typhus Group with different levels of virulence displayed distinct capacities to proliferate within macrophages (Gambrill and Wisseman, 1973b). More recently, we have reported that a pathogenic (*R. conorii,* the causative agent of Mediterranean spotted fever (MSF)) and a non-pathogenic (*R. montanensis,* not associated with disease in humans) member of Spotted Fever group (SFG) *Rickettsia* also differ in their ability to proliferate within THP-1 macrophages (Curto et al., 2016). Combined, these results are suggestive of an association between the ability to replicate in macrophages and rickettsial pathogenicity, which may help to explain why certain species of *Rickettsia* are not associated with disease. However, *Rickettsia*-macrophage interactions are still very poorly understood.

It is known that many pathogenic bacteria have evolved sophisticated strategies to escape macrophage immune defenses, being able to replicate within these (as well as in other) phagocytic cells (Price and Vance, 2014; Sarantis and Grinstein, 2012). In fact, for many intracellular bacteria, replication (or at least survival) within macrophages has been related with the ability to cause disease (Price and Vance, 2014). The diversity of functions that can be performed by macrophages

is directly linked to a high degree of metabolic diversity and plasticity as well as a fast ability to respond to specific environments (Martinez and Gordon, 2014; Murray et al., 2014; Price and Vance, 2014). These features are considered very attractive to be explored by intracellular pathogens as a vast source of cellular resources that can be rapidly remodeled (Eisenreich et al., 2015; Eisenreich et al., 2017; Van den Bossche et al., 2017). Along with the capacity to hijack a wide range of host signaling pathways to their own benefit (Ashida et al., 2014; Friedrich et al., 2017; Reddick and Alto, 2014), it has been reported that several intracellular pathogens are also able to induce distinct host cell metabolic signatures in macrophages to suit their replication requirements (Eisele et al., 2013; Xavier et al., 2013). In fact, the altered metabolic state of M2 macrophages, which has also been associated with reduced antimicrobial capacity, seems to be a beneficial factor that supports the survival and proliferation of several intracellular pathogens (Benoit et al., 2008; Buchacher et al., 2015; Eisele et al., 2013; Mege et al., 2011). Overall, intracellular bacteria appear to be able to capitalize on macrophage intrinsic plasticity for optimal replication during infection (Price and Vance, 2014).

The drastic intracellular phenotypic differences between *R. conorii* and *R. montanensis* in THP-1 macrophages (Curto et al., 2016), suggest substantial alterations in the content of host proteins, that may likely reflect differential macrophage responses to either favor (*R. conorii*) or restrict (*R. montanensis*) intracellular bacterial proliferation. To gain deeper insights into the molecular mechanisms underlying these responses, we herein employed a label-free quantitative proteomics approach (SWATH-MS) (sequential window acquisition of all theoretical mass spectra), to profile proteomic alterations that occur upon infection of THP-1 macrophages with *R. conorii* and *R. montanensis*. SWATH-MS is a highly specific data-independent acquisition method that has been successfully used to compare alterations in protein content in different experimental contexts (Anjo et al., 2017; Gao et al., 2017). Our results revealed substantial differences in protein content between infection conditions, with two main targeted modules – carbon metabolism and protein processing pathways – emerging as differentially affected upon infection with each rickettsial species. Differential changes observed in proteins associated with key metabolic pathways anticipate the induction of distinct metabolic signatures by *R. conorii* and *R. montanensis*,

suggesting that *R. conorii* can substantially reprogram several host metabolic pathways towards an M2-like activation program. Moreover, our results revealed a reduced abundance of different proteasome and immunoproteasome subunits upon infection with both rickettsial species, pointing towards a sophisticated ability of rickettsial species to interfere with this proteolytic machinery, which may help bacteria to escape immune surveillance. Remarkably, the observed ability of *R. conorii*, but not *R. montanensis*, to increase ER protein folding capacity may serve to compensate the stress induced by the accumulation of misfolded proteins during infection. Overall, our results point towards a substantial manipulation of the host by the pathogen *R. conorii* to meet host cell bioenergetics demands and sustain cell viability for bacterial replication, and, likely, to maintain its own metabolic needs.

V.3 | Materials and Methods

V.3.1 | Cell lines, *Rickettsia* Growth and Purification

Vero cells were grown in Dulbecco's modified Eagle's medium (DMEM; Gibco) supplemented with 10% heat-inactivated fetal bovine serum (Atlanta Biologicals), 1x non-essential amino acids (Corning), and 0.5 mM sodium pyruvate (Corning). THP-1 (ATCC TIB-202^{TM}) cells were grown in RPMI-1640 medium (Gibco) supplemented with 10% heat-inactivated fetal bovine serum (Atlanta Biologicals). Differentiation of THP-1 cells into macrophage-like cells was carried out by the addition of 100 nM of phorbol 12-myristate 13-acetate (PMA; Fisher). Cells were allowed to differentiate and adhere for 3 days prior to infection. Both cell lines were maintained in a humidified 5% CO_2 incubator at 34 °C. *R. conorii* isolate Malish7 and *R. montanensis* isolate M5/6 were propagated in Vero cells and purified as previously described (Ammerman et al., 2008; Chan et al., 2009; Chan et al., 2011).

V.3.2 | Sample preparation

PMA-differentiated THP-1 cells monolayers at a cell confluency of 2 x 10^5 cells per well, in 24 well plates (3 wells per condition) were infected with *R. conorii, R. montanensis* at a multiplicity of infection (MOI) of 10 or maintained uninfected. Plates were centrifuged at 300 x g for 5 min at room temperature to induce contact between rickettsiae and host cells, and incubated at 34 °C and 5% CO_2 for 24 hours. At the specified time point, culture medium was removed, cells were washed 1x with PBS and total protein was extracted using 100 µL of protein extraction buffer per well (25 mM Tris/HCl, 5 mM EDTA, 1% Triton X-100 and Pierce protease inhibitors table (ThermoFisher Scientific), pH 7.0). Samples were passed 10 times through Insulin Syringe with 28-gauge needle (Becton Dickinson) and denatured using 6x SDS sample buffer (4x Tris/HCl, 30% glycerol, 10% SDS, 0.6M DTT, 0.012% Bromophenol Blue, pH 6.8) during 10 minutes at 95 °C. Total protein content in each sample was then quantified using 2D Quant kit (GE Healthcare) and kept at -20˚C until further processing. Experiments were done in quadruplicate. After thawing, 10 µg of each replicate sample from each experimental condition were pooled together, creating this way three pooled samples (*R. conorii* pool, *R. montanensis* pool and uninfected pool). At this point, the same

amount of a recombinant protein (Green fluorescent Protein and Maltose-binding periplasmic protein (malE-GFP)) was added to each replicate sample and pooled samples to serve as an internal standard. All the samples were boiled for 5 minutes and acrylamide was added as an alkylating agent.

V.3.3 | In-gel digestion and liquid chromatography coupled to tandem mass spectrometry (LC-MS/MS)

The volume corresponding to 40 µg of each replicate sample as well as pooled samples was then loaded into a precast gel (4-20% Mini-Protean® TGX™ Gel, Bio-Rad), and the SDS-PAGE was partially run for 15 minutes at 110 V (Anjo et al., 2015). After SDS-PAGE, proteins were stained with Colloidal Coomassie Blue as previously described (Manadas et al., 2009).

The lanes were sliced into 3 fractions with the help of a scalpel, and after the excision of the gel bands, each one was sliced into smaller pieces. The gel pieces were destained using a 50 mM ammonium bicarbonate solution with 30% acetonitrile (ACN) followed by a washing step with water (each step was performed in a thermomixer (Eppendorf) at 1,050 x rpm for 15 min). The gel pieces were dehydrated on Concentrador Plus/Vacufuge® Plus (Eppendorf). To each gel band 75 µL of trypsin (0.01 µg/µL solution in 10 mM ammonium bicarbonate) were added to the dried gel bands and left for 15 min at 4°C to rehydrate the gel pieces. After this period, 75 µL of 10 mM ammonium bicarbonate were added and in-gel digestion was performed overnight at room temperature in the dark. After digestion, the excess solution from gel pieces was collected to a low binding microcentrifuge tube (LoBind®, Eppendorf) and peptides were extracted from the gel pieces by sequential addition of three solutions of increasing percentage of acetonitrile (30%, 50%, and 98%) in 1% formic acid (FA). After the addition of each solution, the gel pieces were shaken in a thermomixer (Eppendorf) at 1250 rpm for 15 min and the solution was collected to the tube containing the previous fraction. The peptide mixtures were dried by rotary evaporation under vacuum (Concentrador Plus/Vacufuge® Plus, Eppendorf). The peptides from each fraction of each sample were pooled together for SWATH analysis; the peptides from the pooled samples were kept separated in the three fractions of the digestion procedure.

After digestion, all samples were subjected to solid phase extraction with C18 sorbent (OMIX tip, Agilent Technologies). The eluted peptides were evaporated and solubilized in 30 µL mobile phase, aided by ultrasonication using a cuphorn device (Vibra-cell 750 watt, Sonics) at 40% amplitude for 2 minutes. Samples were then centrifuged for 5 minutes at 14,100 x g (minispin plus, Eppendorf) and analysed by LC-MS/MS.

The Triple TOF™ 5600 System (Sciex) was operated in two phases: information-dependent acquisition (IDA) of each fraction of the pooled samples; followed by SWATH (Sequential Windowed data independent Acquisition of the Total High-resolution Mass Spectra) acquisition of each sample. Peptide separation was performed using liquid chromatography (nanoLC Ultra 2D, Eksigent) on a ChromXP C18CL reverse phase column (300 µm × 15 cm, 3 µm, 120Å, Eksigent) at 5 µL/min with a 45 min gradient from 2% to 35% acetonitrile in 0.1% FA, and the peptides were eluted into the mass spectrometer using an electrospray ionization source (DuoSpray™ Source, Sciex).

Information dependent acquisition (IDA) experiments were performed by analysing 10 µL of each fraction of the pooled samples. The mass spectrometer was set for IDA scanning full spectra (350-1250 m/z) for 250 ms, followed by up to 100 MS/MS scans (100–1500 m/z from a dynamic accumulation time – minimum 30 ms for precursor above the intensity threshold of 1000 counts per second (cps) – in order to maintain a cycle time of 3.3 s). Candidate ions with a charge state between +2 and +5 and counts above a minimum threshold of 10 cps were isolated for fragmentation and one MS/MS spectra was collected before adding those ions to the exclusion list for 25 seconds (mass spectrometer operated by Analyst® TF 1.7, Sciex). Rolling collision energy was used with a collision energy spread of 5.

The SWATH setup was essentially as in Gillet et al (Gillet et al., 2012), with the same chromatographic conditions used for SWATH and IDA acquisitions. For SWATH-MS based experiments, the mass spectrometer was operated in a looped product ion mode. The SWATH-MS setup was designed specifically for the samples to be analysed **(Supplementary Table V.1)**, in order to adapt the SWATH windows to the complexity of this batch of samples. A set of 60 windows of variable width (containing 1 m/z for window overlap) was constructed covering the precursor

mass range of 350-1250 m/z. A 200 ms survey scan (350-1250 m/z) was acquired at the beginning of each cycle for instrument calibration and SWATH MS/MS spectra were collected from 100–1500 m/z for 50 ms resulting in a cycle time of 3.25 s from the precursors ranging from 350 to 1250 m/z. The collision energy for each window was determined according to the calculation for a charge +2 ion centered upon the window with variable collision energy spread (CES) according with the window.

V.3.4 | Protein identification and relative quantification

Specific library of precursor masses and fragment ions were created by combining all files from the IDA experiments, and used for subsequent SWATH processing. The library was obtained using ProteinPilot™ software (v5.0.1, Sciex), with the following search parameters: *Homo Sapiens* SwissProt database (release of March 2017) and malE-GFP; acrylamide alkylated cysteines as fixed modification; and the gel based special focus option. An independent False Discovery Rate (FDR) analysis using the target-decoy approach provided with ProteinPilot™ software was used to assess the quality of the identifications, and positive identifications were considered when identified proteins and peptides reached a 5% local FDR (Sennels et al., 2009; Tang et al., 2008).

Data processing was performed using SWATH™ processing plug-in for PeakView™ (v2.2, Sciex), briefly peptides were selected from the library using the following criteria: (i) the unique peptides for a specific targeted protein were ranked by the intensity of the precursor ion from the IDA analysis as estimated by the ProteinPilot™ software, and (ii) Peptides that contained biological modifications and/or were shared between different protein entries/isoforms were excluded from selection. Up to 15 peptides were chosen per protein, and SWATH™ quantitation was attempted for all proteins in the library file that were identified below 5% local FDR from ProteinPilot™ searches. Peptide's retention time was adjusted by using the malE-GFP peptides. In SWATH™ Acquisition data, peptides are confirmed by finding and scoring peak groups, which are a set of fragment ions for the peptide. Up to 5 target fragment ions were automatically selected and the peak groups were scored following the criteria described in Lambert et al (Lambert et al., 2013). Peak group confidence threshold was determined based on a FDR analysis using the target-decoy

approach and 1% extraction FDR threshold was used for all the analyses. Peptides that met the 1% FDR threshold in at least one pair of technical replicates were retained, and the peak areas of the target fragment ions of those peptides were extracted across the experiments using an extracted-ion chromatogram (XIC) window of 4 minutes. Protein levels were estimated by summing all the transitions from all the peptides for a given protein (Collins et al., 2013) and normalized to the total intensity at the protein level. Statistical tests were performed in SPSS (v23, IBM) using the non-parametric Mann Whitney U-test and proteins were considered altered when an alteration of at least 20% in abundance (fold change ≤ 0.83 or fold change ≥ 1.2) was observed between uninfected and infected conditions.

V.3.5 | Bioinformatics analysis

The correlation plots of the quantitative data from all the proteins quantified were obtained using InfernoRDN (v1.1) software (Polpitiya et al., 2008). Principal components analysis was performed using the software MakerView (v1.2.1, Sciex). The analysis was attempted by importing the quantitative data from the proteins considered as altered upon infection of THP-1 macrophages with *R. conorii* or *R. montanensis*. Functional protein association networks were evaluated using the Search Tool for Retrieval of Interacting Genes/Proteins (STRING) 10.5 (http://string-db.org/) with high confidence (0.7) parameters (Szklarczyk et al., 2017). Quantified proteins that were considered significantly differentially represented in each experimental condition were also upload into KEGG pathway databases (http://www.genome.jp/kegg/pathway.html) to identify significant altered canonical pathways (Kanehisa et al., 2017).

V.3.6 | Data accessibility

The mass spectrometry proteomics data have been deposited to the ProteomeXchange Consortium via the PRIDE (Vizcaino et al., 2016) partner repository, with the identifier PXD010330 (reviewer account username: reviewer65965@ebi.ac.uk; Password: 7jkOjSM3).

V.4 | Results

V.4.1 | Global changes in proteome profiles stimulated by *R. conorii* and *R. montanensis* infection in THP-1 macrophages.

We have previously shown that two members of SFG *Rickettsia* with different pathogenicity attributes display entirely distinct intracellular fates in macrophage-like cells (Curto et al., 2016). At 24 hours post-infection (hpi), *R. conorii* (pathogen) was present as intact bacteria and free in the cytoplasm, whereas *R. montanensis* (non-pathogen) was destroyed with rickettsial debris showing substantial co-localization with lysosomal markers (Curto et al., 2016). To gain insights into molecular changes associated with these opposite phenotypes, we compared host protein abundance in infected and uninfected cells using a label-free quantitative proteomics approach. Total protein extracts were prepared from PMA-differentiated THP-1 cells at 24 hours post-infection with *R. conorii* and *R. montanensis* (MOI=10), and from uninfected cells processed in parallel. The relative protein quantification was performed using LC-SWATH-MS analysis, where a comprehensive library of 1425 confidently identified proteins was created from which a total of 746 proteins were confidently quantified in all samples. Proteins were considered as altered when an alteration of at least 20% in abundance (fold change ≤ 0.83 or fold change ≥ 1.2) was observed between uninfected and infected conditions (Bussey et al., 2018; Rukmangadachar et al., 2016). Using these criteria, THP-1 macrophages infected with *R. conorii* showed significant changes in the content of a total of 385 proteins compared to uninfected cells. Of these, 178 (24%) proteins were found enriched, while 207 (28%) proteins showed reduced abundance **(Figure V.1A, C, and Supplementary Table V.2**). On the other hand, in THP-1 macrophages infected with *R. montanensis,* we identified a total of 358 proteins with significantly altered abundance, 64 (9%) of which identified as enriched and 294 (39%) with lower abundance compared to uninfected cells **(Figure V.1B-C, and Supplementary Table V.2)**. Principal component analysis (PCA) was carried out to assess the sample correlations using the quantification data of altered proteins upon infection of THP-1 macrophages with *R. conorii* or *R. montanensis* **(Supplementary Figure V.1)**.

To provide insights on cellular pathways associated with these significantly altered proteins in each infection condition, we performed a KEGG pathway enrichment analysis (Kanehisa et al., 2017) using STRING databases (Szklarczyk et al., 2017; von Mering et al., 2003).

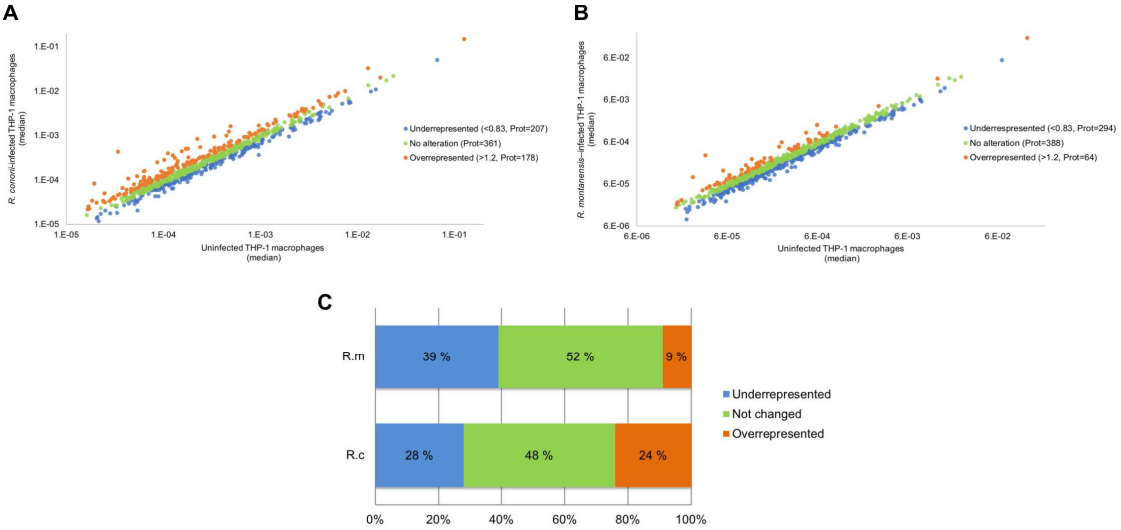

Figure V.1 | Overall analysis of *R. conorii*- and *R. montanensis*-induced changes in global proteome of THP-1 macrophages. (A-B) Scatterplot representation of changes in protein abundance of THP-1 macrophages upon infection with *R. conorii* **(A)** and *R. montanensis* **(B)**. The 746 quantified proteins that were confidently quantified in all 3 experimental conditions were plotted and considered altered when a change of at least 20% in abundance (fold change ≤ 0.83 or fold change ≥ 1.2) was observed between infected and uninfected conditions. Proteins that were considered to decrease, not change or increase its abundance upon infection are represented in blue, green and orange, respectively. **(C)** Bar chart displaying the percentage (out of the 746 quantified proteins that were confidently quantified) of host proteins that were considered to decrease, not change or increase its abundance upon infection with both *R. conorii* and *R. montanensis*. See also **Supplementary Table V.2**.

Top pathways enriched among over and underrepresented proteins in *R. conorii* and *R. montanensis*-infected cells are shown in **Tables V.2-3**, respectively. In *R. conorii*-infected cells, several proteins with either increased and reduced abundance were categorized in broad term categories such as metabolic pathways (KEGG:1100) and carbon metabolism (KEGG:1200), suggesting a significant impact of infection in different pathways of host metabolism, as dissected in detail below. Moreover, accumulating proteins were also associated with protein processing in endoplasmic reticulum (KEGG:4141), while proteins with reduced abundance were associated with proteasome (KEGG:3050). In *R. montanensis*-infected cells, the observed pathway enrichment pattern is different, with top pathways among underrepresented proteins related with proteasome

(KEGG:3050), spliceosome (KEGG:3040), carbon metabolism (KEGG:1200) and metabolic pathways (KEGG:1100), whereas in the group of enriched proteins, the top pathways were related with ribosome (KEGG:3010) and complement and coagulation cascades (KEGG:4610) (although with fewer proteins associated).

Table V.1. KEGG pathways enriched among under and overrepresented proteins upon infection of THP-1 macrophages with *R. conorii*.

***R. conorii*-infected cells – proteins with reduced abundance**			
KEGG Pathways			
ID	**pathway description**	**count in gene set**	**false discovery rate**
1200	Carbon metabolism	13	8.61E-09
1100	Metabolic pathways	38	1.26E-08
30	Pentose phosphate pathway	7	4.90E-07
10	Glycolysis / Gluconeogenesis	9	5.46E-07
3050	Proteasome	8	5.46E-07
1230	Biosynthesis of amino acids	9	1.57E-06
5130	Pathogenic Escherichia coli infection	8	1.88E-06
5203	Viral carcinogenesis	12	1.08E-05
480	Glutathione metabolism	7	1.76E-05
***R. conorii*-infected cells – proteins with enriched abundance**			
KEGG Pathways			
ID	**pathway description**	**count in gene set**	**false discovery rate**
4141	Protein processing in endoplasmic reticulum	23	3.69E-19
5012	Parkinson's disease	16	9.80E-12
1100	Metabolic pathways	36	1.40E-09
5016	Huntington s disease	15	3.68E-09
20	Citrate cycle (TCA cycle)	8	3.72E-09
1200	Carbon metabolism	12	3.72E-09
5010	Alzheimer s disease	12	7.80E-07
510	N-Glycan biosynthesis	7	6.07E-06
4260	Cardiac muscle contraction	8	8.43E-06
3060	Protein export	5	2.99E-05
190	Oxidative phosphorylation	9	4.95E-05

To start distinguishing between common and species-specific host responses to infection, we have sorted these proteins into several groups **(Figure V.2, Supplementary Table V.3)**. As illustrated in the Venn diagram, infection of THP-1 macrophages with *R. conorii* or *R. montanensis* resulted in common changes in protein content of 245 host proteins, corresponding to 52 proteins enriched and 193 proteins with reduced abundance shared between infection conditions.

Table V.2. KEGG pathways enriched among under and overrepresented proteins upon infection of THP-1 macrophages with *R. montanensis*.

***R. montanensis*-infected cells – proteins with reduced abundance**			
KEGG Pathways			
ID	**pathway description**	**count in gene set**	**false discovery rate**
3050	Proteasome	15	4.41E-15
3040	Spliceosome	19	2.06E-12
1200	Carbon metabolism	16	1.19E-10
1100	Metabolic pathways	48	1.90E-09
10	Glycolysis / Gluconeogenesis	11	4.39E-08
30	Pentose phosphate pathway	8	9.36E-08
5130	Pathogenic Escherichia coli infection	9	1.92E-06
1230	Biosynthesis of amino acids	10	2.01E-06
5203	Viral carcinogenesis	14	1.12E-05
480	Glutathione metabolism	8	1.22E-05
5169	Epstein-Barr virus infection	14	1.55E-05
620	Pyruvate metabolism	7	3.35E-05
4114	Oocyte meiosis	10	5.81E-05
***R. montanensis*-infected cells – proteins with enriched abundance**			
KEGG Pathways			
ID	**pathway description**	**count in gene set**	**false discovery rate**
3010	Ribosome	5	0.00773
4610	Complement and coagulation cascades	4	0.00773
5143	African trypanosomiasis	3	0.013
510	N-Glycan biosynthesis	3	0.0238
5144	Malaria	3	0.0238
5150	Staphylococcus aureus infection	3	0.0238
5012	Parkinson's disease	4	0.0344
4141	Protein processing in endoplasmic reticulum	4	0.044
4260	Cardiac muscle contraction	3	0.044
4964	Proximal tubule bicarbonate reclamation	2	0.044

Interestingly, we found that infection with *R. conorii* resulted in specific alterations in the content of 136 host proteins. Of these, 123 proteins were enriched, while 13 showed reduced abundance. On the other hand, *R. montanensis*-specific alterations were observed in 109 proteins (11 proteins found overrepresented and 98 underrepresented). We also identified 4 proteins that are inversely altered in both experimental conditions, with 3 proteins being overrepresented in *R. conorii*-infected cells and underrepresented in *R. montanensis*-infected THP-1 macrophages, and one protein showing the reverse accumulation pattern.

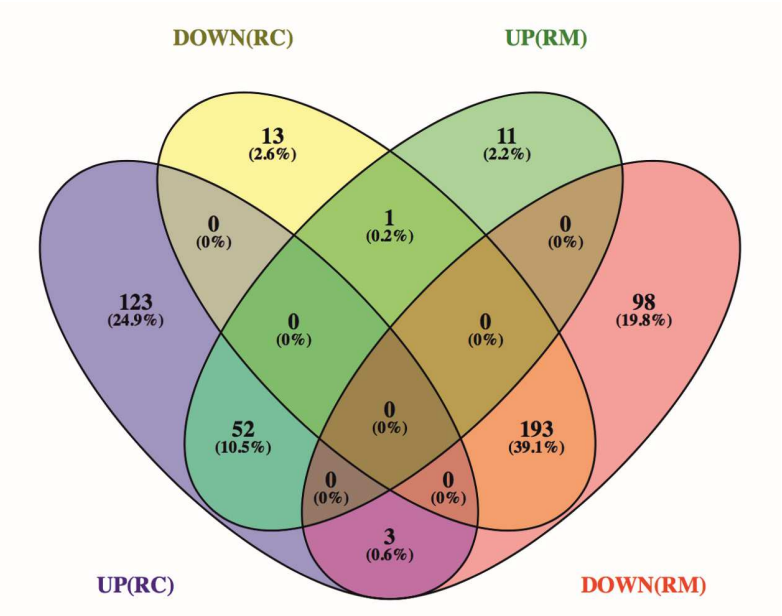

Figure V.2 | Venn diagram depicting the number and distribution of host proteins that changed their abundance upon infection with *R. conorii* or *R. montanensis*. Host proteins that change their abundance in the same direction (increase or decrease abundance) upon infection with both *R. conorii* and *R. montanensis* are considered to be a common response to infection. On the other hand, host proteins that change their abundance in only one infection condition, but show unchanged protein levels in the other, are considered to be a species-specific host response. DOWN(RC), yellow – proteins that are underrepresented in *R. conorii*-infected THP-1 macrophages compared to uninfected THP-1 macrophages; UP(RC), blue – proteins that are overrepresented in *R. conorii*-infected THP-1 macrophages compared to uninfected THP-1 macrophages; DOWN(RM), red - proteins that are underrepresented in *R. montanensis*-infected THP-1 macrophages compared to uninfected THP-1 macrophages; UP(RM), green - proteins that are overrepresented in *R. montanensis*-infected THP-1 macrophages compared to uninfected THP-1 macrophages. Individual information about the proteins in each group of the Venn diagram can be found in **Supplementary Table V.3**. Venn diagrams were obtained using VENNY 2.1 (http://bioinfogp.cnb.csic.es/tools/venny/).

To further identify host processes and molecular pathways that were differentially altered in common and species-specific responses to infection, we performed a Search Tool for Retrieval of Interacting Genes/Proteins (STRING) analysis ((Szklarczyk et al., 2017)) for each of these groups. The global interaction networks obtained for all proteins commonly altered between infection conditions revealed several clusters **(Figure V.3)**, which were particularly evident among proteins with reduced abundance **(Figure V.3A)**.

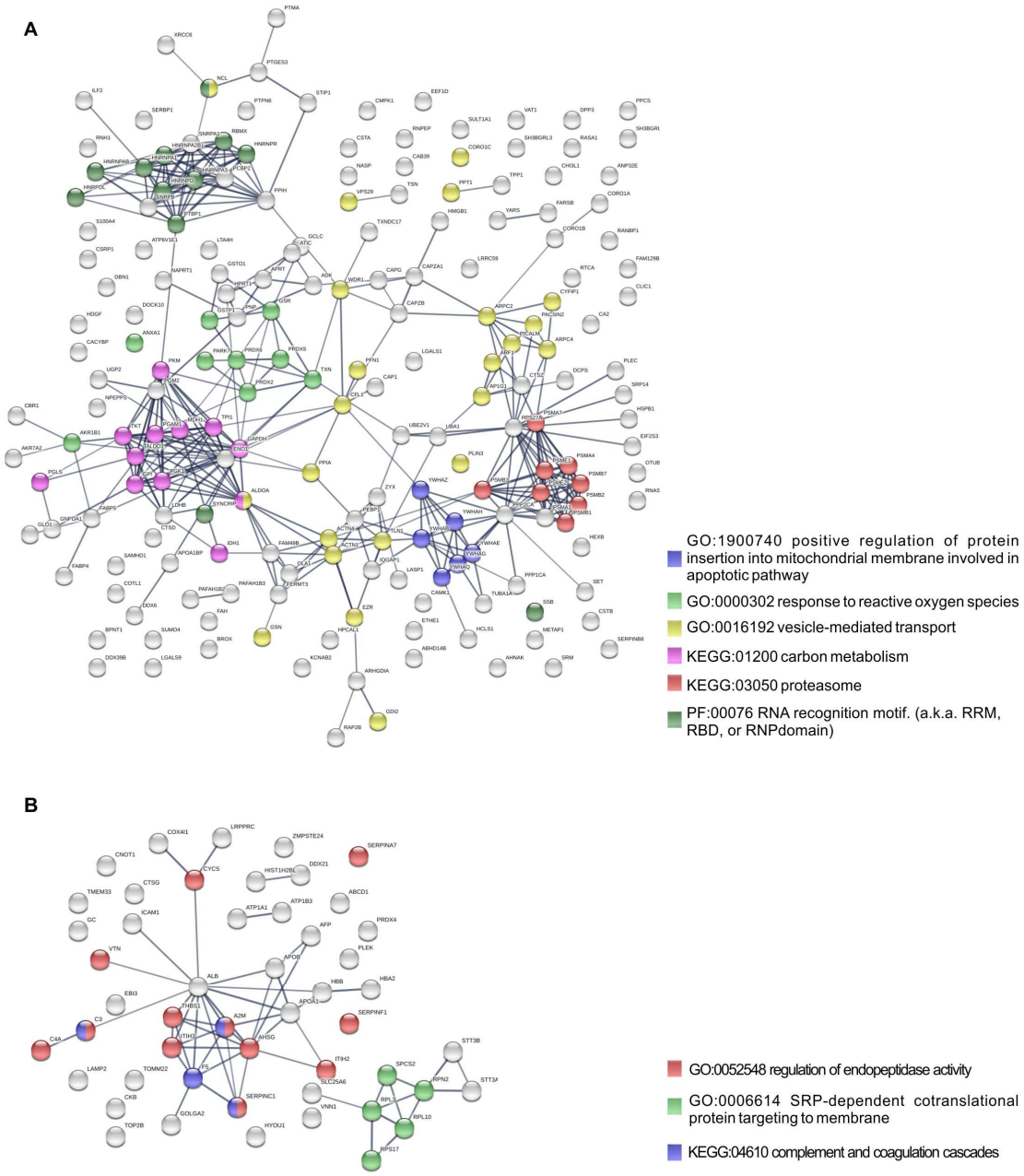

Figure V.3 | Protein network analysis of common responses to infection with both *R. conorii* and *R. montanensis*. (A-B) Clustering of protein-protein interaction networks for the 193 and 52 host proteins commonly altered between infection conditions, found with reduced abundance **(A)** or increased abundance **(B)**, respectively. List of the individual host proteins for each independent analysis can be found in **Supplementary Table V.3**. The analysis was carried out with STRING 10.5 (http://string-db.org/) using high confidence (0.7) score. Nodes are represented with different colors according to their categorization in gene ontology (GO) terms, KEGG pathways or PFAM protein domains.

In this particular functional network, these clusters included GO and KEGG pathway IDs associated with carbon metabolism (KEGG:01200), proteasome (KEGG:03050), positive regulation of protein insertion into mitochondrial membrane involved in apoptotic signaling pathway (GO:1900740), response to reactive oxygen species (GO:0000302), vesicle-mediated transport (GO:0016192) and RNA recognition motif (PF00076), suggesting a common impact of infection with either the pathogenic and non-pathogenic member of SFG *Rickettsia* in different biological processes. For the 52 commonly enriched proteins, the STRING analysis revealed clusters of proteins associated with regulation of endopeptidase activity (GO:0052548), SRP-dependent cotranslational protein targeting to membrane, and complement and coagulation cascades (KEGG:04610) **(Figure V.3B)**. Regarding species-specific induced alterations, the obtained interaction networks are shown in **Figure V.4-5 and Supplementary Figure V.2**.

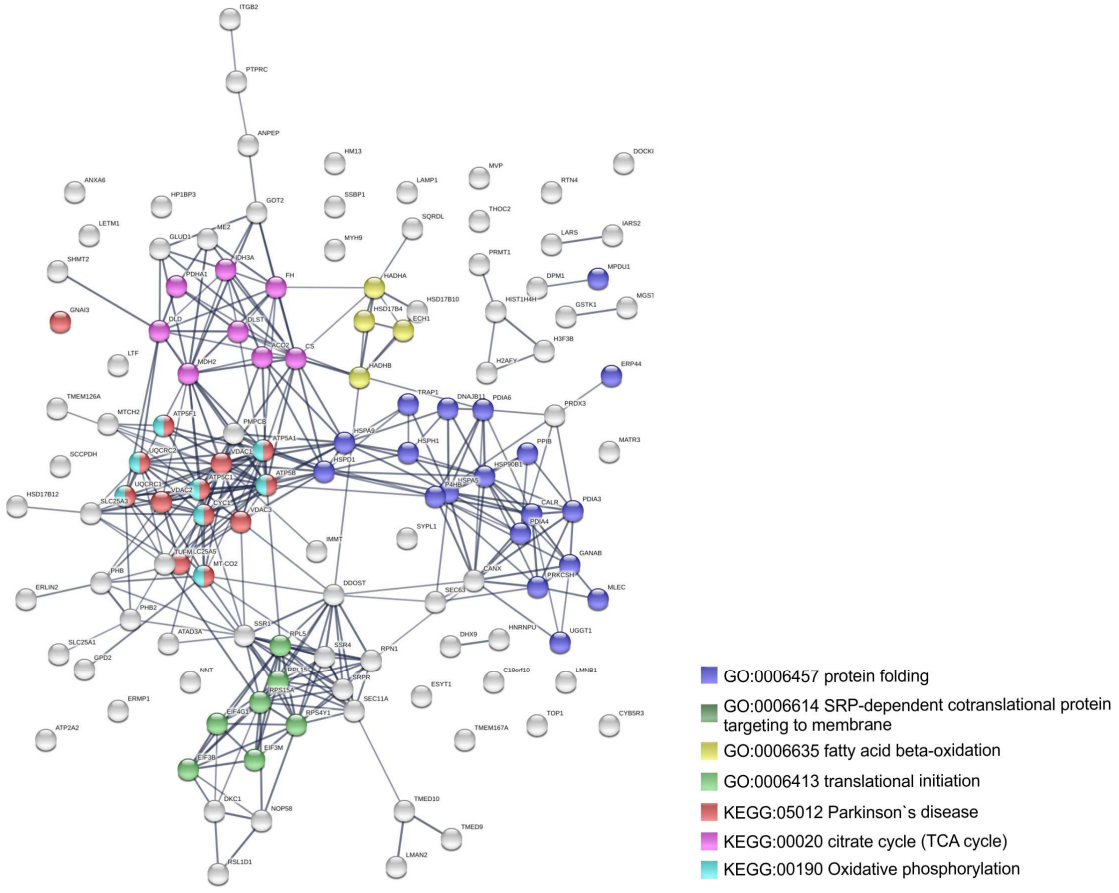

Figure V.4 (previous page) | Clustering of host proteins that specifically increase their abundance upon infection with *R. conorii*. Protein-protein interaction network for the 123 host proteins with increased abundance upon infection with *R. conorii*, but unchanged levels upon infection with *R. montanensis*. List of the individual host proteins for each independent analysis can be found in **Supplementary Table V.3**. The analysis was carried out with STRING 10.5 (http://string-db.org/) using high confidence (0.7) score. Nodes are represented with different colors according to their categorization in gene ontology (GO) terms or KEGG pathways.

The 123 host proteins enriched in THP-1 macrophages infected with *R. conorii* **(Figure V.4)** clustered in diverse cellular functions, such as protein folding (GO:0006457), SRP-dependent cotranslational protein targeting to membrane (GO:0006614), fatty acid beta-oxidation (GO:0006635), translational initiation (GO:0006413), TCA cycle (KEGG:00020), oxidative phosphorylation (KEGG:00190) and Parkinson's disease (GO:05012). Notably, these results suggest a significant impact on the modulation of different host metabolic processes specifically induced by *R. conorii*, on top of the cluster for carbon metabolism already observed for shared proteins with reduced abundance **(Figure V.3A)**. For the 98 host proteins found specifically underrepresented in *R. montanensis*-infected cells **(Figure V.5)**, main clusters associated with mRNA splicing via spliceosome (GO:0000398), nucleocytoplasmic transport (GO:0006913), proteasome-mediated ubiquitin-dependent protein catabolic process (GO:0043161), translational (GO:0006412), carboxylic acid biosynthetic process (GO:0046394) and fatty acid degradation (KEGG:00071).

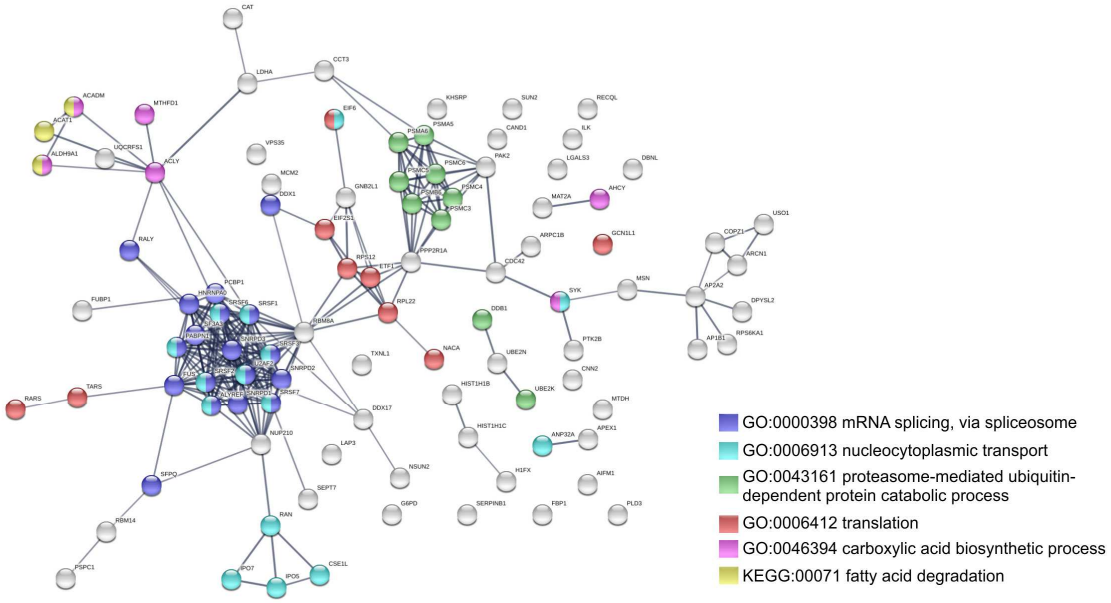

Figure V.5 (previous page) | Clustering of host proteins that specifically decrease their abundance upon infection with *R. montanensis*. Protein-protein interaction network for the 98 host proteins with decreased abundance upon infection with *R. montanensis*, but unchanged protein levels upon infection with *R. conorii*. List of the individual host proteins for each independent analysis can be found in **Supplementary Table V.3**. The analysis was carried out with STRING 10.5 (http://string-db.org/) using high confidence (0.7) score. Nodes are represented with different colors according to their categorization in gene ontology (GO) terms or KEGG pathways.

For the other two groups of proteins uniquely altered by each rickettsial species (*R. conorii*-specific with reduced abundance (13 proteins) and *R. montanensis*-specific with enriched abundance (11 proteins)), no significant clustering was detected **(Supplementary Figure V.2)**.

V.4.2 | A pathogen and a non-pathogen SFG *Rickettsia* trigger differential metabolic signatures in macrophage-like cells

During the past decades, a growing body of knowledge has been emerging showing that macrophages can display high plasticity, being able to adopt various activation states (with different metabolic requirements) to accommodate their diverse functional repertoire (Van den Bossche et al., 2017). Interestingly, the apparent paradox of survival and replication of intracellular pathogens in cells whose primary function is pathogen elimination suggests that different metabolic adaptation processes need to take place, either as a response of the host cell to fight infection or due to bacterial modulation to support its specific metabolic needs (Eisenreich et al., 2017). Indeed, intracellular pathogens are known to employ different strategies to modulate host cell metabolism to create a more permissive replication niche (Abu Kwaik and Bumann, 2015; Eisenreich et al., 2017). Our proteomics results revealed that different host proteins involved in various metabolic processes were differentially altered upon infection of THP-1 macrophages with either *R. conorii* or *R. montanensis*. Central metabolic pathways such as glycolysis, pentose phosphate pathway (PPP), tricarboxylic acid (TCA) cycle, oxidative phosphorylation (OXPHOS), fatty acid metabolism and amino acid metabolism were among the processes where significant alterations were observed **(Table V.3)**.

Regarding glycolysis, the majority of the enzymes involved in the different steps of glucose conversion to pyruvate (names and reactions catalyzed shown in **Figure V.6)**, and lactate dehydrogenase B (LDHB; P07195) which catalyzes the interconversion of pyruvate and lactate in

a post-glycolytic process, were found significantly reduced in abundance under both infection conditions. A similar pattern was observed for several enzymes involved in the PPP **(Table V.3)**. PPP uses intermediates diverted from glycolysis for the production of amino acids for protein synthesis, ribose for nucleotides, and NADPH for the production of reactive oxygen species (ROS) by NADPH oxidase. As the glycolytic metabolism, this pathway assumes a key role by providing intermediates that serve other critical anabolic and catabolic processes (Stincone et al., 2015), with our results suggesting a reduced activity of both metabolic pathways in response to rickettsial infection.

Table V.3. Quantified host proteins involved in several metabolic processes (glycolysis, pentose phosphate pathway, TCA cycle, lipid metabolism and oxidative phosphorylation) and their respective fold change in abundance upon infection of THP-1 macrophages with *R. conorii* (Rc/uninf) or *R. montanensis* (Rm/uninf). Proteins that are considered as altered (fold change ≤ 0.83 or fold change ≥ 1.2) between infected and uninfected conditions were color-coded according the following: decreased (blue), not changed (transparent) or increased (orange) (cont. next pages).

Pathway	Name	UniProt	EC number	Log_2 (Rc/uninf)	Log_2 (Rm/uninf)
Glycolysis	Phosphoglucomutase 2 (PGM2)	Q96G03	5.4.2.2	-0.59	-0.64
	Glucose-6-phosphate isomerase (GPI)	P06744	5.3.1.9	-0.41	-0.40
	Fructose-1,6-biphosphatase I (FBP1)	P09467	3.1.3.11	-0.04	-0.33
	Phosphofructokinase, liver type (PFKL)	P17858	2.7.1.11	0.09	-0.15
	aldolase, fructose-biphosphate A (ALDOA)	P04075	4.1.2.13	-0.39	-0.30
	triosephosphate isomerase (TPI1)	P60174	5.3.1.11	-0.48	-0.40
	glyceraldehyde-3-phosphate dehydrogenase (GADPH)	P04406	1.2.1.12	-0.56	-0.42
	phosphoglycerate kinase 1 (PGK1)	P00558	2.7.2.3	-0.60	-0.62
	phosphoglycerate mutase 1 (PGAM1)	P18669	5.4.2.11	-0.75	-0.60
	enolase 1 (ENO1)	P06733	4.2.1.11	-0.48	-0.39
	pyruvate kinase, muscle (PKM)	P14618	2.7.1.40	-0.45	-0.47
	lactate dehydrogenase A(LDHA)	P00338	1.1.1.27	-0.24	-0.38
	lactate dehydrogenase B(LDHB)	P07195	1.1.1.27	-0.27	-0.38
Pentose Phosphate Pathway	Glucose-6-phosphate dehydrogenase (G6PD)	P11413	1.1.149/1.1.1.343	-0.22	-0.29
	6-phosphogluconolactonase (PGLS)	O95336	3.1.1.31	-0.80	-0.52
	Phosphogluconate dehydrogenase (PGD)	P52209	1.1.1.44/1.1.1.343	-0.48	-0.25
	Glucose-6-phosphate isomerase (GPI)	P06744	5.3.1.9	-0.41	-0.40
	Transketolase (TKT)	P29401	2.2.1.1	-0.64	-0.60

	Transaldolase 1 (TALDO1)	P37837	2.2.1.2	-0.57	-0.43
	Phosphofructokinase, liver type (PFKL)	P17858	2.7.1.11	0.09	-0.15
	Fructose-biphosphatase 1 (FBP1)	P09467	3.1.3.11	-0.04	-0.33
	Aldolase, fructose-biphosphatase A (ALDOA)	P04075	4.1.2.13	-0.39	-0.30
	Phosphoglucomutase 2 (PGM2)	Q96G03	5.4.2.7/5.4.2.2	-0.59	-0.64
TCA cycle	Pyruvate dehydrogenase (lipoamide) alpha 1 (PDHA1)	P08559	1.2.4.1	0.40	0.17
	ATP citrate lyase (ACLY)	P53396	2.3.3.8	-0.23	-0.37
	Citrate synthase (CS)	O75390	2.3.3.1	0.49	0.14
	Aconitase 2 (ACO2)	Q99798	4.2.1.3	0.36	0.02
	Isocitrate dehydrogenase (NADP(+)) 2, mitochondrial (IDH2)	P48735	1.1.1.42	0.23	-0.04
	Isocitrate dehydrogenase 3 (NAD(+)) apha (IDH3A)	P50213	1.1.1.41	0.42	-0.17
	Isocitrate dehydrogenase (NADP(+)) 1, cytosolic (IDH1)	O75874	1.1.1.42	-0.55	-0.80
	Fumarate hydratase (FH)	P07954	4.2.1.2	0.39	0.11
	Malate dehydrogenase 2 (MDH2)	P40926	1.1.1.37	0.46	0.01
	Malate dehydrogenase 1 (MDH1)	P40925	1.1.1.37	-0.67	-0.62
	Dihydrolipoamide S-acetyltransferase (DLAT)	P10515	2.3.1.12	-0.03	0.17
	Dihydrolipoamide dehydrogenase (DLD)	P09622	1.8.1.4	0.58	-0.11
	Dihydrolipoamide S-succinyltransferase (DLST)	P36957	2.3.1.61	0.44	0.11
	Glutamate dehydrogenase 1 (GLUD1)	P00367	1.4.1.3	0.28	-0.02
	Glutamic-oxaloacetic transaminase 2 (GOT2)	P00505	2.6.1.1	0.48	0.12
	Malic enzyme 2 (ME2)	P23368	1.1.1.38	0.45	0.00
Lipid metabolism	hydroxyacyl-CoA dehydrogenase/3-ketoacyl-CoA thiolase/enoyl-CoA hydratase (trifunctional protein), beta subunit (HADHB)	P55084	2.3.1.16	0.32	-0.13
	hydroxyacyl-CoA dehydrogenase (HADH)	Q16836	1.1.1.35	0.20	0.13
	hydroxyacyl-CoA dehydrogenase/3-ketoacyl-CoA thiolase/enoyl-CoA hydratase (trifunctional protein), alpha subunit (HADHA)	P40939	1.1.1.211/4.2.1.17	0.55	0.14
	palmitoyl-protein thioesterase 1 (PPT1)	P50897	3.1.2.22	-1.34	-0.87
	hydroxysteroid 17-beta dehydrogenase 12 (HSD17B12)	Q53GQ0	1.1.1.330	0.50	0.25

	carnitine palmitoyltransferase 2 (CPT2)	P23786	2.3.1.21	0.25	-0.10
	acyl-CoA dehydrogenase, C-4 to C-12 straight chain (ACADM)	P11310	1.3.8.7	0.12	-0.33
	acyl-CoA dehydrogenase, very long chain (ACADVL)	P49748	1.3.8.9	0.25	0.07
	fatty acid synthase (FASN)	P49327	2.3.1.41	0.14	0.08
	apolipoprotein A1 (APOA1)	P02647	-	1.24	1.35
	apolipoprotein B (APOB)	P04114	-	1.35	0.54
Electron chain reaction (complex III)	cytochrome c1 (CYC1)	P08574	1.10.2.2	0.34	0.17
	ubiquinol-cytochrome c reductase core protein I (UQCRC1)	P31930	1.10.2.2	0.55	0.23
	ubiquinol-cytochrome c reductase core protein II (UQCRC2)	P22695	1.10.2.2	0.38	0.15
	ubiquinol-cytochrome c reductase, Rieske iron-sulfur polypeptide 1 (UQCRFS11)	P47985	1.10.2.2	-0.16	-0.46
Electron chain reaction (complex IV)	cytochrome c oxidase subunit 4I1 (COX4I1)	P13073	1.9.3.1	0.42	0.85
	cytochrome c oxidase subunit II (COX2)	P00403	1.9.3.1	0.36	0.12
Electron chain reaction (complex V)	ATP synthase, H+ transporting, mitochondrial F1 complex, alpha subunit 1, cardiac muscle (ATP5A1)	P25705	3.6.3.14	0.43	-0.05
	ATP synthase, H+ transporting, mitochondrial F1 complex, beta polypeptide (ATP5B)	P06576	3.6.3.14	0.47	0.10
	ATP synthase, H+ transporting, mitochondrial F1 complex, gamma polypeptide 1 (ATP5C1)	P36542	3.6.3.14	0.39	-0.05
	ATP synthase, H+ transporting, mitochondrial F1 complex, delta subunit (ATP5D)	P30049	3.6.3.14	0.20	0.12
	ATP synthase, H+ transporting, mitochondrial Fo complex subunit B1 (ATP5F1)	P24539	3.6.3.14	0.35	0.24
	ATPase H+ transporting V1 subunit A (ATP6V1A)	P38606	3.6.3.14	0.08	0.06
	ATPase H+ transporting V1 subunit E1 (ATP6V1E1)	P36543	3.6.3.14	-0.33	-0.36
	ATP synthase, H+ transporting, mitochondrial F1 complex, O subunit (ATP5O)	P48047	3.6.3.14	0.09	0.31
	ATPase H+ transporting V0 subunit d1 (ATP6V0D1)	P61421	3.6.3.14	0.15	-0.11
	ATP synthase, H+ transporting, mitochondrial Fo complex subunit F2 (ATP5J2)	P56134	3.6.3.14	0.10	-0.11

Interestingly, a differential macrophage response to *R. conorii*- versus *R. montanensis*-infection was observed for proteins implicated in other key metabolic pathways **(Table V.3)**. Several TCA cycle enzymes were found enriched in THP-1 macrophages infected with *R. conorii*, but not with *R. montanensis* **(Table V.3)**.

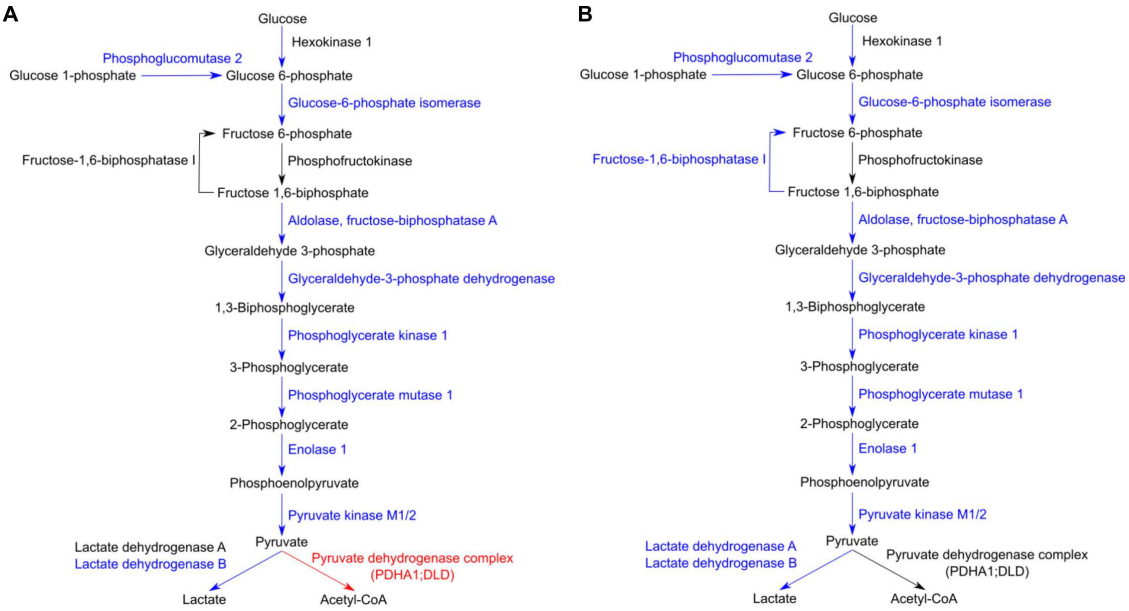

Figure V.6 | Host glycolytic enzymes found in reduced abundance upon infection of THP-1 macrophages with both rickettsial species. (A-B) Infection of THP-1 macrophages with either *R. conorii* **(A)** or *R. montanensis* **(B)** resulted in a decrease in the abundance of several host glycolytic enzymes at 24 hours post-infection. UniProt accession number and the respective fold change upon infection can be found in **Table V.3** for each respective enzyme. Enzymes with unchanged or decreased protein levels, when compared to uninfected cells, are represented in black and blue, respectively. Red represents enzymes of the pyruvate dehydrogenase complex found accumulated in *R. conorii*-infected cells **(Table V.3)**.

More specifically, infection with *R. conorii* resulted in an overrepresentation of citrate synthase (CS, O75390), the enzyme that catalyzes the condensation of acetyl-CoA and oxaloacetate to form citrate; aconitase (ACO2, Q99798), that catalyzes the isomerization of citrate to isocitrate; isocitrate dehydrogenase 3 (IDH3A, P50213), the enzyme responsible for the oxidative decarboxylation of isocitrate to α-ketoglutarate; fumarate hydratase (FH, P07954), which catalyzes the reversible hydration/dehydration of fumarate to malate; and malate dehydrogenase 2 (MDH2, P40926) that catalyzes the reversible oxidation of malate to oxaloacetate **(Figure V.7)**.

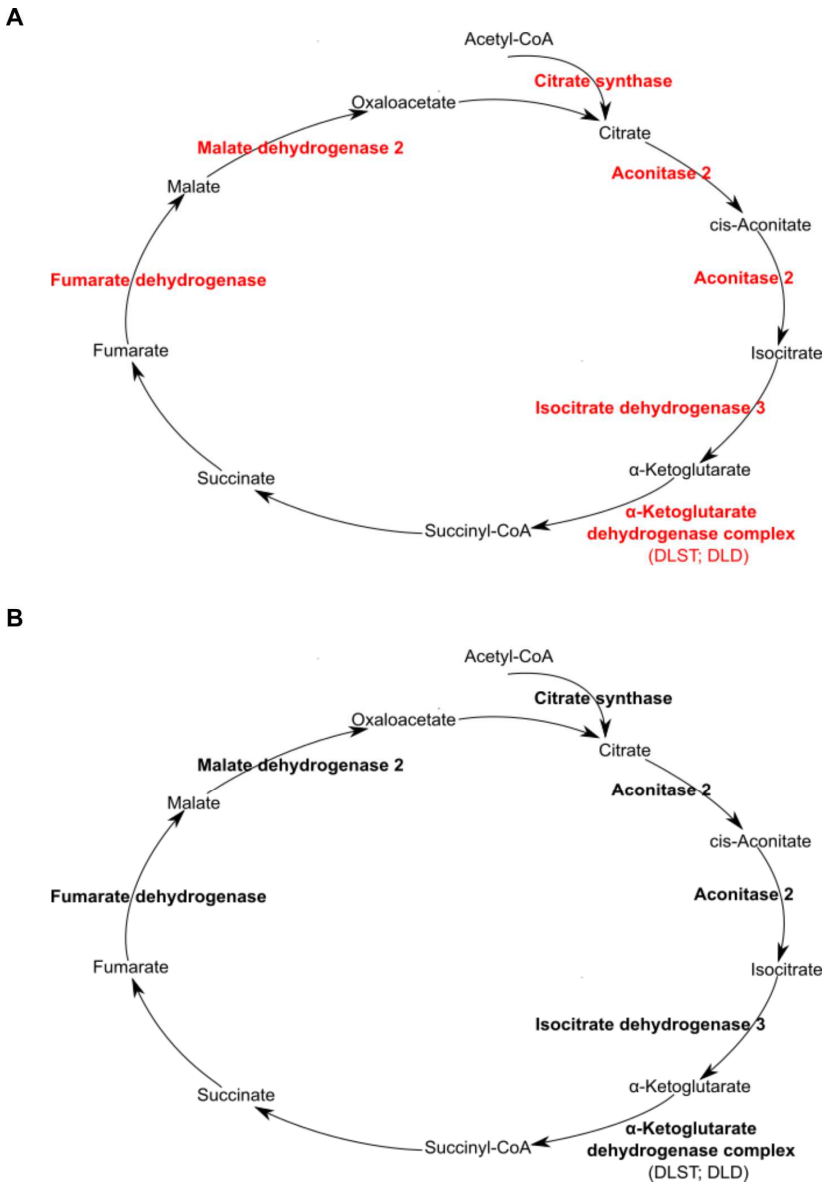

Figure V.7 | *R. conorii*, but not *R. montanensis,* infection increased the abundance of several enzymes of the TCA cycle in THP-1 macrophages. Infection of THP-1 macrophages with either *R. conorii* **(A)** or *R. montanensis* **(B)** resulted in alterations in the abundance of several host TCA cycle enzymes at 24 hours post-infection. UniProt accession number and the respective fold change upon infection can be found in **Table V.3** for each respective enzyme. Enzymes with unchanged or increased protein levels, when compared to uninfected cells, are represented in black and red, respectively.

Two additional enzymes were found in reduced abundance under both infection conditions, isocitrate dehydrogenase 1 (IDH1, O75874) that catalyzes the oxidative decarboxylation of isocitrate to α-ketoglutarate (in the cytoplasm), and malate dehydrogenase 1 (MDH1, P40925) that

catalyzes the reversible cytoplasmic conversion of oxaloacetate to malate. ATP citrate lyase (ACLY, P53396), which catalyzes the cytosolic formation of acetyl-CoA and oxaloacetate from citrate and CoA, was found in significantly reduced abundance only in *R. montanensis*-infected cells.

The TCA cycle coupled to OXPHOS constitute a highly efficient mode for ATP generation, providing for basal subsistence in most cells types (O'Neill et al., 2016). We found that infection of THP-1 macrophages with *R. conorii*, but not with *R. montanensis*, resulted in an enrichment of several proteins of the complex III, IV, and V of the electron transport chain. More specifically, *R. conorii*-infected cells revealed an increased abundance of cytochrome C1 (CYC1, P08574), ubiquinol-cytochrome c reductase core protein 1 (UQCRC1, P31930), and ubiquinol-cytochrome c reductase core protein 2 (UQCRC2, P22695), that are members of the complex III of the electron chain transport. Moreover, members of complex IV of the electron chain transport, cytochrome c oxidase subunit 4I1 (COX4I1, P13073) and cytochrome c oxidase subunit II (COX2, P00403), together with several subunits of F-type ATPase (complex V) also accumulated in *R. conorii*-infected cells **(Table V.3)**. The observed accumulation of several TCA cycle and OXPHOS enzymes in *R. conorii*-infected macrophages suggests differences in the metabolic requirements of infected cells (and between infection conditions).

Multiple intermediates can fuel the TCA cycle. Acetyl-CoA, which is condensed with oxaloacetate to form citrate, can be converted from glucose-derived pyruvate or fatty acids through fatty acid oxidation. Moreover, glutamate is also a critical fuel for the TCA cycle through direct conversion to the intermediate α-ketoglutarate (O'Neill et al., 2016). Although host glycolytic enzymes were found in reduced abundance upon infection with *R. conorii* and *R. montanensis*, we observed significant differences between datasets in the content of proteins involved in mitochondrial pyruvate conversion as well as in lipid and glutamate metabolism **(Table V.3)**. These results suggest that alternative carbon sources may be involved in TCA cycle feeding and that these may be differentially modulated by each bacterial species. Among *R. conorii*-specific responses, we found accumulation of malic enzyme 2 (ME2, P23368), which catalyzes the oxidative decarboxylation of mitochondrial malate to pyruvate, and of proteins of the pyruvate

dehydrogenase complex which irreversibly converts pyruvate to acetyl-CoA (pyruvate dehydrogenase E1 alpha 1 subunit (PDHA1, P08559) and dihydrolipoamide dehydrogenase (DLD, P09622)) **(Figure V.6)**, suggesting the formation of mitochondrial pyruvate that may re-enter the TCA cycle by conversion to acetyl-CoA.

Moreover, several enzymes involved in fatty acid oxidation were differentially altered between infection conditions. The fatty acid oxidation pathway allows the use of fatty acids to yield large amounts of acetyl-CoA, NADH, and $FADH_2$, thereby resulting in the generation of very high amounts of ATP (Houten and Wanders, 2010; Van den Bossche et al., 2017). Our results revealed that subunits alpha and beta of the mitochondrial trifunctional protein (HADHA, P40939; HADHB, P55084) that catalyze three out of four steps in mitochondrial β-oxidation, and Δ(3,5)- Δ(2,4)-dienoyl-CoA isomerase (ECH1, Q13011) that functions in the auxiliary step of β-oxidation are enriched in *R. conorii*-infected THP-1 macrophages, but not in *R. montanensis*-infected cells **(Table V.3)**. In addition, the bifunctional enzyme, HSD17B4, also called as peroxisomal multifunctional enzyme type 2 (P51659) that acts on the peroxisomal β-oxidation also specifically accumulated in *R. conorii*-infected cells **(Table V.3)**, suggesting an increase of activity of both mitochondrial and peroxisomal β-oxidation. Overall, the accumulation of fatty acid β-oxidation enzymes in *R. conorii*-infected cells may indicate an increase of β-oxidation activity to generate acetyl-CoA from lipids, which can then be used to feed the TCA cycle to increase ATP production via OXPHOS. As noted previously, several TCA cycle and OXPHOS enzymes are indeed enriched in this dataset only. The lipid transport proteins apolipoprotein A1 (APOA1, P02647) and apolipoprotein B (APOB, P04114) were overrepresented in both *R. conorii*- and *R. montanensis*-infected cells. Apolipoproteins are reported to influence inflammatory responses, with APOA1 known to display anti-inflammatory functions (Burger and Dayer, 2002; Sirnio et al., 2017).

As previously mentioned, the TCA cycle can also use glutamate as an important anaplerotic substrate. Strikingly, glutamate dehydrogenase 1 (GLUD1, P00367) that converts glutamate into α-ketoglutarate and mitochondrial aspartate transaminase (GOT2, P00505), which generates α-ketoglutarate and aspartate from glutamate and oxaloacetate, are both enriched in *R. conorii*-infected cells only. Moreover, proteins of the α-ketoglutarate dehydrogenase complex

(dihydrolipoamide S-succinyltransferase (DLST, P36957) and dihydrolipoamide dehydrogenase (DLD, P09622)), which catalyzes the conversion of α-ketoglutarate to succinyl-CoA, were also enriched specifically in this dataset. These results point towards an active anaplerotic flux in response to *R. conorii* infection, which may contribute to balance the levels of TCA intermediates. Globally, *R. conorii* appears to positively interfere with different pathways that generate intermediates to feed the TCA cycle (mitochondrial pyruvate conversion, fatty acid oxidation, and glutamate metabolism).

Mitochondria depend on a myriad of membrane transporters and channels that are critical for importing protein precursors as well as for controlling the exchange of metabolic substrates and products required to sustain an efficient metabolism (Gutierrez-Aguilar and Baines, 2013; Palmieri, 2004). Proteins found specifically accumulated in *R. conorii*-infected cells include different types of inner and outer membrane localized transporters **(Table V.4)**.

Table V.4. Quantified host proteins categorized as mitochondrial transporters and their respective fold change in abundance upon infection of THP-1 macrophages with *R. conorii* (Rc/uninf) or *R. montanensis* (Rm/uninf). Proteins that are considered as altered (fold change ≤ 0.83 or fold change ≥ 1.2) between infected and uninfected conditions were color-coded according the following: decreased (blue), not changed (transparent) or increased (orange).

Pathway	Name	UniProt	Log_2 (Rc/uninf)	Log_2 (Rm/uninf)
Mitochondrial transporters	voltage dependent anion channel 1 (VDAC1)	P21796	0.49	-0.01
	voltage dependent anion channel 2 (VDAC2)	P45880	0.37	0.02
	voltage dependent anion channel 3 (VDAC3)	Q9Y277	0.42	0.10
	solute carrier family 25 member 1 (SLC25A1)	P53007	0.38	0.07
	solute carrier family 25 member 3 (SLC25A3)	Q00325	0.66	0.14
	solute carrier family 25 member 5 (SLC25A5)	P05141	0.52	0.24
	solute carrier family 25 member 6 (SLC25A6)	P12236	0.62	0.36
	solute carrier family 25 member 11 (SLC25A11)	Q02978	0.11	0.22
	translocase of outer mitochondrial membrane 22 (TOMM22)	Q9NS69	0.55	0.29
	translocase of outer mitochondrial membrane 40 (TOMM40)	O96008	0.32	-0.29
	mitochondrial carrier 2 (MTCH2)	Q9Y6C9	0.41	0.14

Namely, four members of solute carrier family 25 (SLC25): SCL25A1 (P53007), the citrate (tricarboxylate) carrier which transports citrate out of the mitochondria (exchange with malate); SLC25A3 (Q00325), which transports phosphate groups from the cytosol to the mitochondrial matrix (cotransport protons), and SCL25A5 (P05141) and SLC25A6 (P12236) that catalyze the exchange of ADP and ATP across the mitochondrial inner membrane; mitochondrial carrier 2 (MTCH2, Q9Y6C9) (whose transported substrate is still unknown); the outer membrane voltage-dependent anion channels VDAC1 (P21796), VDAC2 (P45880), VDAC3 (Q9Y277), which permeate different small hydrophilic molecules; and two components of the preprotein translocase complex of the outer mitochondrial membrane (TOM complex) ((TOMM22, Q9NS69) and (TOMM40, O96008)). This accumulation of different mitochondrial transporters is again suggestive of changes in metabolic supply and demand, which appear to be specifically induced by the pathogenic *R. conorii*.

V.4.3 | Differential reprogramming of host protein processing machinery by SFG *Rickettsia* species.

The proteasome is the central proteolytic complex of one of the main protein clearance mechanisms that ensures proteostasis in eukaryotic cells (the ubiquitin-proteasome system (UPS)) (Bentea et al., 2017; Vilchez et al., 2014). By maintaining the levels of many regulatory proteins and removing damaged or misfolded proteins, the UPS is involved in a variety of cellular processes, including quality control of the proteome, antigen presentation or stress responses (Bentea et al., 2017; Vilchez et al., 2014). Bacterial and viral pathogens have evolved various strategies to exploit the UPS depending on their needs (Randow and Lehner, 2009; Zhou and Zhu, 2015), and it is now known that several bacterial effectors can inhibit specific UPS steps to modulate host cell immune responses and bacterial clearance (Kim et al., 2014). We herein found that infection of THP-1 macrophages with either *R. conorii* or *R. montanensis* resulted in significant alterations in the protein content of multiple subunits of the proteasome, which were found in reduced abundance when compared to uninfected cells **(Table V.5)**.

Table V.5. Quantified host proteins categorized in proteasome and protein processing in endoplasmic reticulum and their respective fold change in abundance upon infection of THP-1 macrophages with *R. conorii* (Rc/uninf) or *R. montanensis* (Rm/uninf). Proteins that are considered as altered (fold change ≤ 0.83 or fold change ≥ 1.2) between infected and uninfected conditions were color-coded according the following: decreased (blue), not changed (transparent) or increased (orange) (cont. next pages).

Pathway	Name	UniProt	EC number	Log_2 (Rc/uninf)	Log_2 (Rm/uninf)
Proteasome	26S proteasome non-ATPase regulatory subunit 1 (PSMD1)	Q99460	-	0.04	-0.01
	26S proteasome non-ATPase regulatory subunit 2 (PSMD2)	Q13200	-	-0.12	-0.25
	26S proteasome non-ATPase regulatory subunit 3 (PSMD3)	O43242	-	0.01	0.02
	26S proteasome non-ATPase regulatory subunit 6 (PSMD6)	Q15008	-	0.07	0.06
	26S proteasome non-ATPase regulatory subunit 11 (PSMD11)	O00231	-	0.11	0.02
	26S proteasome non-ATPase regulatory subunit 12 (PSMD12)	O00232	-	0.22	0.15
	26S proteasome non-ATPase regulatory subunit 13 (PSMD13)	Q9UNM6	-	0.06	-0.21
	26S proteasome non-ATPase regulatory subunit 14 (PSMD14)	O00487	-	-0.11	-0.07
	26S proteasome regulatory subunit 4 (PSMC1)	P62191	-	0.02	-0.04
	26S proteasome regulatory subunit 7 (PSMC2)	P35998	-	-0.10	-0.23
	26S proteasome regulatory subunit 6A (PSMC3)	P17980	-	-0.25	-0.42
	26S proteasome regulatory subunit 6B (PSMC4)	P43686	-	-0.19	-0.45
	26S proteasome regulatory subunit 8 (PSMC5)	P62195	-	-0.06	-0.38
	26S proteasome regulatory subunit 10B (PSMC6)	P62333	-	-0.13	-0.30
	Proteasome subunit alpha type-1 (PSMA1)	P25786	3.4.25.1	-0.32	-0.38
	Proteasome subunit alpha type-2 (PSMA2)	P25787	3.4.25.1	-0.11	-0.09
	Proteasome subunit alpha type-3 (PSMA3)	P25788	3.4.25.1	-0.23	-0.26
	Proteasome subunit alpha type-4 (PSMA4)	P25789	3.4.25.1	-0.41	-0.52
	Proteasome subunit alpha type-5 (PSMA5)	P28066	3.4.25.1	-0.15	-0.34

	Proteasome subunit alpha type-6 (PSMA6)	P60900	3.4.25.1	-0.23	-0.29
	Proteasome subunit alpha type-7 (PSMA7)	O14818	3.4.25.1	-0.36	-0.33
	Proteasome subunit beta type-1 (PSMB1)	P20618	3.4.25.1	-0.37	-0.35
	Proteasome subunit beta type-2 (PSMB2)	P49721	3.4.25.1	-0.34	-0.34
	Proteasome subunit beta type-3 (PSMB3)	P49720	3.4.25.1	-0.35	-0.55
	Proteasome subunit beta type-6 (PSMB6)	P28072	3.4.25.1	-0.24	-0.42
	Proteasome subunit beta type-7 (PSMB7)	Q99436	3.4.25.1	-0.49	-0.43
	Proteasome subunit beta type-8 (PSMB8)	P28062	3.4.25.1	-0.01	-0.10
	Proteasome activator complex subunit 1 (PSME1)	Q06323	-	-0.42	-0.47
	Proteasome activator complex subunit 2 (PSME2)	Q9UL46	-	-0.55	-0.29
Protein processing in endoplasmic reticulum	signal sequence receptor subunit 1 (SSR1)	P43307	-	0.41	-0.05
	signal sequence receptor subunit 4 (SSR4)	P51571	-	0.49	0.19
	dolichyl-diphosphooligosaccharide--protein glycosyltransferase non-catalytic subunit (DDOST)	P39656	-	0.44	0.03
	STT3A, catalytic subunit of the oligosaccharyltransferase complex (STT3A)	P46977	2.4.99.18	0.65	0.30
	STT3B, catalytic subunit of the oligosaccharyltransferase complex (STT3B)	Q8TCJ2	2.4.99.18	0.72	0.34
	ribophorin I (RPN1)	P04843	-	0.45	0.04
	ribophorin II (RPN2)	P04844	-	0.51	0.35
	heat shock protein family A (Hsp70) member 5 (HSPA5)	P11021	-	0.57	-0.02
	Calnexin (CANX)	P27824	-	0.70	0.14
	Calreticulin (CALR)	P27797	-	0.47	0.00
	hypoxia up-regulated 1 (HYOU1)	Q9Y4L1	-	0.64	0.29
	DnaJ heat shock protein family (Hsp40) member B11 (DNAJB11)	Q9UBS4	-	0.38	-0.19
	heat shock protein family A (Hsp70) member 8 (HSPA8)	P11142	-	-0.21	-0.12

	heat shock protein 90 alpha family class A member 1 (HSP90AA1)	P07900	-	-0.21	-0.26
	heat shock protein 90 beta family member 1 (HSP90B1)	P14625	-	0.56	0.00
	heat shock protein 90 alpha family class B member 1 (HSP90AB1)	P08238	-	0.14	0.09
	heat shock protein family H (Hsp110) member 1 (HSPH1)	Q92598	-	0.34	-0.04
	protein disulfide isomerase family A member 3 (PDIA3)	P30101	5.3.4.1	0.32	0.03
	protein disulfide isomerase family A member 4 (PDIA4)	P13667	5.3.4.1	0.46	0.04
	protein disulfide isomerase family A member 6 (PDIA6)	Q15084	5.3.4.1	0.49	0.00
	UDP-glucose glycoprotein glucosyltransferase 1 (UGGT1)	Q9NYU2	2.4.1.-	0.43	0.03
	glucosidase II alpha subunit (GANAB)	Q14697	3.2.1.84	0.43	0.14
	protein kinase C substrate 80K-H (PRKCSH)	P14314	-	0.38	-0.07
	lectin, mannose binding 1 (LMAN1)	P49257	-	0.26	0.10
	lectin, mannose binding 2 (LMAN2)	Q12907	-	0.33	0.01
	SEC13 homolog, nuclear pore and COPII coat complex component (SEC13)	P55735	-	0.08	-0.06
	SEC63 homolog, protein translocation regulator (SEC63)	Q9UGP8	-	0.60	0.19
	valosin containing protein (VCP)	P55072	-	-0.06	-0.13
	eukaryotic translation initiation factor 2 subunit alpha (EIF2S1)	P05198	-	-0.17	-0.35

More specifically, from the core particle (20S) of the proteasome, out of the 7 α-subunits that are involved in the formation of the two outer rings 3 were found in lower abundance in the *R. conorii* dataset (subunits α1 (P25786), α4 (P25789), and α7 (O14818)) and 5 in the *R. montanensis* dataset (subunits α1 (P25786), α4 (P25789), α5 (P28066), α6 (P60900) and α7 (O14818)). From the outer ring (subunits β1-β7), we observed the underrepresentation of subunits β1 (P20618), β2

(P49721), β3 (P49720) and β7 (Q99436) in both *R. conorii* and *R. montanensis*-infected cells, with the subunit β6 (P28072) found additionally reduced in the latter. Also, *R. montanensis* infection resulted in a specific underrepresentation of 4 (PSMC3 (P17980), PSMC4 (P43686), PSMC5 (P62195) and PSMC6 (P62333)) out of the 6 AAA-ATPases that are part of the base of the 19S regulatory particle.

A modified type of proteasome called the immunoproteasome is responsible for generating antigen peptides with substantial binding affinity for the major histocompatibility complex I (MHC I) (Kaur and Batra, 2016). The immunoproteasome contains an alternate regulator, known as the PA28 (or 11S), which replaces the 19S regulatory particle and can also activate the core particle. Remarkably, both PA28α (Q06323) and PA28β (Q9UL46) - the α and β immune subunits of the activator PA28 - were found in reduced abundance in THP-1 macrophages infected with *R. conorii* and *R. montanensis*. Overall, these results show a significant interference of both rickettsial species with a key regulatory proteolytic machinery, with potential impact in several cellular processes through impaired proteasome activity.

Any condition that decreases proteasome function may result in the accumulation of misfolded proteins within the endoplasmic reticulum (ER), leading to a state known as “ER stress” (Hetz and Papa, 2018). Given the importance of ER-quality control and ER-associated degradation processes for maintaining cellular homeostasis, the cell responds to ER stress with the activation of elaborate compensatory signals to restore ER homeostasis and to ensure cell survival, a process collectively known as ER stress response or unfolded protein response (UPR) (Martins et al., 2016). Several examples provide evidence that bacterial infections provoke ER stress by a wide range of cellular perturbations (Lin et al., 2008; Shin and Argon, 2015) However, different successful intracellular pathogens are known to interfere with ER stress signaling and to restore ER homeostasis, thereby promoting their survival and replication (Celli and Tsolis, 2015; Galluzzi et al., 2017). In this work, we found significant differences in several proteins clustering with protein processing and quality control in ER between infection conditions **(Table V.5)**. More specifically, *R. conorii* infection led to the accumulation of i) proteins associated with translocation across ER membrane (signal sequence receptor subunits 1 (SSR1, P43307) and 4 (SSR4, P51571)); ii) of

several subunits of the N-oligosaccharyl transferase (OST) complex (dolichyl-diphosphooligosaccharide-protein glycosyltransferase non catalytic subunit (DDOST, P39656), OST catalytic subunits STT3A (P46977) and STT3B (Q8TCJ2), ribophorin I (P04843) and ribophorin II (P04844)); iii) as well as of several proteins comprising chaperone activity, such as BiP (P11021), calnexin (P27824), calreticulin (P27797), hypoxia up-regulated 1 (Q9Y3L1), endoplasmin (P14625), and DnaJ Heat Shock Protein Family (Hsp40) Member B11 (Q9UBS4). In addition, several protein disulfide isomerases (PDI), such as PDI family A members 3, 4 and 6 (P30101, P13667, Q15084, respectively) were also found in higher abundance in *R. conorii*-infected cells. The same accumulation pattern was observed for the protein folding sensor UDP-glucose:glycoprotein glucosyltransferase 1 (Q9NYU2), that recognizes glycoproteins with minor folding defects and reglucosylates them, and glucosidase II alpha subunit (Q14697), another glycan modification enzyme implicated in protein quality control in the ER. In *R. montanensis*-infected cells, with the exception of STT3A (P46977), STT3B (Q8TCJ2), ribophorin II (P04844), HYOU1 (Q9Y4L1), and the eukaryotic translation initiation factor 2 subunit alpha (EIF2S1, P05198) (the latter found in reduced abundance), no significant alterations in abundance were found in the other quantified proteins.

Therefore, this differential accumulation of various proteins involved in protein folding and quality control in the ER anticipates significant differences between bacterial species in their ability to counterbalance ER stress.

V.5 | Discussion

There is growing evidence that the eradication or survival of intracellular bacterial pathogens within macrophages (as well as other immune cells) depend on complex metabolic adaptation programs. The metabolic plasticity of macrophages plays a key role not only in the initiation of the host-cell defense programs aimed to eliminate the invading pathogen (part of a global immune response termed “immunometabolism”), but also in the complex metabolic adaptation reactions that need to take place in both interacting partners for the successful intracellular replication of pathogens (concept recently coined as “pathometabolism”) (Eisenreich et al., 2015; Eisenreich et al., 2017; O'Neill and Pearce, 2016; Van den Bossche et al., 2017). More in-depth knowledge about these mutual metabolic adaptations is growing for different intracellular bacteria (Eisenreich et al., 2017; Xavier et al., 2013). However, for rickettsial species the current state of knowledge on these processes is yet rather poor. In this work, we provide evidence that two rickettsial species with different pathogenicity attributes, and opposite tropisms for macrophages, induce differential changes in proteins associated with key metabolic pathways in these cells. Although both *R. conorii* and *R. montanensis*-infection resulted in a lower accumulation of several enzymes of glycolysis and PPP in THP-1 macrophages, the differences in abundance observed in enzymes involved in TCA cycle, OXPHOS, fatty acid oxidation, glutamate metabolism as well as in different mitochondrial transporters, suggest a significant metabolic reprogramming of macrophages specifically induced by the pathogenic *R. conorii*.

Changes in metabolic pathways are known to regulate macrophage activation states and functions. The best studied are likely the two polarized M1 (pro-inflammatory bactericidal) and M2 (anti-inflammatory) subtypes, characterized by different metabolic signatures (Eisenreich et al., 2017). Two metabolic hallmarks of inflammatory M1-like macrophages are increased glycolysis and elevated activity of the PPP. The induction of glycolysis supports pro-inflammatory functions in different ways, including the production of ATP to sustain phagocytic functions as well as feeding of the PPP for nucleotide and protein synthesis, and generation of ROS by NADPH oxidase. Interestingly, our results suggest a decrease in activity of host glycolysis and reduction in PPP in response to both *R. conorii* and *R. montanensis* at this stage of infection (24 hpi).

Moreover, among the glycolytic enzymes underrepresented in both conditions were GAPDH, ENO1, and PKM, which have been recently demonstrated to promote pro-inflammatory macrophage functions through moonlighting activity (Van den Bossche et al., 2017). A similar downregulation in glycolytic enzymes at early stages of infection has also been observed in *Trypanosoma cruzi*- and HIV-1-infected cells, suggesting a decrease in energy production from glucose at this stage of infection (Li et al., 2016; Ringrose et al., 2008). Interestingly, our transcriptomic data of *R. conorii*-infected THP-1 macrophages also revealed that RRAD (Ras-related glycolysis inhibitor and calcium channel regulator), belongs to one of the most upregulated genes at 1 hour post-infection (unpublished results), which further supports the idea of a reduction in host glycolytic activity at an early stage of infection of THP-1 cells with *R. conorii*. Thus, shutdown in host glycolytic and PPP activities early in infection should be further addressed as a possible mechanism of *Rickettsia* to evade macrophage pro-inflammatory responses.

The metabolic characteristics of the TCA cycle and OXPHOS are also distinct between M1 and M2-like phenotypes. An intact TCA cycle and enhanced OXPHOS characterize M2 macrophages, whereas in inflammatory macrophages the TCA cycle has been shown to be broken in two places and OXPHOS impaired (Van den Bossche et al., 2017). These breaks in the TCA cycle - after citrate due to a decrease in expression of isocitrate dehydrogenase 1 (IDH1) and after succinate - lead to accumulation of citrate to meet the biosynthetic demands of inflammatory macrophages (synthesis of fatty acids, lipids, and prostaglandins) and succinate (an inflammatory signal that stabilizes hypoxia-inducible factor 1 alpha (HIF1α), thereby promoting LPS-induced expression of IL-1α) (Van den Bossche et al., 2017). Remarkably, we also observed a reduction in abundance of host IDH1 upon infection with both species, suggestive of a possible impact on citrate accumulation as described for M1-like macrophages. Since succinate dehydrogenase was not quantified in our dataset, it is not possible to infer the presence or absence of the second break in the TCA cycle at this point. However, the observed accumulation of several TCA cycle and OXPHOS enzymes in *R. conorii*-infected macrophages differ from the typical hallmarks of the bactericidal M1 phenotype, showing instead higher resemblance of these cells with an M2-like phenotype (in contrast to *R. montanensis*-infected cells). Indeed, M2 macrophages obtain much of

their energy from fatty acid oxidation and oxidative metabolism, with a massive induction of an oxidative metabolic program, ranging from fatty acid uptake and oxidation to oxidative phosphorylation and mitochondrial respiration (Mills and O'Neill, 2016). Interestingly, higher accumulation of several fatty acid oxidation enzymes was observed in *R. conorii*-infected cells only, which is again suggestive that this pathogenic SFG *Rickettsia* specifically induces a reprogramming towards an M2-like phenotype. The impact of host cell lipid metabolism during infection has been already studied for several intracellular pathogens (Jordan and Randall, 2017; Shehata et al., 2017). One of the better-documented examples is the ability of dengue virus to promote its replication by inducing lipophagy, a selective autophagy that targets lipid droplets, which further enhances fatty-acid β-oxidation and subsequent viral replication (Jordan and Randall, 2017).

Furthermore, recent findings suggest that α-ketoglutarate produced via glutaminolysis - which enters the TCA cycle to replenish TCA cycle intermediates - is also an anti-inflammatory metabolite that orchestrates M2 activation of macrophages through different reprogramming processes (Liu et al., 2017). The herein observed accumulation of the enzymes GOT2 and GLUD1 in *R. conorii*-infected cells, also suggests the possible use of glutamate to fuel the TCA cycle through conversion into α-ketoglutarate (glutamine is available in RPMI culture medium), further strengthening a more anti-inflammatory M2-like activation program promoted by *R. conorii*.

Recent studies with different intracellular pathogens have indeed demonstrated that the metabolic conditions of M2-like macrophages represent a more favorable replication niche than the inflammatory M1 phenotype (Eisenreich et al., 2017; Price and Vance, 2014). In line with these observations, our results suggest that differences in host cell metabolism promoted by infection with each rickettsial species may indeed reflect differential macrophage activation modes that either favor (*R. conorii*) or restrict (*R. montanensis*) intracellular bacterial proliferation. A summary of the main differences in protein content of metabolic pathway components observed between infection conditions, and potential impact on metabolic fluxes, are illustrated in **Figure V.8**. Overall, our results with *R. conorii* point towards a shift away from glycolysis but with an apparently higher metabolic flux directed to the TCA cycle through other metabolic pathways that are known to fuel this cycle (fatty acid oxidation and glutaminolysis).

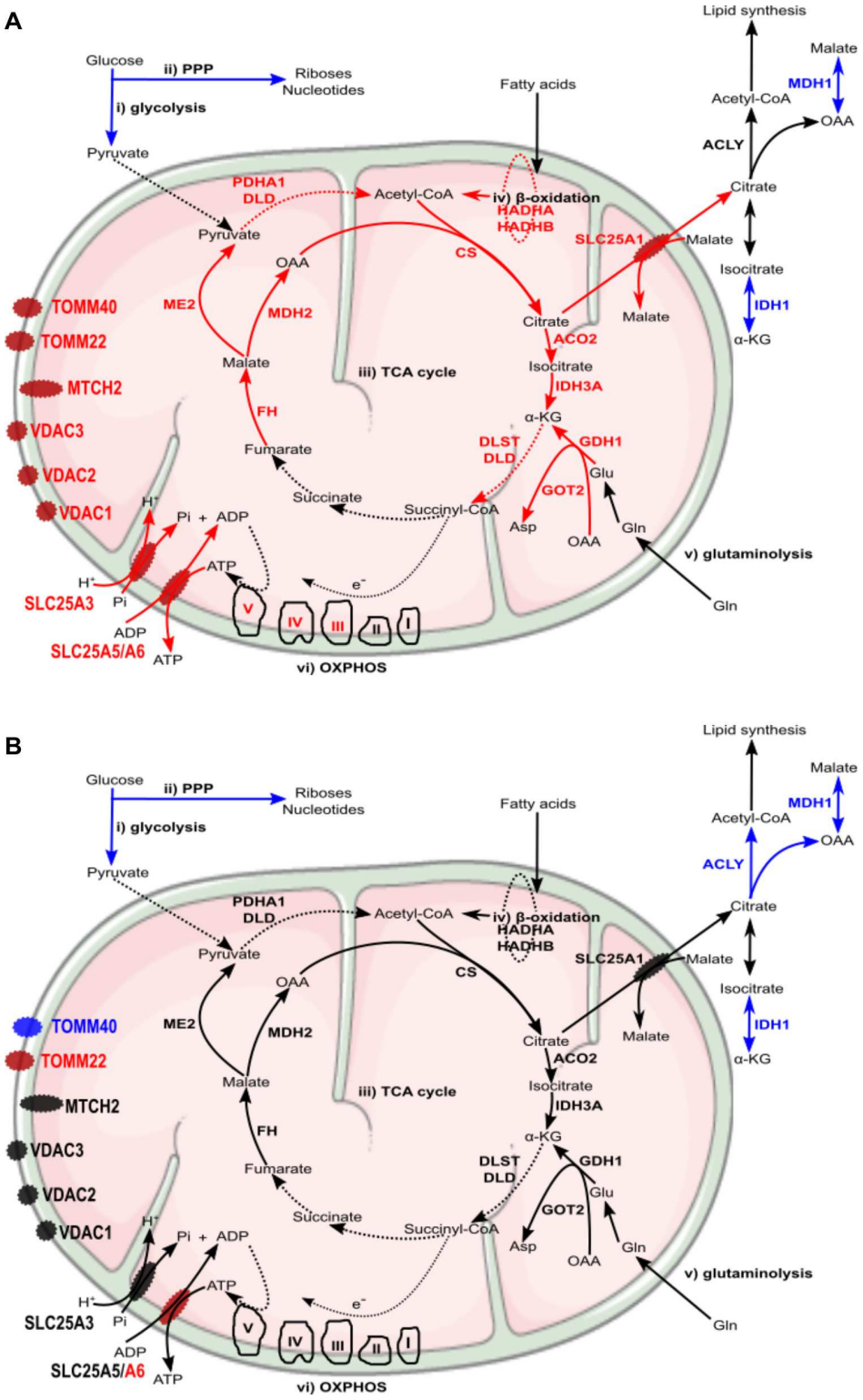
A
Lipid synthesis
Malate
MDH1
Acetyl-CoA
OAA
ACLY
Glucose
ii) PPP
Riboses
Nucleotides
i) glycolysis
Fatty acids
Pyruvate
PDHA1
DLD
Acetyl-CoA
iv) β-oxidation
HADHA
HADHB
Citrate
Pyruvate
SLC25A1
Malate
CS
Isocitrate
IDH1
α-KG
TOMM40
TOMM22
MTCH2
VDAC3
VDAC2
VDAC1
ME2
MDH2
OAA
Citrate
ACO2
Malate
iii) TCA cycle
Isocitrate
IDH3A
FH
α-KG
Fumarate
DLST
DLD
GDH1
Glu
GOT2
Succinate
Succinyl-CoA
Asp
OAA
Gln
v) glutaminolysis
H+
Pi + ADP
ATP
H+
SLC25A3
Pi
ADP
SLC25A5/A6
ATP
e-
V
IV
III
II
I
vi) OXPHOS
Gln
B
Lipid synthesis
Malate
MDH1
Acetyl-CoA
OAA
ACLY
Glucose
ii) PPP
Riboses
Nucleotides
i) glycolysis
Fatty acids
Pyruvate
PDHA1
DLD
Acetyl-CoA
iv) β-oxidation
HADHA
HADHB
Citrate
Pyruvate
SLC25A1
Malate
CS
Isocitrate
IDH1
α-KG
TOMM40
TOMM22
MTCH2
VDAC3
VDAC2
VDAC1
ME2
MDH2
OAA
Citrate
ACO2
Malate
iii) TCA cycle
Isocitrate
IDH3A
FH
α-KG
Fumarate
DLST
DLD
GDH1
Glu
GOT2
Succinate
Succinyl-CoA
Asp
OAA
Gln
v) glutaminolysis
H+
Pi + ADP
ATP
H+
SLC25A3
Pi
ADP
SLC25A5/A6
ATP
e-
V
IV
III
II
I
vi) OXPHOS
Gln

Figure V.8 (previous page) | *R. conorii* and *R. montanensis* trigger a differential metabolic signature in THP-1 macrophages. (A-B) Prediction model of alterations in host cell metabolism, based on changes in the abundance of host proteins induced by infection of THP-1 macrophages with *R. conorii* **(A)** or *R. montanensis* **(B)**. Increase/decrease in the abundance of host enzymes are predicted to contribute with increase/decrease in activity for the respective biological enzymatic activity and are represented in red and blue, respectively. Enzymes quantified in our analysis but with no alteration in abundance upon infection are represented in black **(A)** In *R. conorii*-infected THP-1 macrophages, glycolysis (i) and pentose phosphate pathway (ii) are predicted to be reduced at 24 hours post-infection. This may impact pyruvate production from glycolysis as well as production of riboses, nucleotides and ROS from PPP, globally contributing to reduce pro-inflammatory signals. Several TCA cycle enzymes (iii) were found overrepresented upon infection, suggesting an increase in TCA cycle activity. Acetyl-CoA production from fatty-acid β-oxidation (iv) and glutamine anaplerosis (v) may contribute to replenish the TCA cycle which may result in a sustained ATP production via oxidative phosphorylation (vi). Accumulation of several inner and outer membrane transporters is suggestive of a metabolic configuration with higher needs in metabolic supply and demand. **(B)** In *R. montanensis*-infected THP-1 macrophages, pyruvate production from glycolysis (i) is also predicted to be reduced at this time of infection. However, in contrast with *R. conorii*, unchanged levels of enzymes of the TCA cycle (iii), fatty-acid β-oxidation (iv), glutaminolysis (v) and proteins from the respiratory complex (vi) found in *R. montanensis*-infected cells, together with no alterations observed in most of the quantified mitochondrial transporters, suggests very distinct metabolic requirements between infection conditions. (see **Table V.3** and **Table V.4** for details).

This might be used to increase TCA cycle activity augmenting the levels of NADH, GTP, and $FADH_2$, which could be further used in cellular respiration steps to produce ATP, and/or to replenish the TCA cycle to compensate for diversion of metabolites (e.g., citrate) to other metabolic pathways. In fact, among mitochondrial transporters found in higher abundance in *R. conorii*-infected cells were SLC25A3 and SCL25A5/SLC25A which are important for ADP phosphorylation and ADP/ATP translocation between the mitochondria and the cytosol, SLC25A1 which transports citrate out of the mitochondria, and VDAC1, VDAC2 and VDAC3 that control the flux of various metabolites and ions through the mitochondrial outer membrane.

These metabolic adaptations may not only help to counteract host defense mechanisms, promoting a more comfortable replication niche but may also reflect the complex interconnection with the metabolic and energetic requirements of *R. conorii* itself. Reductive genome evolution has resulted in the loss of many metabolic pathways, which culminates with *Rickettsia* species being strictly dependent on host metabolites to survive and proliferate (Darby et al., 2007). *Rickettsia* display a limited oxidative metabolism. Both glycolysis/gluconeogenesis and PPP enzymatic activities are undetectable although there is evidence of a functional pyruvate dehydrogenase complex and TCA cycle (Coolbaugh et al., 1976; Driscoll et al., 2017; Phibbs and Winkler, 1982;

Renesto et al., 2005; Winkler and Daugherty, 1986). Together with other cofactors, several metabolites have been shown (glutamate, glutamine, serine, glycine) and predicted (malate, pyruvate, α-ketoglutarate) to be imported from the host to fuel the TCA cycle, which in turn feeds the pathways responsible for peptidoglycan synthesis (the TCA-cycle intermediate aspartate, essential for biosynthesis of peptidoglycan precursors, is also predicted to be imported) and for ATP generation (OXPHOS) (Driscoll et al., 2017). In addition, *Rickettsia* is also able to import ATP from the host via an ATP/ADP symporter, and it has been suggested that this dual mechanism for energy supply may reflect the adaptation of *Rickettsia* to the metabolic activity of the host cell (Driscoll et al., 2017; Eisenreich et al., 2013). Interestingly, *R. conorii*-induced host metabolic configuration anticipated in this work **(Figure V.8)** appear to favor the generation of several metabolites also required by *Rickettsia*, such as glutamate, pyruvate, malate, α-ketoglutarate, and aspartate. Moreover, fueling the TCA cycle through fatty acid oxidation can allow the production of very high amounts of ATP by the host, which may also be imported by *R. conorii*. Therefore, promoting the adaptation of host metabolic pathways towards the generation of the carbon substrates and energy required for bacterial proliferation (also needed for sustaining host survival) might be one of the strategies used by *R. conorii* to reduce the metabolic burden put on the host cell by an intracellular pathogen so heavily dependent on host metabolism (Driscoll et al., 2017). Curiously, mitochondrial porins (VDAC), which have been hypothesized to be hijacked by *Rickettsia* to be used as transport systems (Emelyanov, 2009; Emelyanov and Vyssokikh, 2006), were found in higher abundance in *R. conorii*-infected cells, urging for further studies exploring their potential incorporation in rickettsial cells during infection. Understanding rickettsial-host (macrophage) metabolic interconnections and which/how bacterial effectors and transporters control these complex adaptation processes emerge has an exciting area for future research.

The exploitation of the UPS by different pathogens to modulate diverse host cellular responses, such as immune responses, cell death or pathogen clearance has been demonstrated (Kim et al., 2014). However, in the case of bacterial pathogens, this modulation has been mainly associated with interference of ubiquitination/deubiquitination steps by different strategies (Kim et al., 2014). Strikingly, our results show that infection of THP-1 macrophages with both *R. conorii*

and *R. montanensis* have a dramatic impact on the proteasome, with several of the subunits forming this proteolytic machinery found in reduced abundance in infected cells. Among affected subunits, we found several elements of the 20S core particle, including subunits β1 and β2 which display caspase-like and trypsin-like proteolytic activities (Vilchez et al., 2014), as well as both subunits of the proteasome activator complex PA28, important for assembly of the immunoproteasome (McCarthy and Weinberg, 2015). Moreover, several subunits of the 19S regulatory cap were also significantly underrepresented in the *R. montanensis* dataset. The decreased abundance of all these components suggests an impairment of proteasome activity at this time post-infection. To our knowledge, this is the first time the proteasome itself is shown to be affected as a result of a bacterial infection. This raises exciting questions on how and why *Rickettsia* modulate host proteasome function since this likely interferes with different cellular processes. Interestingly, many viruses have mechanisms of interfering with proteasome function by preventing transcriptional upregulation or by direct interaction of viral proteins with immunoproteasome subunits (McCarthy and Weinberg, 2015). In these viral infections, downregulation of immunoproteasome activity has been suggested as a mechanism to reduce the generation of viral peptide antigens to be presented on the MHC class I complex, and thereby avoid host immune surveillance (McCarthy and Weinberg, 2015). Rickettsial antigens can be presented by both MHC class I and MHC class II pathways (Fang et al., 2007; Osterloh, 2017). The herein observed effect on different proteasome and proteasome activator (PA28) subunits, raise the exciting possibility that rickettsial species may also exploit this proteolytic machinery as a sophisticated strategy to decrease antigen peptide generation, decreasing/inhibiting antigen presentation in macrophages. Therefore, the molecular mechanisms underlying this interference with the proteasome and its impact on the regulation of immune responses (and possible contribution to rickettsial evasion of immune surveillance) should be further investigated. As mentioned, impairment of proteasome function may have other implications (Bentea et al., 2017; Ferrington and Gregerson, 2012; Kaur and Batra, 2016). It has been demonstrated that pharmacologic inhibition of the proteasome in macrophages leads to a dysregulation in inflammatory signaling, resulting in a conversion to an anti-inflammatory phenotype (Cuschieri et al., 2004). Although the interference with proteasome

components appears to be a response induced by both rickettsial species, regardless of pathogenicity, we cannot exclude that the potential impact of proteasome dysfunction on the production of inflammatory mediators may also positively contribute to establish a more favorable niche for *R. conorii* survival, combined with the observed changes in cellular metabolism.

An impact in proteasome function is also likely to induce ER stress through the accumulation of unfolded proteins (Thibaudeau et al., 2018; VerPlank et al., 2018). Moreover, a wide range of other cellular perturbations induced by infection, such as nutrient depletion, disruption of the secretory pathway, the accumulation of ROS or increase of free fatty acids, may also result in perturbations in ER homeostasis (Galluzzi et al., 2017). Remarkably, another noticeable difference between *R. conorii* and *R. montanensis*-infected macrophages was the observed *R. conorii*-specific accumulation of various components of the ER quality control machinery. This included proteins associated with translocation across the ER membrane, as well as several proteins related to protein folding and quality control check (several glycosyltransferases, disulfide isomerases, classical and non-classical chaperones, as well as glycan modification enzymes). These results are suggestive of a host response to counteract ER stress, which appears to be specifically triggered by the pathogenic *Rickettsia* only. Indeed, increasing the ER protein folding capacity has been shown as one of the compensatory mechanisms of the UPR to re-establish ER homeostasis (Hetz and Papa, 2018; Janssens et al., 2014; Martins et al., 2016). Whether this impact in ER-quality control machinery (and in the UPR as a whole) is being actively manipulated by *R. conorii* or is an indirect response to other cellular effects remains to be elucidated. However, the differential accumulation patterns in ER proteins observed in *R. conorii* and *R. montanensis* infection datasets, strongly suggests that *R. conorii* may have the ability to manipulate ER stress signaling to its benefit, as demonstrated for other successful intracellular pathogens (Celli and Tsolis, 2015; Galluzzi et al., 2017). Main differences in proteasome and ER protein abundance observed in this work, and possible responses associated with these changes, are summarized in **Figure V.9**. A reduced representation of proteasome subunits, found under both infection conditions, may interfere with *Rickettsia* antigen presentation by MHC class I and recognition by the immune system.

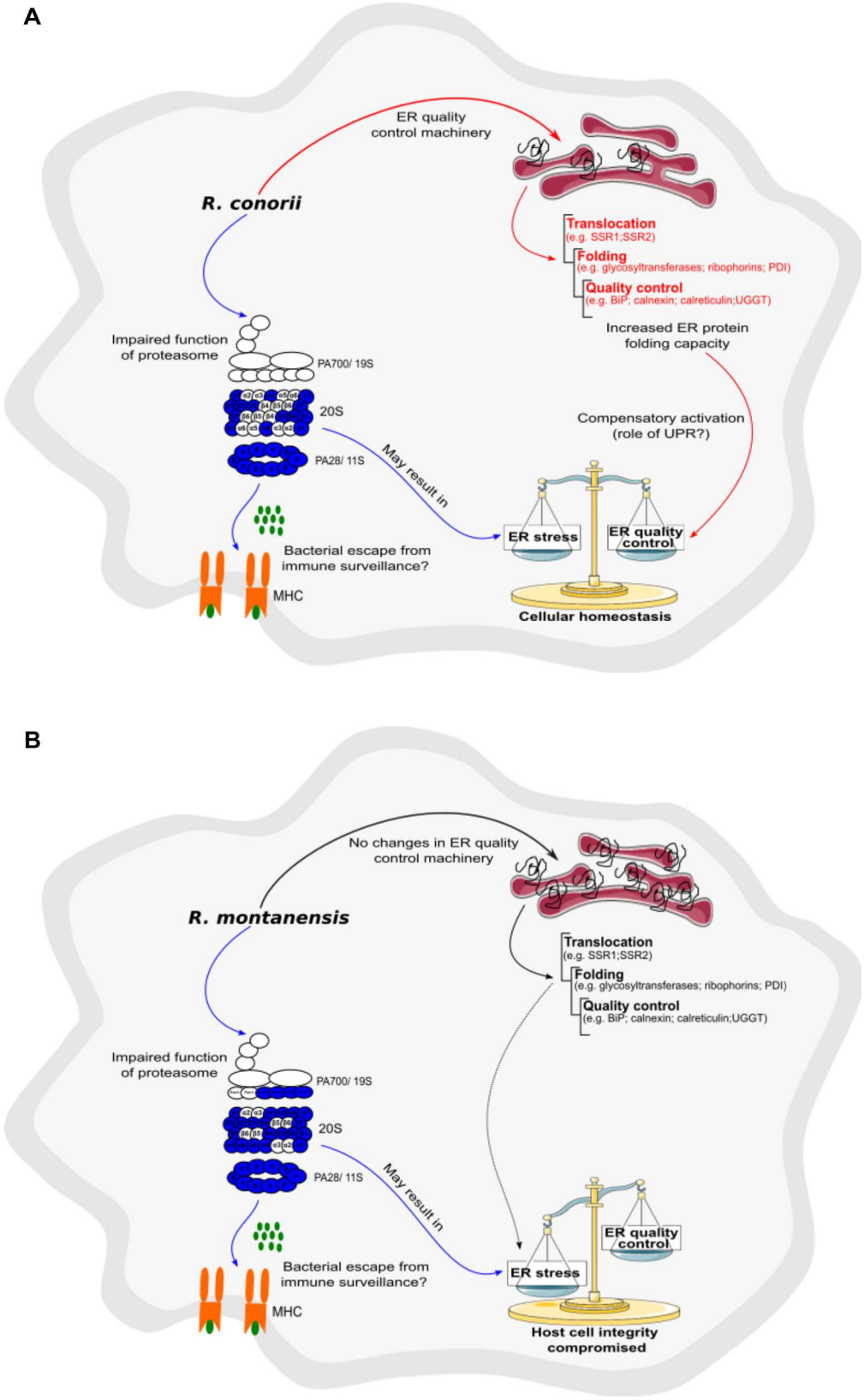
A
ER quality
control machinery
R. conorii
Translocation
(e.g. SSR1;SSR2)
Folding
(e.g. glycosyltransferases; ribophorins; PDI)
Quality control
(e.g. BiP; calnexin; calreticulin;UGGT)
Increased ER protein
folding capacity
Impaired function
of proteasome
PA700/ 19S
20S
PA28/ 11S
May result in
Compensatory activation
(role of UPR?)
ER stress
ER quality
control
Bacterial escape from
immune surveillance?
MHC
Cellular homeostasis
B
No changes in ER quality
control machinery
R. montanensis
Translocation
(e.g. SSR1;SSR2)
Folding
(e.g. glycosyltransferases; ribophorins; PDI)
Quality control
(e.g. BiP; calnexin; calreticulin;UGGT)
Impaired function
of proteasome
PA700/ 19S
20S
PA28/ 11S
May result in
ER quality
control
ER stress
Bacterial escape from
immune surveillance?
MHC
Host cell integrity
compromised

Figure V.9 (previous page) | *R. conorii*, but not *R. montanensis*, may be able to restore host cell homeostasis by increasing ER folding capacity. (A-B) Prediction model of alterations in proteasome and protein processing in endoplasmic reticulum activity, based on changes in the abundance of host proteins, that are induced by the infection of THP-1 macrophages with *R. conorii* **(A)** or *R. montanensis* **(B)**. Increase/decrease in the abundance of host enzymes are predicted to contribute with increase/decrease in activity and are represented in red and blue, respectively. Increase, no alteration, or decrease in the abundance of host enzymes are predicted to contribute with increase, unchanged or decrease activity for the respective biological function and are represented in red, black and blue arrows, respectively. **(A)** In *R. conorii*-infected THP-1 macrophages, several proteasome and immunoproteasome activator subunits are underrepresented at 24 hours post-infection, which may lead to a decrease in antigen peptide generation, and subsequent decrease in antigen presentation by MHC complex Type I, and bacterial evasion from immune system surveillance. Decrease in proteasome activity may lead to an accumulation of misfolded proteins in ER, inducing ER stress. However, *R. conorii* specifically increases the abundance of several ER proteins involved protein translocation, folding and quality control, which may be a compensatory mechanism activated by the UPR. **(B)** In *R. montanensis*-infected THP-1 macrophages, several proteasome and immunoproteasome activator subunits are also underrepresented at 24 hours post-infection, which may lead to a decrease in antigen peptide generation (ii), and subsequent antigen presentation by MHC class I and bacteria evasion from immune system surveillance. Decrease in proteasome activity may lead to an accumulation of misfolded proteins and induction of ER stress. However, in contrast with *R. conorii, R. montanensis* infection did not result in increased levels of ER quality control components, likely resulting in the inability of *R. montanensis* to restore host cell homeostasis. (see **Table V.5** for details).

However, this possible impairment of proteasome function may trigger ER stress through an accumulation of misfolded proteins in the lumen of the ER. While *R. montanensis* promoted no significant changes in host ER proteins, *R. conorii* induced a positive modulation of the ER folding capacity, likely contributing to re-establish ER homeostasis. This may help to restore cellular homeostasis and maintain host cell integrity for pathogen replication. Therefore, the ability (or lack thereof) to restore ER homeostasis may be another critical feature to help defining macrophage-tropic vs. non-tropic interactions during rickettsial infections.

The proteomic profiles herein presented contribute significant insights towards a more in-depth understanding on the modulation of THP-1 macrophage responses upon infection with two rickettsial species that show different intracellular fates in these cells (Curto et al., 2016). Our results evidenced a substantial metabolic reprogramming as well as a modulation of ER folding capacity, specifically induced by the pathogen *R. conorii*. Globally, this helps to unfold the intricate pattern of modulation triggered by a pathogenic *Rickettsia* to control macrophage homeostasis and to maintain a viable intracellular niche. By illuminating the still very poorly studied aspects of macrophage-*Rickettsia* interactions - like metabolic adaptation, the UPR or proteasome dysfunction - our work provides an important framework for future investigations that are likely to

lead to an improved understanding of the link between these mechanisms and rickettsial pathogenicity.

V.6 | Acknowledgements

We would like to acknowledge Dr. Kevin Macaluso (LSU SVM Department of Pathobiological Sciences) for providing *R. montanensis* isolate M5/6. We would like to thank Abigail Fish, Daniel Garza and Sean Riley for helpful suggestions in completion of this study.

Chapter VI

General discussion and conclusions

VI | General discussion and conclusions

Although endothelial cells have long been considered the main target cells for rickettsiae, several studies provided evidence of non-endothelial parasitism in rickettsial infections, suggesting that cells other than the endothelium may play a role during rickettsioses (Banajee et al., 2015; Osterloh et al., 2016; Riley et al., 2016; Walker and Ismail, 2008). It is now becoming evident that the role employed by cells of the immune system during rickettsioses may be an underappreciated aspect of rickettsial biology. A distinctive feature of successful intracellular bacterial pathogens is the ability to escape macrophage immune defenses and establish a replicative niche inside phagocytic cells, raising the so-called “macrophage paradox” (Price and Vance, 2014). Over 40 years ago, it was shown that two TG *Rickettsia* strains have distinct abilities to proliferate in macrophage cell cultures (Gambrill and Wisseman, 1973b). The virulent *R. prowazekii* Breinl strain can replicate within macrophages, whereas the attenuated E strain of *R. prowazekii* does not share the same capacity (Gambrill and Wisseman, 1973b). However, this evidence remained unexplored by the scientific community over the years, and the molecular attributes that distinguish pathogenic and non-pathogenic rickettsial species remained elusive.

We have herein demonstrated that two members of SFG *Rickettsia* with different pathogenicity attributes, the pathogenic (*R. conorii*) and the non-pathogenic (*R. montanensis*), have entirely distinct intracellular fates within macrophage-like cells (Curto et al., 2016) (Chapter II). Again, the pathogenic was able to survive and proliferate, whereas the non-pathogenic was rapidly destroyed. These results raise an enormous amount of exciting questions, including the hypothesis that the ability to proliferate within macrophages can determine pathogenicity in rickettsial species. Indeed, a survey study to determine if there is a correlation between macrophage intracellular fate and rickettsial pathogenicity is now under investigation (Juan J. Martinez (LSU), personal communication: “Understanding the significance of the interactions between spotted fever group *Rickettsia* and mammalian phagocytic cells”, ASR 2018). Moreover, if this phenotype holds true, it raises essential questions about the role of macrophages during rickettsial diseases, suggesting that macrophages may be a central player in the development of

rickettsial infections in humans. Indeed, a recent study demonstrated that OmpB-deficient *R. parkeri,* which can proliferate in endothelial cells but not in wild-type macrophages, was unable to colonize the organs of C57BL/6 (Patrik Engstrom (UC Berkeley), personal communication: "Outer membrane protein B enables *Rickettsia parkeri* to evade antibacterial autophagy", ASR 2018). These results strengthen the potential role of macrophages as critical players in the establishment of rickettsial infections. Interestingly, it has also been demonstrated that high numbers of $CD11b^{+}$ macrophages harboring intact *R. typhi* (that can be recultivated months after infection) are detectable in the brain of C57BL/6 $RAG1^{-/-}$ mice, suggesting that the ability to evade macrophage killing by rickettsial species may serve as a mechanism to spread the infection throughout the body (Osterloh et al., 2016). In fact, and although it is still not completely understood, the hypothesis that these cells may act as shuttles of *R. typhi* into the central nervous system (CNS) has been raised (Osterloh et al., 2016). Therefore, the hypothesis that a successful infection within macrophages may serve to disseminate bacteria throughout the body, thereby contributing to the development of disseminated rickettsial infection, should be promptly addressed.

An essential early event in the life cycle of intracellular pathogens is the entry process into host cells. We demonstrated that *R. conorii* and *R. montanensis* display differences in the ability to bind to THP-1 cells, suggesting the possible use of alternative routes of entry into macrophages. Supported by these findings, we have next employed an inhibitor-based screening to assess the contribution of several host proteins for the entry mechanism of both rickettsial species into THP-1 macrophages (Chapter III). Interestingly, we have determined an unrecognized sensitivity of *R. conorii* entry process into macrophage-like cells to amiloride compounds such as DMA, EIPA and zoniporide, key hallmarks of macropinocytosis. Together, our results suggest that *R. conorii* uses a novel PAK-NHE-TK-dependent macropinocytosis-like mechanism to invade macrophage-like cells. Moreover, our results have shown a differential contribution of host proteins for the entry process of *R. conorii* and *R. montanensis* into macrophage-like cells, suggesting that the route of entry may be one of the factors contributing for rickettsiae tropism in macrophages. Thus, more studies should be carried out to dissect in more detail the entry mechanisms that govern rickettsiae-

macrophage interactions. Interestingly, a complexity of signaling mechanisms underpinning cell entry has been observed for other pathogenic bacteria, being now known that internalization of bacterial pathogens progresses by multiple and potentially redundant routes (Velge et al., 2012). Indeed, contrarily to what was initially thought, it has recently been shown that *Salmonella* can use various invasion pathways mediated by either the trigger or the zipper entry process (Boumart et al., 2014; Velge et al., 2012). Also, the ability to use facets of both zipper and trigger mechanisms has been reported for *Chlamydia trachomatis*, being suggested that *Chlamydia* exploits filopodial capture and a macropinocytosis-like pathway for host cell entry (Ford et al., 2018). Interestingly, the routes of entry used by different bacterial species have been correlated with the subsequent intracellular lifestyle, fate, and pathogenicity. For *Salmonella*, it has been reported that the route of entry employed by different serovars (and in different host cells) are correlated with different intracellular behaviors and pathogenicity (Boumart et al., 2014). Differences in the interplay between distinct forms of *Coxiella* (with different virulent properties) and host cell proteins have also been shown to affect internalization rates of the bacteria, and pathogenicity attributes (Abnave et al., 2017; Cockrell et al., 2017). In this case, among the several virulence factors, the lipopolysaccharide (LPS) of *C. burnetti* (avirulent harbors a truncated form of LPS) has been described as one of the major factors contributing for the invasion process and the subsequent ability to hijack immune defenses (Abnave et al., 2017). Therefore, it will be important to understand if differences in bacterial virulence factors such as LPS composition and/or surface antigen proteins may support the distinct requirement of host proteins for the entry process of SFG *Rickettsia* in macrophage-like cells as well as the subsequent intracellular fate. Indeed, evidence demonstrating the role of the rickettsial antigen-surface protein OmpB in the ability of *R. parkeri* to evade autophagy and subsequent killing by macrophages has recently been provided, strengthening the role of rOmpB as a key virulent factor during rickettsial diseases (Patrik Engstrom, “Outer membrane protein B enables *Rickettsia* parkeri to evade antibacterial autophagy”, ASR 2018). Although the amino acid sequence alignment of rOmpB from *R. conorii* (RC1085), *R. montanensis* (MCI_02705) and *R. parkeri* (MC1_06065) results in high percentage of similarity (around 88%),

the ability (or lack thereof) of rOmpB to mediate *R. conorii* and *R. montanensis* autophagy evasion in macrophages should be further addressed.

Successful intracellular pathogens have evolved sophisticated strategies to modulate host signaling pathways not only to subvert host defenses but also to modify the host cell intracellular environment in conditions more favorable for their lifestyle (Asrat et al., 2015; Eisenreich et al., 2015; Eisenreich et al., 2017; Friedrich et al., 2017). Thus, knowledge about the molecular mechanisms involved in host-pathogen interactions is crucial to a better understanding of the disease progression and, consequently, the development of more targeted therapies. High throughput transcriptomic and proteomic approaches have emerged as powerful techniques to study host and/or pathogen responses to infection (Anjo et al., 2015; Ayllon et al., 2017; Westermann et al., 2017; Westermann et al., 2012). Thus, to start clarifying the molecular determinants involved in rickettsiae-macrophage interactions, we have herein employed a global transcriptomic (RNAseq) (Chapter IV) and proteomics (SWATH-MS) (Chapter V) analysis to evaluate THP-1 macrophages responses to infection by either the pathogen (*R. conorii*) or the non-pathogen (*R. montanensis*) member of SFG *Rickettsia*. Overall, our results revealed that *R. conorii* could substantially reprogram a myriad of host signaling pathways to make intracellular conditions more favorable for a replicative niche.

Our RNAseq analysis revealed that modulation of macrophage inflammatory response is one of the strategies employed by *R. conorii* to circumvent host defenses. Indeed, one of the most striking differences between *R. conorii* and *R. montanensis*-promoted host responses was the observed balance between pro- and anti-inflammatory mediators induced upon infection with the pathogenic *Rickettsia*, which was not observed in *R. montanensis*-infected cells where mainly pro-inflammatory signals were observed. Therefore, understanding how *R. conorii* modulates host immune responses emerges now as a new field of research. It is known that sensing of pathogens by pattern recognition receptors activates several signaling pathways that culminate with pro-inflammatory cytokine production and, subsequently, the recruitment of immune cells to the site of infection to combat the pathogen (Janeway and Medzhitov, 2002). Thus, the observed *R. conorii*-specific downregulation of CD14, a co-receptor that acts along with TLR4 and MD-2 in mediating

LPS signaling, and its implication in subsequent inflammatory responses should be further evaluated. Curiously, it has been already reported that downregulation of CD14 upon infection by *Porphyromonas gingivalis* and *Pseudomonas aeruginosa* is related with hyporesponsiveness to bacterial challenge (Van Belleghem et al., 2017; Wilensky et al., 2015). Interestingly, we have also found that infection of THP-1 macrophages with *R. conorii*, but not *R. montanensis*, renders macrophages unresponsive to a pro-inflammatory stimulus (recombinant LPS), suggesting that modulation of inflammatory responses may be a strategy employed by *R. conorii* to evade innate immune defenses during infection. Indeed, our results also revealed a capacity of *R. conorii*, but not *R. montanensis*, to downregulate several antimicrobial enzymes such as cathepsin G, elastase, and proteinase 3, which are known to be one of the earliest line of defense against bacterial pathogens in innate immunity (Hahn et al., 2011; Korkmaz et al., 2010). Therefore, understanding the mechanisms employed by *R. conorii* to modulate host innate immune and inflammatory responses can bring new insights into how bacterial and viral pathogens escape immune surveillance. The discovery of those factors could enable the design of novel and targeted therapies against rickettsial diseases as well as other infectious diseases. Proteins translocated by secretion systems are known to play significant roles in modulating the host immune response at the levels of sensing, signaling, and interference with host transcription and translation (Asrat et al., 2015). I*n silico* studies exploring the composition and organization of *Rickettsia* secretion systems, as well as the validation of its expression during infection, have been already reported (Gillespie et al., 2009; Gillespie et al., 2015a; Gillespie et al., 2016; Gillespie et al., 2015b). However, more functional studies in *Rickettsia* protein secretion systems and their substrates are still required to identify the complete landscape of rickettsial virulence factors.

In addition to the modulation of host inflammatory responses, it is also known that successful intracellular pathogens also interfere with host apoptotic pathways to their benefit (Friedrich et al., 2017). Interestingly, we have also herein found that *R. conorii*, but not *R. montanensis*, actively modulates pro-survival pathways to sustain macrophage viability during infection. Our results revealed that early in infection, *R. conorii* induces the expression of several anti-apoptotic modulators, including MCL1 and BCL2A1 (two Bcl-2 protein family members that

suppress the pro-apoptotic function of BAX and BAK), PIM3 (a proto-oncogene that can prevent apoptosis and promote cell survival) and SOD2 (protects mitochondria against oxidative stress) (Drane et al., 2001; Mukaida et al., 2011; Willis and Adams, 2005). Thus, inhibition of host cell apoptosis seems to be a strategy employed by *R. conorii* early in infection to maintain the integrity of its replicative niche, whereas host cell viability is rapidly compromised upon infection with *R. montanensis* (Curto et al., 2016). Interestingly, modulation of host cell apoptosis pathways by intracellular pathogens has been widely studied, and while some intracellular pathogens act by inhibiting host cell apoptosis to retain their replicative niche, others induce host cell apoptosis to prevent being killed by the antimicrobial effector molecules of the host cell (Friedrich et al., 2017). Moreover, it has been proposed that most of the pathogens can do both depending on the cellular context (Friedrich et al., 2017). Interestingly, our findings suggest a dynamic and controlled modulation of host cell apoptosis in THP-1 macrophages induced by *R. conorii*. Therefore, it will be interesting to determine the rickettsial effectors responsible for controlling host cell apoptotic pathways during infection as well as to understand how *R. conorii* can differently control host cell apoptosis over the course of the infection. Indeed, additional questions emerge about the mechanisms that allow the bacteria to modulate these pathways in a temporal and/or spatial dependent manner. Thus, it will be interesting to understand if the microenvironment is sensed by *R. conorii* which then releases inhibitors or inducers of apoptosis in a spatially or/and temporally controlled manner or, instead, if the secreted bacterial apoptosis-modulating proteins react in a tissue- or context-dependent manner. In the case that the bacteria continuously sense the cellular environment, tight regulation of the bacterial virulence factor(s) at the transcriptional or post-transcriptional level would be required, opening fascinating interrelations in the rickettsiae-macrophage interface.

To control this multiplicity of cellular processes, *R. conorii* must interfere with host gene expression programs during infection. Indeed, our results revealed that infection of THP-1 macrophages with *R. conorii* resulted in the differential expression of several gene expression modulators such as non-coding RNAs and transcription factors, which can significantly affect the transcription programs generated over the course of the infection. In fact, an increasing number of

studies have reported the ability of pathogens to deliver factors into the host nucleus, “nucleomodulins”, to directly interfere with transcription, chromatin remodeling, RNA splicing or DNA replication and repair (Bierne and Cossart, 2012). However, the mechanisms employed by *R. conorii* to interfere with host gene expression programs remain to be elucidated. In other related pathogens, as the example of *Anaplasma phagocytophilum*, Ankyrin repeat-containing proteins have been identified as regulators of the three-dimensional chromatin architecture, thus coordinating transcriptional programs in the host cell (Dumler et al., 2016). Interestingly, comparative genomic analysis of the secretome of *R. conorii* and *R. montanensis* have revealed significant differences in rarp2, encoding *Rickettsia* Ankyrin Repeat Protein 2 (RARP-2), which is absent in *R. montanensis* genome (Gillespie et al., 2015a). Thus, RARP-2 emerges as a prime candidate in rickettsial species to promote macrophage reprogramming during infection. Moreover, the ability of rickettsial species to invade the nucleus of human cells (Burgdorfer et al., 1968; Ogata et al., 2006) may also favor the potential of this bacteria to interfere with nuclear dynamics and to efficiently reprogram the expression of host genes in programs that may be beneficial for microbial fitness and pathogenicity.

The capacity to modulate host cell metabolism to create a more permissive replication niche has been described for several intracellular bacterial pathogens (Price and Vance, 2014). In this regard, the metabolic plasticity of macrophages is considered a very attractive feature to be explored by pathogens as a vast source of cellular resources that can be rapidly remodeled (Eisenreich et al., 2015; Eisenreich et al., 2017; Van den Bossche et al., 2017). Since many metabolic pathways have been purged throughout reductive genome evolution in *Rickettsia*, it is expected that mutual metabolic adaptations must occur during rickettsial infections (Driscoll et al., 2017). We have herein found *R. conorii* and *R. montanensis* induce different metabolic signatures in macrophage-like cells (Chapter V). Somewhat unexpectedly, infection of THP-1 macrophages with either *R. conorii* or *R. montanensis* resulted in a decrease in abundance of several enzymes involved in glycolysis and pentose phosphate pathways. However, the reasons underlying this decrease in macrophage glycolytic activity remain to be elucidated. Interestingly, it is known that

glycolytic enzymes promote inflammatory macrophage functions (Van den Bossche et al., 2017). Thus, the reduction of glycolytic activity in THP-1 macrophages upon infection with SFG rickettsial species should be evaluated in future studies as a possible strategy employed by the bacteria to block macrophage inflammatory responses early in infection. Remarkably, *R. conorii* seems to be able to compensate host cell energy production by increasing the abundance of several TCA cycle enzymes, components of the electron chain reaction as well as other parallel pathways involved in TCA cycle feeding, such as fatty acid β-oxidation and glutaminolysis. Therefore, our results anticipate a profound metabolic rewriting of macrophages specifically induced by *R. conorii* towards a metabolic signature of an M2-like (anti-inflammatory) activation program, which may result in beneficial conditions for *Rickettsia* proliferation. Moreover, the *R. conorii*-induced host metabolic changes appear to favor the generation of several metabolites that have been shown (or predicted) to be imported from the host by rickettsial species, such as glutamate, pyruvate, malate, α-ketoglutarate, aspartate, and ATP. Therefore, the evaluation of how *Rickettsia* import host metabolites, the metabolic interconnections rickettsiae-macrophage, and which/how bacterial effectors and transporters control these complex adaptation processes emerge as exciting areas of future research. Also, further studies to understand if this metabolic signature is maintained over the course of the infection or if the modulation of macrophage metabolic pathways is a dynamic process should also be addressed.

The ability to escape immune surveillance and persist within the host requires the elaboration of sophisticated strategies by pathogens (Ruby and Monack, 2011). However, the mechanisms by which rickettsia species evade the immune system are still not completely understood. Remarkably, we have herein found that both *R. conorii* and *R. montanensis* infection in THP-1 macrophages reduces the abundance of several proteasome and immunoproteasome activator subunits. This may significantly impact antigen peptide presentation by MHC class I complex and thereby facilitate bacteria to escape immune surveillance. However, the ER stress induced by the accumulation of misfolded proteins, together with the stress caused by the intracellular lifestyle of rickettsial species may also result in ER stress-induced apoptosis if too severe or prolonged (Friedrich et al., 2017). Interestingly, *R. conorii*, but not *R. montanensis*,

specifically induce the accumulation of several ER proteins involved in protein translocation, folding and quality control, which may be a compensatory mechanism to restore host cell homeostasis and retain the replicative niche. To our knowledge, this is the first time the proteasome itself is shown to be affected as a result of a bacterial infection. Our findings raise new questions on how and why *Rickettsia* modulate host proteasome function since this likely interferes with different cellular processes.

This work contributes new insights on how host cell functions and multiple signaling events respond to either clear an infection or to be exploited to the own benefit of an obligate intracellular pathogen. Globally, this helps to unfold the intricate pattern of modulation triggered by a pathogenic *Rickettsia* to control macrophage homeostasis and to maintain a viable intracellular niche. By illuminating still very poorly studied aspects of macrophage-*Rickettsia* interactions, this work provides an important framework for future investigations that are likely to lead to an improved understanding of the link between the capacity to proliferate in macrophages and rickettsial pathogenicity.

VII | References

Abdad, M.Y., Abou Abdallah, R., Fournier, P.E., Stenos, J., and Vasoo, S. (2018). A Concise Review of the Epidemiology and Diagnostics of Rickettsioses: *Rickettsia* and *Orientia* spp. J Clin Microbiol.

Abdullah, Z., Geiger, S., Nino-Castro, A., Bottcher, J.P., Muraliv, E., Gaidt, M., Schildberg, F.A., Riethausen, K., Flossdorf, J., Krebs, W.*, et al.* (2012). Lack of PPARgamma in myeloid cells confers resistance to *Listeria monocytogenes* infection. PLoS One *7*, e37349.

Abell, B.M., Pool, M.R., Schlenker, O., Sinning, I., and High, S. (2004). Signal recognition particle mediates post-translational targeting in eukaryotes. EMBO J *23*, 2755-2764.

Abnave, P., Muracciole, X., and Ghigo, E. (2017). *Coxiella burnetii* Lipopolysaccharide: What Do We Know? Int J Mol Sci *18*.

Abu Kwaik, Y., and Bumann, D. (2015). Host Delivery of Favorite Meals for Intracellular Pathogens. PLoS Pathog *11*, e1004866.

Albert, M.L. (2004). Death-defying immunity: do apoptotic cells influence antigen processing and presentation? Nat Rev Immunol *4*, 223-231.

Alonso, A., and Garcia-del Portillo, F. (2004). Hijacking of eukaryotic functions by intracellular bacterial pathogens. Int Microbiol *7*, 181-191.

Alvarez-Hernandez, G., Roldan, J.F.G., Milan, N.S.H., Lash, R.R., Behravesh, C.B., and Paddock, C.D. (2017). Rocky Mountain spotted fever in Mexico: past, present, and future. Lancet Infect Dis *17*, e189-e196.

Ambite, I., Lutay, N., Stork, C., Dobrindt, U., Wullt, B., and Svanborg, C. (2016). Bacterial Suppression of RNA Polymerase II-Dependent Host Gene Expression. Pathogens *5*.

Ameyar, M., Wisniewska, M., and Weitzman, J.B. (2003). A role for AP-1 in apoptosis: the case for and against. Biochimie *85*, 747-752.

Amit, I., Winter, D.R., and Jung, S. (2016). The role of the local environment and epigenetics in shaping macrophage identity and their effect on tissue homeostasis. Nat Immunol *17*, 18-25.

Ammerman, N.C., Beier-Sexton, M., and Azad, A.F. (2008). Laboratory maintenance of *Rickettsia rickettsii*. Curr Protoc Microbiol *Chapter 3*, Unit 3A 5.

Ammerman, N.C., Swanson, K.I., Anderson, J.M., Schwartz, T.R., Seaberg, E.C., Glass, G.E., and Norris, D.E. (2004). Spotted-fever group *Rickettsia* in Dermacentor variabilis, Maryland. Emerg Infect Dis *10*, 1478-1481.

Amyere, M., Payrastre, B., Krause, U., Van Der Smissen, P., Veithen, A., and Courtoy, P.J. (2000). Constitutive macropinocytosis in oncogene-transformed fibroblasts depends on sequential permanent activation of phosphoinositide 3-kinase and phospholipase C. Mol Biol Cell *11*, 3453-3467.

Andersson, S.G., Zomorodipour, A., Andersson, J.O., Sicheritz-Ponten, T., Alsmark, U.C., Podowski, R.M., Naslund, A.K., Eriksson, A.S., Winkler, H.H., and Kurland, C.G. (1998). The genome sequence of *Rickettsia prowazekii* and the origin of mitochondria. Nature *396*, 133-140.

Angel, P., and Karin, M. (1991). The role of Jun, Fos and the AP-1 complex in cell-proliferation and transformation. Biochim Biophys Acta *1072*, 129-157.

Angelakis, E., Richet, H., Rolain, J.M., La Scola, B., and Raoult, D. (2012). Comparison of real-time quantitative PCR and culture for the diagnosis of emerging Rickettsioses. PLoS Negl Trop Dis *6*, e1540.

Anjo, S.I., Santa, C., and Manadas, B. (2015). Short GeLC-SWATH: a fast and reliable quantitative approach for proteomic screenings. Proteomics *15*, 757-762.

Anjo, S.I., Santa, C., and Manadas, B. (2017). SWATH-MS as a tool for biomarker discovery: From basic research to clinical applications. Proteomics *17*.

Ashida, H., Kim, M., and Sasakawa, C. (2014). Exploitation of the host ubiquitin system by human bacterial pathogens. Nat Rev Microbiol *12*, 399-413.

Ashida, H., and Sasakawa, C. (2014). Shigella hacks host immune responses by reprogramming the host epigenome. EMBO J *33*, 2598-2600.

Asrat, S., Davis, K.M., and Isberg, R.R. (2015). Modulation of the host innate immune and inflammatory response by translocated bacterial proteins. Cell Microbiol *17*, 785-795.

Ayllon, N., Jimenez-Marin, A., Arguello, H., Zaldivar-Lopez, S., Villar, M., Aguilar, C., Moreno, A., De La Fuente, J., and Garrido, J.J. (2017). Comparative Proteomics Reveals Differences in Host-Pathogen Interaction between Infectious and Commensal Relationship with *Campylobacter jejuni*. Front Cell Infect Microbiol *7*, 145.

Banajee, K.H., Embers, M.E., Langohr, I.M., Doyle, L.A., Hasenkampf, N.R., and Macaluso, K.R. (2015). Correction: Amblyomma maculatum Feeding Augments *Rickettsia parkeri* Infection in a *Rhesus Macaque* Model: A Pilot Study. PLoS One *10*, e0137598.

Bar-Sagi, D., and Feramisco, J.R. (1986). Induction of membrane ruffling and fluid-phase pinocytosis in quiescent fibroblasts by ras proteins. Science *233*, 1061-1068.

Bar-Sagi, D., McCormick, F., Milley, R.J., and Feramisco, J.R. (1987). Inhibition of cell surface ruffling and fluid-phase pinocytosis by microinjection of anti-ras antibodies into living cells. J Cell Physiol Suppl *Suppl 5*, 69-73.

Bayer-Santos, E., Marini, M.M., and da Silveira, J.F. (2017). Non-coding RNAs in Host-Pathogen Interactions: Subversion of Mammalian Cell Functions by Protozoan Parasites. Front Microbiol *8*, 474.

Bechah, Y., Capo, C., Mege, J.L., and Raoult, D. (2008a). Epidemic typhus. Lancet Infect Dis *8*, 417-426.

Bechah, Y., Capo, C., Mege, J.L., and Raoult, D. (2008b). Rickettsial diseases: from *Rickettsia*-arthropod relationships to pathophysiology and animal models. Future Microbiol *3*, 223-236.

Bechah, Y., Capo, C., Raoult, D., and Mege, J.L. (2008c). Infection of endothelial cells with virulent *Rickettsia prowazekii* increases the transmigration of leukocytes. J Infect Dis *197*, 142-147.

Bechah, Y., El Karkouri, K., Mediannikov, O., Leroy, Q., Pelletier, N., Robert, C., Medigue, C., Mege, J.L., and Raoult, D. (2010). Genomic, proteomic, and transcriptomic analysis of virulent and avirulent *Rickettsia prowazekii* reveals its adaptive mutation capabilities. Genome Res *20*, 655-663.

Benoit, M., Desnues, B., and Mege, J.L. (2008). Macrophage polarization in bacterial infections. J Immunol *181*, 3733-3739.

Bentea, E., Verbruggen, L., and Massie, A. (2017). The Proteasome Inhibition Model of Parkinson's Disease. J Parkinsons Dis *7*, 31-63.

Bierne, H., and Cossart, P. (2012). When bacteria target the nucleus: the emerging family of nucleomodulins. Cell Microbiol *14*, 622-633.

Billings, A.N., Feng, H.M., Olano, J.P., and Walker, D.H. (2001). Rickettsial infection in murine models activates an early anti-rickettsial effect mediated by NK cells and associated with production of gamma interferon. Am J Trop Med Hyg *65*, 52-56.

Blanc, G., Ngwamidiba, M., Ogata, H., Fournier, P.E., Claverie, J.M., and Raoult, D. (2005). Molecular evolution of rickettsia surface antigens: evidence of positive selection. Mol Biol Evol *22*, 2073-2083.

Blanc, G., Ogata, H., Robert, C., Audic, S., Suhre, K., Vestris, G., Claverie, J.M., and Raoult, D. (2007). Reductive genome evolution from the mother of *Rickettsia*. PLoS Genet *3*, e14.

Bolanos-Rivero, M., Santana-Rodriguez, E., Angel-Moreno, A., Hernandez-Cabrera, M., Liminana-Canal, J.M., Carranza-Rodriguez, C., Martin-Sanchez, A.M., and Perez-Arellano, J.L. (2011). Seroprevalence of *Rickettsia typhi* and *Rickettsia conorii* infections in the Canary Islands (Spain). Int J Infect Dis *15*, e481-485.

Bonilla, F.A., and Oettgen, H.C. (2010). Adaptive immunity. J Allergy Clin Immunol *125*, S33-40.

Botelho-Nevers, E., and Raoult, D. (2011). Host, pathogen and treatment-related prognostic factors in rickettsioses. Eur J Clin Microbiol Infect Dis *30*, 1139-1150.

Botelho-Nevers, E., Socolovschi, C., Raoult, D., and Parola, P. (2012). Treatment of *Rickettsia* spp. infections: a review. Expert Rev Anti Infect Ther *10*, 1425-1437.

Bougneres, L., Girardin, S.E., Weed, S.A., Karginov, A.V., Olivo-Marin, J.C., Parsons, J.T., Sansonetti, P.J., and Van Nhieu, G.T. (2004). Cortactin and Crk cooperate to trigger actin polymerization during Shigella invasion of epithelial cells. J Cell Biol *166*, 225-235.

Boumart, Z., Velge, P., and Wiedemann, A. (2014). Multiple invasion mechanisms and different intracellular Behaviors: a new vision of *Salmonella*-host cell interaction. FEMS Microbiol Lett *361*, 1-7.

Brenner, D., Blaser, H., and Mak, T.W. (2015). Regulation of tumour necrosis factor signalling: live or let die. Nat Rev Immunol *15*, 362-374.

Brossard, M., and Wikel, S.K. (2004). Tick immunobiology. Parasitology *129 Suppl*, S161-176.

Brossart, P., and Bevan, M.J. (1997). Presentation of exogenous protein antigens on major histocompatibility complex class I molecules by dendritic cells: pathway of presentation and regulation by cytokines. Blood *90*, 1594-1599.

Brouqui, P., Bacellar, F., Baranton, G., Birtles, R.J., Bjoersdorff, A., Blanco, J.R., Caruso, G., Cinco, M., Fournier, P.E., Francavilla, E.*, et al.* (2004). Guidelines for the diagnosis of tick-borne bacterial diseases in Europe. Clin Microbiol Infect *10*, 1108-1132.

Brouqui, P., Parola, P., Fournier, P.E., and Raoult, D. (2007). Spotted fever rickettsioses in southern and eastern Europe. FEMS Immunol Med Microbiol *49*, 2-12.

Brown, L.D., and Macaluso, K.R. (2016). *Rickettsia felis*, an Emerging Flea-Borne Rickettsiosis. Curr Trop Med Rep *3*, 27-39.

Buchacher, T., Ohradanova-Repic, A., Stockinger, H., Fischer, M.B., and Weber, V. (2015). M2 Polarization of Human Macrophages Favors Survival of the Intracellular Pathogen *Chlamydia pneumoniae*. PLoS One *10*, e0143593.

Buchmeier, N.A., and Heffron, F. (1991). Inhibition of macrophage phagosome-lysosome fusion by *Salmonella typhimurium*. Infect Immun *59*, 2232-2238.

Burgdorfer, W., Anacker, R.L., Bird, R.G., and Bertram, D.S. (1968). Intranuclear growth of *Rickettsia rickettsii*. J Bacteriol *96*, 1415-1418.

Burgdorfer, W., and Brinton, L.P. (1975). Mechanisms of transovarial infection of spotted fever Rickettsiae in ticks. Ann N Y Acad Sci *266*, 61-72.

Burger, D., and Dayer, J.M. (2002). High-density lipoprotein-associated apolipoprotein A-I: the missing link between infection and chronic inflammation? Autoimmun Rev *1*, 111-117.

Bussey, K.A., Lau, U., Schumann, S., Gallo, A., Osbelt, L., Stempel, M., Arnold, C., Wissing, J., Gad, H.H., Hartmann, R.*, et al.* (2018). The interferon-stimulated gene product oligoadenylate synthetase-like protein enhances replication of Kaposi's sarcoma-associated herpesvirus (KSHV) and interacts with the KSHV ORF20 protein. PLoS Pathog *14*, e1006937.

Cardwell, M.M., and Martinez, J.J. (2009). The Sca2 autotransporter protein from *Rickettsia conorii* is sufficient to mediate adherence to and invasion of cultured mammalian cells. Infect Immun *77*, 5272-5280.

Cardwell, M.M., and Martinez, J.J. (2012). Identification and characterization of the mammalian association and actin-nucleating domains in the *Rickettsia conorii* autotransporter protein, Sca2. Cell Microbiol *14*, 1485-1495.

Carmichael, J.R., and Fuerst, P.A. (2010). Molecular detection of *Rickettsia bellii*, *Rickettsia montanensis*, and *Rickettsia rickettsii* in a *Dermacentor variabilis* tick from nature. Vector Borne Zoonotic Dis *10*, 111-115.

Caro-Gomez, E., Gazi, M., Goez, Y., and Valbuena, G. (2014). Discovery of novel cross-protective *Rickettsia prowazekii* T-cell antigens using a combined reverse vaccinology and in vivo screening approach. Vaccine *32*, 4968-4976.

Carter, G.C., Bernstone, L., Baskaran, D., and James, W. (2011). HIV-1 infects macrophages by exploiting an endocytic route dependent on dynamin, Rac1 and Pak1. Virology *409*, 234-250.

Casadevall, A. (2018). Antibody-based vaccine strategies against intracellular pathogens. Curr Opin Immunol *53*, 74-80.

Cavassani, K.A., Aliberti, J.C., Dias, A.R., Silva, J.S., and Ferreira, B.R. (2005). Tick saliva inhibits differentiation, maturation and function of murine bone-marrow-derived dendritic cells. Immunology *114*, 235-245.

Celli, J., and Tsolis, R.M. (2015). Bacteria, the endoplasmic reticulum and the unfolded protein response: friends or foes? Nat Rev Microbiol *13*, 71-82.

Ceraul, S.M. (2012). Transmission and the Determinants of Transmission Efficiency. In Intracellular Pathogens II: Rickettsiales, G.H. Palmer, and A.F. Azad, eds. (ASM Press), pp. 391-415.

Chan, Y.G., Cardwell, M.M., Hermanas, T.M., Uchiyama, T., and Martinez, J.J. (2009). Rickettsial outer-membrane protein B (rOmpB) mediates bacterial invasion through Ku70 in an actin, c-Cbl, clathrin and caveolin 2-dependent manner. Cell Microbiol *11*, 629-644.

Chan, Y.G., Riley, S.P., Chen, E., and Martinez, J.J. (2011). Molecular basis of immunity to rickettsial infection conferred through outer membrane protein B. Infection and immunity *79*, 2303-2313.

Chan, Y.G., Riley, S.P., and Martinez, J.J. (2010). Adherence to and invasion of host cells by spotted Fever group rickettsia species. Frontiers in microbiology *1*, 139.

Chandran, A., Antony, C., Jose, L., Mundayoor, S., Natarajan, K., and Kumar, R.A. (2015). Mycobacterium tuberculosis Infection Induces HDAC1-Mediated Suppression of IL-12B Gene Expression in Macrophages. Front Cell Infect Microbiol *5*, 90.

Chang, S.H., Hwang, C.S., Yin, J.H., Chen, S.D., and Yang, D.I. (2015). Oncostatin M-dependent Mcl-1 induction mediated by JAK1/2-STAT1/3 and CREB contributes to bioenergetic improvements and protective effects against mitochondrial dysfunction in cortical neurons. Biochim Biophys Acta *1853*, 2306-2325.

Chmielewski, T., Rudzka, D., Fiecek, B., Maczka, I., and Tylewska-Wierzbanowska, S. (2011). [Case of TIBOLA/DEBONEL (tick - borne lymphadenopathy/Dermacentor spp. - borne necrosis - erythema - lymphadenopathy) in Poland]. Przegl Epidemiol *65*, 583-586.

Cirillo, J.D., Cirillo, S.L., Yan, L., Bermudez, L.E., Falkow, S., and Tompkins, L.S. (1999). Intracellular growth in *Acanthamoeba castellanii* affects monocyte entry mechanisms and enhances virulence of *Legionella pneumophila*. Infect Immun *67*, 4427-4434.

Civen, R., and Ngo, V. (2008). Murine typhus: an unrecognized suburban vectorborne disease. Clin Infect Dis *46*, 913-918.

Clark, T.R., Noriea, N.F., Bublitz, D.C., Ellison, D.W., Martens, C., Lutter, E.I., and Hackstadt, T. (2015). Comparative genome sequencing of *Rickettsia rickettsii* strains that differ in virulence. Infect Immun *83*, 1568-1576.

Clifton, D.R., Goss, R.A., Sahni, S.K., van Antwerp, D., Baggs, R.B., Marder, V.J., Silverman, D.J., and Sporn, L.A. (1998). NF-kappa B-dependent inhibition of apoptosis is essential for host cellsurvival during *Rickettsia rickettsii* infection. Proc Natl Acad Sci U S A *95*, 4646-4651.

Clifton, D.R., Rydkina, E., Freeman, R.S., and Sahni, S.K. (2005a). NF-kappaB activation during *Rickettsia rickettsii* infection of endothelial cells involves the activation of catalytic IkappaB kinases IKKalpha and IKKbeta and phosphorylation-proteolysis of the inhibitor protein IkappaBalpha. Infect Immun *73*, 155-165.

Clifton, D.R., Rydkina, E., Huyck, H., Pryhuber, G., Freeman, R.S., Silverman, D.J., and Sahni, S.K. (2005b). Expression and secretion of chemotactic cytokines IL-8 and MCP-1 by human endothelial cells after *Rickettsia rickettsii* infection: regulation by nuclear transcription factor NF-kappaB. Int J Med Microbiol *295*, 267-278.

Cloney, R. (2016). Microbial genetics: Dual RNA-seq for host-pathogen transcriptomics. Nat Rev Genet *17*, 126-127.

Cockrell, D.C., Long, C.M., Robertson, S.J., Shannon, J.G., Miller, H.E., Myers, L., Larson, C.L., Starr, T., Beare, P.A., and Heinzen, R.A. (2017). Robust growth of avirulent phase II *Coxiella burnetii* in bone marrow-derived murine macrophages. PLoS One *12*, e0173528.

Collins, B.C., Gillet, L.C., Rosenberger, G., Rost, H.L., Vichalkovski, A., Gstaiger, M., and Aebersold, R. (2013). Quantifying protein interaction dynamics by SWATH mass spectrometry: application to the 14-3-3 system. Nature methods *10*, 1246-1253.

Colonne, P.M., Sahni, A., and Sahni, S.K. (2011). *Rickettsia conorii* infection stimulates the expression of ISG15 and ISG15 protease UBP43 in human microvascular endothelial cells. Biochem Biophys Res Commun *416*, 153-158.

Colonne, P.M., Winchell, C.G., and Voth, D.E. (2016). Hijacking Host Cell Highways: Manipulation of the Host Actin Cytoskeleton by Obligate Intracellular Bacterial Pathogens. Front Cell Infect Microbiol *6*, 107.

Coolbaugh, J.C., Progar, J.J., and Weiss, E. (1976). Enzymatic activities of cell-free extracts of *Rickettsia typhi*. Infect Immun *14*, 298-305.

Corraliza, I.M., Soler, G., Eichmann, K., and Modolell, M. (1995). Arginase induction by suppressors of nitric oxide synthesis (IL-4, IL-10 and PGE2) in murine bone-marrow-derived macrophages. Biochem Biophys Res Commun *206*, 667-673.

Cossart, P. (2004). Bacterial invasion: a new strategy to dominate cytoskeleton plasticity. Dev Cell *6*, 314-315.

Cruz, R., Huesgen, P., Riley, S.P., Wlodawer, A., Faro, C., Overall, C.M., Martinez, J.J., and Simoes, I. (2014). RC1339/APRc from *Rickettsia conorii* is a novel aspartic protease with properties of retropepsin-like enzymes. PLoS Pathog *10*, e1004324.

Cullen, B.R. (2013). MicroRNAs as mediators of viral evasion of the immune system. Nat Immunol *14*, 205-210.

Curto, P., Simoes, I., Riley, S.P., and Martinez, J.J. (2016). Differences in Intracellular Fate of Two Spotted Fever Group *Rickettsia* in Macrophage-Like Cells. Front Cell Infect Microbiol *6*, 80.

Cuschieri, J., Gourlay, D., Garcia, I., Jelacic, S., and Maier, R.V. (2004). Implications of proteasome inhibition: an enhanced macrophage phenotype. Cell Immunol *227*, 140-147.

Dantas-Torres, F. (2007). Rocky Mountain spotted fever. Lancet Infect Dis *7*, 724-732.

Darby, A.C., Cho, N.H., Fuxelius, H.H., Westberg, J., and Andersson, S.G. (2007). Intracellular pathogens go extreme: genome evolution in the Rickettsiales. Trends Genet *23*, 511-520.

Das, K., Garnica, O., and Dhandayuthapani, S. (2016). Modulation of Host miRNAs by Intracellular Bacterial Pathogens. Front Cell Infect Microbiol *6*, 79.

Davis, A.S., Vergne, I., Master, S.S., Kyei, G.B., Chua, J., and Deretic, V. (2007). Mechanism of inducible nitric oxide synthase exclusion from mycobacterial phagosomes. PLoS Pathog *3*, e186.

de Carvalho, T.M., Barrias, E.S., and de Souza, W. (2015). Macropinocytosis: a pathway to protozoan infection. Front Physiol *6*, 106.

de Sousa, R., Nobrega, S.D., Bacellar, F., and Torgal, J. (2003). Mediterranean spotted fever in Portugal: risk factors for fatal outcome in 105 hospitalized patients. Ann N Y Acad Sci *990*, 285-294.

Demma, L.J., Eremeeva, M., Nicholson, W.L., Traeger, M., Blau, D., Paddock, C., Levin, M., Dasch, G., Cheek, J., Swerdlow, D.*, et al.* (2006). An outbreak of Rocky Mountain Spotted Fever associated with a novel tick vector, Rhipicephalus sanguineus, in Arizona, 2004: preliminary report. Ann N Y Acad Sci *1078*, 342-343.

Demma, L.J., Traeger, M.S., Nicholson, W.L., Paddock, C.D., Blau, D.M., Eremeeva, M.E., Dasch, G.A., Levin, M.L., Singleton, J., Jr., Zaki, S.R., *et al.* (2005). Rocky Mountain spotted fever from an unexpected tick vector in Arizona. N Engl J Med *353*, 587-594.

Deretic, V., Singh, S., Master, S., Harris, J., Roberts, E., Kyei, G., Davis, A., de Haro, S., Naylor, J., Lee, H.H., *et al.* (2006). Mycobacterium tuberculosis inhibition of phagolysosome biogenesis and autophagy as a host defence mechanism. Cell Microbiol *8*, 719-727.

Diop, A., Raoult, D., and Fournier, P.E. (2017). Rickettsial genomics and the paradigm of genome reduction associated with increased virulence. Microbes Infect.

Dobin, A., Davis, C.A., Schlesinger, F., Drenkow, J., Zaleski, C., Jha, S., Batut, P., Chaisson, M., and Gingeras, T.R. (2013). STAR: ultrafast universal RNA-seq aligner. Bioinformatics *29*, 15-21.

Donepudi, M., and Resh, M.D. (2008). c-Src trafficking and co-localization with the EGF receptor promotes EGF ligand-independent EGF receptor activation and signaling. Cell Signal *20*, 1359-1367.

Donnelly, R.P., Loftus, R.M., Keating, S.E., Liou, K.T., Biron, C.A., Gardiner, C.M., and Finlay, D.K. (2014). mTORC1-dependent metabolic reprogramming is a prerequisite for NK cell effector function. J Immunol *193*, 4477-4484.

Doughty, C.A., Bleiman, B.F., Wagner, D.J., Dufort, F.J., Mataraza, J.M., Roberts, M.F., and Chiles, T.C. (2006). Antigen receptor-mediated changes in glucose metabolism in B lymphocytes: role of phosphatidylinositol 3-kinase signaling in the glycolytic control of growth. Blood *107*, 4458-4465.

Drane, P., Bravard, A., Bouvard, V., and May, E. (2001). Reciprocal down-regulation of p53 and SOD2 gene expression-implication in p53 mediated apoptosis. Oncogene *20*, 430-439.

Driscoll, T.P., Verhoeve, V.I., Guillotte, M.L., Lehman, S.S., Rennoll, S.A., Beier-Sexton, M., Rahman, M.S., Azad, A.F., and Gillespie, J.J. (2017). Wholly *Rickettsia*! Reconstructed Metabolic Profile of the Quintessential Bacterial Parasite of Eukaryotic Cells. MBio *8*.

Driskell, L.O., Yu, X.J., Zhang, L., Liu, Y., Popov, V.L., Walker, D.H., Tucker, A.M., and Wood, D.O. (2009). Directed mutagenesis of the *Rickettsia prowazekii* pld gene encoding phospholipase D. Infect Immun *77*, 3244-3248.

Duma, R.J., Sonenshine, D.E., Bozeman, F.M., Veazey, J.M., Jr., Elisberg, B.L., Chadwick, D.P., Stocks, N.I., McGill, T.M., Miller, G.B., Jr., and MacCormack, J.N. (1981). Epidemic typhus in the United States associated with flying squirrels. JAMA *245*, 2318-2323.

Dumler, J.S. (2012). Clinical Disease: Current Treatment and New Challenges. In Intracellular Pathogens II: Rickettsiales, G.H. Palmer, and A.F. Azad, eds. (ASM Press), pp. 1-39.

Dumler, J.S., Sinclair, S.H., Pappas-Brown, V., and Shetty, A.C. (2016). Genome-Wide *Anaplasma phagocytophilum* AnkA-DNA Interactions Are Enriched in Intergenic Regions and Gene Promoters and Correlate with Infection-Induced Differential Gene Expression. Front Cell Infect Microbiol *6*, 97.

Durkop, H., Foss, H.D., Demel, G., Klotzbach, H., Hahn, C., and Stein, H. (1999). Tumor necrosis factor receptor-associated factor 1 is overexpressed in Reed-Sternberg cells of Hodgkin's disease and Epstein-Barr virus-transformed lymphoid cells. Blood *93*, 617-623.

Duval, M., Cossart, P., and Lebreton, A. (2017). Mammalian microRNAs and long noncoding RNAs in the host-bacterial pathogen crosstalk. Semin Cell Dev Biol *65*, 11-19.

ECDC (2013). Epidemiological situation of rickettsioses in EU/EFTA countries (Stockholm).

Edwards, D.C., Sanders, L.C., Bokoch, G.M., and Gill, G.N. (1999). Activation of LIM-kinase by Pak1 couples Rac/Cdc42 GTPase signalling to actin cytoskeletal dynamics. Nat Cell Biol *1*, 253-259.

Eisele, N.A., Ruby, T., Jacobson, A., Manzanillo, P.S., Cox, J.S., Lam, L., Mukundan, L., Chawla, A., and Monack, D.M. (2013). *Salmonella* require the fatty acid regulator PPARdelta for the establishment of a metabolic environment essential for long-term persistence. Cell Host Microbe *14*, 171-182.

Eisenberg, E., and Levanon, E.Y. (2013). Human housekeeping genes, revisited. Trends Genet *29*, 569-574.

Eisenreich, W., Heesemann, J., Rudel, T., and Goebel, W. (2013). Metabolic host responses to infection by intracellular bacterial pathogens. Front Cell Infect Microbiol *3*, 24.

Eisenreich, W., Heesemann, J., Rudel, T., and Goebel, W. (2015). Metabolic Adaptations of Intracellullar Bacterial Pathogens and their Mammalian Host Cells during Infection ("Pathometabolism"). Microbiol Spectr *3*.

Eisenreich, W., Rudel, T., Heesemann, J., and Goebel, W. (2017). To Eat and to Be Eaten: Mutual Metabolic Adaptations of Immune Cells and Intracellular Bacterial Pathogens upon Infection. Front Cell Infect Microbiol *7*, 316.

Eissenberg, L.G., and Wyrick, P.B. (1981). Inhibition of phagolysosome fusion is localized to Chlamydia psittaci-laden vacuoles. Infect Immun *32*, 889-896.

El Karkouri, K., Pontarotti, P., Raoult, D., and Fournier, P.E. (2016). Origin and Evolution of Rickettsial Plasmids. PLoS One *11*, e0147492.

Eldin, C., Mediannikov, O., Davoust, B., Cabre, O., Barre, N., Raoult, D., and Parola, P. (2011). Emergence of Rickettsia africae, Oceania. Emerg Infect Dis *17*, 100-102.

Elfving, K., Olsen, B., Bergstrom, S., Waldenstrom, J., Lundkvist, A., Sjostedt, A., Mejlon, H., and Nilsson, K. (2010). Dissemination of spotted fever rickettsia agents in Europe by migrating birds. PLoS One *5*, e8572.

Eliopoulos, A.G., Waites, E.R., Blake, S.M., Davies, C., Murray, P., and Young, L.S. (2003). TRAF1 is a critical regulator of JNK signaling by the TRAF-binding domain of the Epstein-Barr virus-encoded latent infection membrane protein 1 but not CD40. J Virol *77*, 1316-1328.

Ellison, D.W., Clark, T.R., Sturdevant, D.E., Virtaneva, K., Porcella, S.F., and Hackstadt, T. (2008). Genomic comparison of virulent *Rickettsia rickettsii* Sheila Smith and avirulent *Rickettsia rickettsii* Iowa. Infect Immun *76*, 542-550.

Emelyanov, V.V. (2001). Rickettsiaceae, rickettsia-like endosymbionts, and the origin of mitochondria. Biosci Rep *21*, 1-17.

Emelyanov, V.V. (2009). Mitochondrial porin VDAC 1 seems to be functional in rickettsial cells. Ann N Y Acad Sci *1166*, 38-48.

Emelyanov, V.V., and Vyssokikh, M.Y. (2006). On the nature of obligate intracellular symbiosis of rickettsiae-*Rickettsia prowazekii* cells import mitochondrial porin. Biochemistry (Mosc) *71*, 730-735.

Epelman, S., Lavine, K.J., and Randolph, G.J. (2014). Origin and functions of tissue macrophages. Immunity *41*, 21-35.

Eremeeva, M.E., and Dasch, G.A. (2015). Challenges posed by tick-borne rickettsiae: eco-epidemiology and public health implications. Front Public Health *3*, 55.

Eswaran, J., Soundararajan, M., Kumar, R., and Knapp, S. (2008). UnPAKing the class differences among p21-activated kinases. Trends Biochem Sci *33*, 394-403.

Eulalio, A., Schulte, L., and Vogel, J. (2012). The mammalian microRNA response to bacterial infections. RNA Biol *9*, 742-750.

Faccini-Martinez, A.A., Garcia-Alvarez, L., Hidalgo, M., and Oteo, J.A. (2014). Syndromic classification of rickettsioses: an approach for clinical practice. Int J Infect Dis *28*, 126-139.

Fang, R., Blanton, L.S., and Walker, D.H. (2017). Rickettsiae as Emerging Infectious Agents. Clin Lab Med *37*, 383-400.

Fang, R., Ismail, N., Shelite, T., and Walker, D.H. (2009). CD4+ CD25+ Foxp3- T-regulatory cells produce both gamma interferon and interleukin-10 during acute severe murine spotted fever rickettsiosis. Infect Immun *77*, 3838-3849.

Fang, R., Ismail, N., Soong, L., Popov, V.L., Whitworth, T., Bouyer, D.H., and Walker, D.H. (2007). Differential interaction of dendritic cells with *Rickettsia conorii*: impact on host susceptibility to murine spotted fever rickettsiosis. Infect Immun *75*, 3112-3123.

Feng, H., Popov, V.L., Yuoh, G., and Walker, D.H. (1997). Role of T lymphocyte subsets in immunity to spotted fever group Rickettsiae. J Immunol *158*, 5314-5320.

Feng, H.M., Popov, V.L., and Walker, D.H. (1994). Depletion of gamma interferon and tumor necrosis factor alpha in mice with *Rickettsia conorii*-infected endothelium: impairment of rickettsicidal nitric oxide production resulting in fatal, overwhelming rickettsial disease. Infect Immun *62*, 1952-1960.

Feng, H.M., and Walker, D.H. (2000). Mechanisms of intracellular killing of *Rickettsia conorii* in infected human endothelial cells, hepatocytes, and macrophages. Infect Immun *68*, 6729-6736.

Feng, H.M., Whitworth, T., Olano, J.P., Popov, V.L., and Walker, D.H. (2004). Fc-dependent polyclonal antibodies and antibodies to outer membrane proteins A and B, but not to lipopolysaccharide, protect SCID mice against fatal *Rickettsia conorii* infection. Infect Immun *72*, 2222-2228.

Fernandez-Moreira, E., Helbig, J.H., and Swanson, M.S. (2006). Membrane vesicles shed by *Legionella pneumophila* inhibit fusion of phagosomes with lysosomes. Infect Immun *74*, 3285-3295.

Ferreira, B.R., and Silva, J.S. (1999). Successive tick infestations selectively promote a T-helper 2 cytokine profile in mice. Immunology *96*, 434-439.

Ferrington, D.A., and Gregerson, D.S. (2012). Immunoproteasomes: structure, function, and antigen presentation. Prog Mol Biol Transl Sci *109*, 75-112.

Fodorova, M., Vadovic, P., Skultety, L., Slaba, K., and Toman, R. (2005). Structural features of lipopolysaccharide from *Rickettsia typhi*: the causative agent of endemic typhus. Ann N Y Acad Sci *1063*, 259-260.

Ford, C., Nans, A., Boucrot, E., and Hayward, R.D. (2018). *Chlamydia* exploits filopodial capture and a macropinocytosis-like pathway for host cell entry. PLoS Pathog *14*, e1007051.

Fournier, P.E., Dumler, J.S., Greub, G., Zhang, J., Wu, Y., and Raoult, D. (2003). Gene sequence-based criteria for identification of new rickettsia isolates and description of *Rickettsia heilongjiangensis* sp. nov. J Clin Microbiol *41*, 5456-5465.

Fournier, P.E., Gouriet, F., Brouqui, P., Lucht, F., and Raoult, D. (2005). Lymphangitis-associated rickettsiosis, a new rickettsiosis caused by *Rickettsia sibirica* mongolotimonae: seven new cases and review of the literature. Clin Infect Dis *40*, 1435-1444.

Fournier, P.E., Jensenius, M., Laferl, H., Vene, S., and Raoult, D. (2002). Kinetics of antibody responses in *Rickettsia africae* and *Rickettsia conorii* infections. Clin Diagn Lab Immunol *9*, 324-328.

Fournier, P.E., and Raoult, D. (2009). Current knowledge on phylogeny and taxonomy of *Rickettsia* spp. Ann N Y Acad Sci *1166*, 1-11.

Friedrich, A., Pechstein, J., Berens, C., and Luhrmann, A. (2017). Modulation of host cell apoptotic pathways by intracellular pathogens. Curr Opin Microbiol *35*, 88-99.

Galley, H.F., and Webster, N.R. (2004). Physiology of the endothelium. Br J Anaesth *93*, 105-113.

Galluzzi, L., Diotallevi, A., and Magnani, M. (2017). Endoplasmic reticulum stress and unfolded protein response in infection by intracellular parasites. Future Sci OA *3*, FSO198.

Galvao, M.A., Silva, L.J., Nascimento, E.M., Calic, S.B., Sousa, R., and Bacellar, F. (2005). [Rickettsial diseases in Brazil and Portugal: occurrence, distribution and diagnosis]. Rev Saude Publica *39*, 850-856.

Gambrill, M.R., and Wisseman, C.L., Jr. (1973a). Mechanisms of immunity in typhus infections. 3. Influence of human immune serum and complement on the fate of *Rickettsia mooseri* within the human macrophages. Infect Immun *8*, 631-640.

Gambrill, M.R., and Wisseman, C.L., Jr. (1973b). Mechanisms of immunity in typhus infections. I. Multiplication of typhus rickettsiae in human macrophage cell cultures in the nonimmune system: influence of virulence of rickettsial strains and of chloramphenicol. Infect Immun *8*, 519-527.

Gao, L.Y., and Kwaik, Y.A. (2000). The modulation of host cell apoptosis by intracellular bacterial pathogens. Trends Microbiol *8*, 306-313.

Gao, Y., Wang, X., Sang, Z., Li, Z., Liu, F., Mao, J., Yan, D., Zhao, Y., Wang, H., Li, P.*, et al.* (2017). Quantitative proteomics by SWATH-MS reveals sophisticated metabolic reprogramming in hepatocellular carcinoma tissues. Sci Rep *7*, 45913.

Gaywee, J., Radulovic, S., Higgins, J.A., and Azad, A.F. (2002a). Transcriptional analysis of *Rickettsia prowazekii* invasion gene homolog (invA) during host cell infection. Infect Immun *70*, 6346-6354.

Gaywee, J., Sacci, J.B., Jr., Radulovic, S., Beier, M.S., and Azad, A.F. (2003). Subcellular localization of rickettsial invasion protein, InvA. Am J Trop Med Hyg *68*, 92-96.

Gaywee, J., Xu, W., Radulovic, S., Bessman, M.J., and Azad, A.F. (2002b). The *Rickettsia prowazekii* invasion gene homolog (invA) encodes a Nudix hydrolase active on adenosine (5')-pentaphospho-(5')-adenosine. Mol Cell Proteomics *1*, 179-185.

Gazi, M., Caro-Gomez, E., Goez, Y., Cespedes, M.A., Hidalgo, M., Correa, P., and Valbuena, G. (2013). Discovery of a protective *Rickettsia prowazekii* antigen recognized by CD8+ T cells, RP884, using an in vivo screening platform. PLoS One *8*, e76253.

Ge, H., Chuang, Y.Y., Zhao, S., Temenak, J.J., and Ching, W.M. (2003). Genomic studies of *Rickettsia prowazekii* virulent and avirulent strains. Ann N Y Acad Sci *990*, 671-677.

Gillespie, J.J., Ammerman, N.C., Dreher-Lesnick, S.M., Rahman, M.S., Worley, M.J., Setubal, J.C., Sobral, B.S., and Azad, A.F. (2009). An anomalous type IV secretion system in *Rickettsia* is evolutionarily conserved. PLoS One *4*, e4833.

Gillespie, J.J., Beier, M.S., Rahman, M.S., Ammerman, N.C., Shallom, J.M., Purkayastha, A., Sobral, B.S., and Azad, A.F. (2007). Plasmids and rickettsial evolution: insight from *Rickettsia felis*. PLoS One *2*, e266.

Gillespie, J.J., Joardar, V., Williams, K.P., Driscoll, T., Hostetler, J.B., Nordberg, E., Shukla, M., Walenz, B., Hill, C.A., Nene, V.M*., et al.* (2012a). A *Rickettsia* genome overrun by mobile genetic elements provides insight into the acquisition of genes characteristic of an obligate intracellular lifestyle. J Bacteriol *194*, 376-394.

Gillespie, J.J., Kaur, S.J., Rahman, M.S., Rennoll-Bankert, K., Sears, K.T., Beier-Sexton, M., and Azad, A.F. (2015a). Secretome of obligate intracellular *Rickettsia*. FEMS Microbiol Rev *39*, 47-80.

Gillespie, J.J., Norberg, E., Azad, A.F., and Sobral, B.S. (2012b). Phylogeny and Comparative Genomics: the Shifting Landscape in the Genomics Era. In Intracellular Pathogens II: Rickettsiales, G.H. Palmer, and A.F. Azad, eds. (ASM Press), pp. 84-141.

Gillespie, J.J., Phan, I.Q., Driscoll, T.P., Guillotte, M.L., Lehman, S.S., Rennoll-Bankert, K.E., Subramanian, S., Beier-Sexton, M., Myler, P.J., Rahman, M.S*., et al.* (2016). The *Rickettsia* type IV secretion system: unrealized complexity mired by gene family expansion. Pathog Dis *74*.

Gillespie, J.J., Phan, I.Q., Scheib, H., Subramanian, S., Edwards, T.E., Lehman, S.S., Piitulainen, H., Rahman, M.S., Rennoll-Bankert, K.E., Staker, B.L*., et al.* (2015b). Structural Insight into How Bacteria Prevent Interference between Multiple Divergent Type IV Secretion Systems. MBio *6*, e01867-01815.

Gillespie, J.J., Williams, K., Shukla, M., Snyder, E.E., Nordberg, E.K., Ceraul, S.M., Dharmanolla, C., Rainey, D., Soneja, J., Shallom, J.M*., et al.* (2008). *Rickettsia* phylogenomics: unwinding the intricacies of obligate intracellular life. PLoS One *3*, e2018.

Gillespie, R.D., Dolan, M.C., Piesman, J., and Titus, R.G. (2001). Identification of an IL-2 binding protein in the saliva of the Lyme disease vector tick, *Ixodes scapularis*. J Immunol *166*, 4319-4326.

Gillet, L.C., Navarro, P., Tate, S., Rost, H., Selevsek, N., Reiter, L., Bonner, R., and Aebersold, R. (2012). Targeted data extraction of the MS/MS spectra generated by data-independent acquisition: a new concept for consistent and accurate proteome analysis. Molecular & cellular proteomics : MCP *11*, O111 016717.

Gimenez, D.F. (1964). Staining Rickettsiae in Yolk-Sac Cultures. Stain Technol *39*, 135-140.

Giri, J., Srivastav, S., Basu, M., Palit, S., Gupta, P., and Ukil, A. (2016). *Leishmania donovani* Exploits Myeloid Cell Leukemia 1 (MCL-1) Protein to Prevent Mitochondria-dependent Host Cell Apoptosis. J Biol Chem *291*, 3496-3507.

Goddard, J. (2009). Historical and recent evidence for close relationships among *Rickettsia parkeri*, *R. conorii*, *R. africae*, and *R. sibirica*: implications for rickettsial taxonomy. J Vector Ecol *34*, 238-242.

Gogos, C.A., Drosou, E., Bassaris, H.P., and Skoutelis, A. (2000). Pro- versus anti-inflammatory cytokine profile in patients with severe sepsis: a marker for prognosis and future therapeutic options. J Infect Dis *181*, 176-180.

Goldberg, M.B. (2001). Actin-based motility of intracellular microbial pathogens. Microbiol Mol Biol Rev *65*, 595-626, table of contents.

Goodwin, C.M., Xu, S., and Munger, J. (2015). Stealing the Keys to the Kitchen: Viral Manipulation of the Host Cell Metabolic Network. Trends Microbiol *23*, 789-798.

Gouin, E., Gantelet, H., Egile, C., Lasa, I., Ohayon, H., Villiers, V., Gounon, P., Sansonetti, P.J., and Cossart, P. (1999). A comparative study of the actin-based motilities of the pathogenic bacteria *Listeria monocytogenes*, *Shigella flexneri* and *Rickettsia conorii*. J Cell Sci *112 (Pt 11)*, 1697-1708.

Gray, J.X., Haino, M., Roth, M.J., Maguire, J.E., Jensen, P.N., Yarme, A., Stetler-Stevenson, M.A., Siebenlist, U., and Kelly, K. (1996). CD97 is a processed, seven-transmembrane, heterodimeric receptor associated with inflammation. J Immunol *157*, 5438-5447.

Gross, D., and Schafer, G. (2011). 100th anniversary of the death of Ricketts: Howard Taylor Ricketts (1871-1910). The namesake of the Rickettsiaceae family. Microbes Infect *13*, 10-13.

Gutierrez-Aguilar, M., and Baines, C.P. (2013). Physiological and pathological roles of mitochondrial SLC25 carriers. Biochem J *454*, 371-386.

Hackstadt, T. (1996). The biology of rickettsiae. Infect Agents Dis *5*, 127-143.

Haglund, C.M., Choe, J.E., Skau, C.T., Kovar, D.R., and Welch, M.D. (2010). *Rickettsia* Sca2 is a bacterial formin-like mediator of actin-based motility. Nat Cell Biol *12*, 1057-1063.

Hahn, I., Klaus, A., Janze, A.K., Steinwede, K., Ding, N., Bohling, J., Brumshagen, C., Serrano, H., Gauthier, F., Paton, J.C*., et al.* (2011). Cathepsin G and neutrophil elastase play critical and nonredundant roles in lung-protective immunity against Streptococcus pneumoniae in mice. Infect Immun *79*, 4893-4901.

Halazonetis, T.D., Georgopoulos, K., Greenberg, M.E., and Leder, P. (1988). c-Jun dimerizes with itself and with c-Fos, forming complexes of different DNA binding affinities. Cell *55*, 917-924.

Han, S.C., Guo, H.C., Sun, S.Q., Jin, Y., Wei, Y.Q., Feng, X., Yao, X.P., Cao, S.Z., Xiang Liu, D., and Liu, X.T. (2016). Productive Entry of Foot-and-Mouth Disease Virus via Macropinocytosis Independent of Phosphatidylinositol 3-Kinase. Sci Rep *6*, 19294.

Hannemann, S., and Galan, J.E. (2017). *Salmonella enterica* serovar-specific transcriptional reprogramming of infected cells. PLoS Pathog *13*, e1006532.

Hannemann, S., Gao, B., and Galan, J.E. (2013). *Salmonella* modulation of host cell gene expression promotes its intracellular growth. PLoS Pathog *9*, e1003668.

Harris, E.K., Jirakanwisal, K., Verhoeve, V.I., Fongsaran, C., Suwanbongkot, C., Welch, M.D., and Macaluso, K.R. (2018). The role of Sca2 and RickA in the dissemination of *Rickettsia parkeri* in *Amblyomma maculatum*. Infect Immun.

Harris, E.K., Verhoeve, V.I., Banajee, K.H., Macaluso, J.A., Azad, A.F., and Macaluso, K.R. (2017). Comparative vertical transmission of *Rickettsia* by *Dermacentor variabilis* and *Amblyomma maculatum*. Ticks Tick Borne Dis *8*, 598-604.

Haschemi, A., Kosma, P., Gille, L., Evans, C.R., Burant, C.F., Starkl, P., Knapp, B., Haas, R., Schmid, J.A., Jandl, C.*, et al.* (2012). The sedoheptulose kinase CARKL directs macrophage polarization through control of glucose metabolism. Cell Metab *15*, 813-826.

Hayes, S.F., Burgdorfer, W., and Aeschlimann, A. (1980). Sexual transmission of spotted fever group rickettsiae by infected male ticks: detection of rickettsiae in immature spermatozoa of Ixodes ricinus. Infect Immun *27*, 638-642.

Herrington, F.D., and Nibbs, R.J. (2016). Regulation of the Adaptive Immune Response by the IkappaB Family Protein Bcl-3. Cells *5*.

Hess, J., Angel, P., and Schorpp-Kistner, M. (2004). AP-1 subunits: quarrel and harmony among siblings. J Cell Sci *117*, 5965-5973.

Hetz, C., and Papa, F.R. (2018). The Unfolded Protein Response and Cell Fate Control. Mol Cell *69*, 169-181.

Hillman, R.D., Jr., Baktash, Y.M., and Martinez, J.J. (2013). OmpA-mediated rickettsial adherence to and invasion of human endothelial cells is dependent upon interaction with alpha2beta1 integrin. Cell Microbiol *15*, 727-741.

Hirayama, D., Iida, T., and Nakase, H. (2017). The Phagocytic Function of Macrophage-Enforcing Innate Immunity and Tissue Homeostasis. Int J Mol Sci *19*.

Houten, S.M., and Wanders, R.J. (2010). A general introduction to the biochemistry of mitochondrial fatty acid beta-oxidation. J Inherit Metab Dis *33*, 469-477.

Huang da, W., Sherman, B.T., and Lempicki, R.A. (2009). Systematic and integrative analysis of large gene lists using DAVID bioinformatics resources. Nat Protoc *4*, 44-57.

Husband, A.J. (2001). Overview of the mammalian immune system. Adv Nutr Res *10*, 3-14.

Infantino, V., Convertini, P., Cucci, L., Panaro, M.A., Di Noia, M.A., Calvello, R., Palmieri, F., and Iacobazzi, V. (2011). The mitochondrial citrate carrier: a new player in inflammation. Biochem J *438*, 433-436.

Janeway, C.A., Jr., and Medzhitov, R. (2002). Innate immune recognition. Annu Rev Immunol *20*, 197-216.

Jang, W.J., Choi, Y.J., Kim, J.H., Jung, K.D., Ryu, J.S., Lee, S.H., Yoo, C.K., Paik, H.S., Choi, M.S., Park, K.H.*, et al.* (2005). Seroepidemiology of spotted fever group and typhus group rickettsioses in humans, South Korea. Microbiol Immunol *49*, 17-24.

Janssens, S., Pulendran, B., and Lambrecht, B.N. (2014). Emerging functions of the unfolded protein response in immunity. Nat Immunol *15*, 910-919.

Jeng, R.L., Goley, E.D., D'Alessio, J.A., Chaga, O.Y., Svitkina, T.M., Borisy, G.G., Heinzen, R.A., and Welch, M.D. (2004). A *Rickettsia* WASP-like protein activates the Arp2/3 complex and mediates actin-based motility. Cell Microbiol *6*, 761-769.

Jensenius, M., Fournier, P.E., Vene, S., Hoel, T., Hasle, G., Henriksen, A.Z., Hellum, K.B., Raoult, D., Myrvang, B., and Norwegian African Tick Bite Fever Study, G. (2003). African tick bite fever in travelers to rural sub-Equatorial Africa. Clin Infect Dis *36*, 1411-1417.

Jensenius, M., Hasle, G., Henriksen, A.Z., Vene, S., Raoult, D., Bruu, A.L., and Myrvang, B. (1999). African tick-bite fever imported into Norway: presentation of 8 cases. Scand J Infect Dis *31*, 131-133.

Jha, A.K., Huang, S.C., Sergushichev, A., Lampropoulou, V., Ivanova, Y., Loginicheva, E., Chmielewski, K., Stewart, K.M., Ashall, J., Everts, B.*, et al.* (2015). Network integration of parallel metabolic and transcriptional data reveals metabolic modules that regulate macrophage polarization. Immunity *42*, 419-430.

John Von Freyend, S., Kwok-Schuelein, T., Netter, H.J., Haqshenas, G., Semblat, J.P., and Doerig, C. (2017). Subverting Host Cell P21-Activated Kinase: A Case of Convergent Evolution across Pathogens. Pathogens *6*.

Jordan, J.M., Woods, M.E., Feng, H.M., Soong, L., and Walker, D.H. (2007). Rickettsiae-stimulated dendritic cells mediate protection against lethal rickettsial challenge in an animal model of spotted fever rickettsiosis. J Infect Dis *196*, 629-638.

Jordan, J.M., Woods, M.E., Soong, L., and Walker, D.H. (2009). Rickettsiae stimulate dendritic cells through toll-like receptor 4, leading to enhanced NK cell activation in vivo. J Infect Dis *199*, 236-242.

Jordan, T.X., and Randall, G. (2017). Dengue Virus Activates the AMP Kinase-mTOR Axis To Stimulate a Proviral Lipophagy. J Virol *91*.

Joshi, S.G., Francis, C.W., Silverman, D.J., and Sahni, S.K. (2003). Nuclear factor kappa B protects against host cell apoptosis during *Rickettsia rickettsii* infection by inhibiting activation of apical and effector caspases and maintaining mitochondrial integrity. Infect Immun *71*, 4127-4136.

Joshi, S.G., Francis, C.W., Silverman, D.J., and Sahni, S.K. (2004). NF-kappaB activation suppresses host cell apoptosis during *Rickettsia rickettsii* infection via regulatory effects on intracellular localization or levels of apoptogenic and anti-apoptotic proteins. FEMS Microbiol Lett *234*, 333-341.

Kalamida, D., Karagounis, I.V., Giatromanolaki, A., and Koukourakis, M.I. (2014). Important role of autophagy in endothelial cell response to ionizing radiation. PLoS One *9*, e102408.

Kalin, S., Amstutz, B., Gastaldelli, M., Wolfrum, N., Boucke, K., Havenga, M., DiGennaro, F., Liska, N., Hemmi, S., and Greber, U.F. (2010). Macropinocytotic uptake and infection of human epithelial cells with species B2 adenovirus type 35. J Virol *84*, 5336-5350.

Kalliolias, G.D., and Ivashkiv, L.B. (2016). TNF biology, pathogenic mechanisms and emerging therapeutic strategies. Nat Rev Rheumatol *12*, 49-62.

Kanehisa, M., Furumichi, M., Tanabe, M., Sato, Y., and Morishima, K. (2017). KEGG: new perspectives on genomes, pathways, diseases and drugs. Nucleic Acids Res *45*, D353-D361.

Kaplanski, G., Teysseire, N., Farnarier, C., Kaplanski, S., Lissitzky, J.C., Durand, J.M., Soubeyrand, J., Dinarello, C.A., and Bongrand, P. (1995). IL-6 and IL-8 production from cultured human endothelial cells stimulated by infection with *Rickettsia conorii* via a cell-associated IL-1 alpha-dependent pathway. J Clin Invest *96*, 2839-2844.

Karin, M., and Lin, A. (2002). NF-kappaB at the crossroads of life and death. Nat Immunol *3*, 221-227.

Kaur, G., and Batra, S. (2016). Emerging role of immunoproteasomes in pathophysiology. Immunol Cell Biol *94*, 812-820.

Kawai, T., and Akira, S. (2010). The role of pattern-recognition receptors in innate immunity: update on Toll-like receptors. Nat Immunol *11*, 373-384.

Kelly, D.J., Richards, A.L., Temenak, J., Strickman, D., and Dasch, G.A. (2002). The past and present threat of rickettsial diseases to military medicine and international public health. Clin Infect Dis *34*, S145-169.

Kerr, M.C., and Teasdale, R.D. (2009). Defining macropinocytosis. Traffic *10*, 364-371.

Ketavarapu, J.M., Rodriguez, A.R., Yu, J.J., Cong, Y., Murthy, A.K., Forsthuber, T.G., Guentzel, M.N., Klose, K.E., Berton, M.T., and Arulanandam, B.P. (2008). Mast cells inhibit intramacrophage *Francisella tularensis* replication via contact and secreted products including IL-4. Proc Natl Acad Sci U S A *105*, 9313-9318.

Kim, B.H., Shenoy, A.R., Kumar, P., Bradfield, C.J., and MacMicking, J.D. (2012). IFN-inducible GTPases in host cell defense. Cell Host Microbe *12*, 432-444.

Kim, M., Otsubo, R., Morikawa, H., Nishide, A., Takagi, K., Sasakawa, C., and Mizushima, T. (2014). Bacterial effectors and their functions in the ubiquitin-proteasome system: insight from the modes of substrate recognition. Cells *3*, 848-864.

Kleba, B., Clark, T.R., Lutter, E.I., Ellison, D.W., and Hackstadt, T. (2010). Disruption of the *Rickettsia rickettsii* Sca2 autotransporter inhibits actin-based motility. Infect Immun *78*, 2240-2247.

Korkmaz, B., Horwitz, M.S., Jenne, D.E., and Gauthier, F. (2010). Neutrophil elastase, proteinase 3, and cathepsin G as therapeutic targets in human diseases. Pharmacol Rev *62*, 726-759.

Kotsyfakis, M., Sa-Nunes, A., Francischetti, I.M., Mather, T.N., Andersen, J.F., and Ribeiro, J.M. (2006). Antiinflammatory and immunosuppressive activity of sialostatin L, a salivary cystatin from the tick Ixodes scapularis. J Biol Chem *281*, 26298-26307.

Krachler, A.M., Woolery, A.R., and Orth, K. (2011). Manipulation of kinase signaling by bacterial pathogens. J Cell Biol *195*, 1083-1092.

Kramer, A., Green, J., Pollard, J., Jr., and Tugendreich, S. (2014). Causal analysis approaches in Ingenuity Pathway Analysis. Bioinformatics *30*, 523-530.

Krawczyk, C.M., Holowka, T., Sun, J., Blagih, J., Amiel, E., DeBerardinis, R.J., Cross, J.R., Jung, E., Thompson, C.B., Jones, R.G*., et al.* (2010). Toll-like receptor-induced changes in glycolytic metabolism regulate dendritic cell activation. Blood *115*, 4742-4749.

Krombach, F., Munzing, S., Allmeling, A.M., Gerlach, J.T., Behr, J., and Dorger, M. (1997). Cell size of alveolar macrophages: an interspecies comparison. Environ Health Perspect *105 Suppl 5*, 1261-1263.

Kuhn, S., Lopez-Montero, N., Chang, Y.Y., Sartori-Rupp, A., and Enninga, J. (2017). Imaging macropinosomes during *Shigella* infections. Methods *127*, 12-22.

La Scola, B., and Raoult, D. (1997). Laboratory diagnosis of rickettsioses: current approaches to diagnosis of old and new rickettsial diseases. J Clin Microbiol *35*, 2715-2727.

Lambert, J.P., Ivosev, G., Couzens, A.L., Larsen, B., Taipale, M., Lin, Z.Y., Zhong, Q., Lindquist, S., Vidal, M., Aebersold, R*., et al.* (2013). Mapping differential interactomes by affinity purification coupled with data-independent mass spectrometry acquisition. Nature methods *10*, 1239-1245.

Lateef, Z., Gimenez, G., Baker, E.S., and Ward, V.K. (2017). Transcriptomic analysis of human norovirus NS1-2 protein highlights a multifunctional role in murine monocytes. BMC Genomics *18*, 39.

Lee, S.Y., and Choi, Y. (2007). TRAF1 and its biological functions. Adv Exp Med Biol *597*, 25-31.

Leemans, J.C., te Velde, A.A., Florquin, S., Bennink, R.J., de Bruin, K., van Lier, R.A., van der Poll, T., and Hamann, J. (2004). The epidermal growth factor-seven transmembrane (EGF-TM7) receptor CD97 is required for neutrophil migration and host defense. J Immunol *172*, 1125-1131.

Leick, M., Azcutia, V., Newton, G., and Luscinskas, F.W. (2014). Leukocyte recruitment in inflammation: basic concepts and new mechanistic insights based on new models and microscopic imaging technologies. Cell Tissue Res *355*, 647-656.

Leisching, G., Pietersen, R.D., Mpongoshe, V., van Heerden, C., van Helden, P., Wiid, I., and Baker, B. (2016). The Host Response to a Clinical MDR Mycobacterial Strain Cultured in a Detergent-Free Environment: A Global Transcriptomics Approach. PLoS One *11*, e0153079.

Li, H., and Walker, D.H. (1998). rOmpA is a critical protein for the adhesion of *Rickettsia rickettsii* to host cells. Microb Pathog *24*, 289-298.

Li, M., Gustchina, A., Cruz, R., Simoes, M., Curto, P., Martinez, J., Faro, C., Simoes, I., and Wlodawer, A. (2015). Structure of RC1339/APRc from *Rickettsia conorii*, a retropepsin-like aspartic protease. Acta Crystallogr D Biol Crystallogr *71*, 2109-2118.

Li, Q., and Verma, I.M. (2002). NF-kappaB regulation in the immune system. Nat Rev Immunol *2*, 725-734.

Li, Y., Shah-Simpson, S., Okrah, K., Belew, A.T., Choi, J., Caradonna, K.L., Padmanabhan, P., Ndegwa, D.M., Temanni, M.R., Corrada Bravo, H.*, et al.* (2016). Transcriptome Remodeling in *Trypanosoma cruzi* and Human Cells during Intracellular Infection. PLoS Pathog *12*, e1005511.

Liberali, P., Kakkonen, E., Turacchio, G., Valente, C., Spaar, A., Perinetti, G., Bockmann, R.A., Corda, D., Colanzi, A., Marjomaki, V.*, et al.* (2008). The closure of Pak1-dependent macropinosomes requires the phosphorylation of CtBP1/BARS. EMBO J *27*, 970-981.

Lin, J.H., Walter, P., and Yen, T.S. (2008). Endoplasmic reticulum stress in disease pathogenesis. Annu Rev Pathol *3*, 399-425.

Liu, P.S., Wang, H., Li, X., Chao, T., Teav, T., Christen, S., Di Conza, G., Cheng, W.C., Chou, C.H., Vavakova, M.*, et al.* (2017). alpha-ketoglutarate orchestrates macrophage activation through metabolic and epigenetic reprogramming. Nat Immunol *18*, 985-994.

Lohoefer, F., Reeps, C., Lipp, C., Rudelius, M., Haertl, F., Matevossian, E., Zernecke, A., Eckstein, H.H., and Pelisek, J. (2014). Quantitative expression and localization of cysteine and aspartic proteases in human abdominal aortic aneurysms. Exp Mol Med *46*, e95.

Lommano, E., Bertaiola, L., Dupasquier, C., and Gern, L. (2012). Infections and coinfections of questing *Ixodes ricinus* ticks by emerging zoonotic pathogens in Western Switzerland. Appl Environ Microbiol *78*, 4606-4612.

Lommano, E., Dvorak, C., Vallotton, L., Jenni, L., and Gern, L. (2014). Tick-borne pathogens in ticks collected from breeding and migratory birds in Switzerland. Ticks Tick Borne Dis *5*, 871-882.

Luce-Fedrow, A., Mullins, K., Kostik, A.P., St John, H.K., Jiang, J., and Richards, A.L. (2015). Strategies for detecting rickettsiae and diagnosing rickettsial diseases. Future Microbiol *10*, 537-564.

Lutay, N., Ambite, I., Gronberg Hernandez, J., Rydstrom, G., Ragnarsdottir, B., Puthia, M., Nadeem, A., Zhang, J., Storm, P., Dobrindt, U.*, et al.* (2013). Bacterial control of host gene expression through RNA polymerase II. J Clin Invest *123*, 2366-2379.

Macaluso, K.R., Sonenshine, D.E., Ceraul, S.M., and Azad, A.F. (2002). Rickettsial infection in *Dermacentor variabilis* (Acari: *Ixodidae*) inhibits transovarial transmission of a second *Rickettsia*. J Med Entomol *39*, 809-813.

Madeddu, G., Mancini, F., Caddeo, A., Ciervo, A., Babudieri, S., Maida, I., Fiori, M.L., Rezza, G., and Mura, M.S. (2012). *Rickettsia monacensis* as cause of Mediterranean spotted fever-like illness, Italy. Emerg Infect Dis *18*, 702-704.

Mahajan, S.K. (2012). Rickettsial diseases. J Assoc Physicians India *60*, 37-44.

Mahony, R., Ahmed, S., Diskin, C., and Stevenson, N.J. (2016). SOCS3 revisited: a broad regulator of disease, now ready for therapeutic use? Cell Mol Life Sci *73*, 3323-3336.

Malandrino, M.I., Fucho, R., Weber, M., Calderon-Dominguez, M., Mir, J.F., Valcarcel, L., Escote, X., Gomez-Serrano, M., Peral, B., Salvado, L.*, et al.* (2015). Enhanced fatty acid oxidation in adipocytes and macrophages reduces lipid-induced triglyceride accumulation and inflammation. Am J Physiol Endocrinol Metab *308*, E756-769.

Manadas, B., Santos, A.R., Szabadfi, K., Gomes, J.R., Garbis, S.D., Fountoulakis, M., and Duarte, C.B. (2009). BDNF-induced changes in the expression of the translation machinery in hippocampal neurons: protein levels and dendritic mRNA. Journal of proteome research *8*, 4536-4552.

Mansueto, P., Vitale, G., Cascio, A., Seidita, A., Pepe, I., Carroccio, A., di Rosa, S., Rini, G.B., Cillari, E., and Walker, D.H. (2012). New insight into immunity and immunopathology of Rickettsial diseases. Clin Dev Immunol *2012*, 967852.

Martin, M. (2011). Cutadapt removes adapter sequences from high-throughput sequencing reads. EmbNet Journal.

Martinez, F.O., and Gordon, S. (2014). The M1 and M2 paradigm of macrophage activation: time for reassessment. F1000Prime Rep *6*, 13.

Martinez, J.J., and Cossart, P. (2004). Early signaling events involved in the entry of *Rickettsia conorii* into mammalian cells. J Cell Sci *117*, 5097-5106.

Martinez, J.J., Seveau, S., Veiga, E., Matsuyama, S., and Cossart, P. (2005). Ku70, a component of DNA-dependent protein kinase, is a mammalian receptor for *Rickettsia conorii*. Cell *123*, 1013-1023.

Martins, A.S., Alves, I., Helguero, L., Domingues, M.R., and Neves, B.M. (2016). The Unfolded Protein Response in Homeostasis and Modulation of Mammalian Immune Cells. Int Rev Immunol *35*, 457-476.

Martiny-Baron, G., Kazanietz, M.G., Mischak, H., Blumberg, P.M., Kochs, G., Hug, H., Marme, D., and Schachtele, C. (1993). Selective inhibition of protein kinase C isozymes by the indolocarbazole Go 6976. J Biol Chem *268*, 9194-9197.

Masereel, B., Pochet, L., and Laeckmann, D. (2003). An overview of inhibitors of Na(+)/H(+) exchanger. Eur J Med Chem *38*, 547-554.

McCarthy, M.K., and Weinberg, J.B. (2015). The immunoproteasome and viral infection: a complex regulator of inflammation. Front Microbiol *6*, 21.

McClure, E.E., Chavez, A.S.O., Shaw, D.K., Carlyon, J.A., Ganta, R.R., Noh, S.M., Wood, D.O., Bavoil, P.M., Brayton, K.A., Martinez, J.J.*, et al.* (2017). Engineering of obligate intracellular bacteria: progress, challenges and paradigms. Nat Rev Microbiol *15*, 544-558.

McCutcheon, J.P., and Moran, N.A. (2011). Extreme genome reduction in symbiotic bacteria. Nat Rev Microbiol *10*, 13-26.

McLeod, M.P., Qin, X., Karpathy, S.E., Gioia, J., Highlander, S.K., Fox, G.E., McNeill, T.Z., Jiang, H., Muzny, D., Jacob, L.S.*, et al.* (2004). Complete genome sequence of *Rickettsia typhi* and comparison with sequences of other rickettsiae. J Bacteriol *186*, 5842-5855.

McNeela, E.A., and Mills, K.H. (2001). Manipulating the immune system: humoral versus cell-mediated immunity. Adv Drug Deliv Rev *51*, 43-54.

McQuiston, J., and Paddock, C. (2012). Public Health: Rickettsial Infections and Epidemiology. In Intracellular Pathogens II: Rickettsiales, G.H. Palmer, and A.F. Azad, eds. (ASM Press), pp. 40-83.

McQuiston, J.H., Knights, E.B., Demartino, P.J., Paparello, S.F., Nicholson, W.L., Singleton, J., Brown, C.M., Massung, R.F., and Urbanowski, J.C. (2010). Brill-Zinsser disease in a patient following infection with sylvatic epidemic typhus associated with flying squirrels. Clin Infect Dis *51*, 712-715.

McQuiston, J.H., Zemtsova, G., Perniciaro, J., Hutson, M., Singleton, J., Nicholson, W.L., and Levin, M.L. (2012). Afebrile spotted fever group *Rickettsia* infection after a bite from a *Dermacentor variabilis* tick infected with *Rickettsia montanensis*. Vector Borne Zoonotic Dis *12*, 1059-1061.

Mege, J.L., Mehraj, V., and Capo, C. (2011). Macrophage polarization and bacterial infections. Curr Opin Infect Dis *24*, 230-234.

Mendonca, A.G., Alves, R.J., and Pereira-Leal, J.B. (2011). Loss of genetic redundancy in reductive genome evolution. PLoS Comput Biol *7*, e1001082.

Mercer, J., and Helenius, A. (2009). Virus entry by macropinocytosis. Nat Cell Biol *11*, 510-520.

Mercer, J., and Helenius, A. (2012). Gulping rather than sipping: macropinocytosis as a way of virus entry. Curr Opin Microbiol *15*, 490-499.

Merhej, V., and Raoult, D. (2011). Rickettsial evolution in the light of comparative genomics. Biol Rev Camb Philos Soc *86*, 379-405.

Michalek, R.D., Gerriets, V.A., Jacobs, S.R., Macintyre, A.N., MacIver, N.J., Mason, E.F., Sullivan, S.A., Nichols, A.G., and Rathmell, J.C. (2011). Cutting edge: distinct glycolytic and lipid oxidative metabolic programs are essential for effector and regulatory CD4+ T cell subsets. J Immunol *186*, 3299-3303.

Michelucci, A., Cordes, T., Ghelfi, J., Pailot, A., Reiling, N., Goldmann, O., Binz, T., Wegner, A., Tallam, A., Rausell, A.*, et al.* (2013). Immune-responsive gene 1 protein links metabolism to immunity by catalyzing itaconic acid production. Proc Natl Acad Sci U S A *110*, 7820-7825.

Mills, E.L., Kelly, B., Logan, A., Costa, A.S.H., Varma, M., Bryant, C.E., Tourlomousis, P., Dabritz, J.H.M., Gottlieb, E., Latorre, I.*, et al.* (2016). Succinate Dehydrogenase Supports Metabolic Repurposing of Mitochondria to Drive Inflammatory Macrophages. Cell *167*, 457-470 e413.

Mills, E.L., and O'Neill, L.A. (2016). Reprogramming mitochondrial metabolism in macrophages as an anti-inflammatory signal. Eur J Immunol *46*, 13-21.

Misra, S., Tripathi, M.K., and Chaudhuri, G. (2005). Down-regulation of 7SL RNA expression and impairment of vesicular protein transport pathways by Leishmania infection of macrophages. J Biol Chem *280*, 29364-29373.

Miyata, Y., Nishida, E., Koyasu, S., Yahara, I., and Sakai, H. (1989). Protein kinase C-dependent and -independent pathways in the growth factor-induced cytoskeletal reorganization. J Biol Chem *264*, 15565-15568.

Modolell, M., Corraliza, I.M., Link, F., Soler, G., and Eichmann, K. (1995). Reciprocal regulation of the nitric oxide synthase/arginase balance in mouse bone marrow-derived macrophages by TH1 and TH2 cytokines. Eur J Immunol *25*, 1101-1104.

Mogensen, T.H. (2009). Pathogen recognition and inflammatory signaling in innate immune defenses. Clin Microbiol Rev *22*, 240-273, Table of Contents.

Moncayo, A.C., Cohen, S.B., Fritzen, C.M., Huang, E., Yabsley, M.J., Freye, J.D., Dunlap, B.G., Huang, J., Mead, D.G., Jones, T.F.*, et al.* (2010). Absence of *Rickettsia rickettsii* and occurrence of other spotted fever group rickettsiae in ticks from Tennessee. Am J Trop Med Hyg *83*, 653-657.

Montgomery, R.R., Lusitani, D., De Boisfleury Chevance, A., and Malawista, S.E. (2004). Tick saliva reduces adherence and area of human neutrophils. Infect Immun *72*, 2989-2994.

Moon, J.S., Lee, S., Park, M.A., Siempos, II, Haslip, M., Lee, P.J., Yun, M., Kim, C.K., Howrylak, J., Ryter, S.W.*, et al.* (2015). UCP2-induced fatty acid synthase promotes NLRP3 inflammasome activation during sepsis. J Clin Invest *125*, 665-680.

Mourembou, G., Lekana-Douki, J.B., Mediannikov, O., Nzondo, S.M., Kouna, L.C., Essone, J.C., Fenollar, F., and Raoult, D. (2015). Possible Role of *Rickettsia felis* in Acute Febrile Illness among Children in Gabon. Emerg Infect Dis *21*, 1808-1815.

Mukaida, N., Wang, Y.Y., and Li, Y.Y. (2011). Roles of Pim-3, a novel survival kinase, in tumorigenesis. Cancer Sci *102*, 1437-1442.

Mukhopadhyay, S., Pluddemann, A., and Gordon, S. (2009). Macrophage pattern recognition receptors in immunity, homeostasis and self tolerance. Adv Exp Med Biol *653*, 1-14.

Munder, M., Eichmann, K., and Modolell, M. (1998). Alternative metabolic states in murine macrophages reflected by the nitric oxide synthase/arginase balance: competitive regulation by CD4+ T cells correlates with Th1/Th2 phenotype. J Immunol *160*, 5347-5354.

Murphy, K., and Weaver, C. (2017). Basic Concepts of Immunology. In Janeway's Immunobiology, D. Schanck, M. Toledo, A. Bochicchio, and C. Acevedo-Quiñones, eds. (Garland Science), pp. 1-36.

Murray, G.G., Weinert, L.A., Rhule, E.L., and Welch, J.J. (2016). The Phylogeny of *Rickettsia* Using Different Evolutionary Signatures: How Tree-Like is Bacterial Evolution? Syst Biol *65*, 265-279.

Murray, P.J., Allen, J.E., Biswas, S.K., Fisher, E.A., Gilroy, D.W., Goerdt, S., Gordon, S., Hamilton, J.A., Ivashkiv, L.B., Lawrence, T.*, et al.* (2014). Macrophage activation and polarization: nomenclature and experimental guidelines. Immunity *41*, 14-20.

Murray, P.J., and Wynn, T.A. (2011). Protective and pathogenic functions of macrophage subsets. Nat Rev Immunol *11*, 723-737.

Narayana, Y., and Balaji, K.N. (2008). NOTCH1 up-regulation and signaling involved in *Mycobacterium bovis* BCG-induced SOCS3 expression in macrophages. J Biol Chem *283*, 12501-12511.

Narlik-Grassow, M., Blanco-Aparicio, C., and Carnero, A. (2014). The PIM family of serine/threonine kinases in cancer. Med Res Rev *34*, 136-159.

Narra, H.P., Schroeder, C.L., Sahni, A., Rojas, M., Khanipov, K., Fofanov, Y., and Sahni, S.K. (2016). Small Regulatory RNAs of *Rickettsia conorii*. Sci Rep *6*, 36728.

Newton, K., and Dixit, V.M. (2012). Signaling in innate immunity and inflammation. Cold Spring Harb Perspect Biol *4*.

Niebylski, M.L., Peacock, M.G., and Schwan, T.G. (1999). Lethal effect of *Rickettsia rickettsii* on its tick vector (*Dermacentor andersoni*). Appl Environ Microbiol *65*, 773-778.

Niebylski, M.L., Schrumpf, M.E., Burgdorfer, W., Fischer, E.R., Gage, K.L., and Schwan, T.G. (1997). *Rickettsia peacockii* sp. nov., a new species infecting wood ticks, *Dermacentor andersoni*, in western Montana. Int J Syst Bacteriol *47*, 446-452.

Nogueras, M.M., Cardenosa, N., Sanfeliu, I., Munoz, T., Font, B., and Segura, F. (2006). Serological evidence of infection with *Rickettsia typhi* and *Rickettsia felis* among the human population of Catalonia, in the northeast of Spain. Am J Trop Med Hyg *74*, 123-126.

O'Neill, L.A., Kishton, R.J., and Rathmell, J. (2016). A guide to immunometabolism for immunologists. Nat Rev Immunol *16*, 553-565.

O'Neill, L.A., and Pearce, E.J. (2016). Immunometabolism governs dendritic cell and macrophage function. J Exp Med *213*, 15-23.

Ogata, H., Audic, S., Renesto-Audiffren, P., Fournier, P.E., Barbe, V., Samson, D., Roux, V., Cossart, P., Weissenbach, J., Claverie, J.M.*, et al.* (2001). Mechanisms of evolution in *Rickettsia conorii* and *R. prowazekii*. Science *293*, 2093-2098.

Ogata, H., La Scola, B., Audic, S., Renesto, P., Blanc, G., Robert, C., Fournier, P.E., Claverie, J.M., and Raoult, D. (2006). Genome sequence of *Rickettsia bellii* illuminates the role of amoebae in gene exchanges between intracellular pathogens. PLoS Genet *2*, e76.

Olano, J.P. (2005). Rickettsial infections. Ann N Y Acad Sci *1063*, 187-196.

Osterloh, A. (2017). Immune response against rickettsiae: lessons from murine infection models. Med Microbiol Immunol *206*, 403-417.

Osterloh, A., Papp, S., Moderzynski, K., Kuehl, S., Richardt, U., and Fleischer, B. (2016). Persisting *Rickettsia typhi* Causes Fatal Central Nervous System Inflammation. Infect Immun *84*, 1615-1632.

Oteo, J.A., and Portillo, A. (2012). Tick-borne rickettsioses in Europe. Ticks Tick Borne Dis *3*, 271-278.

Oviedo-Boyso, J., Cortes-Vieyra, R., Huante-Mendoza, A., Yu, H.B., Valdez-Alarcon, J.J., Bravo-Patino, A., Cajero-Juarez, M., Finlay, B.B., and Baizabal-Aguirre, V.M. (2011). The phosphoinositide-3-kinase-Akt signaling pathway is important for *Staphylococcus aureus* internalization by endothelial cells. Infect Immun *79*, 4569-4577.

Ozturk, M.K., Gunes, T., Kose, M., Coker, C., and Radulovic, S. (2003). Rickettsialpox in Turkey. Emerg Infect Dis *9*, 1498-1499.

Paddock, C.D., Zaki, S.R., Koss, T., Singleton, J., Jr., Sumner, J.W., Comer, J.A., Eremeeva, M.E., Dasch, G.A., Cherry, B., and Childs, J.E. (2003). Rickettsialpox in New York City: a persistent urban zoonosis. Ann N Y Acad Sci *990*, 36-44.

Pallen, M.J., and Wren, B.W. (2007). Bacterial pathogenomics. Nature *449*, 835-842.

Palmieri, F. (2004). The mitochondrial transporter family (SLC25): physiological and pathological implications. Pflugers Arch *447*, 689-709.

Pan, X., Luhrmann, A., Satoh, A., Laskowski-Arce, M.A., and Roy, C.R. (2008). Ankyrin repeat proteins comprise a diverse family of bacterial type IV effectors. Science *320*, 1651-1654.

Parkin, J., and Cohen, B. (2001). An overview of the immune system. Lancet *357*, 1777-1789.

Parola, P., Paddock, C.D., and Raoult, D. (2005). Tick-borne rickettsioses around the world: emerging diseases challenging old concepts. Clin Microbiol Rev *18*, 719-756.

Parola, P., Paddock, C.D., Socolovschi, C., Labruna, M.B., Mediannikov, O., Kernif, T., Abdad, M.Y., Stenos, J., Bitam, I., Fournier, P.E.*, et al.* (2013). Update on tick-borne rickettsioses around the world: a geographic approach. Clin Microbiol Rev *26*, 657-702.

Parola, P., Rovery, C., Rolain, J.M., Brouqui, P., Davoust, B., and Raoult, D. (2009). Rickettsia slovaca and R. raoultii in tick-borne Rickettsioses. Emerg Infect Dis *15*, 1105-1108.

Parola, P., Socolovschi, C., Jeanjean, L., Bitam, I., Fournier, P.E., Sotto, A., Labauge, P., and Raoult, D. (2008). Warmer weather linked to tick attack and emergence of severe rickettsioses. PLoS Negl Trop Dis *2*, e338.

Parrini, M.C., Matsuda, M., and de Gunzburg, J. (2005). Spatiotemporal regulation of the Pak1 kinase. Biochem Soc Trans *33*, 646-648.

Paschos, K., and Allday, M.J. (2010). Epigenetic reprogramming of host genes in viral and microbial pathogenesis. Trends Microbiol *18*, 439-447.

Pearce, E.L., and Pearce, E.J. (2013). Metabolic pathways in immune cell activation and quiescence. Immunity *38*, 633-643.

Peng, X., Gralinski, L., Ferris, M.T., Frieman, M.B., Thomas, M.J., Proll, S., Korth, M.J., Tisoncik, J.R., Heise, M., Luo, S.*, et al.* (2011). Integrative deep sequencing of the mouse lung transcriptome reveals differential expression of diverse classes of small RNAs in response to respiratory virus infection. MBio *2*.

Perdiguero, E.G., and Geissmann, F. (2016). The development and maintenance of resident macrophages. Nat Immunol *17*, 2-8.

Petchampai, N., Sunyakumthorn, P., Banajee, K.H., Verhoeve, V.I., Kearney, M.T., and Macaluso, K.R. (2015). Identification of host proteins involved in rickettsial invasion of tick cells. Infect Immun *83*, 1048-1055.

Petchampai, N., Sunyakumthorn, P., Guillotte, M.L., Verhoeve, V.I., Banajee, K.H., Kearney, M.T., and Macaluso, K.R. (2014). Novel identification of *Dermacentor variabilis* Arp2/3 complex and its role in rickettsial infection of the arthropod vector. PLoS One *9*, e93768.

Phibbs, P.V., Jr., and Winkler, H.H. (1982). Regulatory properties of citrate synthase from Rickettsia prowazekii. J Bacteriol *149*, 718-725.

Philip, R.N., Casper, E.A., Ormsbee, R.A., Peacock, M.G., and Burgdorfer, W. (1976). Microimmunofluorescence test for the serological study of rocky mountain spotted fever and typhus. J Clin Microbiol *3*, 51-61.

Pollard, K.M., Cauvi, D.M., Toomey, C.B., Morris, K.V., and Kono, D.H. (2013). Interferon-gamma and systemic autoimmunity. Discov Med *16*, 123-131.

Polpitiya, A.D., Qian, W.J., Jaitly, N., Petyuk, V.A., Adkins, J.N., Camp, D.G., 2nd, Anderson, G.A., and Smith, R.D. (2008). DAnTE: a statistical tool for quantitative analysis of -omics data. Bioinformatics *24*, 1556-1558.

Poltorak, A., He, X., Smirnova, I., Liu, M.Y., Van Huffel, C., Du, X., Birdwell, D., Alejos, E., Silva, M., Galanos, C*., et al.* (1998). Defective LPS signaling in C3H/HeJ and C57BL/10ScCr mice: mutations in Tlr4 gene. Science *282*, 2085-2088.

Price, J.V., and Vance, R.E. (2014). The macrophage paradox. Immunity *41*, 685-693.

Qatsha, K.A., Rudolph, C., Marme, D., Schachtele, C., and May, W.S. (1993). Go 6976, a selective inhibitor of protein kinase C, is a potent antagonist of human immunodeficiency virus 1 induction from latent/low-level-producing reservoir cells in vitro. Proc Natl Acad Sci U S A *90*, 4674-4678.

Radulovic, S., Feng, H.M., Morovic, M., Djelalija, B., Popov, V., Crocquet-Valdes, P., and Walker, D.H. (1996). Isolation of *Rickettsia akari* from a patient in a region where Mediterranean spotted fever is endemic. Clin Infect Dis *22*, 216-220.

Rahman, M.S., Ammerman, N.C., Sears, K.T., Ceraul, S.M., and Azad, A.F. (2010). Functional characterization of a phospholipase A(2) homolog from *Rickettsia typhi*. J Bacteriol *192*, 3294-3303.

Rahman, M.S., Gillespie, J.J., Kaur, S.J., Sears, K.T., Ceraul, S.M., Beier-Sexton, M., and Azad, A.F. (2013). *Rickettsia typhi* possesses phospholipase A2 enzymes that are involved in infection of host cells. PLoS Pathog *9*, e1003399.

Randolph, S.E. (2010). To what extent has climate change contributed to the recent epidemiology of tick-borne diseases? Vet Parasitol *167*, 92-94.

Randow, F., and Lehner, P.J. (2009). Viral avoidance and exploitation of the ubiquitin system. Nat Cell Biol *11*, 527-534.

Raoult, D., Ndihokubwayo, J.B., Tissot-Dupont, H., Roux, V., Faugere, B., Abegbinni, R., and Birtles, R.J. (1998). Outbreak of epidemic typhus associated with trench fever in Burundi. Lancet *352*, 353-358.

Raoult, D., and Roux, V. (1997). Rickettsioses as paradigms of new or emerging infectious diseases. Clin Microbiol Rev *10*, 694-719.

Raoult, D., Woodward, T., and Dumler, J.S. (2004). The history of epidemic typhus. Infect Dis Clin North Am *18*, 127-140.

Ray, K., Marteyn, B., Sansonetti, P.J., and Tang, C.M. (2009). Life on the inside: the intracellular lifestyle of cytosolic bacteria. Nat Rev Microbiol *7*, 333-340.

Reddick, L.E., and Alto, N.M. (2014). Bacteria fighting back: how pathogens target and subvert the host innate immune system. Mol Cell *54*, 321-328.

Reed, S.C., Lamason, R.L., Risca, V.I., Abernathy, E., and Welch, M.D. (2014). *Rickettsia* actin-based motility occurs in distinct phases mediated by different actin nucleators. Curr Biol *24*, 98-103.

Reed, S.C., Serio, A.W., and Welch, M.D. (2012). *Rickettsia parkeri* invasion of diverse host cells involves an Arp2/3 complex, WAVE complex and Rho-family GTPase-dependent pathway. Cell Microbiol *14*, 529-545.

Renesto, P., Ogata, H., Audic, S., Claverie, J.M., and Raoult, D. (2005). Some lessons from *Rickettsia* genomics. FEMS Microbiol Rev *29*, 99-117.

Rennoll-Bankert, K.E., Rahman, M.S., Gillespie, J.J., Guillotte, M.L., Kaur, S.J., Lehman, S.S., Beier-Sexton, M., and Azad, A.F. (2015). Which Way In? The RalF Arf-GEF Orchestrates *Rickettsia* Host Cell Invasion. PLoS Pathog *11*, e1005115.

Rennoll-Bankert, K.E., Rahman, M.S., Guillotte, M.L., Lehman, S.S., Beier-Sexton, M., Gillespie, J.J., and Azad, A.F. (2016). RalF-Mediated Activation of Arf6 Controls *Rickettsia typhi* Invasion by Co-Opting Phosphoinositol Metabolism. Infect Immun *84*, 3496-3506.

Richards, A.L. (2012). Worldwide detection and identification of new and old rickettsiae and rickettsial diseases. FEMS Immunol Med Microbiol *64*, 107-110.

Richards, A.L., Soeatmadji, D.W., Widodo, M.A., Sardjono, T.W., Yanuwiadi, B., Hernowati, T.E., Baskoro, A.D., Roebiyoso, Hakim, L., Soendoro, M.*, et al.* (1997). Seroepidemiologic evidence for murine and scrub typhus in Malang, Indonesia. Am J Trop Med Hyg *57*, 91-95.

Riley, S.P., Cardwell, M.M., Chan, Y.G., Pruneau, L., Del Piero, F., and Martinez, J.J. (2015). Failure of a heterologous recombinant Sca5/OmpB protein-based vaccine to elicit effective protective immunity against *Rickettsia rickettsii* infections in C3H/HeN mice. Pathog Dis *73*, ftv101.

Riley, S.P., Fish, A.I., Del Piero, F., and Martinez, J.J. (2018). Immunity against the Obligate Intracellular Bacterial Pathogen *Rickettsia australis* Requires a Functional Complement System. Infect Immun *86*.

Riley, S.P., Fish, A.I., Garza, D.A., Banajee, K.H., Harris, E.K., Del Piero, F., and Martinez, J.J. (2016). Nonselective Persistence of a *Rickettsia conorii* Extrachromosomal Plasmid during Mammalian Infection. Infect Immun *84*, 790-797.

Riley, S.P., Goh, K.C., Hermanas, T.M., Cardwell, M.M., Chan, Y.G., and Martinez, J.J. (2010). The *Rickettsia conorii* autotransporter protein Sca1 promotes adherence to nonphagocytic mammalian cells. Infect Immun *78*, 1895-1904.

Ringrose, J.H., Jeeninga, R.E., Berkhout, B., and Speijer, D. (2008). Proteomic studies reveal coordinated changes in T-cell expression patterns upon infection with human immunodeficiency virus type 1. J Virol *82*, 4320-4330.

Robinson, D.M., Brown, G., Gan, E., and Huxsoll, D.L. (1976). Adaptation of a microimmunofluorescence test to the study of human *Rickettsia tsutsugamuskh* antibody. Am J Trop Med Hyg *25*, 900-905.

Rodriguez-Prados, J.C., Traves, P.G., Cuenca, J., Rico, D., Aragones, J., Martin-Sanz, P., Cascante, M., and Bosca, L. (2010). Substrate fate in activated macrophages: a comparison between innate, classic, and alternative activation. J Immunol *185*, 605-614.

Rohatgi, R., Ho, H.Y., and Kirschner, M.W. (2000). Mechanism of N-WASP activation by CDC42 and phosphatidylinositol 4, 5-bisphosphate. J Cell Biol *150*, 1299-1310.
Rolain, J.M., Maurin, M., Vestris, G., and Raoult, D. (1998). In vitro susceptibilities of 27 rickettsiae to 13 antimicrobials. Antimicrob Agents Chemother *42*, 1537-1541.

Rosales-Reyes, R., Perez-Lopez, A., Sanchez-Gomez, C., Hernandez-Mote, R.R., Castro-Eguiluz, D., Ortiz-Navarrete, V., and Alpuche-Aranda, C.M. (2012). *Salmonella* infects B cells by macropinocytosis and formation of spacious phagosomes but does not induce pyroptosis in favor of its survival. Microb Pathog *52*, 367-374.

Rothe, M., Wong, S.C., Henzel, W.J., and Goeddel, D.V. (1994). A novel family of putative signal transducers associated with the cytoplasmic domain of the 75 kDa tumor necrosis factor receptor. Cell *78*, 681-692.

Rovery, C., Brouqui, P., and Raoult, D. (2008). Questions on Mediterranean spotted fever a century after its discovery. Emerg Infect Dis *14*, 1360-1367.

Rovery, C., and Raoult, D. (2008). Mediterranean spotted fever. Infect Dis Clin North Am *22*, 515-530, ix.

Ruby, T., and Monack, D.M. (2011). At home with hostility: How do pathogenic bacteria evade mammalian immune surveillance to establish persistent infection? F1000 Biol Rep *3*, 1.

Rukmangadachar, L.A., Makharia, G.K., Mishra, A., Das, P., Hariprasad, G., Srinivasan, A., Gupta, S.D., Ahuja, V., and Acharya, S.K. (2016). Proteome analysis of the macroscopically affected colonic mucosa of Crohn's disease and intestinal tuberculosis. Sci Rep *6*, 23162.

Rydkina, E., Sahni, A., Silverman, D.J., and Sahni, S.K. (2007). Comparative analysis of host-cell signalling mechanisms activated in response to infection with *Rickettsia conorii* and *Rickettsia typhi*. J Med Microbiol *56*, 896-906.

Rydkina, E., Silverman, D.J., and Sahni, S.K. (2005a). Activation of p38 stress-activated protein kinase during *Rickettsia rickettsii* infection of human endothelial cells: role in the induction of chemokine response. Cell Microbiol *7*, 1519-1530.

Rydkina, E., Silverman, D.J., and Sahni, S.K. (2005b). Similarities and differences in host cell signaling following infection with different *Rickettsia* species. Ann N Y Acad Sci *1063*, 203-206.

Sa-Nunes, A., Bafica, A., Lucas, D.A., Conrads, T.P., Veenstra, T.D., Andersen, J.F., Mather, T.N., Ribeiro, J.M., and Francischetti, I.M. (2007). Prostaglandin E2 is a major inhibitor of dendritic cell maturation and function in Ixodes scapularis saliva. J Immunol *179*, 1497-1505.

Sahni, S., Rydkina, E., and Simpson-Haidaris, P.J. (2012). Innate Immune Response and Inflammation: Roles in Pathogenesis and Protection (Rickettsiaceae). In Intracellular Pathogens II: Rickettsiales, G.H. Palmer, and A.F. Azad, eds. (ASM Press), pp. 243-269.

Sahni, S.K., Narra, H.P., Sahni, A., and Walker, D.H. (2013). Recent molecular insights into rickettsial pathogenesis and immunity. Future microbiology *8*, 1265-1288.

Sakharkar, K.R., Dhar, P.K., and Chow, V.T. (2004). Genome reduction in prokaryotic obligatory intracellular parasites of humans: a comparative analysis. Int J Syst Evol Microbiol *54*, 1937-1941.

Saliba, A.E., S, C.S., and Vogel, J. (2017). New RNA-seq approaches for the study of bacterial pathogens. Curr Opin Microbiol *35*, 78-87.

Sanchez-Villamil, J., and Navarro-Garcia, F. (2015). Role of virulence factors on host inflammatory response induced by diarrheagenic *Escherichia coli* pathotypes. Future Microbiol *10*, 1009-1033.

Sandilands, E., Cans, C., Fincham, V.J., Brunton, V.G., Mellor, H., Prendergast, G.C., Norman, J.C., Superti-Furga, G., and Frame, M.C. (2004). RhoB and actin polymerization coordinate Src activation with endosome-mediated delivery to the membrane. Dev Cell *7*, 855-869.

Sarantis, H., and Grinstein, S. (2012). Subversion of phagocytosis for pathogen survival. Cell Host Microbe *12*, 419-431.

Saxena, T., Tandon, B., Sharma, S., Chameettachal, S., Ray, P., Ray, A.R., and Kulshreshtha, R. (2013). Combined miRNA and mRNA signature identifies key molecular players and pathways involved in chikungunya virus infection in human cells. PLoS One *8*, e79886.

Schmutz, C., Ahrne, E., Kasper, C.A., Tschon, T., Sorg, I., Dreier, R.F., Schmidt, A., and Arrieumerlou, C. (2013). Systems-level overview of host protein phosphorylation during Shigella flexneri infection revealed by phosphoproteomics. Mol Cell Proteomics *12*, 2952-2968.

Schroder, K., Hertzog, P.J., Ravasi, T., and Hume, D.A. (2004). Interferon-gamma: an overview of signals, mechanisms and functions. J Leukoc Biol *75*, 163-189.

Schroeder, C., Chowdhury, I., Narra, H., Patel, J., Sahni, A., and Sahni, S. (2016). Human Rickettsioses: Host Response and Molecular Pathogenesis. In Rickettsiales: Biology, Molecular Biology, Epidemiology and Vaccine Development, S. Thomas, ed. (Springer), pp. 399-446.

Sennels, L., Bukowski-Wills, J.C., and Rappsilber, J. (2009). Improved results in proteomics by use of local and peptide-class specific false discovery rates. BMC bioinformatics *10*, 179.

Shehata, H.M., Murphy, A.J., Lee, M.K.S., Gardiner, C.M., Crowe, S.M., Sanjabi, S., Finlay, D.K., and Palmer, C.S. (2017). Sugar or Fat?-Metabolic Requirements for Immunity to Viral Infections. Front Immunol *8*, 1311.

Shin, S., and Argon, Y. (2015). Stressed-Out Endoplasmic Reticulum Inflames the Mitochondria. Immunity *43*, 409-411.

Shishido, S.N., Varahan, S., Yuan, K., Li, X., and Fleming, S.D. (2012). Humoral innate immune response and disease. Clin Immunol *144*, 142-158.

Shuai, K., and Liu, B. (2003). Regulation of JAK-STAT signalling in the immune system. Nat Rev Immunol *3*, 900-911.

Siegler, G., Kremmer, E., Gonnella, R., and Niedobitek, G. (2003). Epstein-Barr virus encoded latent membrane protein 1 (LMP1) and TNF receptor associated factors (TRAF): colocalisation of LMP1 and TRAF1 in primary EBV infection and in EBV associated Hodgkin lymphoma. Mol Pathol *56*, 156-161.

Silverman, D.J., Santucci, L.A., Meyers, N., and Sekeyova, Z. (1992). Penetration of host cells by *Rickettsia rickettsii* appears to be mediated by a phospholipase of rickettsial origin. Infect Immun *60*, 2733-2740.

Sirnio, P., Vayrynen, J.P., Klintrup, K., Makela, J., Makinen, M.J., Karttunen, T.J., and Tuomisto, A. (2017). Decreased serum apolipoprotein A1 levels are associated with poor survival and systemic inflammatory response in colorectal cancer. Sci Rep *7*, 5374.

Sly, L.M., Hingley-Wilson, S.M., Reiner, N.E., and McMaster, W.R. (2003). Survival of *Mycobacterium tuberculosis* in host macrophages involves resistance to apoptosis dependent upon induction of antiapoptotic Bcl-2 family member Mcl-1. J Immunol *170*, 430-437.

Socolovschi, C., Huynh, T.P., Davoust, B., Gomez, J., Raoult, D., and Parola, P. (2009a). Transovarial and trans-stadial transmission of Rickettsiae africae in *Amblyomma variegatum* ticks. Clin Microbiol Infect *15 Suppl 2*, 317-318.

Socolovschi, C., Mediannikov, O., Raoult, D., and Parola, P. (2009b). The relationship between spotted fever group Rickettsiae and ixodid ticks. Vet Res *40*, 34.

Sorensen, L.N., and Paludan, S.R. (2004). Blocking CC chemokine receptor (CCR) 1 and CCR5 during herpes simplex virus type 2 infection in vivo impairs host defence and perturbs the cytokine response. Scand J Immunol *59*, 321-333.

Speir, M., Lawlor, K.E., Glaser, S.P., Abraham, G., Chow, S., Vogrin, A., Schulze, K.E., Schuelein, R., O'Reilly, L.A., Mason, K.*, et al.* (2016). Eliminating *Legionella* by inhibiting BCL-XL to induce macrophage apoptosis. Nat Microbiol *1*, 15034.

St John, A.L., and Abraham, S.N. (2009). *Salmonella* disrupts lymph node architecture by TLR4-mediated suppression of homeostatic chemokines. Nat Med *15*, 1259-1265.

Staedel, C., and Darfeuille, F. (2013). MicroRNAs and bacterial infection. Cell Microbiol *15*, 1496-1507.

Stepanov, G.A., Filippova, J.A., Komissarov, A.B., Kuligina, E.V., Richter, V.A., and Semenov, D.V. (2015). Regulatory role of small nucleolar RNAs in human diseases. Biomed Res Int *2015*, 206849.

Stewart, A., Armstrong, M., Graves, S., and Hajkowicz, K. (2017). *Rickettsia australis* and Queensland Tick Typhus: A Rickettsial Spotted Fever Group Infection in Australia. Am J Trop Med Hyg *97*, 24-29.

Stincone, A., Prigione, A., Cramer, T., Wamelink, M.M., Campbell, K., Cheung, E., Olin-Sandoval, V., Gruning, N.M., Kruger, A., Tauqeer Alam, M.*, et al.* (2015). The return of metabolism: biochemistry and physiology of the pentose phosphate pathway. Biol Rev Camb Philos Soc *90*, 927-963.

Sun, J., Wang, X., Lau, A., Liao, T.Y., Bucci, C., and Hmama, Z. (2010). Mycobacterial nucleoside diphosphate kinase blocks phagosome maturation in murine RAW 264.7 macrophages. PLoS One *5*, e8769.

Szklarczyk, D., Morris, J.H., Cook, H., Kuhn, M., Wyder, S., Simonovic, M., Santos, A., Doncheva, N.T., Roth, A., Bork, P.*, et al.* (2017). The STRING database in 2017: quality-controlled protein-protein association networks, made broadly accessible. Nucleic Acids Res *45*, D362-D368.

Tang, W.H., Shilov, I.V., and Seymour, S.L. (2008). Nonlinear fitting method for determining local false discovery rates from decoy database searches. Journal of proteome research *7*, 3661-3667.

Tannahill, G.M., Curtis, A.M., Adamik, J., Palsson-McDermott, E.M., McGettrick, A.F., Goel, G., Frezza, C., Bernard, N.J., Kelly, B., Foley, N.H.*, et al.* (2013). Succinate is an inflammatory signal that induces IL-1beta through HIF-1alpha. Nature *496*, 238-242.

Teysseire, N., Boudier, J.A., and Raoult, D. (1995). *Rickettsia conorii* entry into Vero cells. Infect Immun *63*, 366-374.

Thibaudeau, T.A., Anderson, R.T., and Smith, D.M. (2018). A common mechanism of proteasome impairment by neurodegenerative disease-associated oligomers. Nat Commun *9*, 1097.

Tomassone, L., Portillo, A., Novakova, M., de Sousa, R., and Oteo, J.A. (2018). Neglected aspects of tick-borne rickettsioses. Parasit Vectors *11*, 263.
Tran Van Nhieu, G., and Arbibe, L. (2009). Genetic reprogramming of host cells by bacterial pathogens. F1000 Biol Rep *1*, 80.

Trapnell, C., Hendrickson, D.G., Sauvageau, M., Goff, L., Rinn, J.L., and Pachter, L. (2013). Differential analysis of gene regulation at transcript resolution with RNA-seq. Nat Biotechnol *31*, 46-53.

Trapnell, C., Roberts, A., Goff, L., Pertea, G., Kim, D., Kelley, D.R., Pimentel, H., Salzberg, S.L., Rinn, J.L., and Pachter, L. (2012). Differential gene and transcript expression analysis of RNA-seq experiments with TopHat and Cufflinks. Nat Protoc *7*, 562-578.

Tsai, Y.S., Wu, Y.H., Kao, P.T., and Lin, Y.C. (2008). African tick bite fever. J Formos Med Assoc *107*, 73-76.

Turvey, S.E., and Broide, D.H. (2010). Innate immunity. J Allergy Clin Immunol *125*, S24-32.

Twigg, H.L., 3rd (2004). Macrophages in innate and acquired immunity. Semin Respir Crit Care Med *25*, 21-31.

Uchiyama, T. (2003). Adherence to and invasion of Vero cells by recombinant Escherichia coli expressing the outer membrane protein rOmpB of *Rickettsia japonica*. Ann N Y Acad Sci *990*, 585-590.

Uchiyama, T. (2012). Tropism and pathogenicity of rickettsiae. Front Microbiol *3*, 230.

Unanue, E.R. (1984). Antigen-presenting function of the macrophage. Annu Rev Immunol *2*, 395-428.

Usami, Y., Ishida, K., Sato, S., Kishino, M., Kiryu, M., Ogawa, Y., Okura, M., Fukuda, Y., and Toyosawa, S. (2013). Intercellular adhesion molecule-1 (ICAM-1) expression correlates with oral cancer progression and induces macrophage/cancer cell adhesion. Int J Cancer *133*, 568-578.

Valbuena, G., Bradford, W., and Walker, D.H. (2003). Expression analysis of the T-cell-targeting chemokines CXCL9 and CXCL10 in mice and humans with endothelial infections caused by rickettsiae of the spotted fever group. Am J Pathol *163*, 1357-1369.

Valbuena, G., Feng, H.M., and Walker, D.H. (2002). Mechanisms of immunity against rickettsiae. New perspectives and opportunities offered by unusual intracellular parasites. Microbes Infect *4*, 625-633.

Valbuena, G., and Walker, D.H. (2004). Effect of blocking the CXCL9/10-CXCR3 chemokine system in the outcome of endothelial-target rickettsial infections. Am J Trop Med Hyg *71*, 393-399.

Valbuena, G., and Walker, D.H. (2009). Infection of the endothelium by members of the order Rickettsiales. Thromb Haemost *102*, 1071-1079.

Valenzuela, J.G. (2004). Exploring tick saliva: from biochemistry to 'sialomes' and functional genomics. Parasitology *129 Suppl*, S83-94.

Van Belleghem, J.D., Clement, F., Merabishvili, M., Lavigne, R., and Vaneechoutte, M. (2017). Pro- and anti-inflammatory responses of peripheral blood mononuclear cells induced by *Staphylococcus aureus* and *Pseudomonas aeruginosa* phages. Sci Rep *7*, 8004.

Van den Bossche, J., Baardman, J., and de Winther, M.P. (2015). Metabolic Characterization of Polarized M1 and M2 Bone Marrow-derived Macrophages Using Real-time Extracellular Flux Analysis. J Vis Exp.

Van den Bossche, J., Baardman, J., Otto, N.A., van der Velden, S., Neele, A.E., van den Berg, S.M., Luque-Martin, R., Chen, H.J., Boshuizen, M.C., Ahmed, M.*, et al.* (2016). Mitochondrial Dysfunction Prevents Repolarization of Inflammatory Macrophages. Cell Rep *17*, 684-696.

Van den Bossche, J., O'Neill, L.A., and Menon, D. (2017). Macrophage Immunometabolism: Where Are We (Going)? Trends Immunol *38*, 395-406.

Vanhaesebroeck, B., Stephens, L., and Hawkins, P. (2012). PI3K signalling: the path to discovery and understanding. Nat Rev Mol Cell Biol *13*, 195-203.

Velge, P., Wiedemann, A., Rosselin, M., Abed, N., Boumart, Z., Chausse, A.M., Grepinet, O., Namdari, F., Roche, S.M., Rossignol, A.*, et al.* (2012). Multiplicity of *Salmonella* entry mechanisms, a new paradigm for *Salmonella* pathogenesis. Microbiologyopen *1*, 243-258.

Vergne, I., Chua, J., Lee, H.H., Lucas, M., Belisle, J., and Deretic, V. (2005). Mechanism of phagolysosome biogenesis block by viable *Mycobacterium tuberculosis*. Proc Natl Acad Sci U S A *102*, 4033-4038.

VerPlank, J.J.S., Lokireddy, S., Feltri, M.L., Goldberg, A.L., and Wrabetz, L. (2018). Impairment of protein degradation and proteasome function in hereditary neuropathies. Glia *66*, 379-395.

Vilchez, D., Saez, I., and Dillin, A. (2014). The role of protein clearance mechanisms in organismal ageing and age-related diseases. Nat Commun *5*, 5659.

Villarino, A.V., Kanno, Y., and O'Shea, J.J. (2017). Mechanisms and consequences of Jak-STAT signaling in the immune system. Nat Immunol *18*, 374-384.

von Both, U., Berk, M., Agapow, P.M., Wright, J.D., Git, A., Hamilton, M.S., Goldgof, G., Siddiqui, N., Bellos, E., Wright, V.J.*, et al.* (2018). *Mycobacterium tuberculosis* Exploits a Molecular Off Switch of the Immune System for Intracellular Survival. Sci Rep *8*, 661.

von Mering, C., Huynen, M., Jaeggi, D., Schmidt, S., Bork, P., and Snel, B. (2003). STRING: a database of predicted functional associations between proteins. Nucleic Acids Res *31*, 258-261.

Walker, D.H. (1989). Rocky Mountain spotted fever: a disease in need of microbiological concern. Clin Microbiol Rev *2*, 227-240.

Walker, D.H. (1997). Endothelial-target rickettsial infection. Lab Anim Sci *47*, 483-485.

Walker, D.H. (2007). Rickettsiae and rickettsial infections: the current state of knowledge. Clin Infect Dis *45 Suppl 1*, S39-44.

Walker, D.H., Feng, H.M., Ladner, S., Billings, A.N., Zaki, S.R., Wear, D.J., and Hightower, B. (1997). Immunohistochemical diagnosis of typhus rickettsioses using an anti-lipopolysaccharide monoclonal antibody. Mod Pathol *10*, 1038-1042.

Walker, D.H., and Gear, J.H. (1985). Correlation of the distribution of *Rickettsia conorii*, microscopic lesions, and clinical features in South African tick bite fever. Am J Trop Med Hyg *34*, 361-371.

Walker, D.H., Hudnall, S.D., Szaniawski, W.K., and Feng, H.M. (1999). Monoclonal antibody-based immunohistochemical diagnosis of rickettsialpox: the macrophage is the principal target. Mod Pathol *12*, 529-533.

Walker, D.H., and Ismail, N. (2008). Emerging and re-emerging rickettsioses: endothelial cell infection and early disease events. Nat Rev Microbiol *6*, 375-386.

Walker, D.H., Olano, J.P., and Feng, H.M. (2001). Critical role of cytotoxic T lymphocytes in immune clearance of rickettsial infection. Infect Immun *69*, 1841-1846.

Walker, D.H., Popov, V.L., Wen, J., and Feng, H.M. (1994). *Rickettsia conorii* infection of C3H/HeN mice. A model of endothelial-target rickettsiosis. Lab Invest *70*, 358-368.

Wan, X.K., Yuan, S.L., Tao, H.X., Diao, L.P., Wang, Y.C., Cao, C., and Liu, C.J. (2016). The Upregulation of TRAF1 Induced by *Helicobacter pylori* Plays an Antiapoptotic Effect on the Infected Cells. Helicobacter *21*, 554-564.

Wang, Q., Liu, S., Tang, Y., Liu, Q., and Yao, Y. (2014). MPT64 protein from Mycobacterium tuberculosis inhibits apoptosis of macrophages through NF-kB-miRNA21-Bcl-2 pathway. PLoS One *9*, e100949.

Wei, X., Song, H., Yin, L., Rizzo, M.G., Sidhu, R., Covey, D.F., Ory, D.S., and Semenkovich, C.F. (2016). Fatty acid synthesis configures the plasma membrane for inflammation in diabetes. Nature *539*, 294-298.

Weiner, A., Mellouk, N., Lopez-Montero, N., Chang, Y.Y., Souque, C., Schmitt, C., and Enninga, J. (2016). Macropinosomes are Key Players in Early *Shigella* Invasion and Vacuolar Escape in Epithelial Cells. PLoS Pathog *12*, e1005602.

Weinert, L.A., Araujo-Jnr, E.V., Ahmed, M.Z., and Welch, J.J. (2015). The incidence of bacterial endosymbionts in terrestrial arthropods. Proc Biol Sci *282*, 20150249.

Weinert, L.A., and Welch, J.J. (2017). Why Might Bacterial Pathogens Have Small Genomes? Trends Ecol Evol *32*, 936-947.

Weinert, L.A., Werren, J.H., Aebi, A., Stone, G.N., and Jiggins, F.M. (2009). Evolution and diversity of *Rickettsia* bacteria. BMC Biol *7*, 6.

Weiss, E., and Strauss, B.S. (1991). The life and career of Howard Taylor Ricketts. Rev Infect Dis *13*, 1241-1242.

Welch, M.D., Reed, S.C., and Haglund, C.M. (2012). Establishing Intracellular Infection: Escape from the Phagosome and Intracellular Colonization (Rickettsiaceae). In Intracellular Pathogens II: Rickettsiales, G.H. Palmer, and A.F. Azad, eds. (ASM Press), pp. 154-174.

Westermann, A.J., Barquist, L., and Vogel, J. (2017). Resolving host-pathogen interactions by dual RNA-seq. PLoS Pathog *13*, e1006033.

Westermann, A.J., Gorski, S.A., and Vogel, J. (2012). Dual RNA-seq of pathogen and host. Nat Rev Microbiol *10*, 618-630.

Whitworth, T., Popov, V.L., Yu, X.J., Walker, D.H., and Bouyer, D.H. (2005). Expression of the *Rickettsia prowazekii* pld or tlyC gene in *Salmonella enterica* serovar Typhimurium mediates phagosomal escape. Infect Immun *73*, 6668-6673.

Wilensky, A., Tzach-Nahman, R., Potempa, J., Shapira, L., and Nussbaum, G. (2015). *Porphyromonas gingivalis* gingipains selectively reduce CD14 expression, leading to macrophage hyporesponsiveness to bacterial infection. J Innate Immun *7*, 127-135.

Williams, K.P., Sobral, B.W., and Dickerman, A.W. (2007). A robust species tree for the alphaproteobacteria. J Bacteriol *189*, 4578-4586.

Willis, S.N., and Adams, J.M. (2005). Life in the balance: how BH3-only proteins induce apoptosis. Curr Opin Cell Biol *17*, 617-625.

Winkler, H.H., and Daugherty, R.M. (1986). Acquisition of glucose by *Rickettsia prowazekii* through the nucleotide intermediate uridine 5'-diphosphoglucose. J Bacteriol *167*, 805-808.

Wixon, J. (2001). Featured organism: reductive evolution in bacteria: *Buchnera* sp., *Rickettsia prowazekii* and *Mycobacterium leprae*. Comp Funct Genomics *2*, 44-48.

Wood, H., and Artsob, H. (2012). Spotted fever group rickettsiae: a brief review and a Canadian perspective. Zoonoses Public Health *59 Suppl 2*, 65-79.

Wright, S.D., Ramos, R.A., Tobias, P.S., Ulevitch, R.J., and Mathison, J.C. (1990). CD14, a receptor for complexes of lipopolysaccharide (LPS) and LPS binding protein. Science *249*, 1431-1433.

Wynne, J.W., Todd, S., Boyd, V., Tachedjian, M., Klein, R., Shiell, B., Dearnley, M., McAuley, A.J., Woon, A.P., Purcell, A.W.*, et al.* (2017). Comparative transcriptomics highlights the role of the AP1 transcription factor in the host response to *Ebolavirus*. J Virol.

Xavier, M.N., Winter, M.G., Spees, A.M., den Hartigh, A.B., Nguyen, K., Roux, C.M., Silva, T.M., Atluri, V.L., Kerrinnes, T., Keestra, A.M.*, et al.* (2013). PPARgamma-mediated increase in glucose availability sustains chronic *Brucella abortus* infection in alternatively activated macrophages. Cell Host Microbe *14*, 159-170.

Yamamoto, M., Sato, S., Hemmi, H., Hoshino, K., Kaisho, T., Sanjo, H., Takeuchi, O., Sugiyama, M., Okabe, M., Takeda, K.*, et al.* (2003). Role of adaptor TRIF in the MyD88-independent toll-like receptor signaling pathway. Science *301*, 640-643.

Yang, Z., Song, L., and Huang, C. (2009). Gadd45 proteins as critical signal transducers linking NF-kappaB to MAPK cascades. Curr Cancer Drug Targets *9*, 915-930.

Yokota, S., Yokosawa, N., Okabayashi, T., Suzutani, T., and Fujii, N. (2005). Induction of suppressor of cytokine signaling-3 by herpes simplex virus type 1 confers efficient viral replication. Virology *338*, 173-181.

Yokota, S., Yokosawa, N., Okabayashi, T., Suzutani, T., Miura, S., Jimbow, K., and Fujii, N. (2004). Induction of suppressor of cytokine signaling-3 by herpes simplex virus type 1 contributes to inhibition of the interferon signaling pathway. J Virol *78*, 6282-6286.

Zavala-Castro, J.E., Zavala-Velazquez, J.E., Peniche-Lara, G.F., and Sulu Uicab, J.E. (2009). Human rickettsialpox, southeastern Mexico. Emerg Infect Dis *15*, 1665-1667.

Zhou, Y., and Zhu, Y. (2015). Diversity of bacterial manipulation of the host ubiquitin pathways. Cell Microbiol *17*, 26-34.

Zur Bruegge, J., Einspanier, R., and Sharbati, S. (2017). A Long Journey Ahead: Long Non-coding RNAs in Bacterial Infections. Front Cell Infect Microbiol *7*, 95.

Chapter VIII

Supplementary Material

VIII | Supplementary material

VIII.1 | Chapter II

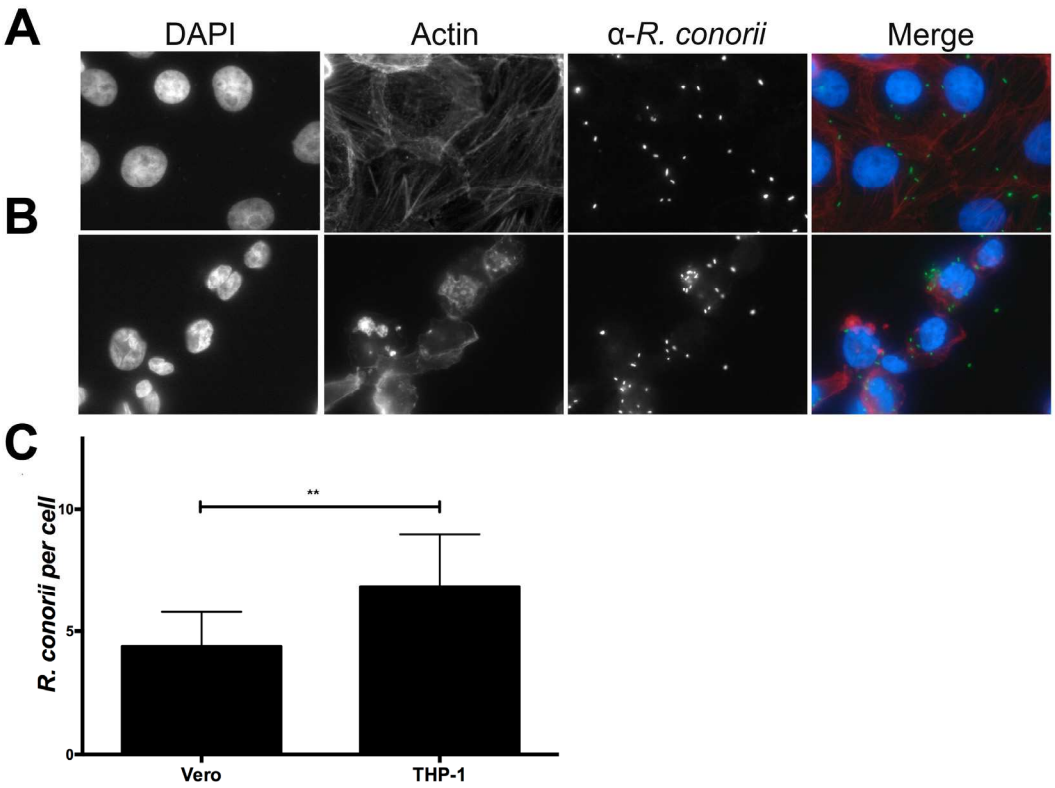

Supplementary Figure II.1 | Unlike *R. montanensis,* adherence of *R. conorii* to THP-1-derived macrophages is not decreased. PMA-differentiated THP-1 cells and Vero cells were infected with *R. conorii* (MOI=10). After 60 min of infection, cells were fixed and stained for immunofluorescence analysis with anti-Rc_{PFA} followed by Alexa Fluor 488 (green) to stain *R. conorii*, DAPI to visualize the host nuclei (blue) and Phalloidin to illustrate the host cytoplasm (red). **(A and B)** Representative immunofluorescence images of *R. conorii* association assays in Vero **(A)** and macrophage-like **(B)** cells. Each row shows, from the left to right, nuclei staining, actin staining, rickettsia staining and merged images. Scale bar = 10 µm. **(C)** Rickettsia and mammalian cells were counted and results are expressed as the ratio of rickettsia to mammalian cells. At least 200 nuclei were counted for each experimental condition. Results are shown as the mean ± SD (P values: ** <0.01).

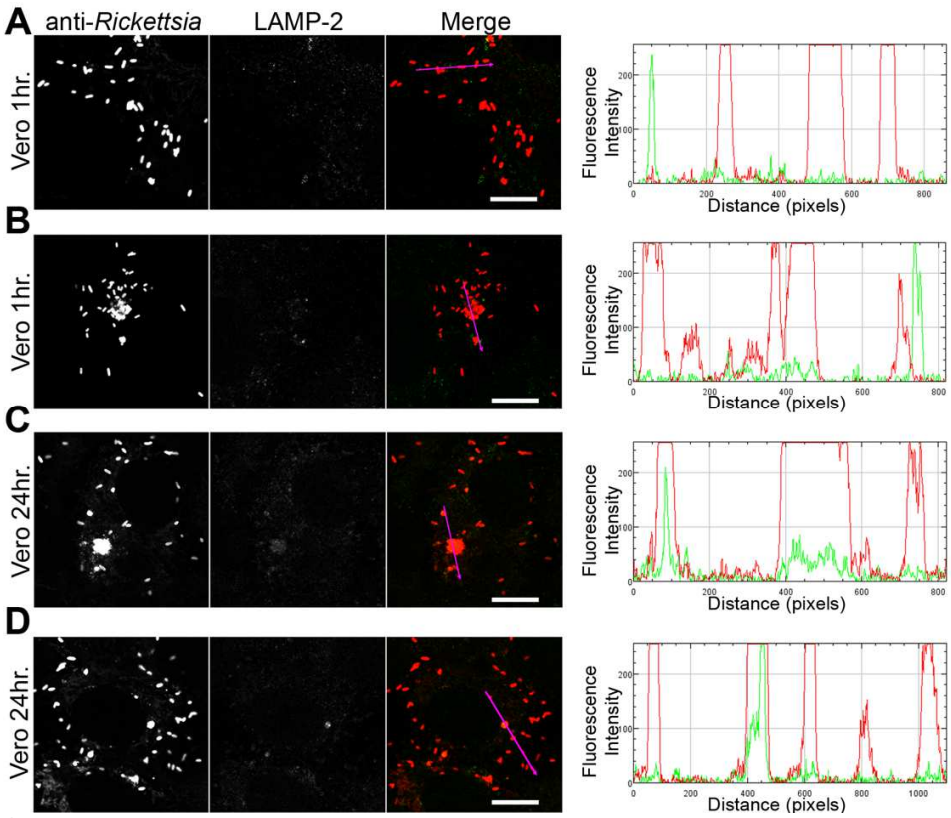

Supplementary Figure II.2 | *R. montanensis* is maintained mostly as morphologically intact bacteria in Vero cells. Vero cells were infected with *R. montanensis* (MOI=10). At 60 min or 24 h post infection, cells were fixed, permeabilized and double stained for immunofluorescence confocal microscopy analysis with NIH/RML I7198 followed by Alexa Fluor 546 (red) to stain *R. montanensis* and the monoclonal antibody for LAMP-2, lysosomal membrane protein followed by Alexa Fluor 488 (green). **(A-D)** Representative images of a single slice from the z stacks. Vero cells at 60 min post infection **(A and B)** and 24 h post infection **(C and D)**. Each row shows, from left to right, *Rickettsia* staining, LAMP-2 staining, the merged image, and a RGB plot profile illustrating the fluorescence intensity along the magenta arrow. Scale bar = 10 µm. **Supplementary movies II.3 and II.4** represent 360 degrees rotation movie of the 3D projection of the stack images shown in panels 3A and 3C, respectively.

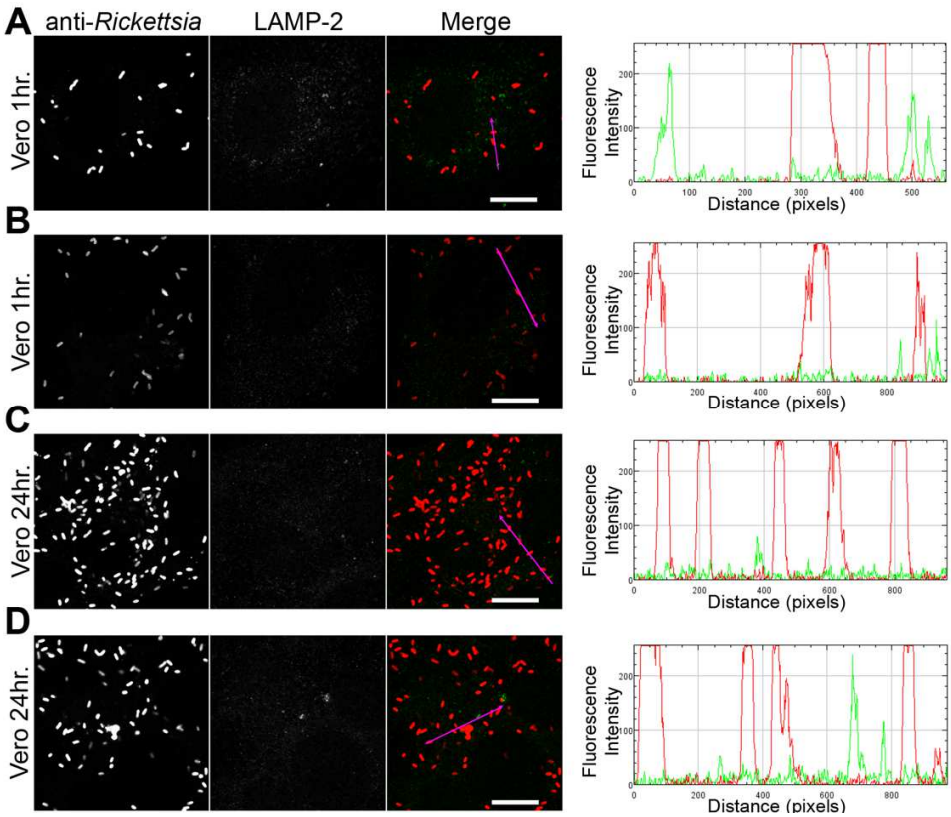

Supplementary Figure II.3 | *R. conorii* maintains an intact morphology in Vero cells. Vero cells were infected with *R. conorii* (MOI=10). At 60 min or 24 h post infection, cells were fixed, permeabilized and double stained for immunofluorescence confocal microscopy analysis with anti-Rc_{PFA} followed by Alexa Fluor 546 (red) to stain *R. conorii* and the monoclonal antibody for LAMP-2, lysosomal membrane protein followed by Alexa Fluor 488 (green). **(A-D)** Representative images of a single slice from the z stacks. Vero cells at 60 min post infection **(A and B)** and 24 h post infection **(C and D)**. Each row shows, from left to right, *Rickettsia* staining, LAMP-2 staining, the merged image, and a RGB plot profile illustrating the fluorescence intensity along the magenta arrow. Scale bar = 10 µm. **Supplementary movies II.7 and II.8** represent 360 degrees rotation movie of the 3D projection of the stack images shown in panels 4A and 4C, respectively.

Supplementary Figure II.4 | Amino acid sequence alignment of Sca0 protein from *R. conorii* and *R. montanensis.* Amino acid sequences of rickettsial Sca0 from *R. conorii* (RC1273) and *R. montanensis* (MCI_03620) were aligned using the ClustalW software. The alignment resulted in a percentage of sequence identity of 75.36 %.

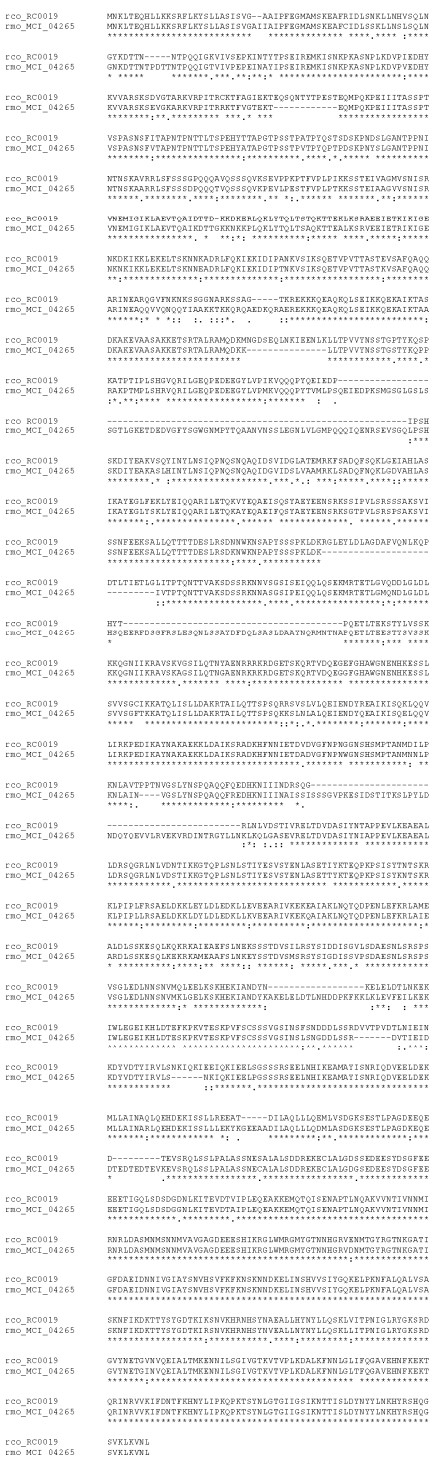

Supplementary Figure II.5 | Amino acid sequence alignment of Sca1 protein from *R. conorii* and *R. montanensis*. Amino acid sequences of rickettsial Sca1 from *R. conorii* (RC0019) and *R. montanensis* (MCI_04265) were aligned using the ClustalW software. The alignment resulted in a percentage of sequence identity of 60.15 %.

Supplementary Figure II.6 | Amino acid sequence alignment of Sca2 protein from *R. conorii* and *R. montanensis*. Amino acid sequences of rickettsial Sca2 from *R. conorii* (RC0110) and *R. montanensis* (MCI_04765) were aligned using the ClustalW software. The alignment resulted in a percentage of sequence identity of 88.47 %.

Supplementary Figure II.7 | Amino acid sequence alignment of Sca5 protein from *R. conorii* and *R. montanensis*. Amino acid sequences of rickettsial Sca5 from *R. conorii* (RC0019) and *R. montanensis* (MCI_02705) were aligned using the ClustalW software. The alignment resulted in a percentage of sequence identity of 88.14 %.

```
rco_RC1270          MKRKNNKFIEISIAFILGIALGLYGQNPDYFTNLISQKSLALSALQIKHYNISELSRSKV
rmo_MCI_03585       MKRRNNKFIEISTAFILGIALGIYGQNPDYFTNLISQKSLALPALQIKHYNISELSRSKV
                    ***:******** *********:******************.*****************

rco_RC1270          STCFTPPAGCTKFIANQIDKAEESIYMQAYGMSDALITTALINAQARGVKVRILLDRSNL
rmo_MCI_03585       STCFTPPAGCTKFIANQIDKAEESIYMQAYGMSDELITTALINAQARGVKVRILLDRSNL
                    ******************************** ************************

rco_RC1270          KQKFSKLHELQRAKIDVDIDKVPGIAHNKVIIIDKKKVITGSFNFTAAADKRNAENVIII
rmo_MCI_03585       KQKFSKLHELQQAKIDVGIDKVPGIAHNKVIIIDKKKVITGSFNFTAAADKRNAENVIII
                    ***********:*****.****************************************

rco_RC1270          EDQELAESYLQNWLNRKASN
rmo_MCI_03585       EDQELAESYLQNWLNRKASN
                    ********************
```

Supplementary Figure II.8 | Amino acid sequence alignment of membranolytic phospholipase D protein from *R. conorii* and *R. montanensis.* Amino acid sequences of rickettsial phospholipase D from *R. conorii* (RC1270) and *R. montanensis* (MCI_03585) were aligned using the ClustalW software. The alignment resulted in a percentage of sequence identity of 96.50 %.

```
rmo_MCI_02955      MLKSSKKEDSSKKNQNNKLIFTVQKLFSPIKNFFRKTKTPDNFFGVIKRLKINSQKMTLD
rco_RC1141         MLKSSKKEDSSKKNQNNKLIFTVRKLFSPIKNFFRKTKTPDNFFGVIKRLKINSQKMTLD
                   ************************:**********************************

rmo_MCI_02955      ERNILANLLELEDKTIEDIMVPRSDIAAIKLTTNLEELSESIKLEVPHTRTLIYDGTLDN
rco_RC1141         ERNILANLLELEDKTIEDIMVPRSDIAAIKLTTNLEELSESIKLEVPHTRTLIYDGTLDN
                   ************************************************************

rmo_MCI_02955      VVGFIHIKDLFKALATKQNGRLKKLIRKHIIAAPSMKLLDLLAKMRRERTHIAIVVDEYG
rco_RC1141         VVGFIHIKDLFKALATKQNGRLKKLIRKHIIAAPSMKLLDLLAKMRRERTHIAIVVDEYG
                   ************************************************************

rmo_MCI_02955      GTDGLVTIEDLIEEIVGRIDDEHDQQLDSDNFKVINNSTIISNARVEVEVLEEIIGEKLQ
rco_RC1141         GTDGLVTIEDLIEEIVGRIDDEHDQQLDSDNFKVINNSTIIANARVEVEVLEEIIGEKLH
                   ************************************:***********************:

rmo_MCI_02955      NDDDEFDTIGGLVLTRVSSVPAIGTRIDISENIEIEVTDATPRSLKQVKIRLKNGLNGK
rco_RC1141         NDYDEFDTIGGLVLTRVSSVPAIGTRIDISENIEIEVTDATPRSLKQVKIRLKNGLNGQ
                   ** ***************************************************:
```

Supplementary Figure II.9 | Amino acid sequence alignment of haemolysin C protein from *R. conorii* and *R. montanensis.* Amino acid sequences of rickettsial haemolysin C from *R. conorii* (RC1141) and *R. montanensis* (MCI_02955) were aligned using the ClustalW software. The alignment resulted in a percentage of sequence identity of 98.34 %.

The following supplementary movies are available in digital format for consultation.

Supplementary Movie II.1 | THP-1-derived macrophages at 60 minutes post infection with *R. montanensis.* This movie corresponds to **Figure II.7A** and represents a 360 degrees rotation movie of the 3D projection of the stack of images (generated with 3D Viewer, ImageJ). Frame rate, 14 fps. (MOV, 1.35 MB)

Supplementary Movie II.2 | THP-1-derived macrophages at 24 hours post infection with *R. montanensis.* This movie corresponds to Figure **II.7C** and represents a 360 degrees rotation movie of the 3D projection of the stack of images (generated with 3D Viewer, ImageJ). Frame rate, 14 fps. (MOV, 1.79 MB)

Supplementary Movie II.3 | Vero cells at 60 minutes post infection with *R. montanensis*. This movie corresponds to **Supplementary Figure II.2A** and represents a 360 degrees rotation movie of the 3D projection of the stack of images (generated with 3D Viewer, ImageJ). Frame rate, 14 fps. (MOV, 1.04 MB)

Supplementary Movie II.4 | Vero cells at 24 hours post infection with *R. montanensis.* This movie corresponds to **Supplementary Figure II.2C** and represents a 360 degrees rotation movie of the 3D projection of the stack of images (generated with 3D Viewer, ImageJ). Frame rate, 14 fps. (MOV, 739.35 KB)

Supplementary Movie II.5 | THP-1-derived macrophages at 60 minutes post infection with *R. conorii.* This movie corresponds to **Figure II.8A** and represents a 360 degrees rotation movie of the 3D projection of the stack of images (generated with 3D Viewer, ImageJ). Frame rate, 14 fps. (MOV, 1.3 MB)

Supplementary Movie II.6 | THP-1-derived macrophages at 24hours post infection with *R. conorii.* This movie corresponds to **Figure II.8C** and represents a 360 degrees rotation movie of the 3D projection of the stack of images (generated with 3D Viewer, ImageJ). Frame rate, 14 fps. (MOV, 1.9 MB)

Supplementary Movie II.7 | Vero cells at 60 minutes post infection with *R. conorii.* This movie corresponds to **Supplementary Figure II.3A** and represents a 360 degrees rotation movie of the 3D projection of the stack of images (generated with 3D Viewer, ImageJ). Frame rate, 14 fps. (MOV, 747.97 KB)

Supplementary Movie 8 | Vero cells at 24 hours post infection with *R. conorii* . This movie corresponds to **Supplementary Figure II.3C** and represents a 360 degrees rotation movie of the 3D projection of the stack of images (generated with 3D Viewer, ImageJ). Frame rate, 14 fps. (MOV, 2.13 MB)

Supplementary Movie II.9 | THP-1-derived macrophages at 60 minutes post infection with *R. montanensis.* This movie corresponds to **Figure II.9B** and represents a 360 degrees rotation movie of the 3D projection of the stack of images (generated with 3D Viewer, ImageJ). Frame rate, 14 fps. (MOV, 1.02 MB)

Supplementary Movie II.10 | THP-1-derived macrophages at 24 hours post infection with *R. montanensis.* This movie corresponds to **Figure II.9C** and represents a 360 degrees rotation movie of the 3D projection of the stack of images (generated with 3D Viewer, ImageJ). Frame rate, 14 fps. (MOV, 2.77 MB)

Supplementary Movie II.11 | THP-1-derived macrophages at 60 minutes post infection with *R. conorii*. This movie corresponds to **Figure II.10B** and represents a 360 degrees rotation movie of the 3D projection of the stack of images (generated with 3D Viewer, ImageJ). Frame rate, 14 fps. (MOV, 1.98 MB)

Supplementary Movie II.12 | THP-1-derived macrophages at 24 hours post infection with *R. conorii.* This movie corresponds to **Figure II.10D** and represents a 360 degrees rotation movie of the 3D projection of the stack of images (generated with 3D Viewer, ImageJ). Frame rate, 14 fps. (MOV, 1.68 MB)

Supplementary Figures

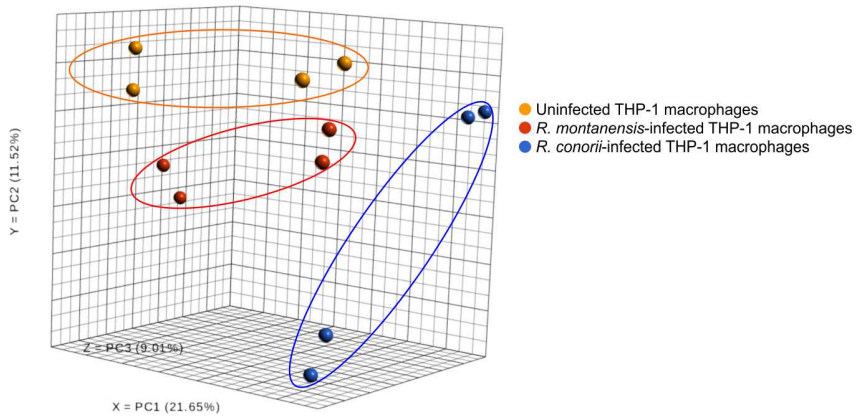

Supplementary Figure IV.1 | 3D principal component analysis (PCA) plots of global transcriptome profiles. 3D PCA plot was performed by importing the mapped read (BAM) files of all RNA-seq data into Partek® Flow® Software. Each sample is represented by a dot and the color label corresponds to the sample group. Orange dots correspond to uninfected THP-1 macrophages, red dots correspond to *R. montanensis*-infected THP-1 macrophages and blue dots correspond to *R. conorii*-infected THP-1 macrophages. The axes show the first three principal components, with the fraction of explained variance in the parenthesis.

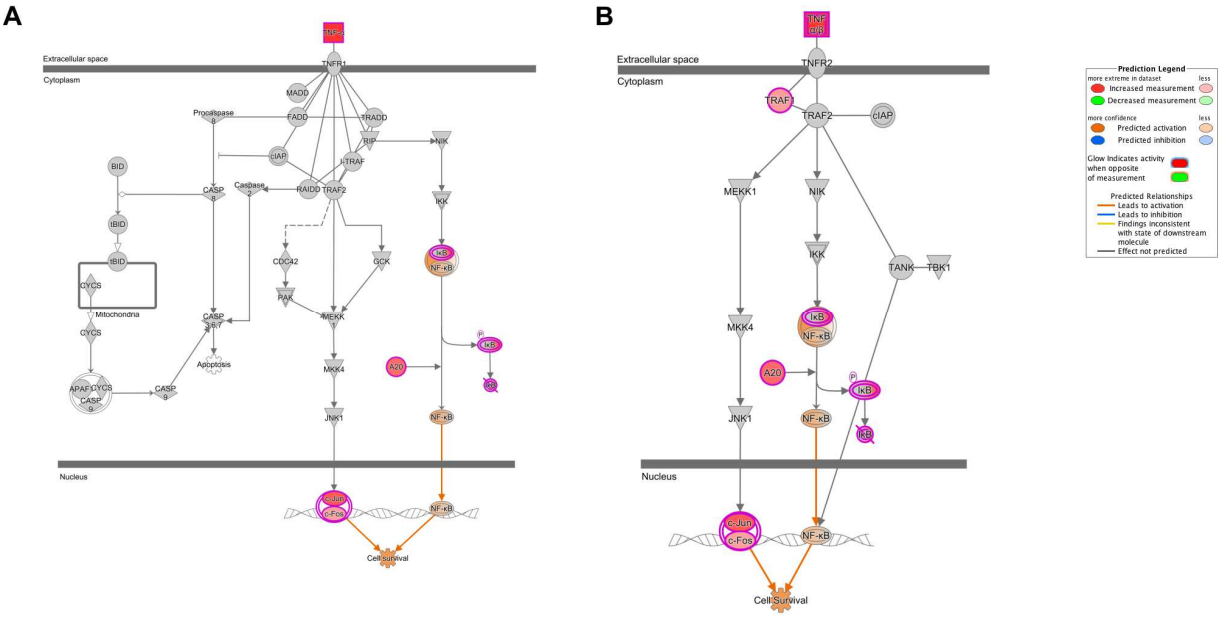

Supplementary Figure IV.2 | IPA depicting predicted activation of the TNFR1 and TNFR2 signaling pathways in *R. conorii*-infected THP-1 macrophages (Associated with Figure IV.3). Statistically significantly DE genes in *R. conorii*- *vs R. montanensis*-infected THP-1 macrophages were uploaded into IPA. Both TNFR1 **(A)** and TNFR2 **(B)** signaling pathways were predicted to be activated for *R. conorii*-infected THP-1 macrophages over *R. montanensis*-infected THP-1 cells (Z-score of 2.236; p-value of 1.45 x 10^{-5} and Z-score of 2.236; p-value of 2.40 x 10^{-8}), respectively.

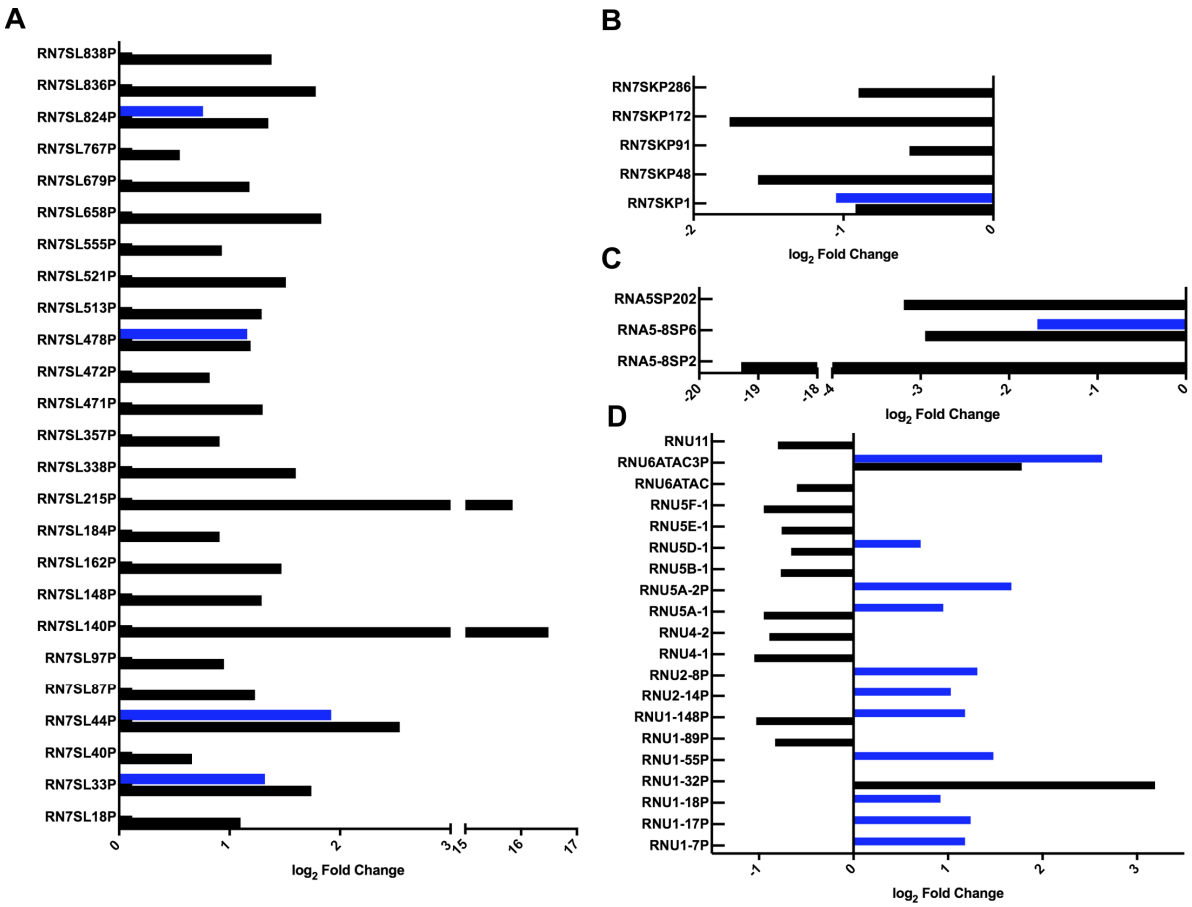

Supplementary Figure IV.3 | List DE non-coding RNAs in *R. conorii*- and *R. montanensis*-infected THP-1 macrophages (Associated with Figure IV.6). (A-D) List of DE non-coding RNAs in THP-1 macrophages infected with *R. conorii* (black) or *R. montanensis* (blue) according its type, 7SL RNAs (signal recognition particle RNAs) **(A)**, 7SK RNAs (7SK small nuclear RNAs) **(B)**, 5S-rRNAs (5S ribosomal RNAs) **(C)** and U-RNA (small nuclear RNAs) **(D)**. A detailed description of genes and log_2 fold change values can be found in **Supplementary table IV.9**.

Supplementary Tables

Supplementary Table IV.1. List of DE genes in *R. conorii*-infected THP-1 macrophages compared with uninfected cells (Associated with Figure IV.1). This table can be found in digital format for consultation.

OFFICIAL_GENE_SYMBOL	Gene_Name	Log_2 (Fold_Change)	locus	p_value	q_value
Y_RNA (1)	Uncharacterized	19.05	20:23457583-23457685	5.00E-05	0.00318053
Y_RNA (2)	Uncharacterized	18.36	17:7537095-7537196	0.0005	0.0217381
NDUFB4P11	NADH:ubiquinone oxidoreductase subunit B4 pseudogene 11(NDUFB4P11)	13.94	14:103139674-103141959	5.00E-05	0.00318053
DNAAF1	dynein axonemal assembly factor 1(DNAAF1)	13.63	16:84145286-84187070	5.00E-05	0.00318053
AP000769.7	Uncharacterized	13.42	11:65497761-65506516	0.0011	0.0394298
RN7SL140P	RNA, 7SL, cytoplasmic 140, pseudogene(RN7SL140P)	13.17	2:20175345-20175639	0.0001	0.00579142
RP4-607I7.1	Uncharacterized	13.17	11:35132654-35138032	5.00E-05	0.00318053
AC061992.2	Uncharacterized	12.91	17:78315728-78347798	5.00E-05	0.00318053
RN7SL215P	RNA, 7SL, cytoplasmic 215, pseudogene(RN7SL215P)	12.53	3:194145673-194145971	0.0004	0.0181532
RP1-140K8.2	Uncharacterized	12.50	6:3913921-3914292	5.00E-05	0.00318053
CCL4L2	C-C motif chemokine ligand 4 like 2(CCL4L2)	8.59	17:36210923-36212878	5.00E-05	0.00318053
TNF	tumor necrosis factor(TNF)	7.93	6:31575566-31578336	5.00E-05	0.00318053
CCL3L3	C-C motif chemokine ligand 3 like 3(CCL3L3)	7.05	17:36183234-36196758	5.00E-05	0.00318053
CXCL1	C-X-C motif chemokine ligand 1(CXCL1)	5.59	4:73869392-73871242	5.00E-05	0.00318053
IL1A	interleukin 1 alpha(IL1A)	5.59	2:112773914-112784590	5.00E-05	0.00318053
CXCL3	C-X-C motif chemokine ligand 3(CXCL3)	5.55	4:74036588-74038807	5.00E-05	0.00318053
CCL3	C-C motif chemokine ligand 3(CCL3)	5.55	17:36072865-36090169	5.00E-05	0.00318053
AC058791.1	Uncharacterized	5.33	7:130853719-130928649	5.00E-05	0.00318053
NFKBIA	NFKB inhibitor alpha(NFKBIA)	5.29	14:35401510-35404749	5.00E-05	0.00318053
DUSP2	dual specificity phosphatase 2(DUSP2)	4.89	2:96143165-96145440	5.00E-05	0.00318053
SOCS3	suppressor of cytokine signaling 3(SOCS3)	4.89	17:78356777-78360077	5.00E-05	0.00318053
PTGS2	prostaglandin-endoperoxide synthase 2(PTGS2)	4.86	1:186671790-186680427	5.00E-05	0.00318053
DUSP1	dual specificity phosphatase 1(DUSP1)	4.68	5:172758225-172777774	5.00E-05	0.00318053
CCL20	C-C motif chemokine ligand 20(CCL20)	4.57	2:227813841-227817564	5.00E-05	0.00318053
NFKBIZ	NFKB inhibitor zeta(NFKBIZ)	4.53	3:101827990-101861022	5.00E-05	0.00318053
CXCL8	C-X-C motif chemokine ligand 8(CXCL8)	4.24	4:73740505-73743716	5.00E-05	0.00318053
ASTL	astacin like metalloendopeptidase(ASTL)	4.23	2:96123849-96138436	5.00E-05	0.00318053
FOSB	FosB proto-oncogene, AP-1 transcription factor subunit(FOSB)	4.02	19:45379633-45478828	5.00E-05	0.00318053
OSM	oncostatin M(OSM)	3.99	22:30262828-30266840	5.00E-05	0.00318053
EGR4	early growth response 4(EGR4)	3.94	2:73290928-73293705	5.00E-05	0.00318053
RRAD	RRAD, Ras related glycolysis inhibitor and calcium channel regulator(RRAD)	3.78	16:66921678-66925644	5.00E-05	0.00318053
CD69	CD69 molecule(CD69)	3.71	12:9752485-9760901	5.00E-05	0.00318053
TNFAIP3	TNF alpha induced protein 3(TNFAIP3)	3.68	6:137823672-137883312	5.00E-05	0.00318053

KCNA3	potassium voltage-gated channel subfamily A member 3(KCNA3)	3.49	1:110672464-110675033	5.00E-05	0.00318053
EGR1	early growth response 1(EGR1)	3.32	5:138465489-138469315	5.00E-05	0.00318053
SOD2	superoxide dismutase 2, mitochondrial(SOD2)	3.25	6:159669056-159789749	5.00E-05	0.00318053
FAM71A	family with sequence similarity 71 member A(FAM71A)	3.23	1:212624283-212626778	5.00E-05	0.00318053
RNU1-32P	RNA, U1 small nuclear 32, pseudogene(RNU1-32P)	3.19	2:60359215-60391375	5.00E-05	0.00318053
JUN	Jun proto-oncogene, AP-1 transcription factor subunit(JUN)	3.14	1:58780787-58784327	5.00E-05	0.00318053
PDGFB	platelet derived growth factor subunit B(PDGFB)	3.10	22:39223358-39244751	0.0003	0.0143713
IER3	immediate early response 3(IER3)	3.09	6:30742928-30744554	5.00E-05	0.00318053
ATF3	activating transcription factor 3(ATF3)	3.08	1:212565333-212620777	5.00E-05	0.00318053
LRRC32	leucine rich repeat containing 32(LRRC32)	3.08	11:76657055-76670747	0.00025	0.0123183
JUNB	JunB proto-oncogene, AP-1 transcription factor subunit(JUNB)	3.06	19:12763002-12874951	5.00E-05	0.00318053
GEM	GTP binding protein overexpressed in skeletal muscle(GEM)	3.05	8:94249252-94262350	5.00E-05	0.00318053
RPL24P2	ribosomal protein L24 pseudogene 2(RPL24P2)	2.99	20:21114722-21115197	5.00E-05	0.00318053
IL1B	interleukin 1 beta(IL1B)	2.98	2:112829750-112836903	5.00E-05	0.00318053
BTG2	BTG anti-proliferation factor 2(BTG2)	2.97	1:203305490-203309602	5.00E-05	0.00318053
LINC00346	long intergenic non-protein coding RNA 346(LINC00346)	2.93	13:110863986-110870251	5.00E-05	0.00318053
C11orf96	chromosome 11 open reading frame 96(C11orf96)	2.79	11:43921058-44001157	5.00E-05	0.00318053
ZFP36	ZFP36 ring finger protein(ZFP36)	2.76	19:39406812-39409412	5.00E-05	0.00318053
SNAI1	snail family transcriptional repressor 1(SNAI1)	2.75	20:49982998-49988886	5.00E-05	0.00318053
RP11-527N22.1	Uncharacterized	2.69	8:37326574-37331984	5.00E-05	0.00318053
RPL7P37	ribosomal protein L7 pseudogene 37(RPL7P37)	2.68	10:35697299-35698037	0.0002	0.0101777
ATP2B1-AS1	Uncharacterized	2.67	12:89561128-89712590	5.00E-05	0.00318053
PPP1R15A	protein phosphatase 1 regulatory subunit 15A(PPP1R15A)	2.66	19:48872391-48876057	5.00E-05	0.00318053
CREB5	cAMP responsive element binding protein 5(CREB5)	2.65	7:28299320-28825894	5.00E-05	0.00318053
CTGF	connective tissue growth factor(CTGF)	2.59	6:131948175-132077393	5.00E-05	0.00318053
LINC01353	long intergenic non-protein coding RNA 1353(LINC01353)	2.56	1:203287151-203288801	0.00035	0.0162645
G0S2	G0/G1 switch 2(G0S2)	2.55	1:209661363-209734950	5.00E-05	0.00318053
RN7SL44P	RNA, 7SL, cytoplasmic 44, pseudogene(RN7SL44P)	2.54	1:153500462-153500764	5.00E-05	0.00318053
CD83	CD83 molecule(CD83)	2.53	6:14117255-14136918	5.00E-05	0.00318053
KLF2	Kruppel like factor 2(KLF2)	2.50	19:16324816-16327874	0.00075	0.0302357
BHLHE40	basic helix-loop-helix family member e40(BHLHE40)	2.49	3:4896808-4985323	5.00E-05	0.00318053
OTUD1	OTU deubiquitinase 1(OTUD1)	2.47	10:23439457-23442390	5.00E-05	0.00318053
KLF10	Kruppel like factor 10(KLF10)	2.40	8:102648778-102655902	5.00E-05	0.00318053
MTRNR2L1	MT-RNR2-like 1(MTRNR2L1)	2.40	17:22523110-22525686	5.00E-05	0.00318053
ZC3H12A	zinc finger CCCH-type containing 12A(ZC3H12A)	2.39	1:37474551-37484379	5.00E-05	0.00318053
ZNF565	zinc finger protein 565(ZNF565)	2.35	19:36182059-36246257	0.00015	0.00816895
UBE3D	ubiquitin protein ligase E3D(UBE3D)	2.32	6:82892397-83065841	5.00E-05	0.00318053
RPL13AP7	ribosomal protein L13a pseudogene 7(RPL13AP7)	2.24	21:25361820-25362431	5.00E-05	0.00318053
HCAR3	hydroxycarboxylic acid receptor 3(HCAR3)	2.18	12:122687124-122716892	5.00E-05	0.00318053

KDM6B	lysine demethylase 6B(KDM6B)	2.17	17:7839903-7854796	5.00E-05	0.00318053
EDN1	endothelin 1(EDN1)	2.15	6:12290362-12297194	5.00E-05	0.00318053
MIR137	microRNA 137(MIR137)	2.13	1:97986739-98049863	5.00E-05	0.00318053
HCAR2	hydroxycarboxylic acid receptor 2(HCAR2)	2.08	12:122687124-122716892	5.00E-05	0.00318053
PIM3	Pim-3 proto-oncogene, serine/threonine kinase(PIM3)	2.06	22:49960512-49964080	5.00E-05	0.00318053
PRDM1	PR/SET domain 1(PRDM1)	2.05	6:106045422-106325791	5.00E-05	0.00318053
ANKRD30BL	ankyrin repeat domain 30B like(ANKRD30BL)	2.03	2:132147590-132257969	5.00E-05	0.00318053
MTRNR2L10	MT-RNR2-like 10(MTRNR2L10)	1.97	X:55181390-55182920	5.00E-05	0.00318053
RGS16	regulator of G-protein signaling 16(RGS16)	1.91	1:182598622-182604408	5.00E-05	0.00318053
RP11-384O8.1	Uncharacterized	1.89	2:222317241-222352989	5.00E-05	0.00318053
LINC02202	Uncharacterized	1.89	5:159100482-159117478	0.0015	0.0495351
BCL3	B-cell CLL/lymphoma 3(BCL3)	1.87	19:44747704-44760044	5.00E-05	0.00318053
RN7SL658P	RNA, 7SL, cytoplasmic 658, pseudogene(RN7SL658P)	1.83	X:16539136-16539439	5.00E-05	0.00318053
CTD-3014M21.1	Uncharacterized	1.80	17:43360040-43361361	5.00E-05	0.00318053
RP11-408P14.1	Uncharacterized	1.80	4:65319562-65698029	5.00E-05	0.00318053
RNU6ATAC3P	RNA, U6atac small nuclear 3, pseudogene(RNU6ATAC3P)	1.78	17:46916769-46923034	0.0011	0.0394298
OSR2	odd-skipped related transciption factor 2(OSR2)	1.78	8:98944402-98952104	0.00105	0.038256
RN7SL836P	RNA, 7SL, cytoplasmic 836, pseudogene(RN7SL836P)	1.78	19:45651509-45651805	5.00E-05	0.00318053
LINC01686	Uncharacterized	1.78	1:182615253-182616629	5.00E-05	0.00318053
CSRNP1	cysteine and serine rich nuclear protein 1(CSRNP1)	1.75	3:39141854-39154723	5.00E-05	0.00318053
PTX3	pentraxin 3(PTX3)	1.75	3:157175222-157533619	5.00E-05	0.00318053
RN7SL33P	RNA, 7SL, cytoplasmic 33, pseudogene(RN7SL33P)	1.74	17:2557752-2558094	5.00E-05	0.00318053
MAFF	MAF bZIP transcription factor F(MAFF)	1.74	22:38111494-38216511	5.00E-05	0.00318053
ARL5B	ADP ribosylation factor like GTPase 5B(ARL5B)	1.72	10:18659404-18681639	5.00E-05	0.00318053
TNFAIP2	TNF alpha induced protein 2(TNFAIP2)	1.71	14:103123441-103137439	5.00E-05	0.00318053
MBD5	methyl-CpG binding domain protein 5(MBD5)	1.71	2:147844516-148516971	5.00E-05	0.00318053
KLF6	Kruppel like factor 6(KLF6)	1.68	10:3775995-3785281	5.00E-05	0.00318053
RASGEF1B	RasGEF domain family member 1B(RASGEF1B)	1.67	4:81426392-82044244	5.00E-05	0.00318053
ANXA2P2	annexin A2 pseudogene 2(ANXA2P2)	1.67	9:33624273-33625293	0.0009	0.0343216
DUSP8	dual specificity phosphatase 8(DUSP8)	1.66	11:1554043-1599184	0.0001	0.00579142
NOCT	nocturnin(NOCT)	1.66	4:139015788-139177218	0.0012	0.0421385
MTRNR2L12	MT-RNR2-like 12(MTRNR2L12)	1.65	3:96617187-96618236	5.00E-05	0.00318053
SHISA2	shisa family member 2(SHISA2)	1.63	13:26044596-26051031	0.00075	0.0302357
ICAM1	intercellular adhesion molecule 1(ICAM1)	1.63	19:10251900-10289019	5.00E-05	0.00318053
RP11-61J19.5	Uncharacterized	1.61	1:212557832-212559731	0.00135	0.0460513
RN7SL338P	RNA, 7SL, cytoplasmic 338, pseudogene(RN7SL338P)	1.60	9:35049270-35049563	5.00E-05	0.00318053
LYPLA2P2	lysophospholipase II pseudogene 2(LYPLA2P2)	1.58	19:7879444-7880120	0.0001	0.00579142
EEF1A1P11	eukaryotic translation elongation factor 1 alpha 1 pseudogene 11(EEF1A1P11)	1.57	1:96446929-96448318	5.00E-05	0.00318053
FAM153C	family with sequence similarity 153, member C, pseudogene(FAM153C)	1.56	5:178006404-178056194	5.00E-05	0.00318053

PTGER4	prostaglandin E receptor 4(PTGER4)	1.55	5:40512332-40755975	5.00E-05	0.00318053
RPL13AP5	ribosomal protein L13a pseudogene 5(RPL13AP5)	1.55	10:96750287-96750899	5.00E-05	0.00318053
IER2	immediate early response 2(IER2)	1.54	19:13150414-13154908	5.00E-05	0.00318053
U1(1)	Uncharacterized	1.54	1:148522600-148522765	5.00E-05	0.00318053
RN7SL521P	RNA, 7SL, cytoplasmic 521, pseudogene(RN7SL521P)	1.51	7:149102783-149126346	5.00E-05	0.00318053
JADE3	jade family PHD finger 3(JADE3)	1.51	X:46912275-47061242	0.0012	0.0421385
SAT1	spermidine/spermine N1-acetyltransferase 1(SAT1)	1.50	X:23783172-23786226	5.00E-05	0.00318053
RN7SL162P	RNA, 7SL, cytoplasmic 162, pseudogene(RN7SL162P)	1.47	22:27851668-28679865	5.00E-05	0.00318053
SPACA6	sperm acrosome associated 6(SPACA6)	1.46	19:51685362-51712387	5.00E-05	0.00318053
GADD45B	growth arrest and DNA damage inducible beta(GADD45B)	1.45	19:2476121-2478259	5.00E-05	0.00318053
PLAU	plasminogen activator, urokinase(PLAU)	1.45	10:73909176-73922777	5.00E-05	0.00318053
TUBB2A	tubulin beta 2A class IIa(TUBB2A)	1.44	6:3153668-3157526	0.0015	0.0495351
TRAF1	TNF receptor associated factor 1(TRAF1)	1.44	9:120902392-120929173	5.00E-05	0.00318053
RP3-340B19.2	Uncharacterized	1.43	6:35555872-35556264	5.00E-05	0.00318053
Y_RNA (3)	Uncharacterized	1.42	11:118836009-118836111	0.0005	0.0217381
RN7SL838P	RNA, 7SL, cytoplasmic 838, pseudogene(RN7SL838P)	1.38	11:417932-442011	5.00E-05	0.00318053
IL23A	interleukin 23 subunit alpha(IL23A)	1.38	12:56334173-56340410	5.00E-05	0.00318053
IER5	immediate early response 5(IER5)	1.37	1:181088711-181092899	5.00E-05	0.00318053
CKS2	CDC28 protein kinase regulatory subunit 2(CKS2)	1.36	9:89311197-89316703	5.00E-05	0.00318053
RN7SL824P	RNA, 7SL, cytoplasmic 824, pseudogene(RN7SL824P)	1.35	1:92402388-92402685	5.00E-05	0.00318053
RP11-810P12.7	Uncharacterized	1.34	11:61967793-61969490	5.00E-05	0.00318053
RP11-553P9.1	Uncharacterized	1.33	4:135045463-135046850	0.0004	0.0181532
RIPK2	receptor interacting serine/threonine kinase 2(RIPK2)	1.32	8:89757746-89791063	5.00E-05	0.00318053
RHOB	ras homolog family member B(RHOB)	1.31	2:20447073-20449445	5.00E-05	0.00318053
XIRP1	xin actin binding repeat containing 1(XIRP1)	1.31	3:39183209-39192596	5.00E-05	0.00318053
RN7SL471P	RNA, 7SL, cytoplasmic 471, pseudogene(RN7SL471P)	1.30	6:28977474-28977773	0.0002	0.0101777
RN7SL513P	RNA, 7SL, cytoplasmic 513, pseudogene(RN7SL513P)	1.29	19:18333275-18333573	5.00E-05	0.00318053
RN7SL148P	RNA, 7SL, cytoplasmic 148, pseudogene(RN7SL148P)	1.29	1:244103931-244104210	0.0001	0.00579142
NDE1	nudE neurodevelopment protein 1(NDE1)	1.29	16:15643266-15857033	5.00E-05	0.00318053
NFE2L2	nuclear factor, erythroid 2 like 2(NFE2L2)	1.28	2:177227594-177559299	5.00E-05	0.00318053
STX11	syntaxin 11(STX11)	1.26	6:144150525-144188370	5.00E-05	0.00318053
F3	coagulation factor III, tissue factor(F3)	1.26	1:94529224-94541800	0.00035	0.0162645
NAMPT	nicotinamide phosphoribosyltransferase(NAMPT)	1.25	7:106248284-106286326	0.00035	0.0162645
TNFSF9	tumor necrosis factor superfamily member 9(TNFSF9)	1.25	19:6530998-6535928	5.00E-05	0.00318053
ERICD	E2F1-regulated inhibitor of cell death (non-protein coding)(ERICD)	1.25	8:140636280-140638283	5.00E-05	0.00318053
RN7SL87P	RNA, 7SL, cytoplasmic 87, pseudogene(RN7SL87P)	1.23	5:144140878-144141166	0.00095	0.0357887
FOS	Fos proto-oncogene, AP-1 transcription factor subunit(FOS)	1.21	14:75278773-75282230	5.00E-05	0.00318053
BCL2A1	BCL2 related protein A1(BCL2A1)	1.20	15:79960888-79971446	5.00E-05	0.00318053
UHRF1BP1	UHRF1 binding protein 1(UHRF1BP1)	1.19	6:34792014-34888089	0.0005	0.0217381

RN7SL478P	RNA, 7SL, cytoplasmic 478, pseudogene(RN7SL478P)	1.19	7:97998324-97998622	5.00E-05	0.00318053
RN7SL679P	RNA, 7SL, cytoplasmic 679, pseudogene(RN7SL679P)	1.18	1:26593242-26593546	5.00E-05	0.00318053
EHD1	EH domain containing 1(EHD1)	1.17	11:64851641-64888296	5.00E-05	0.00318053
RPS3AP6	ribosomal protein S3A pseudogene 6(RPS3AP6)	1.16	15:59768351-59769146	5.00E-05	0.00318053
TRIB1	tribbles pseudokinase 1(TRIB1)	1.15	8:125430320-125438405	5.00E-05	0.00318053
ARRDC3	arrestin domain containing 3(ARRDC3)	1.15	5:91368723-91439085	0.001	0.0371316
PLK3	polo like kinase 3(PLK3)	1.14	1:44800224-44806675	5.00E-05	0.00318053
NLRP3	NLR family pyrin domain containing 3(NLRP3)	1.14	1:247416155-247449108	0.00015	0.00816895
Y_RNA (4)	Uncharacterized	1.12	20:16670640-16670742	0.00015	0.00816895
SNN	stannin(SNN)	1.11	16:11668413-11744506	0.0003	0.0143713
RN7SL18P	RNA, 7SL, cytoplasmic 18, pseudogene(RN7SL18P)	1.10	2:62491177-62491468	5.00E-05	0.00318053
BCL6	B-cell CLL/lymphoma 6(BCL6)	1.10	3:187698258-187746028	0.00105	0.038256
NFKB2	nuclear factor kappa B subunit 2(NFKB2)	1.10	10:102394109-102402529	0.00025	0.0123183
Y_RNA (5)	Uncharacterized	1.09	10:10232610-10232712	0.0014	0.0472378
YBX1P10	Y-box binding protein 1 pseudogene 10(YBX1P10)	1.08	9:35971343-35972318	5.00E-05	0.00318053
ETS2	ETS proto-oncogene 2, transcription factor(ETS2)	1.07	21:38805306-38824955	5.00E-05	0.00318053
RPL24P4	ribosomal protein L24 pseudogene 4(RPL24P4)	1.05	6:42956344-42956765	0.00115	0.0407515
RGS1	regulator of G-protein signaling 1(RGS1)	1.05	1:192575726-192580031	5.00E-05	0.00318053
CCRL2	C-C motif chemokine receptor like 2(CCRL2)	1.05	3:46407162-46412997	5.00E-05	0.00318053
EPOP	Elongin BC and polycomb repressive complex 2 associated protein(EPOP)	1.05	17:38671702-38675421	5.00E-05	0.00318053
FTH1	ferritin heavy chain 1(FTH1)	1.04	11:61949820-61967660	5.00E-05	0.00318053
MTRNR2L6	MT-RNR2-like 6(MTRNR2L6)	1.04	7:142666271-142667718	0.0007	0.0287426
PRKCQ-AS1	PRKCQ antisense RNA 1(PRKCQ-AS1)	1.04	10:6580418-6616452	0.0009	0.0343216
RPL6P27	ribosomal protein L6 pseudogene 27(RPL6P27)	1.03	18:6462143-6463015	0.00015	0.00816895
PMAIP1	phorbol-12-myristate-13-acetate-induced protein 1(PMAIP1)	1.02	18:59899947-59904306	5.00E-05	0.00318053
RND3	Rho family GTPase 3(RND3)	1.02	2:150468194-150539011	5.00E-05	0.00318053
FOSL1	FOS like 1, AP-1 transcription factor subunit(FOSL1)	1.01	11:65892048-65900573	5.00E-05	0.00318053
YBX1P1	Y-box binding protein 1 pseudogene 1(YBX1P1)	1.00	14:66012829-66013789	5.00E-05	0.00318053
RPL3P4	ribosomal protein L3 pseudogene 4(RPL3P4)	0.99	14:98972878-98973301	0.0001	0.00579142
SGK1	serum/glucocorticoid regulated kinase 1(SGK1)	0.99	6:134169245-134318112	5.00E-05	0.00318053
RP11-475C16.1	Uncharacterized	0.99	6:153231319-153347488	5.00E-05	0.00318053
ZNF697	zinc finger protein 697(ZNF697)	0.98	1:119619421-119647773	5.00E-05	0.00318053
DUSP5	dual specificity phosphatase 5(DUSP5)	0.96	10:110497837-110511544	5.00E-05	0.00318053
PPP1R14C	protein phosphatase 1 regulatory inhibitor subunit 14C(PPP1R14C)	0.96	6:150143075-150250357	5.00E-05	0.00318053
RN7SL97P	RNA, 7SL, cytoplasmic 97, pseudogene(RN7SL97P)	0.95	18:25818233-25818532	0.00065	0.0268315
RN7SL555P	RNA, 7SL, cytoplasmic 555, pseudogene(RN7SL555P)	0.93	20:3094170-3094509	5.00E-05	0.00318053
PLAGL2	PLAG1 like zinc finger 2(PLAGL2)	0.93	20:32192502-32207791	5.00E-05	0.00318053
PHLDA1	pleckstrin homology like domain family A member 1(PHLDA1)	0.92	12:76025446-76033932	5.00E-05	0.00318053
EGR2	early growth response 2(EGR2)	0.91	10:62811995-62919900	0.0002	0.0101777

RN7SL357P	RNA, 7SL, cytoplasmic 357, pseudogene(RN7SL357P)	0.91	4:56805833-56806131	0.0001	0.00579142
RN7SL184P	RNA, 7SL, cytoplasmic 184, pseudogene(RN7SL184P)	0.91	4:113419839-113420136	0.0002	0.0101777
GBP1	guanylate binding protein 1(GBP1)	0.90	1:89052318-89065360	0.0011	0.0394298
MARCKS	myristoylated alanine rich protein kinase C substrate(MARCKS)	0.90	6:113857361-113863471	5.00E-05	0.00318053
MSC	musculin(MSC)	0.89	8:71828166-72118393	5.00E-05	0.00318053
B3GNT5	UDP-GlcNAc:betaGal beta-1,3-N-acetylglucosaminyltransferase 5(B3GNT5)	0.89	3:183178042-183428778	0.0014	0.0472378
CITED4	Cbp/p300 interacting transactivator with Glu/Asp rich carboxy-terminal domain 4(CITED4)	0.88	1:40861050-40862366	5.00E-05	0.00318053
ZBTB10	zinc finger and BTB domain containing 10(ZBTB10)	0.88	8:80484560-80526265	5.00E-05	0.00318053
SRGAP2D	SLIT-ROBO Rho GTPase activating protein 2D (pseudogene)(SRGAP2D)	0.88	1:143975086-144068350	0.00095	0.0357887
EIF3FP3	eukaryotic translation initiation factor 3 subunit F pseudogene 3(EIF3FP3)	0.87	2:58251439-58252525	0.0001	0.00579142
RGS2	regulator of G-protein signaling 2(RGS2)	0.87	1:192809038-192812283	5.00E-05	0.00318053
RPS19P1	ribosomal protein S19 pseudogene 1(RPS19P1)	0.86	20:18504632-18505066	0.00015	0.00816895
EEF1A1P9	eukaryotic translation elongation factor 1 alpha 1 pseudogene 9(EEF1A1P9)	0.86	4:105484697-105486080	5.00E-05	0.00318053
TNFSF15	tumor necrosis factor superfamily member 15(TNFSF15)	0.86	9:114784634-114806126	5.00E-05	0.00318053
TNFAIP8	TNF alpha induced protein 8(TNFAIP8)	0.86	5:119268691-119399688	0.0004	0.0181532
SMAD7	SMAD family member 7(SMAD7)	0.85	18:48919852-48950711	0.0005	0.0217381
EEF1A1P12	eukaryotic translation elongation factor 1 alpha 1 pseudogene 12(EEF1A1P12)	0.85	2:106697330-106698676	0.00115	0.0407515
SLC2A6	solute carrier family 2 member 6(SLC2A6)	0.85	9:133471094-133479137	5.00E-05	0.00318053
NUDT15	nudix hydrolase 15(NUDT15)	0.85	13:48037566-48047222	0.00095	0.0357887
UQCRHL	ubiquinol-cytochrome c reductase hinge protein like(UQCRHL)	0.84	1:15807168-15809348	5.00E-05	0.00318053
YRDC	yrdC N6-threonylcarbamoyltransferase domain containing(YRDC)	0.84	1:37802943-37809454	0.0001	0.00579142
CH507-42P11.8	Uncharacterized	0.84	21:6111133-6123739	0.0002	0.0101777
EIF1	eukaryotic translation initiation factor 1(EIF1)	0.83	17:41688884-41692668	5.00E-05	0.00318053
NFKBIE	NFKB inhibitor epsilon(NFKBIE)	0.83	6:44258165-44265788	5.00E-05	0.00318053
PLEK	pleckstrin(PLEK)	0.82	2:68361213-68397453	5.00E-05	0.00318053
RN7SL472P	RNA, 7SL, cytoplasmic 472, pseudogene(RN7SL472P)	0.82	14:102077179-102077472	5.00E-05	0.00318053
MXD1	MAX dimerization protein 1(MXD1)	0.81	2:69893559-69942945	0.00015	0.00816895
ACKR3	atypical chemokine receptor 3(ACKR3)	0.81	2:236567786-236582358	5.00E-05	0.00318053
RPS2P46	ribosomal protein S2 pseudogene 46(RPS2P46)	0.80	17:19417803-19492991	0.0004	0.0181532
JUND	JunD proto-oncogene, AP-1 transcription factor subunit(JUND)	0.80	19:18279759-18281622	0.00035	0.0162645
FLOT1	flotillin 1(FLOT1)	0.80	6:30727708-30742733	0.00095	0.0357887
MCL1	BCL2 family apoptosis regulator(MCL1)	0.78	1:150548561-150579738	0.00065	0.0268315
DDIT4	DNA damage inducible transcript 4(DDIT4)	0.78	10:72273919-72276036	0.00025	0.0123183
SDC4	syndecan 4(SDC4)	0.78	20:45325287-45348424	5.00E-05	0.00318053
E2F7	E2F transcription factor 7(E2F7)	0.78	12:77021246-77065580	5.00E-05	0.00318053
DUSP10	dual specificity phosphatase 10(DUSP10)	0.77	1:221701423-221742176	0.0001	0.00579142
ZBTB5	zinc finger and BTB domain containing 5(ZBTB5)	0.77	9:37438113-37465399	5.00E-05	0.00318053
ZC3H12C	zinc finger CCCH-type containing 12C(ZC3H12C)	0.77	11:110093360-110171841	5.00E-05	0.00318053

PNRC1	proline rich nuclear receptor coactivator 1(PNRC1)	0.76	6:89080750-89085160	0.0001	0.00579142
JRKL	JRK-like(JRKL)	0.76	11:96389988-96507574	0.0004	0.0181532
CAP1P2	CAP1 pseudogene 2(CAP1P2)	0.75	10:43604842-43606251	5.00E-05	0.00318053
CITED2	Cbp/p300 interacting transactivator with Glu/Asp rich carboxy-terminal domain 2(CITED2)	0.74	6:139371806-139374620	0.00015	0.00816895
RNF19B	ring finger protein 19B(RNF19B)	0.74	1:32936444-32964685	5.00E-05	0.00318053
KB-1042C11.5	Uncharacterized	0.73	8:102656463-102687118	0.00135	0.0460513
HIST1H2BG	histone cluster 1 H2B family member g(HIST1H2BG)	0.72	6:26215158-26216692	5.00E-05	0.00318053
MYC	v-myc avian myelocytomatosis viral oncogene homolog(MYC)	0.71	8:127735433-127741434	0.0008	0.0315949
RNVU1-15	RNA, variant U1 small nuclear 15(RNVU1-15)	0.71	1:144412575-144412740	0.0001	0.00579142
MZT1	mitotic spindle organizing protein 1(MZT1)	0.70	13:72708356-72727687	0.00045	0.0199556
ZFP36L1	ZFP36 ring finger protein like 1(ZFP36L1)	0.69	14:68787659-68796253	5.00E-05	0.00318053
HIST1H4E	histone cluster 1 H4 family member e(HIST1H4E)	0.69	6:26204551-26206038	5.00E-05	0.00318053
RPL9P9	Uncharacterized	0.68	15:82355141-82439153	5.00E-05	0.00318053
H3F3B	H3 histone family member 3B(H3F3B)	0.67	17:75776433-75825799	0.00055	0.023647
CDKN1A	cyclin dependent kinase inhibitor 1A(CDKN1A)	0.67	6:36676459-36687339	0.00065	0.0268315
GBP2	guanylate binding protein 2(GBP2)	0.67	1:89106131-89176040	5.00E-05	0.00318053
REL	REL proto-oncogene, NF-kB subunit(REL)	0.66	2:60881520-60931610	0.0012	0.0421385
RN7SL40P	RNA, 7SL, cytoplasmic 40, pseudogene(RN7SL40P)	0.66	2:202357075-202357417	5.00E-05	0.00318053
NINJ1	ninjurin 1(NINJ1)	0.65	9:93121488-93134288	0.0002	0.0101777
CCNL1	cyclin L1(CCNL1)	0.65	3:157146507-157160760	0.00065	0.0268315
LCP2	lymphocyte cytosolic protein 2(LCP2)	0.65	5:170232446-170298227	0.0009	0.0343216
CEBPD	CCAAT/enhancer binding protein delta(CEBPD)	0.62	8:47736908-47739086	0.0009	0.0343216
SDE2	SDE2 telomere maintenance homolog(SDE2)	0.60	1:225982701-225999331	0.0001	0.00579142
SERTAD1	SERTA domain containing 1(SERTAD1)	0.59	19:40421591-40426025	0.0001	0.00579142
PTGES3	prostaglandin E synthase 3(PTGES3)	0.59	12:56663340-56688408	0.00045	0.0199556
CYTOR	cytoskeleton regulator RNA(CYTOR)	0.58	2:87439522-87606805	0.0004	0.0181532
PLIN2	perilipin 2(PLIN2)	0.58	9:19108374-19149290	0.00075	0.0302357
CH17-373J23.1	Uncharacterized	0.56	1:145281115-145281462	0.00035	0.0162645
RN7SL767P	RNA, 7SL, cytoplasmic 767, pseudogene(RN7SL767P)	0.55	3:113632703-113632998	0.0002	0.0101777
ETV3	ETS variant 3(ETV3)	0.54	1:157121190-157138474	0.00095	0.0357887
COMMD6	COMM domain containing 6(COMMD6)	0.54	13:75525218-75549439	0.001	0.0371316
KPNA3	karyopherin subunit alpha 3(KPNA3)	0.54	13:49699306-49793307	0.0009	0.0343216
CHMP1B	charged multivesicular body protein 1B(CHMP1B)	0.54	18:11688955-11909223	0.0014	0.0472378
H1F0	H1 histone family member 0(H1F0)	0.53	22:37805092-37807436	0.0003	0.0143713
TICAM1	toll like receptor adaptor molecule 1(TICAM1)	0.53	19:4815931-4831704	0.00085	0.0333153
AC024592.12	Uncharacterized	0.52	19:5865825-5904006	0.00075	0.0302357
MID1IP1	MID1 interacting protein 1(MID1IP1)	0.51	X:38801431-38806537	0.0014	0.0472378
OSTF1	osteoclast stimulating factor 1(OSTF1)	0.50	9:75088542-75147265	0.00105	0.038256

H1FX	H1 histone family member X(H1FX)	0.49	3:129314770-129326225	0.0009	0.0343216
NFIL3	nuclear factor, interleukin 3 regulated(NFIL3)	0.47	9:91409044-91423862	0.0013	0.0448384
FUCA1	fucosidase, alpha-L- 1, tissue(FUCA1)	-0.47	1:23845076-23868294	0.0013	0.0448384
SLC30A1	solute carrier family 30 member 1(SLC30A1)	-0.48	1:211571567-211578742	0.00115	0.0407515
CD1D	CD1d molecule(CD1D)	-0.49	1:158179946-158184896	0.00105	0.038256
CECR6	cat eye syndrome chromosome region, candidate 6(CECR6)	-0.50	22:17116298-17121367	0.0008	0.0315949
TBCC	tubulin folding cofactor C(TBCC)	-0.50	6:42744480-42746096	0.001	0.0371316
ORAI1	ORAI calcium release-activated calcium modulator 1(ORAI1)	-0.50	12:121626549-121642677	0.0013	0.0448384
TMEM185B	transmembrane protein 185B(TMEM185B)	-0.51	2:120221277-120223408	0.0015	0.0495351
NOMO3	NODAL modulator 3(NOMO3)	-0.51	16:16232494-16294814	0.00025	0.0123183
CALU	calumenin(CALU)	-0.53	7:128739291-128771807	0.0011	0.0394298
LMF2	lipase maturation factor 2(LMF2)	-0.53	22:50502948-50507691	0.00125	0.0435983
TUBGCP6	tubulin gamma complex associated protein 6(TUBGCP6)	-0.53	22:50217688-50244992	0.00065	0.0268315
ME3	malic enzyme 3(ME3)	-0.54	11:86431589-86672636	0.0014	0.0472378
SLC22A16	solute carrier family 22 member 16(SLC22A16)	-0.54	6:110424686-110476641	0.00115	0.0407515
SEMA4C	semaphorin 4C(SEMA4C)	-0.54	2:96859715-96870757	0.0008	0.0315949
P2RX1	purinergic receptor P2X 1(P2RX1)	-0.55	17:3896591-3916500	0.0006	0.025514
ABCB6	ATP binding cassette subfamily B member 6 (Langereis blood group)(ABCB6)	-0.55	2:219209767-219229717	0.00035	0.0162645
SCARNA13	small Cajal body-specific RNA 13(SCARNA13)	-0.55	14:95532296-95544724	0.00065	0.0268315
TM9SF4	transmembrane 9 superfamily member 4(TM9SF4)	-0.55	20:32109505-32167258	0.00145	0.0486079
RN7SKP91	RNA, 7SK small nuclear pseudogene 91(RN7SKP91)	-0.56	1:30843822-30844110	0.0011	0.0394298
CCR1	C-C motif chemokine receptor 1(CCR1)	-0.56	3:46163603-46266706	0.0002	0.0101777
NID1	nidogen 1(NID1)	-0.57	1:235975829-236065162	0.0001	0.00579142
AGT	angiotensinogen(AGT)	-0.57	1:230702522-230802003	0.00025	0.0123183
GBA	glucosylceramidase beta(GBA)	-0.57	1:155234451-155244699	0.00105	0.038256
NPTX1	neuronal pentraxin 1(NPTX1)	-0.58	17:80467147-80477843	0.0003	0.0143713
CCDC130	coiled-coil domain containing 130(CCDC130)	-0.58	19:13731759-13763296	0.0008	0.0315949
SLC29A1	solute carrier family 29 member 1 (Augustine blood group)(SLC29A1)	-0.58	6:44219504-44234151	0.0003	0.0143713
NUP210	nucleoporin 210(NUP210)	-0.59	3:13316234-13420309	0.0005	0.0217381
LOXL4	lysyl oxidase like 4(LOXL4)	-0.59	10:98247689-98268250	0.0001	0.00579142
EGFL7	EGF like domain multiple 7(EGFL7)	-0.59	9:136648609-136672678	0.00075	0.0302357
SLC12A9	solute carrier family 12 member 9(SLC12A9)	-0.59	7:100802564-100867009	0.00035	0.0162645
TMEM201	transmembrane protein 201(TMEM201)	-0.59	1:9588921-9614873	0.00075	0.0302357
ZNF692	zinc finger protein 692(ZNF692)	-0.59	1:248850005-248859144	0.0015	0.0495351
CD180	CD180 molecule(CD180)	-0.59	5:67179612-67196799	0.00035	0.0162645
GRIN2D	glutamate ionotropic receptor NMDA type subunit 2D(GRIN2D)	-0.59	19:48394874-48444931	0.00015	0.00816895
SIGMAR1	sigma non-opioid intracellular receptor 1(SIGMAR1)	-0.59	9:34634721-34637809	0.00135	0.0460513
RP11-244H3.4	Uncharacterized	-0.59	1:34974355-35031968	0.00105	0.038256
CTD-3252C9.4	Uncharacterized	-0.59	19:13834515-13836359	0.00065	0.0268315

SCARB1	scavenger receptor class B member 1(SCARB1)	-0.59	12:124776855-124882668	0.001	0.0371316
RET	ret proto-oncogene(RET)	-0.60	10:43077026-43130351	0.0002	0.0101777
RNU6ATAC	RNA, U6atac small nuclear (U12-dependent splicing)(RNU6ATAC)	-0.60	9:134164438-134164564	0.00075	0.0302357
RP11-473M20.9	Uncharacterized	-0.61	16:3065296-3087100	0.0009	0.0343216
TIMP1	TIMP metallopeptidase inhibitor 1(TIMP1)	-0.61	X:47561099-47630305	0.0013	0.0448384
PKDCC	protein kinase domain containing, cytoplasmic(PKDCC)	-0.61	2:42048019-42058528	0.0003	0.0143713
C16orf54	chromosome 16 open reading frame 54(C16orf54)	-0.61	16:29742462-29748299	5.00E-05	0.00318053
CCNL2	cyclin L2(CCNL2)	-0.61	1:1385710-1399328	0.001	0.0371316
ADGRE4P	adhesion G protein-coupled receptor E4, pseudogene(ADGRE4P)	-0.61	19:6952499-6997872	0.00025	0.0123183
LGALS3BP	galectin 3 binding protein(LGALS3BP)	-0.61	17:78971237-78980109	0.00105	0.038256
COL8A2	collagen type VIII alpha 2 chain(COL8A2)	-0.62	1:36095235-36125220	0.00015	0.00816895
LINC01125	long intergenic non-protein coding RNA 1125(LINC01125)	-0.62	2:97664216-97703064	0.00125	0.0435983
TIMP3	TIMP metallopeptidase inhibitor 3(TIMP3)	-0.63	22:32512551-33058372	0.0002	0.0101777
MFSD3	major facilitator superfamily domain containing 3(MFSD3)	-0.64	8:144509073-144511213	0.0001	0.00579142
CHST14	carbohydrate sulfotransferase 14(CHST14)	-0.64	15:40470997-40474571	5.00E-05	0.00318053
REEP4	receptor accessory protein 4(REEP4)	-0.65	8:22138019-22141951	0.0001	0.00579142
METTL17	methyltransferase like 17(METTL17)	-0.65	14:20989769-20999163	0.0002	0.0101777
ADGRE5	adhesion G protein-coupled receptor E5(ADGRE5)	-0.66	19:14380500-14408725	0.001	0.0371316
RNU5D-1	RNA, U5D small nuclear 1(RNU5D-1)	-0.66	1:44731054-44731170	0.0002	0.0101777
SLC35F5	solute carrier family 35 member F5(SLC35F5)	-0.67	2:113705010-113756823	0.00135	0.0460513
PHB2	prohibitin 2(PHB2)	-0.67	12:6964948-6970825	0.0008	0.0315949
ALG3	ALG3, alpha-1,3- mannosyltransferase(ALG3)	-0.68	3:184230428-184249548	0.0004	0.0181532
CFAP206	cilia and flagella associated protein 206(CFAP206)	-0.68	6:87407982-87512336	0.0001	0.00579142
LINC00235	long intergenic non-protein coding RNA 235(LINC00235)	-0.68	16:525154-527407	0.00055	0.023647
ANPEP	alanyl aminopeptidase, membrane(ANPEP)	-0.68	15:89784888-89815401	0.00065	0.0268315
CTSG	cathepsin G(CTSG)	-0.69	14:24573521-24576260	0.00015	0.00816895
SNORD92	small nucleolar RNA, C/D box 92(SNORD92)	-0.69	2:28894642-28948222	0.0003	0.0143713
SNORD3C	small nucleolar RNA, C/D box 3C(SNORD3C)	-0.69	17:19189664-19190245	5.00E-05	0.00318053
SOWAHD	sosondowah ankyrin repeat domain family member D(SOWAHD)	-0.70	X:119758612-119760164	0.00085	0.0333153
SNORA38B	small nucleolar RNA, H/ACA box 38B(SNORA38B)	-0.70	17:67717832-67744531	5.00E-05	0.00318053
NOTCH1	notch 1(NOTCH1)	-0.70	9:136494443-136545862	0.00045	0.0199556
SPINT1	serine peptidase inhibitor, Kunitz type 1(SPINT1)	-0.70	15:40835807-40858207	0.0004	0.0181532
ELANE	elastase, neutrophil expressed(ELANE)	-0.71	19:851013-856247	5.00E-05	0.00318053
MRM1	mitochondrial rRNA methyltransferase 1(MRM1)	-0.71	17:36601571-36608971	0.0005	0.0217381
TPBG	trophoblast glycoprotein(TPBG)	-0.73	6:82363205-82370828	5.00E-05	0.00318053
ZNF536	zinc finger protein 536(ZNF536)	-0.73	19:30219665-30713538	0.0002	0.0101777
PRTN3	proteinase 3(PRTN3)	-0.73	19:840959-848175	0.00045	0.0199556
ADAMTS14	ADAM metallopeptidase with thrombospondin type 1 motif 14(ADAMTS14)	-0.73	10:70672802-70762441	0.0002	0.0101777
C9orf106	chromosome 9 open reading frame 106(C9orf106)	-0.73	9:129321015-129324905	5.00E-05	0.00318053

SNORD67	small nucleolar RNA, C/D box 67(SNORD67)	-0.74	11:46743047-46846308	5.00E-05	0.00318053
GP1BB	glycoprotein Ib platelet beta subunit(GP1BB)	-0.74	22:19714463-19724772	0.0011	0.0394298
ECM1	extracellular matrix protein 1(ECM1)	-0.74	1:150508061-150513789	5.00E-05	0.00318053
KIR3DX1	killer cell immunoglobulin like receptor, three Ig domains X1(KIR3DX1)	-0.75	19:54532691-54545771	0.00145	0.0486079
U3(1)	Uncharacterized	-0.75	17:48133439-48430275	0.0002	0.0101777
NUAK2	NUAK family kinase 2(NUAK2)	-0.75	1:205302058-205321791	5.00E-05	0.00318053
ENG	endoglin(ENG)	-0.75	9:127815011-127854756	5.00E-05	0.00318053
VSIG4	V-set and immunoglobulin domain containing 4(VSIG4)	-0.76	X:66021737-66040125	5.00E-05	0.00318053
RNU5E-1	RNA, U5E small nuclear 1(RNU5E-1)	-0.76	1:11908151-11908271	5.00E-05	0.00318053
DCHS1	dachsous cadherin-related 1(DCHS1)	-0.76	11:6621322-6655854	5.00E-05	0.00318053
VTRNA2-1	vault RNA 2-1(VTRNA2-1)	-0.76	5:136080470-136080597	5.00E-05	0.00318053
EPHB2	EPH receptor B2(EPHB2)	-0.77	1:22710838-22921500	0.0001	0.00579142
MBOAT7	membrane bound O-acyltransferase domain containing 7(MBOAT7)	-0.77	19:54173411-54189882	0.0009	0.0343216
AHNAK	AHNAK nucleoprotein(AHNAK)	-0.77	11:62433541-62556235	0.00145	0.0486079
RNU5B-1	RNA, U5B small nuclear 1(RNU5B-1)	-0.77	15:65304676-65304792	5.00E-05	0.00318053
U1(2)	Uncharacterized	-0.77	1:145465616-145465780	5.00E-05	0.00318053
SNORD60	small nucleolar RNA, C/D box 60(SNORD60)	-0.80	16:2154796-2155358	5.00E-05	0.00318053
TMBIM1	transmembrane BAX inhibitor motif containing 1(TMBIM1)	-0.80	2:218270391-218368099	0.00055	0.023647
RCN3	reticulocalbin 3(RCN3)	-0.80	19:49527617-49546962	0.00135	0.0460513
RNU11	RNA, U11 small nuclear(RNU11)	-0.80	1:28648599-28648733	5.00E-05	0.00318053
U3(2)	Uncharacterized	-0.81	15:58760465-58760681	5.00E-05	0.00318053
MLNR	motilin receptor(MLNR)	-0.82	13:49220337-49222377	5.00E-05	0.00318053
RNU1-89P	RNA, U1 small nuclear 89, pseudogene(RNU1-89P)	-0.83	4:135995928-135996092	0.00125	0.0435983
SNORA2A	small nucleolar RNA, H/ACA box 2A(SNORA2A)	-0.83	12:48653400-48682238	0.00015	0.00816895
MYBPC3	myosin binding protein C, cardiac(MYBPC3)	-0.83	11:47331396-47352702	0.0006	0.025514
SNORA71B	small nucleolar RNA, H/ACA box 71B(SNORA71B)	-0.84	20:38420587-38435353	0.00035	0.0162645
SNORA47	small nucleolar RNA, H/ACA box 47(SNORA47)	-0.84	5:77072071-77166909	0.00015	0.00816895
SNORA80B	small nucleolar RNA, H/ACA box 80B(SNORA80B)	-0.85	2:10439967-10448504	0.0006	0.025514
TMEM259	transmembrane protein 259(TMEM259)	-0.85	19:999795-1021179	0.00025	0.0123183
SNORD17	small nucleolar RNA, C/D box 17(SNORD17)	-0.85	20:17941596-18059188	5.00E-05	0.00318053
CD14	CD14 molecule(CD14)	-0.86	5:140631727-140633701	5.00E-05	0.00318053
PTMAP5	prothymosin, alpha pseudogene 5(PTMAP5)	-0.86	13:81689910-81691072	0.0001	0.00579142
SNORA7B	small nucleolar RNA, H/ACA box 7B(SNORA7B)	-0.87	3:129381297-129399655	5.00E-05	0.00318053
SLC22A31	solute carrier family 22 member 31(SLC22A31)	-0.87	16:89195760-89201664	5.00E-05	0.00318053
ADAMTS15	ADAM metallopeptidase with thrombospondin type 1 motif 15(ADAMTS15)	-0.87	11:130448973-130476641	5.00E-05	0.00318053
SLX1A	SLX1 homolog A, structure-specific endonuclease subunit(SLX1A)	-0.88	16:30192933-30204310	0.00065	0.0268315
SNORA79	small nucleolar RNA, H/ACA box 79(SNORA79)	-0.89	14:20311367-20333312	5.00E-05	0.00318053
RNU4-2	RNA, U4 small nuclear 2(RNU4-2)	-0.89	12:120291762-120291903	0.00015	0.00816895
MIR223	microRNA 223(MIR223)	-0.89	X:66015460-66020422	0.00015	0.00816895

LPAR2	lysophosphatidic acid receptor 2(LPAR2)	-0.89	19:19623667-19628930	0.0003	0.0143713
RN7SKP286	RNA, 7SK small nuclear pseudogene 286(RN7SKP286)	-0.90	2:138863596-138863895	5.00E-05	0.00318053
KRT17P1	keratin 17 pseudogene 1(KRT17P1)	-0.91	17:16840742-16845883	0.00085	0.0333153
RN7SKP1	RNA, 7SK small nuclear pseudogene 1(RN7SKP1)	-0.92	13:37166351-37166658	0.0001	0.00579142
PODXL	podocalyxin like(PODXL)	-0.93	7:131500261-131558217	0.00035	0.0162645
RP11-1334A24.5	Uncharacterized	-0.94	5:177476630-177479656	5.00E-05	0.00318053
RHBDL1	rhomboid like 1(RHBDL1)	-0.94	16:675665-678268	0.00045	0.0199556
RNU5A-1	RNA, U5A small nuclear 1(RNU5A-1)	-0.95	15:65234459-65300618	5.00E-05	0.00318053
RP11-274B21.3	Uncharacterized	-0.95	7:128653689-128654722	5.00E-05	0.00318053
RNU5F-1	RNA, U5F small nuclear 1(RNU5F-1)	-0.95	1:44674691-44725591	5.00E-05	0.00318053
SNORA54	small nucleolar RNA, H/ACA box 54(SNORA54)	-0.97	11:2944430-2992377	0.0002	0.0101777
MIR424	microRNA 424(MIR424)	-0.97	X:134543336-134546711	0.00055	0.023647
SCARNA8	small Cajal body-specific RNA 8(SCARNA8)	-0.97	9:19053142-19103119	0.0008	0.0315949
ANO7	anoctamin 7(ANO7)	-0.98	2:241188508-241225377	0.00015	0.00816895
SNORA23	small nucleolar RNA, H/ACA box 23(SNORA23)	-0.98	11:9384621-9448126	5.00E-05	0.00318053
CLDN15	claudin 15(CLDN15)	-0.98	7:101232091-101238820	5.00E-05	0.00318053
SNORA74B	small nucleolar RNA, H/ACA box 74B(SNORA74B)	-0.98	5:172983756-173035445	5.00E-05	0.00318053
MAN2A2	mannosidase alpha class 2A member 2(MAN2A2)	-0.98	15:90902217-90922584	5.00E-05	0.00318053
SCG2	secretogranin II(SCG2)	-0.99	2:223596939-223602503	0.00045	0.0199556
SNORA80E	small nucleolar RNA, H/ACA box 80E(SNORA80E)	-1.00	1:155913042-155934400	0.0002	0.0101777
FBN2	fibrillin 2(FBN2)	-1.02	5:128257908-129033642	5.00E-05	0.00318053
MT-TA	Uncharacterized	-1.02	MT:5586-5891	5.00E-05	0.00318053
SNORA37	small nucleolar RNA, H/ACA box 37(SNORA37)	-1.03	18:54151600-54224788	5.00E-05	0.00318053
RNU1-148P	RNA, U1 small nuclear 148, pseudogene(RNU1-148P)	-1.03	8:24076996-24077158	5.00E-05	0.00318053
NPIPB3	nuclear pore complex interacting protein family member B3(NPIPB3)	-1.04	16:21402236-21520444	5.00E-05	0.00318053
RNU4-1	RNA, U4 small nuclear 1(RNU4-1)	-1.05	12:120293096-120293237	5.00E-05	0.00318053
CCDC146	coiled-coil domain containing 146(CCDC146)	-1.07	7:76959834-77416400	0.0013	0.0448384
ADRB2	adrenoceptor beta 2(ADRB2)	-1.08	5:148825244-148828687	5.00E-05	0.00318053
SLCO2B1	solute carrier organic anion transporter family member 2B1(SLCO2B1)	-1.11	11:75099171-75206549	5.00E-05	0.00318053
SLC25A3	solute carrier family 25 member 3(SLC25A3)	-1.12	12:98593590-98606379	0.0002	0.0101777
LINC01230	long intergenic non-protein coding RNA 1230(LINC01230)	-1.13	9:1045624-1048641	5.00E-05	0.00318053
TSPAN33	tetraspanin 33(TSPAN33)	-1.14	7:129144891-129169697	0.0001	0.00579142
RP11-274B21.2	Uncharacterized	-1.14	7:128651184-128652334	5.00E-05	0.00318053
MYO7A	myosin VIIA(MYO7A)	-1.14	11:77128263-77215239	0.0006	0.025514
MTND2P28	mitochondrially encoded NADH:ubiquinone oxidoreductase core subunit 2 pseudogene 28(MTND2P28)	-1.16	1:585988-859446	5.00E-05	0.00318053
SCARNA1	small Cajal body-specific RNA 1(SCARNA1)	-1.16	1:27830777-27851676	0.0015	0.0495351
SLC16A13	solute carrier family 16 member 13(SLC16A13)	-1.19	17:7036074-7040121	5.00E-05	0.00318053
CPNE6	copine 6(CPNE6)	-1.20	14:24070836-24078100	0.00105	0.038256

TBC1D3L	TBC1 domain family member 3L(TBC1D3L)	-1.21	17:37977971-37989048	0.0009	0.0343216
LINC00899	long intergenic non-protein coding RNA 899(LINC00899)	-1.23	22:46039906-46044853	0.0002	0.0101777
RP11-448A19.1	Uncharacterized	-1.23	7:129604547-129611630	5.00E-05	0.00318053
ID1	inhibitor of DNA binding 1, HLH protein(ID1)	-1.23	20:31605282-31606515	5.00E-05	0.00318053
RP11-54O7.3	Uncharacterized	-1.24	1:916864-921016	0.0008	0.0315949
MT-TP	Uncharacterized	-1.24	MT:15955-16023	0.00065	0.0268315
MTATP6P1	mitochondrially encoded ATP synthase 6 pseudogene 1(MTATP6P1)	-1.28	1:585988-859446	0.00115	0.0407515
RP11-600F24.7	Uncharacterized	-1.29	14:103525009-103529072	5.00E-05	0.00318053
CAPN10-AS1	CAPN10 antisense RNA 1 (head to head)(CAPN10-AS1)	-1.30	2:240582699-240586699	5.00E-05	0.00318053
SNORA5C	small nucleolar RNA, H/ACA box 5C(SNORA5C)	-1.33	7:45100099-45112047	0.0007	0.0287426
CTB-31O20.2	Uncharacterized	-1.35	19:1874870-1876169	5.00E-05	0.00318053
LINC00638	long intergenic non-protein coding RNA 638(LINC00638)	-1.35	14:104821200-104823718	0.00045	0.0199556
NALT1	NOTCH1 associated lncRNA in T-cell acute lymphoblastic leukemia 1(NALT1)	-1.36	9:136546172-136549893	0.0002	0.0101777
RP11-1E4.1	Uncharacterized	-1.38	8:10050484-10054254	0.0005	0.0217381
MBTPS2	membrane bound transcription factor peptidase, site 2(MBTPS2)	-1.42	X:21839635-21885424	5.00E-05	0.00318053
RP11-572O17.1	Uncharacterized	-1.45	4:1712820-1713622	5.00E-05	0.00318053
AC079922.3	Uncharacterized	-1.46	2:112641831-112645690	5.00E-05	0.00318053
RP11-274B21.4	Uncharacterized	-1.47	7:128652840-128653243	5.00E-05	0.00318053
KLHL23	kelch like family member 23(KLHL23)	-1.50	2:169694453-169776989	0.0009	0.0343216
MLPH	melanophilin(MLPH)	-1.51	2:237485427-237555318	5.00E-05	0.00318053
RP11-262H14.5	Uncharacterized	-1.51	9:62837747-62838372	0.0015	0.0495351
RUFY3	RUN and FYVE domain containing 3(RUFY3)	-1.52	4:70703746-70807315	0.00015	0.00816895
CTD-3064M3.7	Uncharacterized	-1.52	8:141433828-141507230	0.0001	0.00579142
GARNL3	GTPase activating Rap/RanGAP domain like 3(GARNL3)	-1.53	9:127224264-127393660	5.00E-05	0.00318053
RP11-981G7.1	Uncharacterized	-1.55	8:10433671-10438312	5.00E-05	0.00318053
CTD-3193O13.12	Uncharacterized	-1.55	19:7888504-7903542	0.00025	0.0123183
BRSK2	BR serine/threonine kinase 2(BRSK2)	-1.56	11:1389898-1462689	0.00025	0.0123183
RN7SKP48	RNA, 7SK small nuclear pseudogene 48(RN7SKP48)	-1.57	4:85100495-85100823	0.0012	0.0421385
SEMA6B	semaphorin 6B(SEMA6B)	-1.59	19:4542592-4559808	5.00E-05	0.00318053
HID1	HID1 domain containing(HID1)	-1.68	17:74950742-74975728	0.00015	0.00816895
SMAD1	SMAD family member 1(SMAD1)	-1.75	4:145481193-145558079	0.0001	0.00579142
LINC00896	long intergenic non-protein coding RNA 896(LINC00896)	-1.75	22:20206396-20208524	5.00E-05	0.00318053
RN7SKP172	RNA, 7SK small nuclear pseudogene 172(RN7SKP172)	-1.76	12:76315750-76316048	0.0015	0.0495351
LINC00599	long intergenic non-protein coding RNA 599(LINC00599)	-1.77	8:9900063-9905366	5.00E-05	0.00318053
RP4-758J18.13	Uncharacterized	-1.80	1:1409095-1410618	0.00025	0.0123183
CDO1	cysteine dioxygenase type 1(CDO1)	-1.82	5:115804732-115816954	0.0008	0.0315949
ADGRG1	adhesion G protein-coupled receptor G1(ADGRG1)	-1.83	16:57610651-57665580	5.00E-05	0.00318053
U2	Uncharacterized	-1.91	17:43211834-43305397	5.00E-05	0.00318053
CTD-2649C14.2	Uncharacterized	-1.98	16:21950217-21951708	0.0011	0.0394298

RP1-118J21.25	Uncharacterized	-2.15	1:39788975-39790171	5.00E-05	0.00318053
PTGES2-AS1	PTGES2 antisense RNA 1 (head to head)(PTGES2-AS1)	-2.17	9:128128528-128130628	5.00E-05	0.00318053
C1orf101	chromosome 1 open reading frame 101(C1orf101)	-2.20	1:244454376-244641177	5.00E-05	0.00318053
RBBP8	RB binding protein 8, endonuclease(RBBP8)	-2.55	18:22699480-23026488	5.00E-05	0.00318053
RP11-573D15.8	Uncharacterized	-2.94	3:186538440-186773476	5.00E-05	0.00318053
RNA5-8SP6	RNA, 5.8S ribosomal pseudogene 6(RNA5-8SP6)	-2.95	Y:10200154-10200306	5.00E-05	0.00318053
RP5-884M6.1	Uncharacterized	-3.13	7:106775010-106795564	0.00065	0.0268315
RNA5SP202	RNA, 5S ribosomal pseudogene 202(RNA5SP202)	-3.19	6:4427962-4428081	5.00E-05	0.00318053
PCDH11Y	protocadherin 11 Y-linked(PCDH11Y)	-4.00	Y:5000225-5742224	0.00045	0.0199556
FAM83C-AS1	FAM83C antisense RNA 1(FAM83C-AS1)	-11.97	20:35285250-35292401	0.0009	0.0343216
RNA5-8SP2	RNA, 5.8S ribosomal pseudogene 2(RNA5-8SP2)	-15.97	16:34162958-34163110	0.0003	0.0143713

Supplementary Table IV.2. List of DE genes in *R. montanensis*-infected THP-1 macrophages compared with uninfected cells (Associated with Figure IV.1). This table can be found in digital format for consultation.

OFFICIAL_GENE_SYMBOL	Gene_Name	Log_2 (Fold_Change)	locus	p_value	q_value_FDR
RP11-483F11.7	Uncharacterized	13.42	10:99651988-99653905	0.0001	0.0203867
CTD-2288F12.1	Uncharacterized	12.38	16:18926862-18937043	5.00E-05	0.0107676
CCL4L2	C-C motif chemokine ligand 4 like 2(CCL4L2)	6.48	17:36210923-36212878	5.00E-05	0.0107676
TNF	tumor necrosis factor(TNF)	5.34	6:31575566-31578336	5.00E-05	0.0107676
CCL3L3	C-C motif chemokine ligand 3 like 3(CCL3L3)	5.08	17:36183234-36196758	5.00E-05	0.0107676
AC058791.1	Uncharacterized	3.93	7:130853719-130928649	5.00E-05	0.0107676
CXCL1	C-X-C motif chemokine ligand 1(CXCL1)	3.84	4:73869392-73871242	5.00E-05	0.0107676
CCL3	C-C motif chemokine ligand 3(CCL3)	3.78	17:36072865-36090169	5.00E-05	0.0107676
NR2F2	nuclear receptor subfamily 2 group F member 2(NR2F2)	3.69	15:95990581-96340263	5.00E-05	0.0107676
KLF5	Kruppel like factor 5(KLF5)	3.65	13:73054975-73077542	5.00E-05	0.0107676
CXCL3	C-X-C motif chemokine ligand 3(CXCL3)	3.35	4:74036588-74038807	5.00E-05	0.0107676
MTRNR2L1	MT-RNR2-like 1(MTRNR2L1)	3.34	17:22523110-22525686	5.00E-05	0.0107676
NFKBIA	NFKB inhibitor alpha(NFKBIA)	3.16	14:35401510-35404749	5.00E-05	0.0107676
CCL20	C-C motif chemokine ligand 20(CCL20)	2.97	2:227813841-227817564	5.00E-05	0.0107676
CXCL8	C-X-C motif chemokine ligand 8(CXCL8)	2.95	4:73740505-73743716	5.00E-05	0.0107676
PLCB1	phospholipase C beta 1(PLCB1)	2.90	20:8077250-8968360	5.00E-05	0.0107676
HOTTIP	HOXA distal transcript antisense RNA(HOTTIP)	2.79	7:27193502-27207259	0.0002	0.0368434
NFKBIZ	NFKB inhibitor zeta(NFKBIZ)	2.78	3:101827990-101861022	5.00E-05	0.0107676
PTGS2	prostaglandin-endoperoxide synthase 2(PTGS2)	2.74	1:186671790-186680427	5.00E-05	0.0107676
RNU6ATAC3P	RNA, U6atac small nuclear 3, pseudogene(RNU6ATAC3P)	2.63	17:46916769-46923034	0.0002	0.0368434
ANKRD30BL	ankyrin repeat domain 30B like(ANKRD30BL)	2.62	2:132147590-132257969	5.00E-05	0.0107676
FAM13A-AS1	FAM13A antisense RNA 1(FAM13A-AS1)	2.59	4:88709788-89111398	5.00E-05	0.0107676

MTRNR2L10	MT-RNR2-like 10(MTRNR2L10)	2.52	X:55181390-55182920	5.00E-05	0.0107676
DUSP1	dual specificity phosphatase 1(DUSP1)	2.37	5:172758225-172777774	5.00E-05	0.0107676
WT1-AS	WT1 antisense RNA(WT1-AS)	2.23	11:32387774-32458769	5.00E-05	0.0107676
CD69	CD69 molecule(CD69)	2.20	12:9752485-9760901	5.00E-05	0.0107676
TNFSF11	tumor necrosis factor superfamily member 11(TNFSF11)	2.12	13:42562735-42608013	5.00E-05	0.0107676
MTRNR2L12	MT-RNR2-like 12(MTRNR2L12)	2.09	3:96617187-96618236	5.00E-05	0.0107676
TNFAIP3	TNF alpha induced protein 3(TNFAIP3)	2.08	6:137823672-137883312	5.00E-05	0.0107676
RN7SL44P	RNA, 7SL, cytoplasmic 44, pseudogene(RN7SL44P)	1.92	1:153500462-153500764	5.00E-05	0.0107676
MTRNR2L6	MT-RNR2-like 6(MTRNR2L6)	1.88	7:142666271-142667718	5.00E-05	0.0107676
GEM	GTP binding protein overexpressed in skeletal muscle(GEM)	1.85	8:94249252-94262350	5.00E-05	0.0107676
HCAR3	hydroxycarboxylic acid receptor 3(HCAR3)	1.79	12:122687124-122716892	5.00E-05	0.0107676
IER3	immediate early response 3(IER3)	1.76	6:30742928-30744554	5.00E-05	0.0107676
SPACA6	sperm acrosome associated 6(SPACA6)	1.69	19:51685362-51712387	5.00E-05	0.0107676
RNU5A-2P	RNA, U5A small nuclear 2, pseudogene(RNU5A-2P)	1.67	4:81334302-81334418	5.00E-05	0.0107676
EDN1	endothelin 1(EDN1)	1.62	6:12290362-12297194	5.00E-05	0.0107676
DUSP2	dual specificity phosphatase 2(DUSP2)	1.54	2:96143165-96145440	5.00E-05	0.0107676
RNU1-55P	RNA, U1 small nuclear 55, pseudogene(RNU1-55P)	1.48	20:5890054-5890212	5.00E-05	0.0107676
TMC5	transmembrane channel like 5(TMC5)	1.42	16:19410495-19499113	5.00E-05	0.0107676
IL1B	interleukin 1 beta(IL1B)	1.41	2:112829750-112836903	5.00E-05	0.0107676
JUN	Jun proto-oncogene, AP-1 transcription factor subunit(JUN)	1.35	1:58780787-58784327	5.00E-05	0.0107676
ATF3	activating transcription factor 3(ATF3)	1.34	1:212565333-212620777	5.00E-05	0.0107676
RN7SL33P	RNA, 7SL, cytoplasmic 33, pseudogene(RN7SL33P)	1.32	17:2557752-2558094	5.00E-05	0.0107676
RNU2-8P	RNA, U2 small nuclear 8, pseudogene(RNU2-8P)	1.31	6:121580331-121580521	5.00E-05	0.0107676
JUNB	JunB proto-oncogene, AP-1 transcription factor subunit(JUNB)	1.30	19:12763002-12874951	5.00E-05	0.0107676
RNU1-17P	RNA, U1 small nuclear 17, pseudogene(RNU1-17P)	1.24	5:180729585-180729737	0.00015	0.0294038
CTGF	connective tissue growth factor(CTGF)	1.21	6:131948175-132077393	5.00E-05	0.0107676
RPL13AP5	ribosomal protein L13a pseudogene 5(RPL13AP5)	1.20	10:96750287-96750899	5.00E-05	0.0107676
MIR663A	microRNA 663a(MIR663A)	1.20	20:26186919-26251526	5.00E-05	0.0107676
RNU1-148P	RNA, U1 small nuclear 148, pseudogene(RNU1-148P)	1.18	8:24076996-24077158	5.00E-05	0.0107676
RNU1-7P	RNA, U1 small nuclear 7, pseudogene(RNU1-7P)	1.18	1:8202428-8215210	5.00E-05	0.0107676
RN7SL478P	RNA, 7SL, cytoplasmic 478, pseudogene(RN7SL478P)	1.16	7:97998324-97998622	5.00E-05	0.0107676
OTUD1	OTU deubiquitinase 1(OTUD1)	1.13	10:23439457-23442390	5.00E-05	0.0107676
EEF1A1P11	eukaryotic translation elongation factor 1 alpha 1 pseudogene 11(EEF1A1P11)	1.13	1:96446929-96448318	0.00025	0.0444477
CD83	CD83 molecule(CD83)	1.11	6:14117255-14136918	5.00E-05	0.0107676
RPS3AP6	ribosomal protein S3A pseudogene 6(RPS3AP6)	1.11	15:59768351-59769146	5.00E-05	0.0107676
BTG2	BTG anti-proliferation factor 2(BTG2)	1.07	1:203305490-203309602	5.00E-05	0.0107676
ZC3H12A	zinc finger CCCH-type containing 12A(ZC3H12A)	1.06	1:37474551-37484379	0.0002	0.0368434
RNU2-14P	RNA, U2 small nuclear 14, pseudogene(RNU2-14P)	1.03	14:65124351-65124542	5.00E-05	0.0107676
UHRF1BP1	UHRF1 binding protein 1(UHRF1BP1)	1.03	6:34792014-34888089	0.00015	0.0294038

TNFSF15	tumor necrosis factor superfamily member 15(TNFSF15)	1.03	9:114784634 -114806126	5.00E-05	0.0107676
Y_RNA	Uncharacterized	0.95	10:92710498 -92710608	0.00025	0.0444477
RNU5A-1	RNA, U5A small nuclear 1(RNU5A-1)	0.95	15:65234459 -65300618	5.00E-05	0.0107676
G0S2	G0/G1 switch 2(G0S2)	0.94	1:209661363 -209734950	5.00E-05	0.0107676
RNU1-18P	RNA, U1 small nuclear 18, pseudogene(RNU1-18P)	0.92	6:122211647 -122211811	5.00E-05	0.0107676
LINC01686	Uncharacterized	0.91	1:182615253 -182616629	5.00E-05	0.0107676
KLF10	Kruppel like factor 10(KLF10)	0.85	8:102648778 -102655902	5.00E-05	0.0107676
RP3-340B19.2	Uncharacterized	0.84	6:35555872-35556264	0.00015	0.0294038
PPP1R15A	protein phosphatase 1 regulatory subunit 15A(PPP1R15A)	0.84	19:48872391 -48876057	5.00E-05	0.0107676
CTD-3014M21.1	Uncharacterized	0.82	17:43360040 -43361361	0.0002	0.0368434
EGR1	early growth response 1(EGR1)	0.80	5:138465489 -138469315	0.0001	0.0203867
ZFP36	ZFP36 ring finger protein(ZFP36)	0.76	19:39406812 -39409412	5.00E-05	0.0107676
RN7SL824P	RNA, 7SL, cytoplasmic 824, pseudogene(RN7SL824P)	0.76	1:92402388-92402685	0.00025	0.0444477
RNU5D-1	RNA, U5D small nuclear 1(RNU5D-1)	0.71	1:44731054-44731170	5.00E-05	0.0107676
MBTPS2	membrane bound transcription factor peptidase, site 2(MBTPS2)	-0.94	X:21839635-21885424	5.00E-05	0.0107676
RP11-661A12.4	Uncharacterized	-0.99	8:143541972 -143549729	5.00E-05	0.0107676
RN7SKP1	RNA, 7SK small nuclear pseudogene 1(RN7SKP1)	-1.05	13:37166351 -37166658	5.00E-05	0.0107676
CTD-3252C9.4	Uncharacterized	-1.16	19:13834515 -13836359	5.00E-05	0.0107676
RNA5-8SP6	RNA, 5.8S ribosomal pseudogene 6(RNA5-8SP6)	-1.68	Y:10200154-10200306	5.00E-05	0.0107676
RGS6	regulator of G-protein signaling 6(RGS6)	-1.85	14:71932438 -72595125	0.0002	0.0368434
SLC40A1	solute carrier family 40 member 1(SLC40A1)	-1.92	2:189560578 -189583758	0.0001	0.0203867
NSRP1	nuclear speckle splicing regulatory protein 1(NSRP1)	-2.50	17:29560546 -30186475	0.0001	0.0203867
RBBP8	RB binding protein 8, endonuclease(RBBP8)	-2.57	18:22699480 -23026488	5.00E-05	0.0107676
ZNF813	zinc finger protein 813(ZNF813)	-2.78	19:53467734 -53496255	5.00E-05	0.0107676
RP11-84C10.2	Uncharacterized	-13.44	14:20897984 -20936255	5.00E-05	0.0107676

Supplementary Table IV.3. Genes targeted for qPCR validation, primer sequences, and calculated log_2 fold changes **(Associated with Figure IV.1)**.

Gene I.D.	Primer Name	Primer Sequence	Product Size (b. p.)	qPCR Log_2Fold Change (*R.con*/Uninf.)	qPCR Log_2Fold Change (*R.mont.*/Uninf.)
CXCL3	CXCL3_F	AGA AAG CTT GTC TCA ACC CCG	74	7.8	3.2
	CXCL3_R	GGT GCT CCC CTT GTT CAG TA			
B2M	B2M_F	GTG CTC GCG CTA CTC TCT C	50	1.2	0.3
	B2M_R	GGA CTA CGC TGG ATA GCC TC			
PTGS2	PTGS2_F	GGC CAT GGG GTG GAC TTA AA	70	4.4	0.1
	PTGS2_R	TGA AAA GGC GCA GTT TAC GC			
IER3	IER3_F	CTT CGG AGC CCT CGG ACT A	52	3.9	2.2
	IER3_R	TGT TGC TGG AGG AAA GTG CT			
CCL4L2	CCL4L2_F	GGA AGG ATC CCA TCC ACC AG	65	11.4	8.0
	CCL4L2_R	GGT AGG CAT CTT CCT CTG CC			
PP1R15A	PP1R15A_F	GGC ATG TAT GGT GAG CGA GA	59	2.3	0.6
	PP1R15A_R	GCA AAT TGA CTT CCC TGC CC			
MBTPS2	MBTPS2_F	GGA TGC CAC CCT TAC CTC AG	77	1.0	1.2
	MBTPS2_R	TGC CAC CCA GCA AGA TGA AA			
RBBP8	RBBP8_F	TGA ACA TCT CGG GAA GCA GC	50	0.6	0.0
	RBBP8_R	AGA TGT ATC TGC AGA GTT AGG GC			
KLF10	KLF10_F	AAG GCG CTG TCA TGT TTG TG	58	3.3	0.7
	KLF10_R	ACC GGA GGC TTT GAA CTC TG			
EMC7	EMC7_F	TCT GGC AAA TCT AGC AGC GG	55	0.3	1.1
	EMC7_R	TTT TGC CAG CCC CAC TTT TG			
G6PD	G6PD_F	TTT GCC CGC AAC TCC TAT GT	79	0	0.0
	G6PD_R	GGG CAT TCA TGT GGC TGT TG			
EGR1	EGR1_F	AAG TTT GCC AGG AGC GAT GA	65	3.0	0.8
	EGR1_R	TTC TTG TCC TTC TGC CGC AA			
BTG2	BTG2_F	TGA GGT GTC CTA CCG CAT TG	56	3.2	1.1
	BTG2_R	CCT CCT CGT ACA AGA CGC AG			
MTRNR2L6	MTRNR2L6_F	CAC GAG GGT TCA GCT GTC TC	59	0.4	0.6
	MTRNR2L6_R	CCT CTT CAC AGG CAG GTC AG			
OTUD1	OTUD1_F	CCG ACC ATC TCG ACC ACT TC	70	3.2	1.1
	OTUD1_R	TGG GCA GCA GCG ATG ATA AA			
CD69	CD69_F	AGG AAC ACT GGG TTG GAC TG	50	4.2	1.5
	CD69_R	CCA CTT CCA TGG GTG ACC AG			
CCL3	CCL3_F	TGT CAT CTT CCT AAC CAA GAG AGG	69	6.5	2.2
	CCL3_R	TAT TTC TGG ACC CAC TCC TCA			

Supplementary Table IV.4. List of common and specifically DE *in R. conorii*- and *R. montanensis*-infected THP-1 macrophages compared with uninfected cells and list of canonical pathways identified by IPA (Associated with Figure IV.2). (xls) This table can be found in digital format for consultation.

Supplementary Table IV.5. **Categorization of common, *R. conorii*-specific and *R. montanensis*-specific DE genes according to gene ontology (GO) terms (biological process and cellular component) and canonical pathways (Associated with Figure IV.2)**. (PDF) This table can be found in digital format for consultation.

Supplementary Table IV.6. Expression patterns of DE genes categorized in inflammatory and innate immune responses to infection in *R. conorii*- and *R. montanensis*-infected THP-1 macrophages (Associated with Figure IV.3). (xls) This table can be found in digital format for consultation.

Supplementary Table IV.7. Fold change of DE genes categorized in JAK/STAT pathway according to KEGG pathways in THP-1 cells infected with *R. conorii* or *R. montanensis*. (PDF) This table can be found in digital format for consultation.

Supplementary Table IV.8. **Contribution of DE genes in *R. conorii*- and *R. montanensis*-infected THP-1 macrophages for negative regulation of apoptotic process according to biological process GO terms and cell survival according to IPA (Associated with Figure IV.5)**. (xls) This table can be found in digital format for consultation.

Supplementary Table IV.9. Fold change of non-coding transcripts in *R. conorii*- or *R. montanensis*-infected THP-1 macrophages (Associated with Figure IV.6). (PDF) This table can be found in digital format for consultation.

Supplementary Table IV.10. Contribution of DE genes in *R. conorii*- and *R. montanensis*-infected THP-1 macrophages for positive and negative regulation of transcription from RNA polymerase II promoter according to biological process GO terms and transcription according to IPA (Associated with Figure IV.7). (xls) This table can be found in digital format for consultation.

Supplementary Table IV.11. Predicted contribution of DE genes in *R. conorii*- and *R. montanensis*-THP-1 macrophages for inflammatory response based on "Diseases and Functions" category by IPA (Associated with Figure IV.4). (PDF) This table can be found in digital format for consultation.

Supplementary Figures

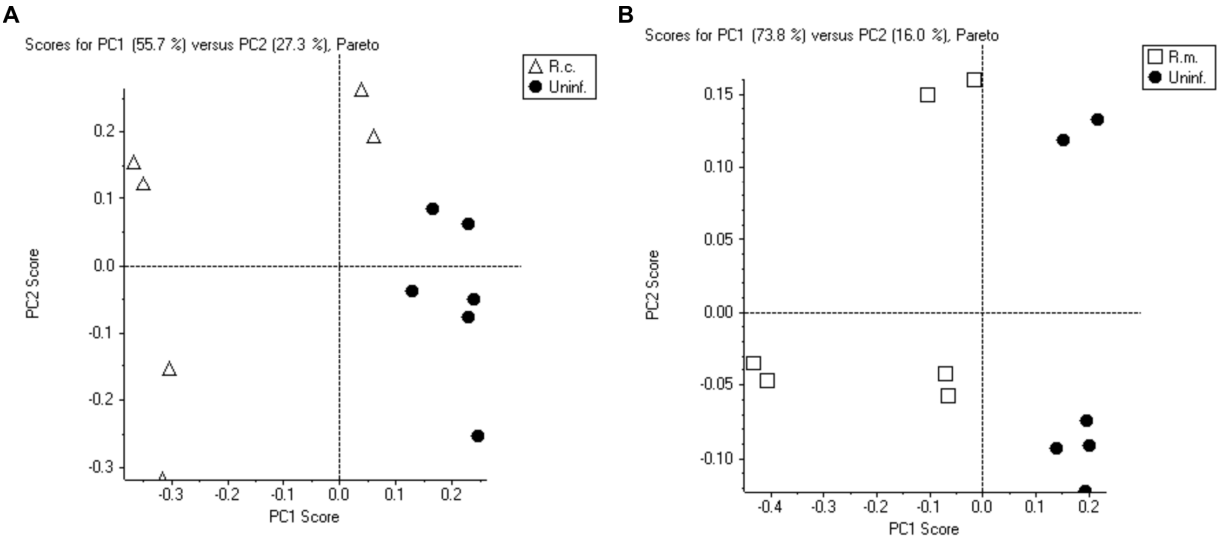

Supplementary Figure V.1 | Principal component analysis (PCA) plots of global changes in proteome profiles. (A-B) PCA plot was performed by importing the quantification data of all proteins considered as altered for *R. conorii*-infected THP-1 macrophages *vs.* uninfected cells **(A)** and for *R. montanensis*-infected THP-1 macrophages *vs.* uninfected cells **(B)**. PCA was performed using the software MarkerView (v1.2.1, Sciex) and the axes show the first two principal components, with the fraction of explained variance in the parenthesis.

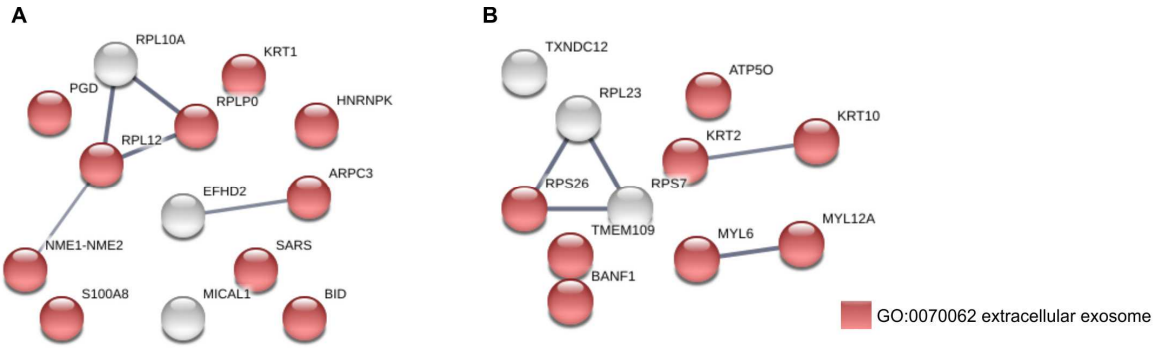

Supplementary Figure V.2 | Protein-protein interaction networks of host proteins with altered abundance in one infection condition. (A-B) Protein-protein interaction network for the 13 host proteins with decreased abundance in *R. conorii*-infected THP-1 macrophages but unchanged levels in *R. montanensis*-infected cells **(A)** and the 11 host proteins with increased abundance in *R. montanensis*-infected THP-1 macrophages but unchanged levels in *R. conorii*-infected cells **(B)**. List of the individual host proteins for each independent analysis can be found in **Supplementary Table V.1**. The analysis was carried out with STRING 10.5 (http://string-db.org/)

using high confidence (0.7) score. Nodes are represented with different colors according to their categorization in gene ontology (GO) terms.

Supplementary Tables

Supplementary Table V.1. Information about the windows used in SWATH acquisition. Table can also be found in digital format for consultation.

Window	Start Mass (Da)	Stop Mass (Da)	Mass Interval (Da)	CES
Window 1	349.5	360.9	11.4	5
Window 2	359.9	375.2	15.3	5
Window 3	374.2	389.2	15	5
Window 4	388.2	402.2	14	5
Window 5	401.2	415.3	14.1	5
Window 6	414.3	427.4	13.1	5
Window 7	426.4	439.1	12.7	5
Window 8	438.1	449.9	11.8	5
Window 9	448.9	460.7	11.8	5
Window 10	459.7	471.1	11.4	5
Window 11	470.1	480.5	10.4	5
Window 12	479.5	490	10.5	5
Window 13	489	499	10	5
Window 14	498	508	10	5
Window 15	507	516.5	9.5	5
Window 16	515.5	525.1	9.6	5
Window 17	524.1	533.2	9.1	5
Window 18	532.2	540.8	8.6	5
Window 19	539.8	548.5	8.7	5
Window 20	547.5	555.7	8.2	5
Window 21	554.7	563.4	8.7	5
Window 22	562.4	570.6	8.2	5
Window 23	569.6	577.8	8.2	5

Window 24	576.8	585.4	8.6	5
Window 25	584.4	592.6	8.2	5
Window 26	591.6	600.3	8.7	5
Window 27	599.3	607.9	8.6	5
Window 28	606.9	615.6	8.7	5
Window 29	614.6	623.2	8.6	5
Window 30	622.2	630.9	8.7	5
Window 31	629.9	638.5	8.6	5
Window 32	637.5	646.2	8.7	5
Window 33	645.2	653.8	8.6	5
Window 34	652.8	661.5	8.7	5
Window 35	660.5	669.1	8.6	5
Window 36	668.1	677.2	9.1	5
Window 37	676.2	685.3	9.1	5
Window 38	684.3	693.9	9.6	5
Window 39	692.9	702.9	10	5
Window 40	701.9	711.9	10	5
Window 41	710.9	721.3	10.4	5
Window 42	720.3	731.2	10.9	5
Window 43	730.2	741.6	11.4	5
Window 44	740.6	752.4	11.8	5
Window 45	751.4	763.6	12.2	5
Window 46	762.6	775.8	13.2	5
Window 47	774.8	787.9	13.1	5
Window 48	786.9	800.5	13.6	8
Window 49	799.5	814.5	15	8
Window 50	813.5	829.3	15.8	8

Window 51	828.3	845.5	17.2	8
Window 52	844.5	865.3	20.8	8
Window 53	864.3	886.5	22.2	8
Window 54	885.5	911.2	25.7	8
Window 55	910.2	939.1	28.9	8
Window 56	938.1	972	33.9	8
Window 57	971	1008.4	37.4	10
Window 58	1007.4	1053.4	46	10
Window 59	1052.4	1120	67.6	10
Window 60	1119	1249.6	130.6	10

Supplementary Table V.2. List of the 746 host proteins that were confidently quantified in all experimental conditions. This table can also be found in digital format for consultation where proteins that are considered as altered (fold change ≤ 0.83 or fold change ≥ 1.2) between infected and uninfected conditions are color-coded according the following: decreased (blue), not changed (transparent) or increased (orange). (xls)

UniProt_Acession	Name	Fold change (R.c/uninf.)	LOG2 (R.c/uninf.)	P-value (R.c/uninf.)	Fold change (R.m/uninf.)	LOG2 (R.m/uninf.)	P-value (R.m/uninf.)
P06454	prothymosin, alpha(PTMA)	0.3837	-1.3818	0.065	0.7330	-0.4481	0.065
P50897	palmitoyl-protein thioesterase 1(PPT1)	0.3952	-1.3392	0.002	0.5475	-0.8690	0.002
P50225	sulfotransferase family 1A member 1(SULT1A1)	0.4938	-1.0181	0.002	0.5030	-0.9913	0.002
P15090	fatty acid binding protein 4(FABP4)	0.4976	-1.0070	0.18	0.5284	-0.9202	0.002
P55263	adenosine kinase(ADK)	0.5247	-0.9304	0.132	0.4316	-1.2121	0.132
Q9BR76	coronin 1B(CORO1B)	0.5266	-0.9252	0.002	0.5899	-0.7614	0.002
O00584	ribonuclease T2(RNASET2)	0.5324	-0.9093	0.002	0.6362	-0.6524	0.002
Q9HAB8	phosphopantothenoylcysteine synthetase(PPCS)	0.5351	-0.9020	0.009	0.5984	-0.7408	0.002
Q9UNF0	protein kinase C and casein kinase substrate in neurons 2(PACSIN2)	0.5425	-0.8824	0.002	0.6360	-0.6529	0.002
P27348	tyrosine 3-monooxygenase/tryptophan 5-monooxygenase activation protein theta(YWHAQ)	0.5560	-0.8470	0.026	0.6226	-0.6836	0.132
Q96C86	decapping enzyme, scavenger(DCPS)	0.5596	-0.8375	0.015	0.6596	-0.6003	0.015
P32119	peroxiredoxin 2(PRDX2)	0.5651	-0.8234	0.004	0.5829	-0.7786	0.004
P16152	carbonyl reductase 1(CBR1)	0.5660	-0.8210	0.009	0.6146	-0.7023	0.026
Q9Y376	calcium binding protein 39(CAB39)	0.5732	-0.8028	0.026	0.4613	-1.1161	0.002
O95336	6-phosphogluconolactonase(PGLS)	0.5749	-0.7986	0.009	0.6956	-0.5237	0.009
Q01469	fatty acid binding protein 5(FABP5)	0.5778	-0.7913	0.002	0.5677	-0.8167	0.002
P21291	cysteine and glycine rich protein 1(CSRP1)	0.5829	-0.7788	0.002	0.5770	-0.7933	0.004

P09960	leukotriene A4 hydrolase(LTA4H)	0.5859	-0.7713	0.004	0.6704	-0.5768	0.002
P18669	phosphoglycerate mutase 1(PGAM1)	0.5936	-0.7525	0.026	0.6614	-0.5964	0.015
Q9H4A4	arginyl aminopeptidase(RNPEP)	0.5964	-0.7457	0.002	0.6653	-0.5878	0.002
P00491	purine nucleoside phosphorylase(PNP)	0.6012	-0.7341	0.002	0.6532	-0.6145	0.002
Q13838	DExD-box helicase 39B(DDX39B)	0.6049	-0.7252	0.041	0.5061	-0.9825	0.004
P50452	serpin family B member 8(SERPINB8)	0.6097	-0.7138	0.065	0.7376	-0.4390	0.065
P68402	platelet activating factor acetylhydrolase 1b catalytic subunit 2(PAFAH1B2)	0.6097	-0.7138	0.002	0.6499	-0.6216	0.002
Q04917	tyrosine 3-monooxygenase/tryptophan 5-monooxygenase activation protein eta(YWHAH)	0.6134	-0.7051	0.004	0.6530	-0.6149	0.015
Q9BTT0	acidic nuclear phosphoprotein 32 family member E(ANP32E)	0.6189	-0.6923	0.24	0.4421	-1.1774	0.026
P48506	glutamate-cysteine ligase catalytic subunit(GCLC)	0.6190	-0.6921	0.065	0.6341	-0.6573	0.015
P09211	glutathione S-transferase pi 1(GSTP1)	0.6196	-0.6906	0.002	0.6755	-0.5660	0.002
P78417	glutathione S-transferase omega 1(GSTO1)	0.6232	-0.6822	0.002	0.7024	-0.5097	0.002
P31146	coronin 1A(CORO1A)	0.6237	-0.6812	0.002	0.6698	-0.5781	0.002
P07686	hexosaminidase subunit beta(HEXB)	0.6241	-0.6802	0.002	0.6532	-0.6145	0.002
P22626	heterogeneous nuclear ribonucleoprotein A2/B1(HNRNPA2B1)	0.6273	-0.6729	0.015	0.6931	-0.5288	0.002
P07339	cathepsin D(CTSD)	0.6294	-0.6680	0.002	0.6286	-0.6697	0.002
P31946	tyrosine 3-monooxygenase/tryptophan 5-monooxygenase activation protein beta(YWHAB)	0.6313	-0.6635	0.041	0.7620	-0.3922	0.18
Q14012	calcium/calmodulin dependent protein kinase I(CAMK1)	0.6317	-0.6627	0.004	0.5027	-0.9921	0.002
P40925	malate dehydrogenase 1(MDH1)	0.6322	-0.6615	0.002	0.6511	-0.6190	0.002
Q14019	coactosin like F-actin binding protein 1(COTL1)	0.6382	-0.6480	0.004	0.6338	-0.6580	0.002
P19623	spermidine synthase(SRM)	0.6415	-0.6404	0.041	0.6992	-0.5163	0.002
P29401	transketolase(TKT)	0.6419	-0.6397	0.009	0.6604	-0.5986	0.002
Q96FW1	OTU deubiquitinase, ubiquitin aldehyde binding 1(OTUB1)	0.6420	-0.6394	0.002	0.7171	-0.4797	0.002
Q96IU4	abhydrolase domain containing 14B(ABHD14B)	0.6423	-0.6386	0.004	0.6115	-0.7097	0.004
O00182	galectin 9(LGALS9)	0.6453	-0.6318	0.009	0.6067	-0.7210	0.004
P01040	cystatin A(CSTA)	0.6502	-0.6210	0.132	0.6737	-0.5699	0.18
Q86UX7	fermitin family member 3(FERMT3)	0.6545	-0.6116	0.065	0.7010	-0.5124	0.015
Q15942	zyxin(ZYX)	0.6547	-0.6112	0.002	0.5001	-0.9998	0.002
Q9NUQ9	family with sequence similarity 49 member B(FAM49B)	0.6562	-0.6079	0.002	0.7112	-0.4917	0.002
P30041	peroxiredoxin 6(PRDX6)	0.6567	-0.6066	0.002	0.6981	-0.5186	0.002
P55786	aminopeptidase puromycin sensitive(NPEPPS)	0.6576	-0.6047	0.026	0.6642	-0.5903	0.015
P00558	phosphoglycerate kinase 1(PGK1)	0.6601	-0.5993	0.026	0.6492	-0.6232	0.002
O14773	tripeptidyl peptidase 1(TPP1)	0.6603	-0.5988	0.002	0.6614	-0.5963	0.009
P30085	cytidine/uridine monophosphate kinase 1(CMPK1)	0.6614	-0.5965	0.002	0.6435	-0.6360	0.002
O43447	peptidylprolyl isomerase H(PPIH)	0.6636	-0.5917	0.132	0.5421	-0.8833	0.026
Q15102	platelet activating factor acetylhydrolase 1b catalytic subunit 3(PAFAH1B3)	0.6641	-0.5906	0.002	0.6697	-0.5784	0.004
P30086	phosphatidylethanolamine binding protein 1(PEBP1)	0.6641	-0.5905	0.002	0.7646	-0.3873	0.002
Q96G03	phosphoglucomutase 2(PGM2)	0.6652	-0.5882	0.002	0.6426	-0.6380	0.002

P23528	cofilin 1(CFL1)	0.6660	-0.5865	0.041	0.6582	-0.6035	0.009
O00299	chloride intracellular channel 1(CLIC1)	0.6670	-0.5843	0.004	0.7023	-0.5098	0.002
P29350	protein tyrosine phosphatase, non-receptor type 6(PTPN6)	0.6680	-0.5820	0.093	0.7296	-0.4549	0.026
P26447	S100 calcium binding protein A4(S100A4)	0.6711	-0.5753	0.002	0.7394	-0.4356	0.026
Q96TA1	family with sequence similarity 129 member B(FAM129B)	0.6742	-0.5687	0.132	0.5954	-0.7480	0.026
P37837	transaldolase 1(TALDO1)	0.6748	-0.5674	0.041	0.7423	-0.4299	0.041
P62136	protein phosphatase 1 catalytic subunit alpha(PPP1CA)	0.6754	-0.5661	0.093	0.5265	-0.9254	0.026
P13489	ribonuclease/angiogenin inhibitor 1(RNH1)	0.6757	-0.5655	0.002	0.6892	-0.5371	0.002
P04406	glyceraldehyde-3-phosphate dehydrogenase(GAPDH)	0.6768	-0.5633	0.002	0.7457	-0.4233	0.002
Q9UBQ0	VPS29, retromer complex component(VPS29)	0.6770	-0.5628	0.004	0.7747	-0.3682	0.026
O43488	aldo-keto reductase family 7 member A2(AKR7A2)	0.6775	-0.5618	0.002	0.6603	-0.5988	0.002
Q9Y490	talin 1(TLN1)	0.6811	-0.5540	0.009	0.7272	-0.4595	0.002
O75874	isocitrate dehydrogenase (NADP(+)) 1, cytosolic(IDH1)	0.6811	-0.5540	0.009	0.5725	-0.8047	0.004
P04792	heat shock protein family B (small) member 1(HSPB1)	0.6819	-0.5523	0.002	0.6739	-0.5693	0.002
P00918	carbonic anhydrase 2(CA2)	0.6822	-0.5518	0.002	0.6772	-0.5624	0.002
P31939	5-aminoimidazole-4-carboxamide ribonucleotide formyltransferase/IMP cyclohydrolase(ATIC)	0.6840	-0.5479	0.004	0.6883	-0.5390	0.002
Q9UL46	proteasome activator subunit 2(PSME2)	0.6848	-0.5462	0.002	0.8191	-0.2878	0.002
Q9ULV4	coronin 1C(CORO1C)	0.6868	-0.5420	0.065	0.7654	-0.3857	0.041
Q14847	LIM and SH3 protein 1(LASP1)	0.6875	-0.5405	0.004	0.5780	-0.7910	0.002
Q8NCW5	NAD(P)HX epimerase(NAXE)	0.6885	-0.5385	0.004	0.7305	-0.4531	0.009
Q9Y3Z3	SAM and HD domain containing deoxynucleoside triphosphate triphosphohydrolase 1(SAMHD1)	0.6893	-0.5367	0.015	0.6352	-0.6547	0.065
P46926	glucosamine-6-phosphate deaminase 1(GNPDA1)	0.6896	-0.5361	0.093	0.4133	-1.2746	0.24
P12814	actinin alpha 1(ACTN1)	0.6902	-0.5348	0.002	0.7189	-0.4761	0.002
P52907	capping actin protein of muscle Z-line alpha subunit 1(CAPZA1)	0.6943	-0.5263	0.002	0.7574	-0.4009	0.002
P15311	ezrin(EZR)	0.6944	-0.5263	0.026	0.5384	-0.8933	0.009
P38159	RNA binding motif protein, X-linked(RBMX)	0.6967	-0.5214	0.041	0.7516	-0.4120	0.002
Q9H299	SH3 domain binding glutamate rich protein like 3(SH3BGRL3)	0.6970	-0.5207	0.132	0.6194	-0.6911	0.132
P37108	signal recognition particle 14(SRP14)	0.6981	-0.5186	0.026	0.7959	-0.3294	0.026
P54577	tyrosyl-tRNA synthetase(YARS)	0.6983	-0.5181	0.041	0.6901	-0.5352	0.065
P05455	Sjogren syndrome antigen B(SSB)	0.6995	-0.5156	0.31	0.5860	-0.7710	0.065
P31948	stress induced phosphoprotein 1(STIP1)	0.6999	-0.5148	0.004	0.7013	-0.5120	0.002
Q14103	heterogeneous nuclear ribonucleoprotein D(HNRNPD)	0.7012	-0.5120	0.004	0.7031	-0.5083	0.002
Q71U36	tubulin alpha 1a(TUBA1A)	0.7026	-0.5092	0.002	0.7478	-0.4192	0.002
Q9NTK5	Obg like ATPase 1(OLA1)	0.7031	-0.5082	0.065	0.7727	-0.3720	0.009
Q99497	Parkinsonism associated deglycase(PARK7)	0.7032	-0.5080	0.394	0.7720	-0.3733	0.394
P10599	thioredoxin(TXN)	0.7033	-0.5078	0.132	0.5194	-0.9452	0.132
O95861	3'(2'), 5'-bisphosphate nucleotidase 1(BPNT1)	0.7040	-0.5063	0.093	0.6228	-0.6832	0.132
P62258	tyrosine 3-monooxygenase/tryptophan 5-monooxygenase activation protein epsilon(YWHAE)	0.7041	-0.5061	0.002	0.7520	-0.4112	0.002

Q15149	plectin(PLEC)	0.7063	-0.5016	0.041	0.6519	-0.6173	0.004
Q9UBR2	cathepsin Z(CTSZ)	0.7072	-0.4997	0.132	0.4254	-1.2331	0.132
P14317	hematopoietic cell-specific Lyn substrate 1(HCLS1)	0.7075	-0.4992	0.015	0.6692	-0.5796	0.041
Q99536	vesicle amine transport 1(VAT1)	0.7101	-0.4939	0.132	0.5956	-0.7476	0.18
Q99436	proteasome subunit beta 7(PSMB7)	0.7106	-0.4929	0.004	0.7416	-0.4312	0.026
P30044	peroxiredoxin 5(PRDX5)	0.7107	-0.4927	0.041	0.6127	-0.7068	0.009
P52565	Rho GDP dissociation inhibitor alpha(ARHGDIA)	0.7155	-0.4830	0.015	0.7178	-0.4783	0.002
P36222	chitinase 3 like 1(CHI3L1)	0.7157	-0.4826	0.002	0.6697	-0.5785	0.004
P52209	phosphogluconate dehydrogenase(PGD)	0.7158	-0.4824	0.31	0.8425	-0.2472	0.004
Q15631	translin(TSN)	0.7172	-0.4795	0.18	0.7318	-0.4506	0.18
P60174	triosephosphate isomerase 1(TPI1)	0.7185	-0.4769	0.002	0.7565	-0.4026	0.002
P00492	hypoxanthine phosphoribosyltransferase 1(HPRT1)	0.7187	-0.4765	0.24	0.6719	-0.5736	0.041
P04264	keratin 1(KRT1)	0.7189	-0.4762	0.31	1.1702	0.2268	0.485
P06733	enolase 1(ENO1)	0.7189	-0.4760	0.002	0.7651	-0.3863	0.002
P00390	glutathione-disulfide reductase(GSR)	0.7205	-0.4729	0.002	0.6987	-0.5174	0.009
O75368	SH3 domain binding glutamate rich protein like(SH3BGRL)	0.7265	-0.4610	0.132	0.5608	-0.8344	0.132
P14678	small nuclear ribonucleoprotein polypeptides B and B1(SNRPB)	0.7282	-0.4575	0.041	0.6781	-0.5604	0.026
O60664	perilipin 3(PLIN3)	0.7304	-0.4533	0.009	0.8272	-0.2737	0.009
P14618	pyruvate kinase, muscle(PKM)	0.7308	-0.4525	0.18	0.7229	-0.4681	0.026
P51858	hepatoma-derived growth factor(HDGF)	0.7315	-0.4511	0.002	0.7797	-0.3591	0.002
Q8NC51	SERPINE1 mRNA binding protein 1(SERBP1)	0.7342	-0.4458	0.009	0.7619	-0.3923	0.009
P41091	eukaryotic translation initiation factor 2 subunit gamma(EIF2S3)	0.7342	-0.4457	0.18	0.7308	-0.4524	0.24
Q99729	heterogeneous nuclear ribonucleoprotein A/B(HNRNPAB)	0.7355	-0.4432	0.041	0.7042	-0.5060	0.002
O75083	WD repeat domain 1(WDR1)	0.7360	-0.4422	0.009	0.7541	-0.4072	0.002
P62906	ribosomal protein L10a(RPL10A)	0.7378	-0.4386	0.589	0.8606	-0.2166	0.24
Q15366	poly(rC) binding protein 2(PCBP2)	0.7391	-0.4361	0.004	0.7173	-0.4793	0.004
Q15185	prostaglandin E synthase 3(PTGES3)	0.7393	-0.4357	0.004	0.6479	-0.6262	0.002
P40121	capping actin protein, gelsolin like(CAPG)	0.7419	-0.4308	0.18	0.7975	-0.3265	0.24
P62937	peptidylprolyl isomerase A(PPIA)	0.7431	-0.4284	0.002	0.7728	-0.3718	0.002
P22314	ubiquitin like modifier activating enzyme 1(UBA1)	0.7436	-0.4275	0.004	0.7569	-0.4018	0.002
P47756	capping actin protein of muscle Z-line beta subunit(CAPZB)	0.7452	-0.4244	0.009	0.7593	-0.3974	0.002
O15145	actin related protein 2/3 complex subunit 3(ARPC3)	0.7466	-0.4216	0.093	0.8663	-0.2071	0.394
O00442	RNA 3'-terminal phosphate cyclase(RTCA)	0.7478	-0.4193	0.002	0.8009	-0.3202	0.015
Q06323	proteasome activator subunit 1(PSME1)	0.7479	-0.4191	0.002	0.7197	-0.4745	0.004
P53582	methionyl aminopeptidase 1(METAP1)	0.7482	-0.4185	0.041	0.7218	-0.4703	0.002
Q16851	UDP-glucose pyrophosphorylase 2(UGP2)	0.7499	-0.4151	0.004	0.7377	-0.4389	0.004
P06744	glucose-6-phosphate isomerase(GPI)	0.7509	-0.4134	0.002	0.7557	-0.4041	0.002
Q12905	interleukin enhancer binding factor 2(ILF2)	0.7515	-0.4121	0.041	0.7825	-0.3538	0.009
P49321	nuclear autoantigenic sperm protein(NASP)	0.7528	-0.4096	0.004	0.6340	-0.6575	0.026

P25789	proteasome subunit alpha 4(PSMA4)	0.7533	-0.4087	0.026	0.6968	-0.5211	0.026
O60506	synaptotagmin binding cytoplasmic RNA interacting protein(SYNCRIP)	0.7557	-0.4042	0.31	0.6123	-0.7077	0.041
P09651	heterogeneous nuclear ribonucleoprotein A1(HNRNPA1)	0.7573	-0.4011	0.394	0.7101	-0.4939	0.015
Q9NY33	dipeptidyl peptidase 3(DPP3)	0.7574	-0.4009	0.24	0.6522	-0.6167	0.093
Q01105	SET nuclear proto-oncogene(SET)	0.7629	-0.3904	0.002	0.6254	-0.6772	0.002
Q6XQN6	nicotinate phosphoribosyltransferase(NAPRT)	0.7631	-0.3900	0.002	0.5620	-0.8313	0.004
P07737	profilin 1(PFN1)	0.7648	-0.3868	0.002	0.6696	-0.5786	0.002
P04075	aldolase, fructose-bisphosphate A(ALDOA)	0.7655	-0.3856	0.009	0.8113	-0.3017	0.004
P07741	adenine phosphoribosyltransferase(APRT)	0.7657	-0.3851	0.002	0.7080	-0.4982	0.015
Q04760	glyoxalase I(GLO1)	0.7661	-0.3845	0.041	0.6960	-0.5227	0.002
Q13303	potassium voltage-gated channel subfamily A regulatory beta subunit 2(KCNAB2)	0.7682	-0.3805	0.015	0.7244	-0.4652	0.004
P67775	protein phosphatase 2 catalytic subunit alpha(PPP2CA)	0.7689	-0.3792	0.004	0.7965	-0.3283	0.004
P59998	actin related protein 2/3 complex subunit 4(ARPC4)	0.7712	-0.3749	0.002	0.7808	-0.3570	0.002
P20618	proteasome subunit beta 1(PSMB1)	0.7720	-0.3733	0.002	0.7869	-0.3458	0.004
Q96AG4	leucine rich repeat containing 59(LRRC59)	0.7742	-0.3692	0.065	0.7612	-0.3936	0.041
P37235	hippocalcin like 1(HPCAL1)	0.7744	-0.3689	0.009	0.8056	-0.3118	0.004
P61225	RAP2B, member of RAS oncogene family(RAP2B)	0.7745	-0.3687	0.394	0.8032	-0.3161	0.18
Q13492	phosphatidylinositol binding clathrin assembly protein(PICALM)	0.7752	-0.3674	0.009	0.6626	-0.5937	0.004
Q01518	adenylate cyclase associated protein 1(CAP1)	0.7762	-0.3655	0.002	0.8246	-0.2782	0.002
P26196	DEAD-box helicase 6(DDX6)	0.7790	-0.3603	0.24	0.7561	-0.4033	0.065
O14818	proteasome subunit alpha 7(PSMA7)	0.7792	-0.3599	0.009	0.7966	-0.3281	0.009
P26599	polypyrimidine tract binding protein 1(PTBP1)	0.7799	-0.3586	0.009	0.7988	-0.3241	0.002
Q13404	ubiquitin conjugating enzyme E2 V1(UBE2V1)	0.7802	-0.3580	0.015	0.7302	-0.4536	0.093
Q9HB71	calcyclin binding protein(CACYBP)	0.7811	-0.3564	0.093	0.6712	-0.5753	0.015
P09661	small nuclear ribonucleoprotein polypeptide A'(SNRPA1)	0.7813	-0.3561	0.009	0.7859	-0.3475	0.065
P09382	galectin 1(LGALS1)	0.7822	-0.3544	0.002	0.6576	-0.6048	0.002
O43747	adaptor related protein complex 1 gamma 1 subunit(AP1G1)	0.7827	-0.3535	0.065	0.7734	-0.3707	0.026
P61978	heterogeneous nuclear ribonucleoprotein K(HNRNPK)	0.7827	-0.3534	0.002	0.8471	-0.2394	0.002
Q8TDZ2	microtubule associated monooxygenase, calponin and LIM domain containing 1(MICAL1)	0.7844	-0.3503	0.485	0.8457	-0.2418	0.31
P49720	proteasome subunit beta 3(PSMB3)	0.7846	-0.3499	0.041	0.6815	-0.5532	0.009
P09429	high mobility group box 1(HMGB1)	0.7847	-0.3498	0.24	0.7649	-0.3867	0.18
Q8IZP2	suppression of tumorigenicity 13 (colon carcinoma) (Hsp70 interacting protein) pseudogene 4(ST13P4)	0.7852	-0.3489	0.093	0.7374	-0.4395	0.18
P20936	RAS p21 protein activator 1(RASA1)	0.7863	-0.3469	0.009	0.6150	-0.7014	0.002
P29692	eukaryotic translation elongation factor 1 delta(EEF1D)	0.7866	-0.3464	0.009	0.8160	-0.2934	0.009
P51991	heterogeneous nuclear ribonucleoprotein A3(HNRNPA3)	0.7869	-0.3457	0.132	0.7855	-0.3483	0.002
P43487	RAN binding protein 1(RANBP1)	0.7873	-0.3449	0.041	0.8199	-0.2864	0.004
O95571	ETHE1, persulfide dioxygenase(ETHE1)	0.7886	-0.3426	0.394	0.7868	-0.3460	0.24
P49721	proteasome subunit beta 2(PSMB2)	0.7898	-0.3404	0.004	0.7893	-0.3414	0.015

Q09666	AHNAK nucleoprotein(AHNAK)	0.7904	-0.3393	0.065	0.7545	-0.4064	0.002
P15121	aldo-keto reductase family 1 member B(AKR1B1)	0.7905	-0.3391	0.485	0.7149	-0.4841	0.065
P61981	tyrosine 3-monooxygenase/tryptophan 5-monooxygenase activation protein gamma(YWHAG)	0.7936	-0.3334	0.015	0.8267	-0.2745	0.015
O43707	actinin alpha 4(ACTN4)	0.7945	-0.3318	0.002	0.7358	-0.4427	0.002
P36543	ATPase H+ transporting V1 subunit E1(ATP6V1E1)	0.7959	-0.3294	0.24	0.7785	-0.3612	0.818
P19338	nucleolin(NCL)	0.7963	-0.3287	0.004	0.7922	-0.3360	0.002
O15144	actin related protein 2/3 complex subunit 2(ARPC2)	0.8025	-0.3175	0.026	0.8092	-0.3054	0.004
P25786	proteasome subunit alpha 1(PSMA1)	0.8033	-0.3161	0.18	0.7671	-0.3825	0.31
O14979	heterogeneous nuclear ribonucleoprotein D like(HNRNPDL)	0.8035	-0.3156	0.026	0.6854	-0.5449	0.004
Q5VW32	BRO1 domain and CAAX motif containing(BROX)	0.8053	-0.3124	0.394	0.6181	-0.6942	0.065
P22392	NME/NM23 nucleoside diphosphate kinase 2(NME2)	0.8073	-0.3089	0.002	0.8503	-0.2340	0.002
Q6EEV6	small ubiquitin-like modifier 4(SUMO4)	0.8081	-0.3073	0.24	0.7865	-0.3464	0.18
P55957	BH3 interacting domain death agonist(BID)	0.8089	-0.3060	0.132	1.0383	0.0542	0.699
P49591	seryl-tRNA synthetase(SARS)	0.8102	-0.3037	0.065	0.8341	-0.2616	0.009
P12956	X-ray repair cross complementing 6(XRCC6)	0.8115	-0.3013	0.065	0.7864	-0.3466	0.041
P30050	ribosomal protein L12(RPL12)	0.8119	-0.3007	0.485	1.0639	0.0893	0.699
P62979	ribosomal protein S27a(RPS27A)	0.8123	-0.3000	0.132	0.7232	-0.4676	0.132
P84077	ADP ribosylation factor 1(ARF1)	0.8127	-0.2992	0.065	0.7200	-0.4740	0.002
O43390	heterogeneous nuclear ribonucleoprotein R(HNRNPR)	0.8146	-0.2959	0.818	0.6502	-0.6211	0.18
Q96C19	EF-hand domain family member D2(EFHD2)	0.8146	-0.2958	0.132	0.9125	-0.1321	0.041
P35527	keratin 9(KRT9)	0.8169	-0.2917	0.24	1.4634	0.5493	0.485
P46940	IQ motif containing GTPase activating protein 1(IQGAP1)	0.8184	-0.2890	0.009	0.7959	-0.3294	0.002
P50395	GDP dissociation inhibitor 2(GDI2)	0.8193	-0.2875	0.015	0.7878	-0.3441	0.004
Q16643	drebrin 1(DBN1)	0.8199	-0.2864	0.394	0.7270	-0.4599	0.18
Q7L576	cytoplasmic FMR1 interacting protein 1(CYFIP1)	0.8201	-0.2862	0.065	0.7463	-0.4222	0.015
P63104	tyrosine 3-monooxygenase/tryptophan 5-monooxygenase activation protein zeta(YWHAZ)	0.8202	-0.2859	0.009	0.7710	-0.3752	0.065
P16930	fumarylacetoacetate hydrolase(FAH)	0.8212	-0.2842	0.065	0.8023	-0.3178	0.026
P04080	cystatin B(CSTB)	0.8227	-0.2816	0.132	0.7686	-0.3797	0.132
P42167	thymopoietin(TMPO)	0.8233	-0.2805	0.18	0.8166	-0.2923	0.18
Q9BRA2	thioredoxin domain containing 17(TXNDC17)	0.8243	-0.2787	0.009	0.6696	-0.5787	0.026
P05109	S100 calcium binding protein A8(S100A8)	0.8248	-0.2778	0.589	0.8908	-0.1668	0.394
P06396	gelsolin(GSN)	0.8264	-0.2751	0.002	0.8260	-0.2758	0.026
Q9NSD9	phenylalanyl-tRNA synthetase beta subunit(FARSB)	0.8273	-0.2735	0.24	0.6761	-0.5647	0.093
P04083	annexin A1(ANXA1)	0.8275	-0.2732	0.041	0.7910	-0.3383	0.093
P07195	lactate dehydrogenase B(LDHB)	0.8281	-0.2721	0.132	0.7704	-0.3763	0.132
P05388	ribosomal protein lateral stalk subunit P0(RPLP0)	0.8288	-0.2708	0.093	0.8591	-0.2191	0.065
Q96BY6	dedicator of cytokinesis 10(DOCK10)	0.8294	-0.2699	0.009	0.8066	-0.3102	0.004
P27695	apurinic/apyrimidinic endodeoxyribonuclease 1(APEX1)	0.8302	-0.2685	0.065	0.6528	-0.6153	0.18

P35268	ribosomal protein L22(RPL22)	0.8307	-0.2675	0.394	0.8173	-0.2911	0.24
Q13177	p21 (RAC1) activated kinase 2(PAK2)	0.8321	-0.2651	0.065	0.8186	-0.2888	0.132
P28838	leucine aminopeptidase 3(LAP3)	0.8329	-0.2638	0.004	0.7182	-0.4775	0.041
Q13148	TAR DNA binding protein(TARDBP)	0.8330	-0.2636	0.026	0.8362	-0.2580	0.041
P26640	valyl-tRNA synthetase(VARS)	0.8338	-0.2622	0.004	0.8511	-0.2326	0.009
O60763	USO1 vesicle transport factor(USO1)	0.8341	-0.2617	0.132	0.7841	-0.3509	0.093
Q15154	pericentriolar material 1(PCM1)	0.8352	-0.2598	0.065	0.8512	-0.2324	0.041
Q86VP6	cullin associated and neddylation dissociated 1(CAND1)	0.8368	-0.2571	0.002	0.8277	-0.2728	0.041
P46783	ribosomal protein S10(RPS10)	0.8370	-0.2566	0.132	0.9418	-0.0865	0.937
P61158	ARP3 actin related protein 3 homolog(ACTR3)	0.8380	-0.2551	0.004	0.8790	-0.1860	0.002
P62995	transformer 2 beta homolog (Drosophila)(TRA2B)	0.8384	-0.2543	0.24	0.8827	-0.1800	0.31
P63151	protein phosphatase 2 regulatory subunit Balpha(PPP2R2A)	0.8390	-0.2532	0.002	0.8986	-0.1542	0.093
Q15365	poly(rC) binding protein 1(PCBP1)	0.8392	-0.2529	0.24	0.7657	-0.3851	0.24
Q01130	serine and arginine rich splicing factor 2(SRSF2)	0.8394	-0.2525	0.041	0.7097	-0.4948	0.093
P31153	methionine adenosyltransferase 2A(MAT2A)	0.8396	-0.2522	0.132	0.6756	-0.5657	0.041
P26038	moesin(MSN)	0.8396	-0.2522	0.065	0.7986	-0.3244	0.004
Q16555	dihydropyrimidinase like 2(DPYSL2)	0.8411	-0.2496	0.132	0.7999	-0.3221	0.002
O43396	thioredoxin like 1(TXNL1)	0.8412	-0.2495	0.24	0.8160	-0.2934	0.132
Q92945	KH-type splicing regulatory protein(KHSRP)	0.8417	-0.2486	0.093	0.7392	-0.4360	0.093
O00410	importin 5(IPO5)	0.8421	-0.2479	0.132	0.8195	-0.2872	0.015
Q9Y5S9	RNA binding motif protein 8A(RBM8A)	0.8426	-0.2471	0.132	0.7547	-0.4061	0.065
P17980	proteasome 26S subunit, ATPase 3(PSMC3)	0.8433	-0.2460	0.132	0.7475	-0.4198	0.041
P84103	serine and arginine rich splicing factor 3(SRSF3)	0.8434	-0.2457	0.026	0.7819	-0.3549	0.132
P67936	tropomyosin 4(TPM4)	0.8445	-0.2439	0.24	0.9299	-0.1048	0.394
P07203	glutathione peroxidase 1(GPX1)	0.8450	-0.2431	0.026	0.9065	-0.1416	0.065
P28072	proteasome subunit beta 6(PSMB6)	0.8454	-0.2424	0.093	0.7497	-0.4157	0.24
Q96QK1	VPS35, retromer complex component(VPS35)	0.8461	-0.2412	0.24	0.8086	-0.3065	0.18
Q08J23	NOP2/Sun RNA methyltransferase family member 2(NSUN2)	0.8461	-0.2411	0.18	0.6578	-0.6043	0.026
P00338	lactate dehydrogenase A(LDHA)	0.8478	-0.2382	0.132	0.7671	-0.3825	0.026
P18621	ribosomal protein L17(RPL17)	0.8499	-0.2346	0.699	1.0157	0.0224	1
Q14204	dynein cytoplasmic 1 heavy chain 1(DYNC1H1)	0.8505	-0.2337	0.132	0.8666	-0.2065	0.589
P84098	ribosomal protein L19(RPL19)	0.8507	-0.2333	0.394	0.8316	-0.2661	0.18
P24534	eukaryotic translation elongation factor 1 beta 2(EEF1B2)	0.8507	-0.2333	0.065	0.8852	-0.1759	0.041
P68371	tubulin beta 4B class IVb(TUBB4B)	0.8510	-0.2328	0.009	0.8350	-0.2602	0.004
P53396	ATP citrate lyase(ACLY)	0.8511	-0.2326	0.026	0.7760	-0.3659	0.004
P56537	eukaryotic translation initiation factor 6(EIF6)	0.8513	-0.2323	0.589	0.7374	-0.4394	0.31
P60900	proteasome subunit alpha 6(PSMA6)	0.8514	-0.2321	0.009	0.8175	-0.2906	0.041
P61086	ubiquitin conjugating enzyme E2 K(UBE2K)	0.8527	-0.2298	0.065	0.6368	-0.6511	0.015
Q16181	septin 7(SEPT7)	0.8529	-0.2296	0.132	0.7732	-0.3710	0.009

Q96AE4	far upstream element binding protein 1(FUBP1)	0.8537	-0.2283	0.026	0.7317	-0.4506	0.041
P25398	ribosomal protein S12(RPS12)	0.8539	-0.2278	0.132	0.8290	-0.2705	0.132
P25788	proteasome subunit alpha 3(PSMA3)	0.8541	-0.2275	0.015	0.8365	-0.2576	0.132
Q07955	serine and arginine rich splicing factor 1(SRSF1)	0.8544	-0.2271	0.009	0.6559	-0.6086	0.041
P23526	adenosylhomocysteinase(AHCY)	0.8545	-0.2269	0.065	0.7776	-0.3630	0.009
P39687	acidic nuclear phosphoprotein 32 family member A(ANP32A)	0.8547	-0.2265	0.065	0.8204	-0.2857	0.041
O14980	exportin 1(XPO1)	0.8548	-0.2263	0.132	0.9001	-0.1518	0.026
P30740	serpin family B member 1(SERPINB1)	0.8551	-0.2259	0.065	0.6425	-0.6381	0.009
P11413	glucose-6-phosphate dehydrogenase(G6PD)	0.8561	-0.2241	0.041	0.8170	-0.2915	0.065
P55060	chromosome segregation 1 like(CSE1L)	0.8568	-0.2229	0.24	0.8172	-0.2913	0.093
P50570	dynamin 2(DNM2)	0.8569	-0.2228	0.026	0.8877	-0.1719	0.065
P62826	RAN, member RAS oncogene family(RAN)	0.8571	-0.2225	0.009	0.7783	-0.3617	0.002
Q12906	interleukin enhancer binding factor 3(ILF3)	0.8579	-0.2212	0.065	0.8525	-0.2303	0.004
P47914	ribosomal protein L29(RPL29)	0.8587	-0.2198	0.485	0.8415	-0.2490	0.589
O94973	adaptor related protein complex 2 alpha 2 subunit(AP2A2)	0.8596	-0.2182	0.485	0.7126	-0.4889	0.132
P60953	cell division cycle 42(CDC42)	0.8607	-0.2164	0.026	0.7767	-0.3645	0.026
P15531	NME/NM23 nucleoside diphosphate kinase 1(NME1)	0.8610	-0.2159	0.699	0.9550	-0.0664	0.699
Q10567	adaptor related protein complex 1 beta 1 subunit(AP1B1)	0.8618	-0.2145	0.015	0.7638	-0.3888	0.015
P11142	heat shock protein family A (Hsp70) member 8(HSPA8)	0.8622	-0.2139	0.065	0.9185	-0.1226	0.041
P26641	eukaryotic translation elongation factor 1 gamma(EEF1G)	0.8623	-0.2137	0.004	0.8397	-0.2521	0.002
P62495	eukaryotic translation termination factor 1(ETF1)	0.8626	-0.2132	0.394	0.8180	-0.2899	0.18
P15153	ras-related C3 botulinum toxin substrate 2 (rho family, small GTP binding protein Rac2)(RAC2)	0.8640	-0.2109	0.015	0.8923	-0.1644	0.18
Q16629	serine and arginine rich splicing factor 7(SRSF7)	0.8649	-0.2094	0.31	0.7251	-0.4637	0.24
P07900	heat shock protein 90 alpha family class A member 1(HSP90AA1)	0.8650	-0.2093	0.004	0.8376	-0.2556	0.004
P26639	threonyl-tRNA synthetase(TARS)	0.8651	-0.2091	0.041	0.8250	-0.2776	0.065
P23246	splicing factor proline and glutamine rich(SFPQ)	0.8675	-0.2050	0.041	0.7704	-0.3763	0.002
Q7L1Q6	basic leucine zipper and W2 domains 1(BZW1)	0.8708	-0.1995	0.065	0.8406	-0.2505	0.002
P34932	heat shock protein family A (Hsp70) member 4(HSPA4)	0.8709	-0.1993	0.18	0.8977	-0.1557	0.026
Q8IV08	phospholipase D family member 3(PLD3)	0.8712	-0.1989	0.18	0.7667	-0.3833	0.026
P07910	heterogeneous nuclear ribonucleoprotein C (C1/C2)(HNRNPC)	0.8713	-0.1988	0.132	0.8782	-0.1874	0.041
P48444	archain 1(ARCN1)	0.8746	-0.1932	0.31	0.7453	-0.4240	0.065
P31943	heterogeneous nuclear ribonucleoprotein H1 (H)(HNRNPH1)	0.8760	-0.1910	0.041	0.8641	-0.2108	0.026
P42766	ribosomal protein L35(RPL35)	0.8763	-0.1905	0.699	1.1568	0.2101	0.818
P11586	methylenetetrahydrofolate dehydrogenase, cyclohydrolase and formyltetrahydrofolate synthetase 1(MTHFD1)	0.8778	-0.1881	0.041	0.8078	-0.3079	0.041
P54136	arginyl-tRNA synthetase(RARS)	0.8782	-0.1873	0.004	0.8213	-0.2840	0.065
P17931	galectin 3(LGALS3)	0.8784	-0.1871	0.009	0.8119	-0.3007	0.065
Q9UH99	Sad1 and UNC84 domain containing 2(SUN2)	0.8788	-0.1864	0.31	0.8076	-0.3083	0.24
P43686	proteasome 26S subunit, ATPase 4(PSMC4)	0.8789	-0.1862	0.394	0.7318	-0.4505	0.31

O76094	signal recognition particle 72(SRP72)	0.8791	-0.1860	1	0.9917	-0.0121	0.699
Q13151	heterogeneous nuclear ribonucleoprotein A0(HNRNPA0)	0.8808	-0.1831	0.485	0.7802	-0.3581	0.065
P46776	ribosomal protein L27a(RPL27A)	0.8810	-0.1828	0.394	0.9922	-0.0113	1
Q9Y696	chloride intracellular channel 4(CLIC4)	0.8842	-0.1775	0.937	0.9336	-0.0991	0.699
Q9UKM9	RALY heterogeneous nuclear ribonucleoprotein(RALY)	0.8855	-0.1754	0.31	0.8145	-0.2960	0.132
P22234	phosphoribosylaminoimidazole carboxylase; phosphoribosylaminoimidazolesuccinocarboxamide synthase(PAICS)	0.8860	-0.1746	0.026	0.8929	-0.1634	0.026
Q15418	ribosomal protein S6 kinase A1(RPS6KA1)	0.8861	-0.1744	0.31	0.8118	-0.3007	0.132
Q99439	calponin 2(CNN2)	0.8869	-0.1732	0.24	0.5338	-0.9055	0.026
O00160	myosin IF(MYO1F)	0.8869	-0.1731	0.589	0.8575	-0.2218	0.394
O15143	actin related protein 2/3 complex subunit 1B(ARPC1B)	0.8889	-0.1699	0.18	0.8267	-0.2745	0.009
P05198	eukaryotic translation initiation factor 2 subunit alpha(EIF2S1)	0.8908	-0.1669	0.093	0.7865	-0.3464	0.065
P30153	protein phosphatase 2 scaffold subunit Aalpha(PPP2R1A)	0.8908	-0.1668	0.065	0.7254	-0.4631	0.065
P13010	X-ray repair cross complementing 5(XRCC5)	0.8916	-0.1655	0.026	0.8541	-0.2275	0.041
P46063	RecQ like helicase(RECQL)	0.8921	-0.1648	0.065	0.8031	-0.3164	0.093
P49189	aldehyde dehydrogenase 9 family member A1(ALDH9A1)	0.8940	-0.1617	0.026	0.7619	-0.3923	0.132
E9PAV3	nascent polypeptide-associated complex alpha subunit(NACA)	0.8940	-0.1616	0.18	0.6807	-0.5550	0.18
P60842	eukaryotic translation initiation factor 4A1(EIF4A1)	0.8965	-0.1577	0.394	0.9580	-0.0619	0.485
P47985	ubiquinol-cytochrome c reductase, Rieske iron-sulfur polypeptide 1(UQCRFS1)	0.8973	-0.1564	0.589	0.7253	-0.4634	0.818
Q86U42	poly(A) binding protein nuclear 1(PABPN1)	0.8978	-0.1556	0.24	0.7860	-0.3473	0.132
P13796	lymphocyte cytosolic protein 1(LCP1)	0.8985	-0.1543	0.485	0.9118	-0.1332	0.093
P13693	tumor protein, translationally-controlled 1(TPT1)	0.8987	-0.1542	0.132	0.8782	-0.1874	0.015
Q13045	FLII, actin remodeling protein(FLII)	0.8987	-0.1542	0.132	0.8820	-0.1811	0.18
P17812	CTP synthase 1(CTPS1)	0.8990	-0.1536	0.041	0.8860	-0.1747	0.026
P28066	proteasome subunit alpha 5(PSMA5)	0.9006	-0.1511	0.24	0.7883	-0.3433	0.093
Q13247	serine and arginine rich splicing factor 6(SRSF6)	0.9031	-0.1470	0.18	0.7843	-0.3505	0.24
P29144	tripeptidyl peptidase 2(TPP2)	0.9051	-0.1439	0.18	0.9307	-0.1036	0.699
P49736	minichromosome maintenance complex component 2(MCM2)	0.9073	-0.1403	0.485	0.7672	-0.3823	0.24
Q9P0L0	VAMP associated protein A(VAPA)	0.9073	-0.1403	0.589	0.8525	-0.2303	0.485
P55010	eukaryotic translation initiation factor 5(EIF5)	0.9091	-0.1375	0.589	0.9517	-0.0714	0.589
P61088	ubiquitin conjugating enzyme E2 N(UBE2N)	0.9107	-0.1350	0.31	0.8130	-0.2987	0.041
P62333	proteasome 26S subunit, ATPase 6(PSMC6)	0.9138	-0.1301	0.132	0.8096	-0.3047	0.132
P07437	tubulin beta class I(TUBB)	0.9172	-0.1246	0.041	0.8950	-0.1601	0.041
P41252	isoleucyl-tRNA synthetase(IARS)	0.9184	-0.1228	0.31	0.8634	-0.2119	0.18
Q14157	ubiquitin associated protein 2 like(UBAP2L)	0.9193	-0.1214	0.24	0.9525	-0.0702	0.132
Q15907	RAB11B, member RAS oncogene family(RAB11B)	0.9193	-0.1214	0.18	0.9333	-0.0996	0.394
P50990	chaperonin containing TCP1 subunit 8(CCT8)	0.9215	-0.1180	0.065	0.8718	-0.1979	0.009
P48643	chaperonin containing TCP1 subunit 5(CCT5)	0.9221	-0.1170	0.009	0.9057	-0.1429	0.18
Q13200	proteasome 26S subunit, non-ATPase 2(PSMD2)	0.9221	-0.1170	0.699	0.8410	-0.2498	0.093

O00487	proteasome 26S subunit, non-ATPase 14(PSMD14)	0.9236	-0.1147	0.093	0.9527	-0.0699	0.485
Q03252	lamin B2(LMNB2)	0.9239	-0.1142	0.937	0.9725	-0.0402	0.937
P25787	proteasome subunit alpha 2(PSMA2)	0.9239	-0.1142	0.132	0.9366	-0.0945	0.31
P49368	chaperonin containing TCP1 subunit 3(CCT3)	0.9243	-0.1136	0.132	0.8283	-0.2719	0.18
Q14974	karyopherin subunit beta 1(KPNB1)	0.9244	-0.1134	0.699	0.8393	-0.2528	0.589
Q16531	damage specific DNA binding protein 1(DDB1)	0.9244	-0.1134	0.699	0.7371	-0.4401	0.24
O00186	syntaxin binding protein 3(STXBP3)	0.9267	-0.1097	1	0.9554	-0.0658	0.589
Q07021	complement C1q binding protein(C1QBP)	0.9275	-0.1086	0.937	0.8560	-0.2243	1
Q92499	DEAD-box helicase 1(DDX1)	0.9281	-0.1077	0.394	0.7323	-0.4495	0.18
P33993	minichromosome maintenance complex component 7(MCM7)	0.9284	-0.1071	0.589	1.0091	0.0131	0.937
Q12874	splicing factor 3a subunit 3(SF3A3)	0.9286	-0.1069	0.31	0.8076	-0.3083	0.18
P60866	ribosomal protein S20(RPS20)	0.9289	-0.1065	0.31	1.0161	0.0230	0.818
Q8NBQ5	hydroxysteroid 17-beta dehydrogenase 11(HSD17B11)	0.9291	-0.1061	0.818	0.9264	-0.1103	0.937
Q9BUF5	tubulin beta 6 class V(TUBB6)	0.9296	-0.1053	0.132	0.8509	-0.2330	0.026
P35998	proteasome 26S subunit, ATPase 2(PSMC2)	0.9299	-0.1049	0.24	0.8549	-0.2261	0.026
P40227	chaperonin containing TCP1 subunit 6A(CCT6A)	0.9303	-0.1042	0.026	0.8483	-0.2374	0.132
P62318	small nuclear ribonucleoprotein D3 polypeptide(SNRPD3)	0.9306	-0.1037	0.093	0.7761	-0.3656	0.015
P63241	eukaryotic translation initiation factor 5A(EIF5A)	0.9307	-0.1036	0.132	0.9504	-0.0733	0.818
P62277	ribosomal protein S13(RPS13)	0.9317	-0.1020	0.485	0.9891	-0.0159	0.818
O75533	splicing factor 3b subunit 1(SF3B1)	0.9322	-0.1013	0.937	0.8557	-0.2248	0.18
Q9UHD8	septin 9(SEPT9)	0.9327	-0.1005	0.818	0.8976	-0.1559	0.31
P46779	ribosomal protein L28(RPL28)	0.9331	-0.0998	0.818	0.9779	-0.0322	0.699
Q14011	cold inducible RNA binding protein(CIRBP)	0.9335	-0.0992	0.31	0.8427	-0.2468	0.24
P62316	small nuclear ribonucleoprotein D2 polypeptide(SNRPD2)	0.9340	-0.0985	0.31	0.7545	-0.4063	0.132
P06753	tropomyosin 3(TPM3)	0.9351	-0.0968	0.31	0.9449	-0.0818	0.31
Q14739	lamin B receptor(LBR)	0.9353	-0.0965	0.394	0.8497	-0.2349	0.065
Q13418	integrin linked kinase(ILK)	0.9376	-0.0929	0.394	0.7630	-0.3902	0.004
O75694	nucleoporin 155(NUP155)	0.9385	-0.0916	1	1.0124	0.0178	0.699
Q14108	scavenger receptor class B member 2(SCARB2)	0.9388	-0.0911	0.818	0.9697	-0.0444	0.937
Q02878	ribosomal protein L6(RPL6)	0.9417	-0.0867	0.818	0.9560	-0.0649	0.818
P07814	glutamyl-prolyl-tRNA synthetase(EPRS)	0.9423	-0.0858	0.041	0.8915	-0.1657	0.041
P50991	chaperonin containing TCP1 subunit 4(CCT4)	0.9450	-0.0816	0.18	0.9324	-0.1009	0.18
P50552	vasodilator-stimulated phosphoprotein(VASP)	0.9456	-0.0807	0.937	0.8394	-0.2525	0.18
O00754	mannosidase alpha class 2B member 1(MAN2B1)	0.9457	-0.0805	1	0.9352	-0.0966	0.699
P61160	ARP2 actin related protein 2 homolog(ACTR2)	0.9460	-0.0800	0.485	0.9623	-0.0554	0.31
Q8WXF1	paraspeckle component 1(PSPC1)	0.9489	-0.0757	0.485	0.7826	-0.3537	0.026
P62081	ribosomal protein S7(RPS7)	0.9489	-0.0756	0.485	1.2511	0.3232	0.394
P62854	ribosomal protein S26(RPS26)	0.9495	-0.0748	0.699	1.2140	0.2798	0.31
P62249	ribosomal protein S16(RPS16)	0.9497	-0.0744	1	0.9551	-0.0662	1

P53618	coatomer protein complex subunit beta 1(COPB1)	0.9504	-0.0734	0.065	0.9222	-0.1169	0.041
Q15233	non-POU domain containing, octamer-binding(NONO)	0.9510	-0.0724	0.937	0.8521	-0.2309	0.093
P04040	catalase(CAT)	0.9517	-0.0714	0.31	0.8015	-0.3193	0.026
P47897	glutaminyl-tRNA synthetase(QARS)	0.9523	-0.0705	0.394	0.8553	-0.2255	0.026
O75643	small nuclear ribonucleoprotein U5 subunit 200(SNRNP200)	0.9550	-0.0664	0.589	0.8864	-0.1740	0.589
P08865	ribosomal protein SA(RPSA)	0.9552	-0.0662	0.093	0.8869	-0.1731	0.065
P98179	RNA binding motif (RNP1, RRM) protein 3(RBM3)	0.9553	-0.0660	0.699	0.9531	-0.0693	0.31
P55072	valosin containing protein(VCP)	0.9566	-0.0641	0.31	0.9166	-0.1257	0.015
P53999	SUB1 homolog, transcriptional regulator(SUB1)	0.9571	-0.0632	0.394	0.9228	-0.1159	0.132
O15511	actin related protein 2/3 complex subunit 5(ARPC5)	0.9575	-0.0626	0.394	1.0994	0.1368	0.818
P52566	Rho GDP dissociation inhibitor beta(ARHGDIB)	0.9581	-0.0618	0.24	0.9393	-0.0904	0.24
Q92616	GCN1, eIF2 alpha kinase activator homolog(GCN1)	0.9582	-0.0616	0.818	0.8216	-0.2834	0.093
P60709	actin beta(ACTB)	0.9582	-0.0616	0.394	0.9266	-0.1100	0.394
P43405	spleen associated tyrosine kinase(SYK)	0.9587	-0.0609	0.589	0.8078	-0.3079	0.24
P26368	U2 small nuclear RNA auxiliary factor 2(U2AF2)	0.9590	-0.0604	0.699	0.7430	-0.4286	0.041
P51148	RAB5C, member RAS oncogene family(RAB5C)	0.9591	-0.0603	0.699	1.0901	0.1245	0.093
P46459	N-ethylmaleimide sensitive factor, vesicle fusing ATPase(NSF)	0.9591	-0.0603	0.065	0.8548	-0.2263	0.065
P25205	minichromosome maintenance complex component 3(MCM3)	0.9592	-0.0601	0.041	0.9252	-0.1121	0.31
Q99832	chaperonin containing TCP1 subunit 7(CCT7)	0.9597	-0.0594	0.394	0.9704	-0.0433	0.31
P35637	FUS RNA binding protein(FUS)	0.9606	-0.0581	0.394	0.8283	-0.2718	0.18
P62195	proteasome 26S subunit, ATPase 5(PSMC5)	0.9611	-0.0573	0.24	0.7674	-0.3820	0.041
P78371	chaperonin containing TCP1 subunit 2(CCT2)	0.9629	-0.0546	0.818	0.9370	-0.0939	0.394
P63244	receptor for activated C kinase 1(RACK1)	0.9647	-0.0518	0.394	0.7945	-0.3318	0.24
Q15046	lysyl-tRNA synthetase(KARS)	0.9649	-0.0515	0.394	0.9901	-0.0144	0.589
P35908	keratin 2(KRT2)	0.9654	-0.0508	0.589	1.2898	0.3672	0.24
P62280	ribosomal protein S11(RPS11)	0.9664	-0.0494	1	0.9169	-0.1251	0.485
P62241	ribosomal protein S8(RPS8)	0.9672	-0.0482	0.937	1.0146	0.0208	1
P62913	ribosomal protein L11(RPL11)	0.9681	-0.0468	1	0.9335	-0.0993	0.589
O95831	apoptosis inducing factor, mitochondria associated 1(AIFM1)	0.9690	-0.0454	0.818	0.7837	-0.3517	0.132
Q08945	structure specific recognition protein 1(SSRP1)	0.9694	-0.0449	0.699	0.9700	-0.0439	0.937
P61923	coatomer protein complex subunit zeta 1(COPZ1)	0.9695	-0.0447	0.818	0.7987	-0.3242	0.002
P83731	ribosomal protein L24(RPL24)	0.9702	-0.0437	0.937	0.9453	-0.0812	0.589
Q86UE4	metadherin(MTDH)	0.9705	-0.0433	0.937	0.8060	-0.3112	0.24
P09467	fructose-bisphosphatase 1(FBP1)	0.9750	-0.0365	0.699	0.7936	-0.3335	0.31
P61019	RAB2A, member RAS oncogene family(RAB2A)	0.9756	-0.0356	0.699	0.9713	-0.0420	0.31
Q8N163	cell cycle and apoptosis regulator 2(CCAR2)	0.9759	-0.0352	0.589	0.8555	-0.2251	0.065
Q92608	dedicator of cytokinesis 2(DOCK2)	0.9765	-0.0343	0.485	0.8744	-0.1936	0.041
Q9Y265	RuvB like AAA ATPase 1(RUVBL1)	0.9766	-0.0342	0.589	1.0187	0.0267	1
P62879	G protein subunit beta 2(GNB2)	0.9780	-0.0320	1	0.8468	-0.2400	0.31

P53621	coatomer protein complex subunit alpha(COPA)	0.9790	-0.0306	0.937	0.9673	-0.0480	0.589
P13804	electron transfer flavoprotein alpha subunit(ETFA)	0.9791	-0.0304	0.818	1.0044	0.0064	0.818
Q9Y4P3	transducin beta like 2(TBL2)	0.9792	-0.0303	0.589	0.8801	-0.1843	0.132
P10515	dihydrolipoamide S-acetyltransferase(DLAT)	0.9798	-0.0294	0.394	0.8682	-0.2039	0.394
Q99829	copine 1(CPNE1)	0.9808	-0.0280	0.699	0.8653	-0.2087	0.093
P19105	myosin light chain 12A(MYL12A)	0.9810	-0.0277	0.699	1.2972	0.3754	0.065
P32969	ribosomal protein L9(RPL9)	0.9814	-0.0271	0.818	1.0428	0.0605	0.937
Q16881	thioredoxin reductase 1(TXNRD1)	0.9826	-0.0253	0.937	0.9125	-0.1321	0.132
Q9P258	regulator of chromosome condensation 2(RCC2)	0.9858	-0.0207	0.818	0.8928	-0.1635	0.065
P78527	protein kinase, DNA-activated, catalytic polypeptide(PRKDC)	0.9859	-0.0204	1	0.9914	-0.0124	0.699
Q96PK6	RNA binding motif protein 14(RBM14)	0.9863	-0.0199	0.818	0.8271	-0.2739	0.818
Q16795	NADH:ubiquinone oxidoreductase subunit A9(NDUFA9)	0.9875	-0.0182	0.589	1.0288	0.0410	0.485
Q6DRA6	histone cluster 2 H2B family member d (pseudogene)(HIST2H2BD)	0.9878	-0.0177	0.818	1.0471	0.0664	0.394
P09525	annexin A4(ANXA4)	0.9902	-0.0142	0.818	0.8570	-0.2226	0.937
P62847	ribosomal protein S24(RPS24)	0.9913	-0.0126	0.485	1.0321	0.0456	0.937
P28062	proteasome subunit beta 8(PSMB8)	0.9921	-0.0114	0.589	0.9338	-0.0988	0.31
Q07666	KH RNA binding domain containing, signal transduction associated 1(KHDRBS1)	0.9923	-0.0111	0.818	0.8383	-0.2544	0.093
P07305	H1 histone family member 0(H1F0)	0.9924	-0.0110	0.937	0.8854	-0.1756	0.24
P04899	G protein subunit alpha i2(GNAI2)	0.9924	-0.0110	0.818	0.8327	-0.2641	0.589
P14866	heterogeneous nuclear ribonucleoprotein L(HNRNPL)	0.9940	-0.0087	0.818	0.8721	-0.1974	0.132
Q06830	peroxiredoxin 1(PRDX1)	0.9940	-0.0087	0.589	0.9765	-0.0343	0.699
P67809	Y-box binding protein 1(YBX1)	0.9945	-0.0080	0.699	0.9475	-0.0779	0.937
P62851	ribosomal protein S25(RPS25)	0.9951	-0.0071	0.937	1.1876	0.2481	0.041
P60660	myosin light chain 6(MYL6)	0.9973	-0.0038	0.699	1.4590	0.5450	0.24
P14868	aspartyl-tRNA synthetase(DARS)	0.9986	-0.0020	0.937	0.8470	-0.2396	0.24
P62269	ribosomal protein S18(RPS18)	0.9988	-0.0017	0.818	1.0952	0.1311	0.818
P08134	ras homolog family member C(RHOC)	0.9992	-0.0012	1	0.9483	-0.0766	0.31
P16403	histone cluster 1 H1 family member c(HIST1H1C)	0.9993	-0.0010	0.589	0.7467	-0.4215	0.485
P51149	RAB7A, member RAS oncogene family(RAB7A)	1.0008	0.0012	1	1.0151	0.0216	0.818
Q09028	RB binding protein 4, chromatin remodeling factor(RBBP4)	1.0033	0.0048	1	0.8751	-0.1925	0.041
P26373	ribosomal protein L13(RPL13)	1.0042	0.0060	0.937	1.0326	0.0463	0.818
P62314	small nuclear ribonucleoprotein D1 polypeptide(SNRPD1)	1.0057	0.0082	0.818	0.8240	-0.2793	0.093
O43242	proteasome 26S subunit, non-ATPase 3(PSMD3)	1.0061	0.0088	0.937	1.0164	0.0235	0.699
P06748	nucleophosmin(NPM1)	1.0073	0.0105	1	0.8760	-0.1910	0.589
Q9Y3A6	transmembrane p24 trafficking protein 5(TMED5)	1.0082	0.0118	0.485	1.0134	0.0193	0.699
Q99613	eukaryotic translation initiation factor 3 subunit C(EIF3C)	1.0090	0.0129	0.937	0.9233	-0.1151	0.18
P61353	ribosomal protein L27(RPL27)	1.0102	0.0146	0.937	1.1614	0.2158	0.394
P46778	ribosomal protein L21(RPL21)	1.0105	0.0150	0.589	1.1224	0.1666	0.394
P13645	keratin 10(KRT10)	1.0106	0.0153	0.937	1.5856	0.6650	0.065

P62191	proteasome 26S subunit, ATPase 1(PSMC1)	1.0112	0.0160	0.699	0.9725	-0.0402	0.31
P36578	ribosomal protein L4(RPL4)	1.0112	0.0161	0.485	0.9948	-0.0075	1
Q07020	ribosomal protein L18(RPL18)	1.0118	0.0170	0.699	1.0412	0.0582	1
Q8NBM8	prenylcysteine oxidase 1 like(PCYOX1L)	1.0137	0.0196	0.394	0.9857	-0.0207	0.699
Q9Y678	coatomer protein complex subunit gamma 1(COPG1)	1.0162	0.0232	0.818	0.8698	-0.2013	0.004
P61247	ribosomal protein S3A(RPS3A)	1.0167	0.0239	0.18	0.9870	-0.0189	0.818
P62424	ribosomal protein L7a(RPL7A)	1.0170	0.0243	0.485	1.0104	0.0150	0.699
Q8WU79	small ArfGAP2(SMAP2)	1.0174	0.0249	0.589	1.0531	0.0746	0.699
Q13310	poly(A) binding protein cytoplasmic 4(PABPC4)	1.0203	0.0290	1	0.8823	-0.1807	0.394
Q16658	fascin actin-bundling protein 1(FSCN1)	1.0208	0.0297	0.818	0.8961	-0.1582	0.015
P33991	minichromosome maintenance complex component 4(MCM4)	1.0208	0.0297	0.937	0.9654	-0.0509	0.485
Q7KZF4	staphylococcal nuclease and tudor domain containing 1(SND1)	1.0222	0.0316	0.699	0.9105	-0.1352	0.132
P48651	phosphatidylserine synthase 1(PTDSS1)	1.0233	0.0332	0.485	1.0334	0.0474	0.589
Q96FN4	copine 2(CPNE2)	1.0247	0.0352	0.937	0.8423	-0.2476	0.065
O15371	eukaryotic translation initiation factor 3 subunit D(EIF3D)	1.0254	0.0361	0.589	0.9716	-0.0415	0.589
Q9H2U2	pyrophosphatase (inorganic) 2(PPA2)	1.0254	0.0362	0.937	0.9673	-0.0479	0.818
P40429	ribosomal protein L13a(RPL13A)	1.0259	0.0369	0.485	0.9938	-0.0089	1
P17987	t-complex 1(TCP1)	1.0261	0.0372	0.937	0.9609	-0.0576	0.589
Q9UQ80	proliferation-associated 2G4(PA2G4)	1.0268	0.0381	0.589	0.9793	-0.0302	0.485
P20701	integrin subunit alpha L(ITGAL)	1.0281	0.0399	0.699	0.8491	-0.2359	0.589
Q99460	proteasome 26S subunit, non-ATPase 1(PSMD1)	1.0281	0.0400	0.937	0.9950	-0.0072	0.937
Q9UM54	myosin VI(MYO6)	1.0289	0.0411	0.589	1.0002	0.0003	0.699
P16401	histone cluster 1 H1 family member b(HIST1H1B)	1.0295	0.0420	0.589	0.7466	-0.4216	0.485
P46781	ribosomal protein S9(RPS9)	1.0299	0.0425	0.818	1.1051	0.1441	0.394
Q9UPN3	microtubule-actin crosslinking factor 1(MACF1)	1.0329	0.0466	0.937	1.0368	0.0522	0.937
P62917	ribosomal protein L8(RPL8)	1.0338	0.0479	0.937	0.9784	-0.0315	0.818
P55209	nucleosome assembly protein 1 like 1(NAP1L1)	1.0358	0.0507	0.699	0.8834	-0.1788	0.937
Q14289	protein tyrosine kinase 2 beta(PTK2B)	1.0361	0.0511	0.485	0.7392	-0.4360	0.589
P49207	ribosomal protein L34(RPL34)	1.0379	0.0537	0.818	1.1573	0.2108	0.093
Q15393	splicing factor 3b subunit 3(SF3B3)	1.0398	0.0563	1	0.8307	-0.2676	0.699
P62753	ribosomal protein S6(RPS6)	1.0399	0.0565	0.132	1.0140	0.0201	0.937
Q9UNM6	proteasome 26S subunit, non-ATPase 13(PSMD13)	1.0413	0.0584	0.31	0.8650	-0.2092	0.699
P54819	adenylate kinase 2(AK2)	1.0452	0.0638	0.818	1.0372	0.0527	0.699
P08670	vimentin(VIM)	1.0453	0.0640	0.394	0.8809	-0.1830	0.093
Q15008	proteasome 26S subunit, non-ATPase 6(PSMD6)	1.0480	0.0677	0.589	1.0444	0.0627	0.937
P61026	RAB10, member RAS oncogene family(RAB10)	1.0489	0.0688	0.818	1.0650	0.0908	0.699
Q9UJU6	drebrin like(DBNL)	1.0495	0.0697	0.818	0.7881	-0.3435	0.132
O75396	SEC22 homolog B, vesicle trafficking protein (gene/pseudogene)(SEC22B)	1.0502	0.0706	0.18	1.1555	0.2086	0.041
Q6NVY1	3-hydroxyisobutyryl-CoA hydrolase(HIBCH)	1.0544	0.0765	0.31	0.8614	-0.2152	0.31

P62750	ribosomal protein L23a(RPL23A)	1.0551	0.0773	0.31	1.1015	0.1395	0.937
P52272	heterogeneous nuclear ribonucleoprotein M(HNRNPM)	1.0553	0.0776	0.31	0.9209	-0.1190	0.485
P55735	SEC13 homolog, nuclear pore and COPII coat complex component(SEC13)	1.0558	0.0783	0.485	0.9593	-0.0600	0.485
P38606	ATPase H+ transporting V1 subunit A(ATP6V1A)	1.0572	0.0802	0.31	1.0415	0.0587	0.394
P18085	ADP ribosylation factor 4(ARF4)	1.0617	0.0864	0.818	0.8953	-0.1596	0.31
Q92841	DEAD-box helicase 17(DDX17)	1.0618	0.0865	0.589	0.7852	-0.3489	0.093
P48047	ATP synthase, H+ transporting, mitochondrial F1 complex, O subunit(ATP5O)	1.0654	0.0914	0.699	1.2358	0.3054	0.026
Q86V81	Aly/REF export factor(ALYREF)	1.0658	0.0920	0.589	0.6436	-0.6358	0.31
Q9NX63	coiled-coil-helix-coiled-coil-helix domain containing 3(CHCHD3)	1.0662	0.0924	0.699	0.8954	-0.1593	0.818
P23381	tryptophanyl-tRNA synthetase(WARS)	1.0662	0.0924	0.818	0.9094	-0.1370	1
P17858	phosphofructokinase, liver type(PFKL)	1.0669	0.0935	0.31	0.8990	-0.1537	0.699
P62266	ribosomal protein S23(RPS23)	1.0670	0.0935	0.18	0.9956	-0.0064	0.818
Q8TDN6	BRX1, biogenesis of ribosomes(BRIX1)	1.0674	0.0940	0.31	0.9932	-0.0098	1
Q9NVJ2	ADP ribosylation factor like GTPase 8B(ARL8B)	1.0679	0.0947	0.18	0.9514	-0.0719	0.699
P02545	lamin A/C(LMNA)	1.0682	0.0952	0.132	0.8930	-0.1633	0.31
P12268	inosine monophosphate dehydrogenase 2(IMPDH2)	1.0685	0.0955	0.394	1.0635	0.0889	0.699
Q8TEM1	nucleoporin 210(NUP210)	1.0686	0.0958	0.589	0.7049	-0.5045	0.394
P56134	ATP synthase, H+ transporting, mitochondrial Fo complex subunit F2(ATP5J2)	1.0692	0.0965	0.589	0.9260	-0.1110	0.699
P62829	ribosomal protein L23(RPL23)	1.0693	0.0966	0.18	1.2451	0.3163	0.132
P50995	annexin A11(ANXA11)	1.0695	0.0969	0.31	0.9181	-0.1233	0.589
Q5VTE0	eukaryotic translation elongation factor 1 alpha 1 pseudogene 5(EEF1A1P5)	1.0705	0.0983	0.132	1.0979	0.1348	0.394
P37802	transgelin 2(TAGLN2)	1.0705	0.0983	0.699	1.1168	0.1593	0.818
Q9Y3U8	ribosomal protein L36(RPL36)	1.0741	0.1031	0.24	1.1697	0.2262	0.015
O95881	thioredoxin domain containing 12(TXNDC12)	1.0743	0.1034	0.589	1.3239	0.4048	0.026
O43615	translocase of inner mitochondrial membrane 44(TIMM44)	1.0778	0.1081	0.18	0.9677	-0.0474	0.818
Q00610	clathrin heavy chain(CLTC)	1.0803	0.1115	0.24	0.9725	-0.0402	0.937
O00231	proteasome 26S subunit, non-ATPase 11(PSMD11)	1.0809	0.1123	0.937	1.0136	0.0195	0.818
Q02978	solute carrier family 25 member 11(SLC25A11)	1.0822	0.1139	0.589	1.1667	0.2224	0.065
Q92522	H1 histone family member X(H1FX)	1.0833	0.1154	0.699	0.7335	-0.4472	0.31
P11215	integrin subunit alpha M(ITGAM)	1.0882	0.1219	0.818	0.8929	-0.1635	0.394
Q71UI9	H2A histone family member V(H2AFV)	1.0884	0.1223	0.18	1.1139	0.1556	0.31
O43143	DEAH-box helicase 15(DHX15)	1.0885	0.1223	0.18	0.9232	-0.1153	0.394
P11310	acyl-CoA dehydrogenase, C-4 to C-12 straight chain(ACADM)	1.0905	0.1250	0.589	0.7928	-0.3350	0.24
P20702	integrin subunit alpha X(ITGAX)	1.0908	0.1254	0.485	0.8480	-0.2378	0.093
O00303	eukaryotic translation initiation factor 3 subunit F(EIF3F)	1.0944	0.1302	0.394	1.0660	0.0922	0.818
A0FGR8	extended synaptotagmin 2(ESYT2)	1.0952	0.1313	0.31	1.1118	0.1529	0.132
P36776	lon peptidase 1, mitochondrial(LONP1)	1.0954	0.1315	0.394	1.0231	0.0329	0.589
P09874	poly(ADP-ribose) polymerase 1(PARP1)	1.0962	0.1325	0.065	1.0213	0.0304	1

Q9Y262	eukaryotic translation initiation factor 3 subunit L(EIF3L)	1.0968	0.1333	0.818	0.9381	-0.0921	0.699
P38117	electron transfer flavoprotein beta subunit(ETFB)	1.0992	0.1364	0.24	0.9605	-0.0581	0.394
P49327	fatty acid synthase(FASN)	1.1011	0.1389	0.24	1.0539	0.0757	0.818
P62701	ribosomal protein S4, X-linked(RPS4X)	1.1047	0.1437	0.394	0.9781	-0.0319	1
P13639	eukaryotic translation elongation factor 2(EEF2)	1.1050	0.1441	0.394	1.0864	0.1196	0.818
P08238	heat shock protein 90 alpha family class B member 1(HSP90AB1)	1.1053	0.1444	0.31	1.0637	0.0890	0.699
P61254	ribosomal protein L26(RPL26)	1.1058	0.1451	0.24	1.1099	0.1504	0.699
P61421	ATPase H+ transporting V0 subunit d1(ATP6V0D1)	1.1082	0.1482	0.132	0.9297	-0.1051	0.31
Q96CW1	adaptor related protein complex 2 mu 1 subunit(AP2M1)	1.1130	0.1544	0.589	0.9564	-0.0643	0.818
Q02543	ribosomal protein L18a(RPL18A)	1.1143	0.1562	0.18	0.9361	-0.0953	0.485
Q13740	activated leukocyte cell adhesion molecule(ALCAM)	1.1145	0.1564	0.18	1.0451	0.0636	0.937
Q5JTV8	torsin 1A interacting protein 1(TOR1AIP1)	1.1162	0.1585	0.589	0.9990	-0.0014	1
P35606	coatomer protein complex subunit beta 2(COPB2)	1.1176	0.1604	0.394	0.9441	-0.0829	0.485
P61106	RAB14, member RAS oncogene family(RAB14)	1.1232	0.1676	0.132	1.0382	0.0541	0.24
O75489	NADH:ubiquinone oxidoreductase core subunit S3(NDUFS3)	1.1263	0.1716	0.31	1.0374	0.0529	0.24
Q6P2Q9	pre-mRNA processing factor 8(PRPF8)	1.1319	0.1787	0.24	1.0241	0.0343	0.937
P07355	annexin A2(ANXA2)	1.1324	0.1794	0.394	0.9770	-0.0336	0.818
P17844	DEAD-box helicase 5(DDX5)	1.1326	0.1796	0.015	0.9482	-0.0767	0.818
P22307	sterol carrier protein 2(SCP2)	1.1335	0.1808	1	1.0963	0.1327	0.589
O75531	barrier to autointegration factor 1(BANF1)	1.1348	0.1825	0.818	1.4478	0.5339	0.31
P23219	prostaglandin-endoperoxide synthase 1(PTGS1)	1.1356	0.1835	0.394	0.9014	-0.1498	0.485
P15880	ribosomal protein S2(RPS2)	1.1357	0.1835	0.818	1.0770	0.1070	0.485
Q9NZ08	endoplasmic reticulum aminopeptidase 1(ERAP1)	1.1362	0.1843	0.394	1.0177	0.0253	0.937
P24752	acetyl-CoA acetyltransferase 1(ACAT1)	1.1366	0.1848	0.394	0.8029	-0.3167	0.818
P11940	poly(A) binding protein cytoplasmic 1(PABPC1)	1.1416	0.1911	0.026	1.0871	0.1204	0.699
Q16836	hydroxyacyl-CoA dehydrogenase(HADH)	1.1493	0.2007	0.394	1.0976	0.1344	0.18
Q13263	tripartite motif containing 28(TRIM28)	1.1512	0.2031	0.31	0.9678	-0.0472	0.699
P30049	ATP synthase, H+ transporting, mitochondrial F1 complex, delta subunit(ATP5D)	1.1520	0.2042	0.937	1.0886	0.1224	0.818
Q12965	myosin IE(MYO1E)	1.1532	0.2056	0.24	1.1387	0.1874	0.18
P18124	ribosomal protein L7(RPL7)	1.1559	0.2090	0.093	1.1189	0.1620	0.132
Q16698	2,4-dienoyl-CoA reductase 1, mitochondrial(DECR1)	1.1619	0.2164	0.589	0.9135	-0.1305	0.699
P30040	endoplasmic reticulum protein 29(ERP29)	1.1625	0.2172	0.394	0.8992	-0.1533	0.699
P23396	ribosomal protein S3(RPS3)	1.1644	0.2196	0.004	1.1052	0.1443	0.18
P08758	annexin A5(ANXA5)	1.1653	0.2207	0.009	1.0672	0.0938	0.31
P62263	ribosomal protein S14(RPS14)	1.1670	0.2228	0.065	1.0604	0.0847	0.589
Q9H7B2	ribosome production factor 2 homolog(RPF2)	1.1676	0.2235	0.065	0.9598	-0.0591	0.937
O00232	proteasome 26S subunit, non-ATPase 12(PSMD12)	1.1678	0.2238	0.18	1.1127	0.1540	0.589
P50914	ribosomal protein L14(RPL14)	1.1698	0.2262	0.132	1.0344	0.0488	0.818

P23141	carboxylesterase 1(CES1)	1.1711	0.2279	0.24	1.0838	0.1162	0.31
P48735	isocitrate dehydrogenase (NADP(+)) 2, mitochondrial(IDH2)	1.1762	0.2341	0.24	0.9725	-0.0403	0.818
P35030	protease, serine 3(PRSS3)	1.1767	0.2347	0.589	0.8995	-0.1528	0.937
O00148	DExD-box helicase 39A(DDX39A)	1.1772	0.2354	0.065	0.9704	-0.0434	0.818
O00571	DEAD-box helicase 3, X-linked(DDX3X)	1.1781	0.2365	0.015	1.1002	0.1377	0.485
O95373	importin 7(IPO7)	1.1880	0.2485	0.041	0.8056	-0.3119	0.24
P23786	carnitine palmitoyltransferase 2(CPT2)	1.1891	0.2499	0.31	0.9350	-0.0970	0.589
Q9BVC6	transmembrane protein 109(TMEM109)	1.1907	0.2518	0.015	1.3503	0.4333	0.009
P49748	acyl-CoA dehydrogenase, very long chain(ACADVL)	1.1923	0.2537	0.394	1.0488	0.0687	0.589
Q6PI48	aspartyl-tRNA synthetase 2, mitochondrial(DARS2)	1.1941	0.2559	0.31	0.9824	-0.0256	1
Q9Y5X1	sorting nexin 9(SNX9)	1.1944	0.2563	0.065	1.0848	0.1174	0.818
Q7LGA3	heparan sulfate 2-O-sulfotransferase 1(HS2ST1)	1.1951	0.2571	0.589	1.0249	0.0354	0.394
P49257	lectin, mannose binding 1(LMAN1)	1.1999	0.2630	0.041	1.0745	0.1036	0.394
Q8NF50	dedicator of cytokinesis 8(DOCK8)	1.2000	0.2631	0.065	1.1810	0.2400	0.065
P84243	H3 histone family member 3A(H3F3A)	1.2033	0.2670	0.589	1.0084	0.0121	0.937
Q9NVI7	ATPase family, AAA domain containing 3A(ATAD3A)	1.2036	0.2674	0.18	1.0318	0.0451	0.589
Q7Z2K6	endoplasmic reticulum metallopeptidase 1(ERMP1)	1.2047	0.2686	0.24	1.0555	0.0779	0.818
O75367	H2A histone family member Y(H2AFY)	1.2048	0.2688	0.132	0.9351	-0.0969	0.24
O60832	dyskerin pseudouridine synthase 1(DKC1)	1.2062	0.2705	0.18	1.0947	0.1306	0.485
P05107	integrin subunit beta 2(ITGB2)	1.2086	0.2733	0.31	0.9709	-0.0426	0.818
Q9H061	transmembrane protein 126A(TMEM126A)	1.2106	0.2757	0.24	1.0052	0.0075	0.699
P62805	histone cluster 1 H4 family member i(HIST1H4I)	1.2108	0.2760	0.026	1.1752	0.2329	0.009
P20292	arachidonate 5-lipoxygenase activating protein(ALOX5AP)	1.2123	0.2777	0.699	0.8058	-0.3115	0.18
P00367	glutamate dehydrogenase 1(GLUD1)	1.2144	0.2803	0.394	0.9831	-0.0247	0.699
I00001	#N/A	1.2155	0.2816	0.093	1.4535	0.5395	0.041
P08708	ribosomal protein S17(RPS17)	1.2208	0.2878	0.699	1.3753	0.4597	0.485
P23284	peptidylprolyl isomerase B(PPIB)	1.2216	0.2888	0.24	1.0210	0.0299	0.589
Q04837	single stranded DNA binding protein 1(SSBP1)	1.2224	0.2897	0.589	0.9088	-0.1379	0.937
Q7L2H7	eukaryotic translation initiation factor 3 subunit M(EIF3M)	1.2237	0.2913	0.31	1.0832	0.1153	0.24
O14880	microsomal glutathione S-transferase 3(MGST3)	1.2274	0.2956	0.24	0.8901	-0.1679	0.394
Q99880	histone cluster 1 H2B family member l(HIST1H2BL)	1.2278	0.2960	0.24	1.5368	0.6199	0.24
P35579	myosin heavy chain 9(MYH9)	1.2278	0.2960	0.394	1.0845	0.1170	0.31
P08133	annexin A6(ANXA6)	1.2282	0.2965	0.093	1.0321	0.0455	0.24
O60762	dolichyl-phosphate mannosyltransferase subunit 1, catalytic(DPM1)	1.2329	0.3021	0.31	1.0974	0.1341	0.31
P55884	eukaryotic translation initiation factor 3 subunit B(EIF3B)	1.2353	0.3049	0.065	1.1616	0.2161	0.937
P61604	heat shock protein family E (Hsp10) member 1(HSPE1)	1.2386	0.3087	0.818	0.8065	-0.3103	0.485
P00387	cytochrome b5 reductase 3(CYB5R3)	1.2412	0.3118	0.31	1.0520	0.0732	0.394
Q08211	DExH-box helicase 9(DHX9)	1.2425	0.3133	0.009	1.0611	0.0856	0.394
Q99623	prohibitin 2(PHB2)	1.2439	0.3148	0.093	1.0006	0.0008	1

P55084	hydroxyacyl-CoA dehydrogenase/3-ketoacyl-CoA thiolase/enoyl-CoA hydratase (trifunctional protein), beta subunit(HADHB)	1.2471	0.3186	0.31	0.9143	-0.1293	0.589
Q5SSJ5	heterochromatin protein 1 binding protein 3(HP1BP3)	1.2476	0.3191	0.132	0.9096	-0.1368	0.132
P30101	protein disulfide isomerase family A member 3(PDIA3)	1.2495	0.3213	0.132	1.0188	0.0268	0.132
P33897	ATP binding cassette subfamily D member 1(ABCD1)	1.2502	0.3222	0.18	1.2075	0.2720	0.394
P30048	peroxiredoxin 3(PRDX3)	1.2507	0.3227	0.394	1.0114	0.0163	1
O96008	translocase of outer mitochondrial membrane 40(TOMM40)	1.2509	0.3230	0.24	0.8170	-0.2917	0.818
Q12907	lectin, mannose binding 2(LMAN2)	1.2591	0.3324	0.485	1.0097	0.0139	0.937
Q99714	hydroxysteroid 17-beta dehydrogenase 10(HSD17B10)	1.2607	0.3342	0.394	1.0651	0.0910	0.015
P16615	ATPase sarcoplasmic/endoplasmic reticulum Ca2+ transporting 2(ATP2A2)	1.2642	0.3382	0.132	1.1796	0.2383	0.041
P62244	ribosomal protein S15a(RPS15A)	1.2649	0.3390	0.132	1.1350	0.1826	1
P04004	vitronectin(VTN)	1.2658	0.3401	0.065	1.2027	0.2663	0.132
P08574	cytochrome c1(CYC1)	1.2669	0.3413	0.394	1.1213	0.1652	0.093
Q92598	heat shock protein family H (Hsp110) member 1(HSPH1)	1.2698	0.3446	0.065	0.9760	-0.0350	0.937
P08240	SRP receptor alpha subunit(SRPRA)	1.2715	0.3465	0.24	1.0428	0.0604	0.31
Q8TBQ9	transmembrane protein 167A(TMEM167A)	1.2770	0.3527	0.132	0.9020	-0.1488	0.24
P24539	ATP synthase, H+ transporting, mitochondrial Fo complex subunit B1(ATP5F1)	1.2787	0.3547	0.026	1.1809	0.2399	0.002
P00403	cytochrome c oxidase subunit II(COX2)	1.2821	0.3585	0.093	1.0896	0.1238	0.31
P13473	lysosomal associated membrane protein 2(LAMP2)	1.2822	0.3586	0.485	1.2286	0.2971	0.132
Q99798	aconitase 2(ACO2)	1.2835	0.3601	0.24	1.0114	0.0164	0.589
P20700	lamin B1(LMNB1)	1.2836	0.3602	0.132	0.8882	-0.1710	0.589
P43304	glycerol-3-phosphate dehydrogenase 2(GPD2)	1.2868	0.3638	0.24	1.0746	0.1038	0.31
Q16891	inner membrane mitochondrial protein(IMMT)	1.2869	0.3640	0.24	0.9902	-0.0142	0.818
P45880	voltage dependent anion channel 2(VDAC2)	1.2902	0.3676	0.394	1.0158	0.0227	0.937
P69905	hemoglobin subunit alpha 1(HBA1)	1.2921	0.3697	0.065	2.6573	1.4100	0.132
P46777	ribosomal protein L5(RPL5)	1.2938	0.3716	0.026	1.0488	0.0687	0.589
P53007	solute carrier family 25 member 1(SLC25A1)	1.2971	0.3753	0.24	1.0466	0.0657	0.24
P22695	ubiquinol-cytochrome c reductase core protein II(UQCRC2)	1.3028	0.3816	0.394	1.1085	0.1486	0.589
Q9Y2X3	NOP58 ribonucleoprotein(NOP58)	1.3039	0.3828	0.041	0.9786	-0.0312	0.937
Q9UBS4	DnaJ heat shock protein family (Hsp40) member B11(DNAJB11)	1.3043	0.3833	0.24	0.8767	-0.1898	0.818
Q9NQC3	reticulon 4(RTN4)	1.3056	0.3848	0.065	1.1085	0.1486	0.041
P14314	protein kinase C substrate 80K-H(PRKCSH)	1.3058	0.3850	0.31	0.9507	-0.0729	1
P36542	ATP synthase, H+ transporting, mitochondrial F1 complex, gamma polypeptide 1(ATP5C1)	1.3074	0.3867	0.394	0.9683	-0.0465	0.589
P07954	fumarate hydratase(FH)	1.3095	0.3890	0.31	1.0805	0.1117	0.24
Q13011	enoyl-CoA hydratase 1(ECH1)	1.3096	0.3891	0.093	1.1976	0.2601	0.002
P61313	ribosomal protein L15(RPL15)	1.3161	0.3963	0.026	1.0835	0.1157	0.093
P08559	pyruvate dehydrogenase (lipoamide) alpha 1(PDHA1)	1.3231	0.4039	0.093	1.1259	0.1711	0.18
Q9Y6C9	mitochondrial carrier 2(MTCH2)	1.3250	0.4060	0.132	1.1056	0.1448	0.065
P11279	lysosomal associated membrane protein 1(LAMP1)	1.3275	0.4088	0.699	1.0405	0.0572	0.937

O76021	ribosomal L1 domain containing 1(RSL1D1)	1.3277	0.4089	0.065	1.1118	0.1529	0.24
P51659	hydroxysteroid 17-beta dehydrogenase 4(HSD17B4)	1.3297	0.4111	0.31	0.9926	-0.0108	0.937
P43307	signal sequence receptor subunit 1(SSR1)	1.3317	0.4133	0.394	0.9636	-0.0535	0.818
P13073	cytochrome c oxidase subunit 4I1(COX4I1)	1.3334	0.4151	0.31	1.8080	0.8544	0.026
Q9Y277	voltage dependent anion channel 3(VDAC3)	1.3377	0.4197	0.24	1.0747	0.1040	0.31
P50213	isocitrate dehydrogenase 3 (NAD(+)) alpha(IDH3A)	1.3411	0.4234	0.132	0.8907	-0.1670	0.24
Q14165	malectin(MLEC)	1.3426	0.4250	0.31	0.9277	-0.1082	0.699
P08575	protein tyrosine phosphatase, receptor type C(PTPRC)	1.3428	0.4253	0.065	1.1178	0.1607	0.18
Q9NYU2	UDP-glucose glycoprotein glucosyltransferase 1(UGGT1)	1.3433	0.4257	0.31	1.0178	0.0255	0.937
P25705	ATP synthase, H+ transporting, mitochondrial F1 complex, alpha subunit 1, cardiac muscle(ATP5A1)	1.3435	0.4260	0.394	0.9661	-0.0498	1
P15144	alanyl aminopeptidase, membrane(ANPEP)	1.3459	0.4286	0.065	1.1459	0.1964	0.24
A5YKK6	CCR4-NOT transcription complex subunit 1(CNOT1)	1.3479	0.4308	0.485	1.2231	0.2905	0.394
Q9NSE4	isoleucyl-tRNA synthetase 2, mitochondrial(IARS2)	1.3480	0.4309	0.24	1.0470	0.0662	0.589
Q14697	glucosidase II alpha subunit(GANAB)	1.3502	0.4332	0.18	1.0981	0.1351	0.041
P39656	dolichyl-diphosphooligosaccharide--protein glycosyltransferase non-catalytic subunit(DDOST)	1.3533	0.4364	0.18	1.0234	0.0334	0.394
Q8NI27	THO complex 2(THOC2)	1.3567	0.4401	0.18	1.1115	0.1526	0.699
P36957	dihydrolipoamide S-succinyltransferase(DLST)	1.3584	0.4420	0.18	1.0782	0.1086	0.394
Q9BS26	endoplasmic reticulum protein 44(ERP44)	1.3594	0.4430	0.132	1.0842	0.1166	0.132
P23368	malic enzyme 2(ME2)	1.3615	0.4452	0.394	1.0012	0.0018	1
P04843	ribophorin I(RPN1)	1.3699	0.4541	0.132	1.0299	0.0425	0.24
P35232	prohibitin(PHB)	1.3752	0.4597	0.093	1.0812	0.1127	0.699
P40926	malate dehydrogenase 2(MDH2)	1.3754	0.4598	0.24	1.0076	0.0110	0.589
P67812	SEC11 homolog A, signal peptidase complex subunit(SEC11A)	1.3756	0.4600	0.041	1.0361	0.0511	0.132
P43243	matrin 3(MATR3)	1.3772	0.4618	0.015	1.1495	0.2010	0.485
P13667	protein disulfide isomerase family A member 4(PDIA4)	1.3774	0.4619	0.18	1.0247	0.0352	1
Q969H8	myeloid derived growth factor(MYDGF)	1.3785	0.4631	0.24	1.0541	0.0760	0.31
Q9P2J5	leucyl-tRNA synthetase(LARS)	1.3806	0.4653	0.394	0.9088	-0.1380	0.589
P06576	ATP synthase, H+ transporting, mitochondrial F1 complex, beta polypeptide(ATP5B)	1.3813	0.4660	0.394	1.0697	0.0972	0.093
P22090	ribosomal protein S4, Y-linked 1(RPS4Y1)	1.3860	0.4710	0.093	0.9715	-0.0417	0.937
Q15005	signal peptidase complex subunit 2(SPCS2)	1.3874	0.4723	0.485	1.3956	0.4809	0.026
P49411	Tu translation elongation factor, mitochondrial(TUFM)	1.3875	0.4725	0.24	0.9846	-0.0223	0.818
P27797	calreticulin(CALR)	1.3879	0.4729	0.132	1.0032	0.0046	0.937
P08754	G protein subunit alpha i3(GNAI3)	1.3879	0.4729	0.24	1.0051	0.0073	0.589
P27635	ribosomal protein L10(RPL10)	1.3883	0.4733	0.18	1.3220	0.4028	0.041
Q9BSJ8	extended synaptotagmin 1(ESYT1)	1.3936	0.4788	0.394	1.0108	0.0154	1
P00505	glutamic-oxaloacetic transaminase 2(GOT2)	1.3940	0.4793	0.132	1.0893	0.1234	0.589
Q16563	synaptophysin like 1(SYPL1)	1.3986	0.4840	0.394	1.0512	0.0720	0.394
Q00839	heterogeneous nuclear ribonucleoprotein U(HNRNPU)	1.4006	0.4861	0.015	1.1522	0.2044	0.065

P21796	voltage dependent anion channel 1(VDAC1)	1.4037	0.4892	0.31	0.9950	-0.0072	0.589
O75390	citrate synthase(CS)	1.4037	0.4893	0.065	1.1024	0.1407	0.093
P51571	signal sequence receptor subunit 4(SSR4)	1.4039	0.4895	0.132	1.1438	0.1938	0.026
Q9Y2Q3	glutathione S-transferase kappa 1(GSTK1)	1.4047	0.4903	0.093	1.1042	0.1430	0.818
Q15084	protein disulfide isomerase family A member 6(PDIA6)	1.4068	0.4924	0.24	1.0017	0.0024	0.394
Q14764	major vault protein(MVP)	1.4088	0.4945	0.009	1.1768	0.2348	0.485
Q53GQ0	hydroxysteroid 17-beta dehydrogenase 12(HSD17B12)	1.4168	0.5027	0.394	1.1910	0.2522	0.24
Q04637	eukaryotic translation initiation factor 4 gamma 1(EIF4G1)	1.4186	0.5044	0.004	1.1855	0.2455	0.699
P04844	ribophorin II(RPN2)	1.4214	0.5073	0.041	1.2742	0.3496	0.026
Q8NBX0	saccharopine dehydrogenase (putative)(SCCPDH)	1.4230	0.5089	0.394	1.0186	0.0266	1
O75439	peptidase, mitochondrial processing beta subunit(PMPCB)	1.4349	0.5209	0.093	1.1374	0.1857	0.394
P05141	solute carrier family 25 member 5(SLC25A5)	1.4365	0.5225	0.18	1.1805	0.2394	0.015
P49755	transmembrane p24 trafficking protein 10(TMED10)	1.4398	0.5258	0.009	1.1935	0.2552	0.18
P34897	serine hydroxymethyltransferase 2(SHMT2)	1.4491	0.5352	0.132	1.1856	0.2457	0.002
P54709	ATPase Na+/K+ transporting subunit beta 3(ATP1B3)	1.4512	0.5373	0.015	1.3019	0.3806	0.065
O94905	ER lipid raft associated 2(ERLIN2)	1.4550	0.5410	0.24	1.1213	0.1652	0.31
P07237	prolyl 4-hydroxylase subunit beta(P4HB)	1.4576	0.5436	0.132	1.0405	0.0572	0.31
P31930	ubiquinol-cytochrome c reductase core protein I(UQCRC1)	1.4601	0.5460	0.041	1.1729	0.2301	0.002
Q9NS69	translocase of outer mitochondrial membrane 22(TOMM22)	1.4622	0.5481	0.026	1.2237	0.2913	0.18
Q99873	protein arginine methyltransferase 1(PRMT1)	1.4654	0.5513	0.132	0.9070	-0.1409	0.818
Q9Y6N5	sulfide quinone reductase-like (yeast)(SQRDL)	1.4671	0.5530	0.065	1.0744	0.1036	0.394
P40939	hydroxyacyl-CoA dehydrogenase/3-ketoacyl-CoA thiolase/enoyl-CoA hydratase (trifunctional protein), alpha subunit(HADHA)	1.4691	0.5550	0.24	1.1025	0.1407	0.002
P14625	heat shock protein 90 beta family member 1(HSP90B1)	1.4760	0.5617	0.394	1.0024	0.0034	0.589
P11021	heat shock protein family A (Hsp70) member 5(HSPA5)	1.4863	0.5717	0.31	0.9868	-0.0192	0.937
P09622	dihydrolipoamide dehydrogenase(DLD)	1.4912	0.5764	0.18	0.9241	-0.1139	0.699
O95202	leucine zipper and EF-hand containing transmembrane protein 1(LETM1)	1.5016	0.5865	0.132	1.0836	0.1158	0.394
Q13423	nicotinamide nucleotide transhydrogenase(NNT)	1.5093	0.5939	0.18	1.0868	0.1201	0.394
P39023	ribosomal protein L3(RPL3)	1.5105	0.5950	0.002	1.3277	0.4089	0.004
Q12931	TNF receptor associated protein 1(TRAP1)	1.5139	0.5983	0.18	1.1185	0.1616	0.009
Q9UGP8	SEC63 homolog, protein translocation regulator(SEC63)	1.5139	0.5983	0.18	1.1415	0.1909	0.18
Q8TCT9	histocompatibility minor 13(HM13)	1.5189	0.6030	0.132	1.0701	0.0978	0.026
P12236	solute carrier family 25 member 6(SLC25A6)	1.5338	0.6171	0.026	1.2801	0.3563	0.009
P38646	heat shock protein family A (Hsp70) member 9(HSPA9)	1.5433	0.6260	0.18	1.0824	0.1143	0.002
Q08379	golgin A2(GOLGA2)	1.5491	0.6314	0.009	1.3412	0.4235	0.485
Q9Y4L1	hypoxia up-regulated 1(HYOU1)	1.5615	0.6430	0.132	1.2195	0.2863	0.065
P46977	STT3A, catalytic subunit of the oligosaccharyltransferase complex(STT3A)	1.5663	0.6474	0.132	1.2290	0.2975	0.009
P10809	heat shock protein family D (Hsp60) member 1(HSPD1)	1.5664	0.6475	0.394	1.1359	0.1838	0.015
Q00325	solute carrier family 25 member 3(SLC25A3)	1.5777	0.6578	0.026	1.0984	0.1354	0.026

P42704	leucine rich pentatricopeptide repeat containing(LRPPRC)	1.5911	0.6700	0.093	1.2544	0.3270	0.015
Q13162	peroxiredoxin 4(PRDX4)	1.5986	0.6769	0.132	1.2185	0.2851	0.015
P99999	cytochrome c, somatic(CYCS)	1.6059	0.6833	0.093	1.3426	0.4250	0.065
P27824	calnexin(CANX)	1.6213	0.6971	0.132	1.0997	0.1371	0.015
P05023	ATPase Na+/K+ transporting subunit alpha 1(ATP1A1)	1.6413	0.7148	0.132	1.2474	0.3189	0.065
Q9BVK6	transmembrane p24 trafficking protein 9(TMED9)	1.6497	0.7222	0.004	1.2000	0.2630	0.026
Q8TCJ2	STT3B, catalytic subunit of the oligosaccharyltransferase complex(STT3B)	1.6517	0.7240	0.009	1.2627	0.3365	0.31
P57088	transmembrane protein 33(TMEM33)	1.6653	0.7358	0.132	1.2111	0.2763	0.026
P11387	topoisomerase (DNA) I(TOP1)	1.6779	0.7466	0.31	0.9555	-0.0656	0.485
P0C0L4	complement C4A (Rodgers blood group)(C4A)	1.7483	0.8060	0.31	1.5466	0.6291	0.699
P01892	major histocompatibility complex, class I, A(HLA-A)	1.7919	0.8415	0.093	1.4344	0.5204	0.18
O75844	zinc metallopeptidase STE24(ZMPSTE24)	1.7968	0.8454	0.002	1.4805	0.5661	0.002
P08311	cathepsin G(CTSG)	1.8304	0.8722	0.093	1.4279	0.5139	0.24
P08567	pleckstrin(PLEK)	1.8760	0.9076	0.002	1.5838	0.6634	0.093
Q02880	topoisomerase (DNA) II beta(TOP2B)	1.9075	0.9317	0.026	1.3883	0.4733	0.394
Q9NR30	DExD-box helicase 21(DDX21)	1.9238	0.9439	0.002	1.4780	0.5637	0.004
P12259	coagulation factor V(F5)	2.0929	1.0655	0.002	3.5894	1.8437	0.026
Q14213	Epstein-Barr virus induced 3(EBI3)	2.2492	1.1694	0.132	2.2583	1.1753	0.132
P68871	hemoglobin subunit beta(HBB)	2.3095	1.2076	0.015	2.4174	1.2734	0.026
P02647	apolipoprotein A1(APOA1)	2.3573	1.2371	0.31	2.5577	1.3549	0.18
P36955	serpin family F member 1(SERPINF1)	2.4669	1.3027	0.18	1.5123	0.5967	0.699
P07996	thrombospondin 1(THBS1)	2.5317	1.3401	0.132	1.3401	0.4223	0.485
P04114	apolipoprotein B(APOB)	2.5576	1.3548	0.132	1.4535	0.5395	0.394
O95497	vanin 1(VNN1)	2.5691	1.3612	0.18	1.3759	0.4604	0.699
P02768	albumin(ALB)	2.6309	1.3956	0.132	1.5435	0.6262	0.394
P02765	alpha 2-HS glycoprotein(AHSG)	2.6494	1.4057	0.18	1.5003	0.5852	0.31
P01023	alpha-2-macroglobulin(A2M)	2.8501	1.5110	0.132	1.4464	0.5324	0.485
Q06033	inter-alpha-trypsin inhibitor heavy chain 3(ITIH3)	2.8998	1.5359	0.132	1.4619	0.5478	0.485
P01024	complement C3(C3)	2.9009	1.5365	0.132	1.4065	0.4921	0.485
P02771	alpha fetoprotein(AFP)	2.9222	1.5470	0.132	1.4804	0.5660	0.31
P01008	serpin family C member 1(SERPINC1)	2.9411	1.5563	0.18	1.6455	0.7185	0.485
P05543	serpin family A member 7(SERPINA7)	2.9965	1.5833	0.132	1.5650	0.6462	0.485
P02788	lactotransferrin(LTF)	2.9974	1.5837	0.18	1.1153	0.1575	0.589
P19823	inter-alpha-trypsin inhibitor heavy chain 2(ITIH2)	3.3714	1.7533	0.132	1.3816	0.4663	0.485
P02774	GC, vitamin D binding protein(GC)	3.6354	1.8621	0.18	2.1758	1.1216	0.31
P12277	creatine kinase B(CKB)	3.8162	1.9321	0.002	2.1222	1.0855	0.002
O75352	mannose-P-dolichol utilization defect 1(MPDU1)	4.3710	2.1280	0.093	1.1062	0.1456	0.31
P05362	intercellular adhesion molecule 1(ICAM1)	13.1237	3.7141	0.002	8.6182	3.1074	0.002

Supplementary Table V.3. List of common and specific differentially represented host proteins in *R. conorii*- and *R. montanensis*-infected THP-1 macrophages compared with uninfected cells. Associated with **Figure V.3**. (xls) This table can be found in digital format for consultation